國立中央大學天文研究所
鹿林天文台年報

2006

No.4

國立中央大學天文研究所編

This page is intentionally left blank.

序言

鹿林天文台的建設，是中央大學投入十多年的精神與心血而成。這位於玉山國家公園鹿林前山（海拔 2,862 公尺）的天文研究基地，正帶領台灣天文研究邁向跨國的天文研究中心。幾年來的累積，鹿林天文台多個具前瞻性的研究計畫，已經有一些重要的成果，

- 歷年來鹿林天文台相關國際期刊論文(10+)、會議論文(30+)及通告(67)累計達上百篇。研究範圍涵蓋天文各個領域。
- 自 2003 年 7 月開始，鹿林天文台一米望遠鏡(LOT)加入伽瑪射線爆光學餘暉觀測的行列，並與日本、大陸以及韓國的天文台合作成立了東亞伽瑪射線爆測網(EAFON)。在 3 年的觀測時間內，LOT 對 41 個伽瑪射線爆進行光學後續觀測，並成功的觀測 15 個伽瑪射線爆光學餘暉。
- 在新天體的發現上，自 2002 年發現台灣第一顆小行星以來累計超過 280 顆，其中有 6 顆已取得正式編號，擁有命名權，成為亞洲發現小行星最活躍的地方。
- 台灣超新星巡天計畫自 2003 年發現台灣第一顆超新星迄今已發現 11 顆超新星。
- 除了一米望遠鏡(LOT)、SLT(40 公分)望遠鏡、中美掩星計畫(TAOS)和發射線巡天計畫(LELIS)外，鹿林天文台做為一個科學基地，還擔任支持其他科學領域的角色。如中大大氣系/環工所的亞洲大氣污染物長程輸送與衝擊研究、中大太空所 airglow imager、成功大學物理系的紅色精靈地面觀測與極低頻無線電波偵測系統(ELF)，以及環保署鹿林空氣品質背景測站(LABS)，都設置在鹿林天文台基地，開展各領域相關的研究計畫。其中成大的紅色精靈和中大太空所的 airglow imager 都是與華衛二號 ISUAL 聯合之地面觀測。

鹿林天文台的觀測工作都是應用小型望遠鏡和台灣觀測條件的優勢。目前我們正籌建兩米望遠鏡，並同時參與美國夏威夷大學天文所及美國空軍合作的泛星計劃(Pan-STARRS)。從天文學研究大架構的建立，到以鹿林天文台做為培育人才的搖籃，中央大學天文研究所更進一步想凝聚研究能量的中心，以期提倡國內天文研究與教育，實現科技富國的美好遠景。

鹿林天文台 台長

林宏欽

2007/03/19

This page is intentionally left blank.

目錄

This page is intentionally left blank.

研究報告

The Astronomical Journal, 131:3040–3046, 2006 June

EVIDENCE FOR A BINARY ORIGIN OF THE YOUNG PLANETARY NEBULA HUBBLE 12

Chih Hao Hsia,[1,2] Wing Huen Ip,[1] and Jin Zeng Li[2]
Received 2005 October 7; accepted 2006 February 17

ABSTRACT

Young planetary nebulae play an important role in stellar evolution when intermediate- to low-mass stars (0.8–8 $M_{\odot}$) evolve from the proto–planetary nebula phase to the planetary nebula phase. Many young planetary nebulae display distinct bipolar structures as they evolve away from the proto–planetary nebula phase. One possible cause of their bipolarity could be a binary origin for their energy source. Here we report on our detailed investigation of the young planetary nebula Hubble 12, which is well known for its extended hourglass-like envelope. We present evidence with time-series photometric observations for the existence of an eclipsing binary at the center of Hubble 12. In addition, low-resolution spectra of the central source show absorption features such as CN, *G* band, and Mg *b*, which can be suggestive of a low-mass nature for the secondary component.

Key words: binaries: general — planetary nebulae: individual (Hubble 12)

1. INTRODUCTION

The young planetary nebula (PN) Hubble 12 (HB 12; PN G111.8−02.8) plays an important role in the study of PNe. The line ratios of its strong fluorescent molecular hydrogen emission (Dinerstein et al. 1988) match closely pure fluorescent emission (Black & van Dishoeck 1987), which might have originated from shock excitation via collisional interaction of a strong wind from the central star against a circumstellar gaseous disk (Kastner & Weintraub 1994). The bipolar structure of HB 12 is also of particular interest. Early radio continuum observations from the Very Large Array (Bignell 1983) first disclosed its bipolar configuration. Miranda & Solf (1989) later confirmed the double-lobe structure along the north-south axis through long-slit spectroscopy. In addition, Hora & Latter (1996) and Welch et al. (1999) showed the existence of a ringlike structure near the central core from near-infrared and [Fe II] imaging. Recent *Hubble Space Telescope* (*HST*) NICMOS observations have revealed clearly detailed structure of the inner torus and its bipolar lobes (Hora et al. 2000). The origin of the axisymmetric morphology of young PNe has long been an unresolved issue. In classification of PNe based on their morphology, Zuckerman & Aller (1986) and Soker (1997) found that a large majority of PNe have nonspherical shapes, some indicating extreme bipolar or axisymmetric structure. Such structures could be generated by strong bipolar outflows during the late asymptotic giant branch (AGB) or post-AGB phase and may be transient phenomena (Kwok et al. 2000). The bipolar flows in turn could be produced by close binaries (Morris 1990; Soker et al. 1998; Soker 2000), or rather focusing effects from the associated magnetic field (Garcia-Segura et al. 1999, 2000), among various potential mechanisms suggested. Note that observational evidence has been found in support of the binary model (De Marco et al. 2004; Hillwig 2004; Sorensen & Pollacco 2004). Detailed investigations of the physical nature and dynamical properties of the central source are therefore of fundamental importance to our understanding of the origin and evolution of PNe.

We have initiated a program combining efforts from the photometric measurements obtained by the 1 m telescope (LOT) at the Lulin Observatory in central Taiwan and the spectrographic observations carried out with the 2.16 m telescope at the Xing-Long station of the National Astronomical Observatory of the Chinese Academy of Sciences (NAOC). Our main objective is to search for the possible presence of periodic variations in the light curves of the nucleus of HB 12, NSV 26083. Properties of the binary components could also perhaps be inferred from spectral observations of the central source. We describe in § 2 the observations and data reduction. The photometric light curves are presented in § 3, and then a discussion of the results and interpretations in § 4. The spectral features possibly originating from the cool secondary are investigated in § 5, which is followed by a summary of the main results of this study.

2. OBSERVATIONS AND DATA REDUCTION

2.1. *Time-Series Broadband Photometric Imaging*

High-speed broadband photometric observations were performed in the queue mode on the nights of 2003 December 3–5 using Johnson *R*- and *I*-band filters with the LOT telescope of the National Central University in Taiwan. The camera was operated with a Princeton Instruments 1340 × 1300 pixel CCD, giving a field of view of $11' \times 11'$. The CCD has a readout noise of 15.7 *e* and a gain of 4.4. The setup results in a pixel scale of $0''.62$ pixel^{-1}. Flat-field exposures were obtained on the twilight sky. The seeing condition all through this run of observations varied between $1''.3$ and $1''.9$. The journal of observations is summarized in Table 1.

More than 800 snapshots of HB 12 were made, with each snapshot containing a 10 s exposure in *R* and another 5 s in *I*. The data reduction includes bias and dark current correction and flat-fielding based on standard packages and procedures in the NOAO IRAF (ver. 2.12). Differential magnitudes of the central core of HB 12 were measured using the DAOPHOT package with three stars in the same field as reference stars. The signal-to-noise (S/N) ratios of all stars are >100. No apparent variations were found with the reference stars. The differential magnitudes in the *R* and *I* bands have accuracies within 0.04 and 0.02 mag, respectively.

2.2. *Optical Spectroscopy*

Low-resolution spectroscopy was obtained by the 2.16 m telescope of NAOC. The journal of observations in two separate sessions is given in Table 2. In the 2004 session, measurement

[1] Institute of Astronomy, National Central University, Chung Li 32054, Taiwan; d929001@astro.ncu.edu.tw.
[2] National Astronomical Observatories, Chinese Academy of Sciences, Beijing 100012, China; ljz@bao.ac.cn.

TABLE 1
JOURNAL OF PHOTOMETRIC OBSERVATIONS OF HB 12

Observation Date	Start (UT)	Start (HJD 2,452,900+)	Duration (hr)	Filter	Number of Exposures
2003 Dec 3	10:56	76.9557	4.3	*R*	132
2003 Dec 3	10:57	76.9568	4.3	*I*	132
2003 Dec 4	10:51	77.9527	4.4	*R*	139
2003 Dec 4	10:52	77.9540	4.4	*I*	139
2003 Dec 5	10:38	78.9434	4.5	*R*	143
2003 Dec 5	10:40	78.9452	4.5	*I*	143

was performed in the spectral range 4800–10500 Å on the night of 2004 August 8. The spectral dispersion was 3.1 Å pixel^{-1}. The Beijing Faint Object Spectrograph and Camera and a thinned back-illuminated Orbit 2048 × 2048 CCD were used. A slit width of 3.″6 was set. The exposure times ranged from 300 to 900 s. S/N ratios of the continuum of >90 were achieved. Exposures of Fe-Ne arcs were obtained right before and after each stellar spectrum and were used for the wavelength calibration.

In the 2005 session, spectroscopy was performed in the blue (3800–6200 Å) spectral range on the night of 2005 September 26. The 100 Å mm^{-1} grating was used, which resulted in a 2 pixel resolution of ~4.8 Å. The slit was placed at P.A. = 170°, in parallel to the main axis of HB 12 as indicated in Figure 1. The slit width was set to 2″. An Optomechanics Research, Inc., spectrograph and a Tektronix 1024 × 1024 CCD were used. The exposures ranged from 3600 to 7200 s, resulting in S/N ratios of >60. Wavelength calibration was performed based on He-Ar lamps exposed right before and after the target spectrum.

The spectral data were reduced following standard procedures in the NOAO IRAF (ver. 2.12) software package. The CCD reductions included bias and flat-field correction, successful background subtraction, and cosmic-ray removal. Flux calibration was derived with observations of at least two of the Kitt Peak National Observatory standard stars per spectral range per night. The atmospheric extinction was corrected by the mean extinction coefficients measured for Xing-Long station, where the 2.16 m telescope is located.

3. SEARCH FOR PERIODICITIES IN THE LIGHT CURVES

The multiband photometric results of HB 12 are presented in Figure 2. The method of phase dispersion minimization (PDM; Stellingwerf 1978) was used to analyze the light curves of NSV 26083. The PDM code was employed to derive the period, maximum magnitude, and amplitude of the light variation. Before calculating the power spectra, we set the nightly mean magnitude to zero and calculated the amplitude spectra of these data. The *I*-band data clearly cover three primary minima. A linear least-squares fit results in a period of $P = 0.1415 \pm 0.0015$ days. The *R*-band light curve was fitted simultaneously using the period of the *I*-band data because of their distinct primary minima. The power spectra of the photometric data are presented in Figure 3. A prominent amplitude peak is found at 7.06 cycles day^{-1}, which is 3.4 hr. The corresponding phase diagrams are shown in Figure 4. The profiles are sinusoidal for both the *R* and *I* bands. The period shows an amplitude of 0.06 ± 0.0074 mag in *R* and 0.08 ± 0.0046 mag in *I*. This suggests that NSV 26083 displays in its multiband time-series observations periodic variation and indicates a probable eclipsing binary origin for HB 12. It is the first time that a clear signature of periodicity has been evidenced toward the exciting source of HB 12, which may have important implications on the physical nature of bipolar structures associated with other young PNe.

Note that the dip in the *R*-band light curve seems to be shallower and smoother than that in the *I* band light curve. This wavelength dependence could probably be due to effects from Hα emission of the companion star, which is encompassed by the *R*-band observations, or other reflection effects from the illuminated surface of the less luminous star (Grauer & Bond 1983; Bruch et al. 2001).

If we alternatively suppose the periodic variations of NSV 26083 to be due to rotation modulation of stellar spot(s), the rotational period can be estimated as follows (Reid et al. 1993):

$$P_{\rm crit} = \frac{2\pi R_e^{3/2}}{\sqrt{GM}} = 2.78 R_e^{3/2} M^{-1/2}, \quad (1)$$

where $P_{\rm crit}$ is the rotational period of the star in hours, R_e is the equatorial radius, and M is the mass of the star in solar units. Following the discussion by Reid et al. (1993), we use $R_e = 1.5R_*$, where R_* is the radius of NSV 26083. If Zhang & Kwok's (1993) results of $T_{\rm eff} = 31{,}800$ K, $\log g = 3.1$, and $M = 0.8\,M_\odot$ are adopted, the rotational period $P_{\rm crit}$ would be as large as 48 hr. This is inconsistent with our estimation of 3.4 hr as presented above and helps to exclude the possibility of modulation by stellar spots.

4. STELLAR PROPERTIES OF THE BINARY COMPONENTS

The mass of the central source of HB 12 has been determined to be 0.8 $M_\odot$ by Zhang & Kwok (1993) based on existing infrared

TABLE 2
JOURNAL OF SPECTRAL OBSERVATIONS OF HB 12

Observation Date	Wavelength (Å)	Resolution (Å pixel^{-1})	Width of Slit (arcsec)	Integration Time (s)
2004 Aug 8	4800–10500	3.1	3.6	300
2004 Aug 8	4800–10500	3.1	3.6	900
2005 Sep 26	3800–6200	2.4	2	2 × 3600

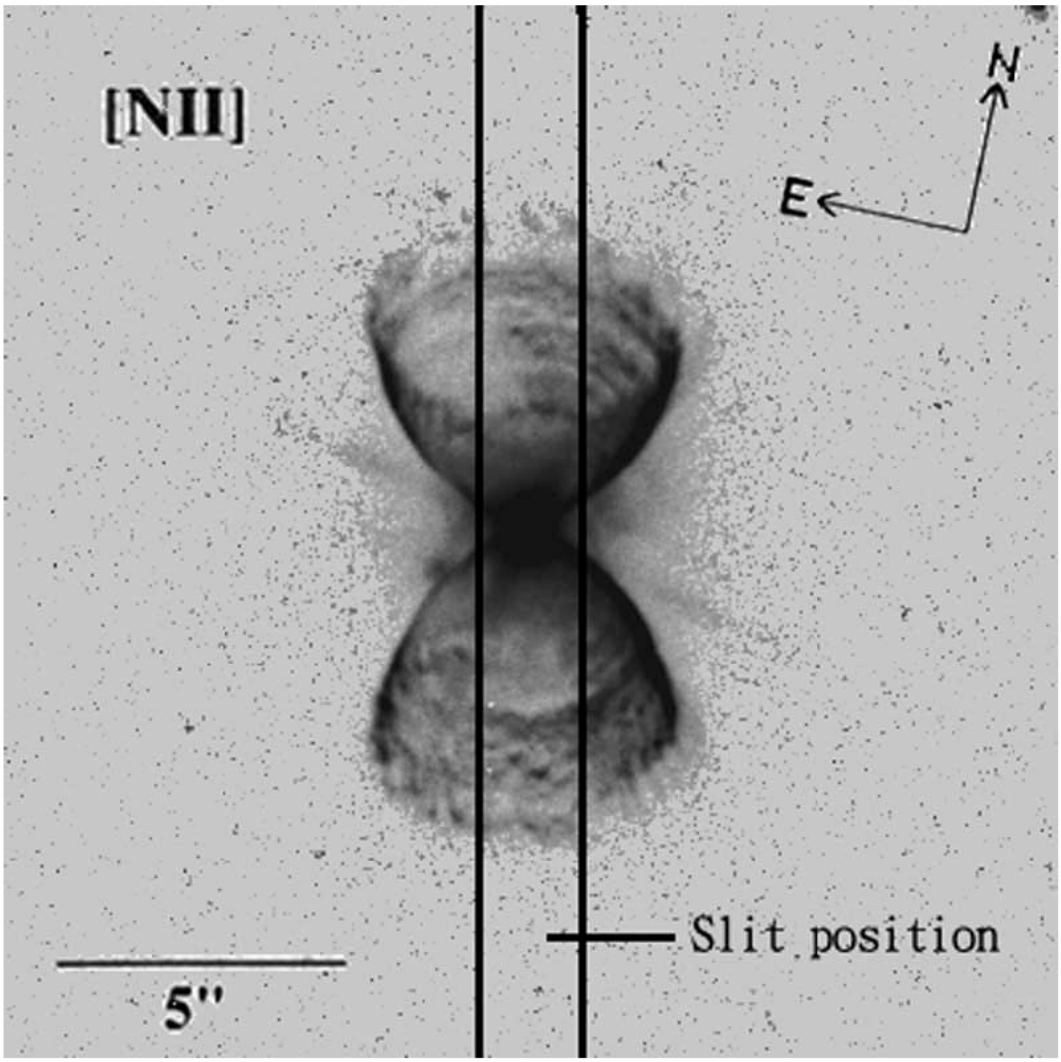

FIG. 1.—*HST* WFPC2 narrowband [N II] (F658N) image of HB 12, displayed with a linear gray scale. We present here the combined data sets (U6CI0405, U6CI0406, U6CI0407, and U6CI0408) of B. Balick. The total exposure time is 1300 s, and the field of view is $18'' \times 18''$. The slit position is shown against the image of the core of the PN.

and radio data. We present below an estimation of the mass and radius of the proposed secondary component of the system.

First, the secondary star, with an orbital period of hours to days, was suggested to have a mass of less than 0.5 $M_\odot$ (Chen et al. 1995). If a mass ratio $M_2/M_1 < 0.8$ (M_1 is the mass of the primary star) is supposed, the upper limits of the mass and radius of the secondary would satisfy the following condition (Paczyński 1981):

$$8.85\sqrt{\frac{R_2^3}{M_2}} < P, \tag{2}$$

where P is the orbital period in hours and M_2 and R_2 are the mass and radius of the secondary in solar units, respectively.

Second, assume that the mass-radius relation of the lower main sequence stars can be applied to the secondary (Rappaport et al. 1982):

$$\frac{R_2}{R_\odot} = 0.76\left(\frac{M_2}{M_\odot}\right)^{0.78}. \tag{3}$$

We can combine equation (2) with equation (3) to obtain

$$M_2 < 0.443\ M_\odot, \quad R_2 < 0.403\ R_\odot. \tag{4}$$

There is a general agreement (Schönberner 1981; Heap & Augensen 1987; Weidemann 1989; Tylenda et al. 1991b; Zhang & Kwok 1993; Stasińska et al. 1997) that the dispersion of the central stellar masses of PNe, averaged to around 0.6 $M_\odot$, should be rather small. If we assume a mass 0.6 $M_\odot$ for the primary star, for $M_1 = 0.6$ and $0.08 < M_2 < 0.443$, the separation of the stars $a = 1.163 \pm 0.063\ R_\odot$. In turn, the radius of the Roche lobe of the secondary is

$$l_2 = a[0.5 + 0.227 \log (M_2/M_1)].$$

This results in an estimation of $0.547 \pm 0.03\ R_\odot$, and the hemisphere of the secondary must be illuminated and heated by the primary source.

The distance to HB 12 has been estimated to be 2.24 kpc by Cahn et al. (1992) based on existing optical and radio data; Hora & Latter (1996) determined an $E(B-V)$ value of 0.28 measuring

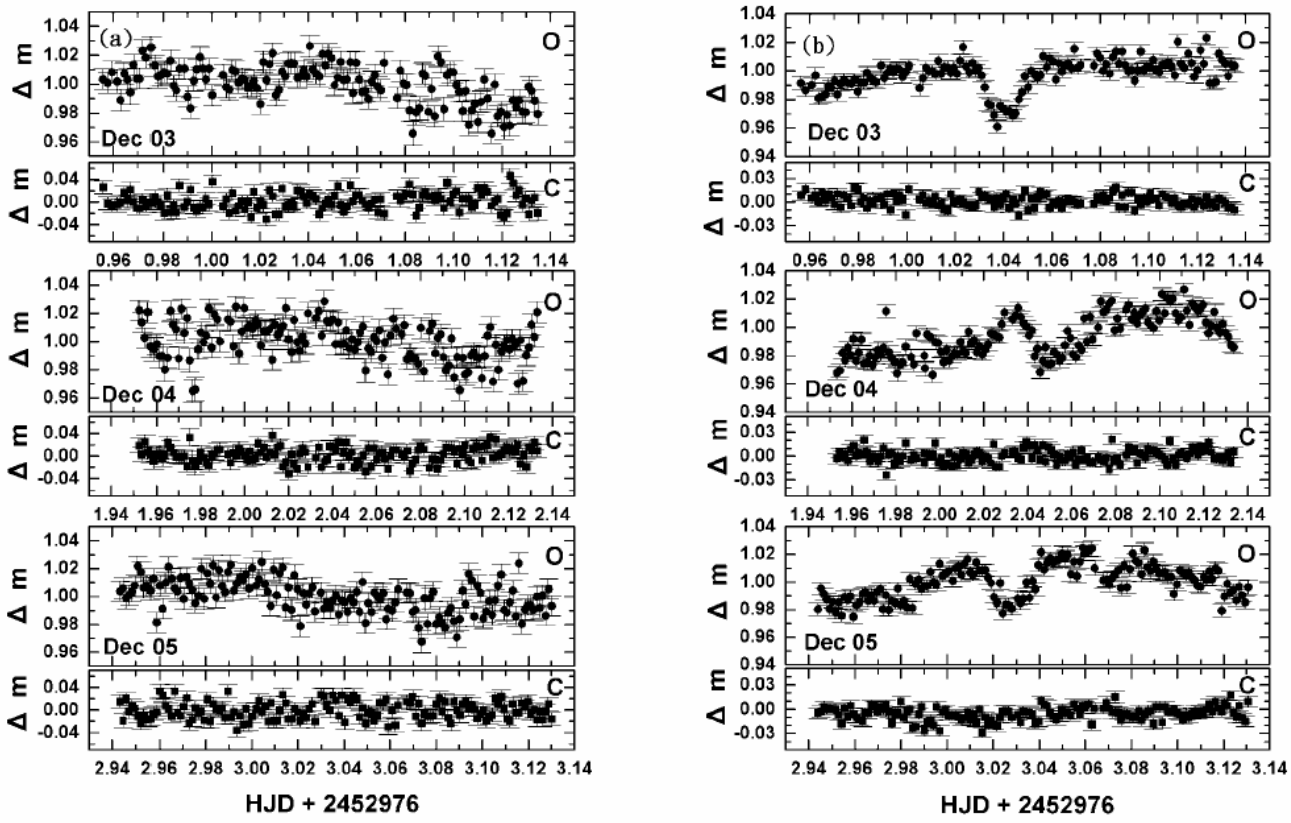

FIG. 2.—Differential photometric light curves of NSV 26083 in both (*a*) the *R* band and (*b*) the *I* band.

from the Brackett line flux of the near-IR spectrum; and the *V* magnitude determined by Tylenda et al. (1991a) for the cool stellar component of HB 12 is 13.6. If these results are adopted, the absolute visual magnitude M_v of the central star of HB 12 is 0.98. Suppose that the primary component has a mass of 0.6 $M_\odot$ and $M_v = 0.98$ at an effective temperature of 31,800 K (Zhang & Kwok 1993). The corresponding radius of the primary is estimated to be $R_1 = 0.19\ R_\odot$.

5. THE SPECTRA OF NSV 26083

In order to examine the nature of the putative binary companion of NSV 26083, we have initiated a project of spectrographic measurements at the NAOC using the 2.16 m telescope. Figure 5 shows the low-resolution spectrum of NSV 26083 taken on 2004 August 8, which apparently indicates various emission lines characteristic of a photoionized medium. The profiles of Hα and Hβ are broader than other emission lines, which here is most likely attributed to effects of Rayleigh-Raman scatting (Arrieta & Torres-Peimbert 2003).

To search for further evidence on the possible binary origin of the nucleus of HB 12, we examine closely the spectra taken on 2005 September 26 for photospheric absorption features characteristic of a cool companion. The spectrum between 4150 and 4550 Å is shown in Figure 6*a* in an expanded scale. An apparent *G*-band feature characteristic of late-type stars is seen, and molecular CN λ4216 absorption can also be identified. Furthermore, absorption features due to the *s*-process elements such as Y and Sr are found in the spectrum, with Y II λ4178 and Sr I λ4607 being the primary features. The molecular $C^{13}C^{13}$ λ4752 is also seen in absorption in the spectrum, as shown in Figure 6*b*. The spectrum ranges from 5150 to 5600 Å, clearly indicating C_2 features at 5165 and 5585 Å, and is presented in Figure 6*c*. The Mg I triplet (5167, 5172, and 5183 Å) is also marginally seen in the spectrum.

The above-mentioned features seem to suggest the existence of a cool companion to the exciting source of HB 12 with a spectral type of G to early K. However, this introduces a discrepancy with our mass estimation based on the light curves, which give a spectral type of M. Note that an M dwarf in isolation cannot be detected at all at the distance of HB 12 of about 2.24 kpc (Cahn et al. 1992). This discrepancy cannot be reconciled unless additional physical processes are involved. The spectral change of the cool secondary here is most likely attributed to external heating of its upper atmosphere by the hot primary (Grauer & Bond 1983). Further investigations of this system based on high-resolution spectroscopic observations are highly needed to have this issued resolved, which may come with a more reliable determination of the spectral type of the secondary. However, this uncertainty with the spectral determination does not affect in any way our inference of the binary origin of the nucleus of HB 12 based on our photometric results.

6. SUMMARY

Based on time-series multiband photometric observations and low-resolution spectroscopy, our study of the physical nature of

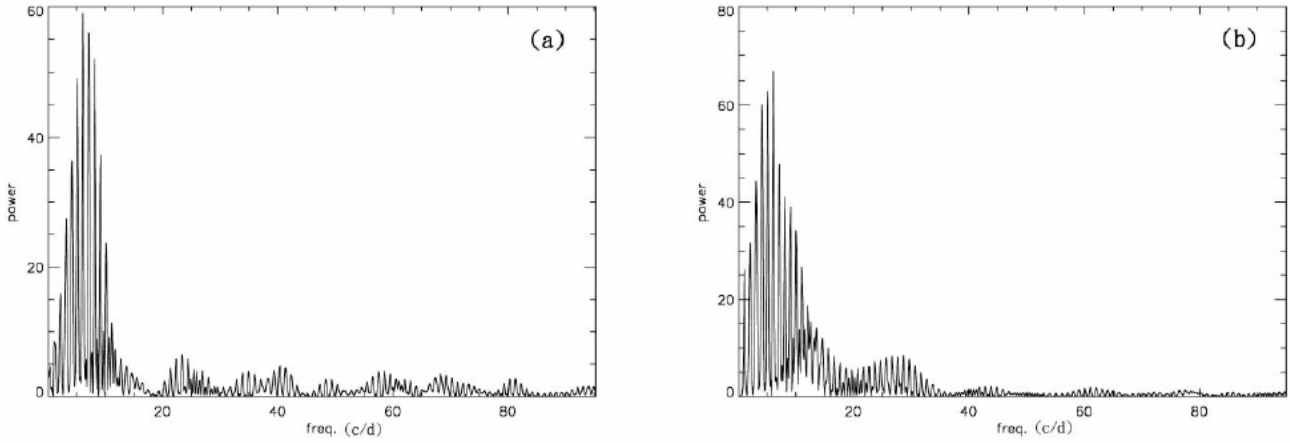

FIG. 3.—Power spectra of the time-series photometric data in both (*a*) *R* and (*b*) *I*.

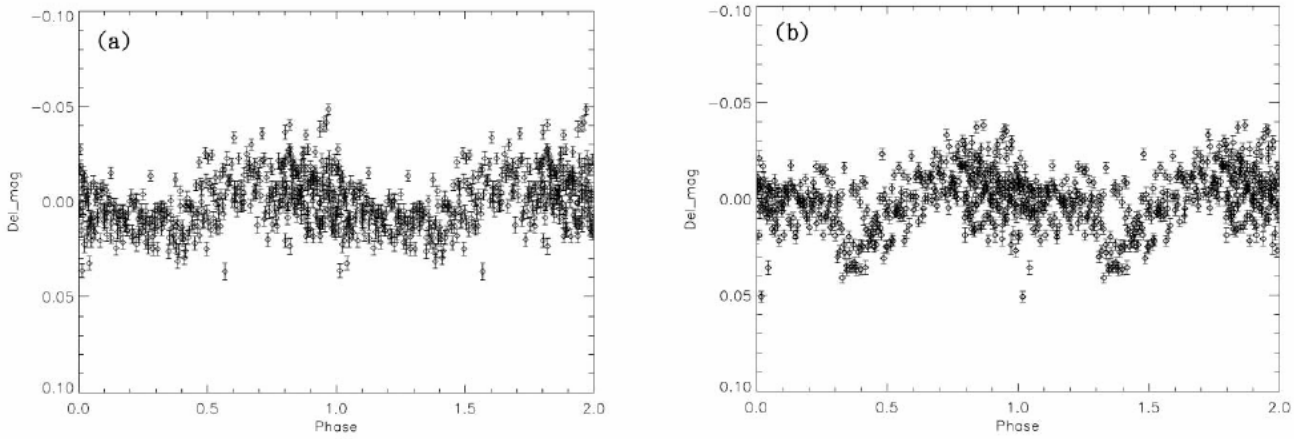

FIG. 4.—Phase diagrams of the photometric data in (*a*) *R* and (*b*) *I*. The periodic variations are believed to be due to the eclipsing binary nature of the central source. The average error of the phase bin is ±0.0074 mag for the *R* band and ±0.0046 mag for the *I* band.

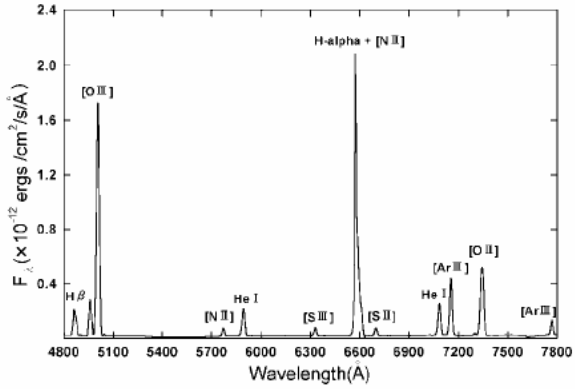

FIG. 5.—Spectrum of HB 12 in the wavelength range from 4800 to 7800 Å.

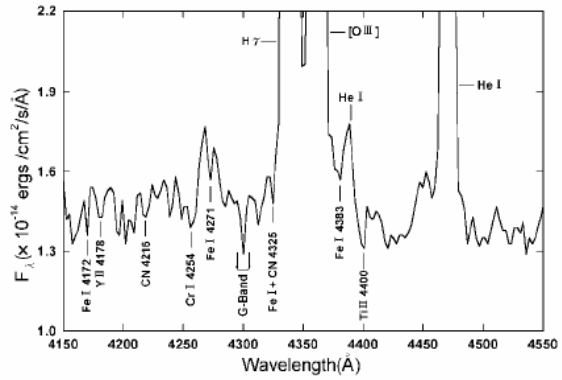

FIG. 6*a*

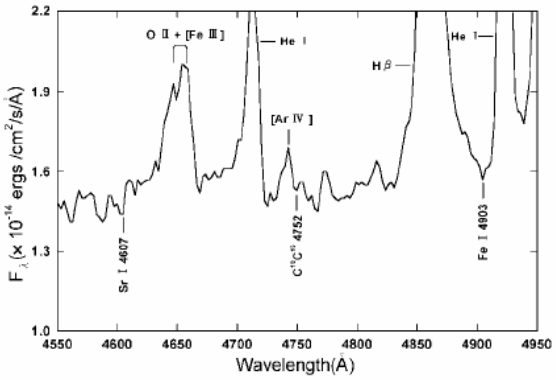

FIG. 6*b*

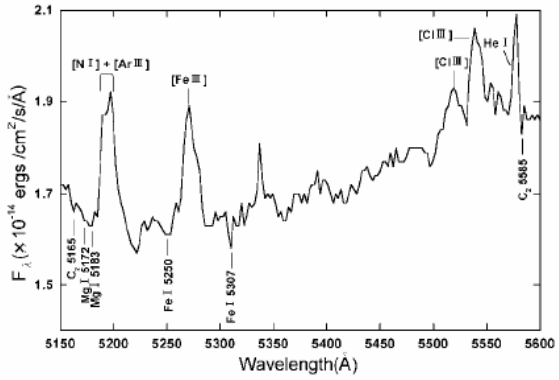

FIG. 6*c*

FIG. 6.—Enlarged spectrum of HB 12 in the ranges (*a*) 4150–4550 Å, (*b*) 4550–4950 Å, and (*c*) 5150–5600 Å.

the nucleus (NSV 26083) of the young PN HB 12 has led to the following results:

1. The central star is probably a close binary with an orbital period of 3.4 hr. This provides further support to the theory of a binary origin for bipolar PNe.

2. The difference in the *R* and *I* light curves is indicative of a reflection effect from the illuminated surface of the secondary.

3. Assuming a mass of 0.6 $M_\odot$ for the primary, upper limits to the mass and radius of the secondary star can be estimated to be $M_2 < 0.443\,M_\odot$ and $R_2 < 0.403\,R_\odot$, respectively. This results in an estimation of a physical separation of $\sim$1.163 $R_\odot$ of the close binary in association with NSV 26083. The hemisphere of the secondary can be suffering from reflection and heating effects from the hot primary. This thermal coupling may well lead to a spectral change of the secondary and deserves to be investigated in further detail.

We are grateful to the referee for useful comments, and Sun Kwok at the University of Hong Kong, Yi Chou at National Central University, and Yu-Lei Qiu, Jian-Yan Wei, and Jing-Yao Hu at the National Astronomical Observatory of the Chinese Academy of Sciences for useful discussions. This work was partially supported by the National Science Council of Taiwan under NSC 93-2752-M-008-001-PAE, NSC 93-2112-M-008-006, NSC 94-2752-M-008-001-PAE, and NSC 94-2112-M-008-002. Finally, we acknowledge funding from the National Natural Science Foundation of China through grant O611081001.

REFERENCES

Arrieta, A., & Torres-Peimbert, S. 2003, ApJS, 147, 97
Bignell, R. C. 1983, in Planetary Nebulae, ed. D. R. Flower (Dordrecht: Reidel), 69
Black, J. H., & van Dishoeck, E. F. 1987, ApJ, 322, 412
Bruch, A., Vaz, L. P. R., & Diaz, M. P. 2001, A&A, 377, 898
Cahn, J., Kaler, J. B., & Stanghellini, L. 1992, A&AS, 94, 399
Chen, A., O'Donoghue, D., Stobie, R. S., Kilkenny, D., Roberts, G., & van Wyk, F. 1995, MNRAS, 275, 100
De Marco, O., Bond, H. E., Harmer, D., & Fleming, A. J. 2004, ApJ, 602, L93
Dinerstein, H. L., Lester, D. F., Carr, J. S., & Harvey, P. M. 1988, ApJ, 327, L27
Garcia-Segura, G., Franco, J., & López, J. A. 2000, in ASP Conf. Ser. 199, Asymmetrical Planetary Nebulae II: From Origins to Microstructures, ed. J. H. Kastner, N. Soker, & S. Rappaport (San Francisco: ASP), 235
Garcia-Segura, G., Langer, N., Rózyczka, M., & Franco, J. 1999, ApJ, 517, 767
Grauer, A. D., & Bond, H. E. 1983, ApJ, 271, 259

Heap, S. R., & Augensen, H. J. 1987, ApJ, 313, 268
Hillwig, T. 2004, in ASP Conf. Ser. 313, Asymmetrical Planetary Nebulae III: Winds, Structure, and the Thunderbird, ed. M. Meixner et al. (San Francisco: ASP), 529
Hora, J. L., & Latter, W. B. 1996, ApJ, 461, 288
Hora, J. L., Latter, W. B., Dayal, A., Bieging, J., Kelly, D. M., Tielens, A. G. G. M., & Trammell, S. R. 2000, in ASP Conf. Ser. 199, Asymmetrical Planetary Nebulae II: From Origins to Microstructures, ed. J. H. Kastner, N. Soker, & S. Rappaport (San Francisco: ASP), 267
Kastner, J. H., & Weintraub, D. A. 1994, ApJ, 434, 719
Kwok, S., Hrivnak, B. J., Zhang, C. Y., & Langill, P. L. 2000, ApJ, 544, L149
Miranda, L. F., & Solf, J. 1989, A&A, 214, 353
Morris, M. 1990, in From Miras to Planetary Nebulae: Which Path for Stellar Evolution?, ed. M. O. Mennessier & A. Omont (Gif-sur-Yvette: Editions Frontières), 520
Paczyński, B. 1981, Acta Astron., 31, 1
Rappaport, S., Joss, P. C., & Webbink, R. F. 1982, ApJ, 254, 616
Reid, A. H. N., et al. 1993, ApJ, 417, 320
Schönberner, D. 1981, A&A, 103, 119
Soker, N. 1997, ApJS, 112, 487
———. 2000, in ASP Conf. Ser. 199, Asymmetrical Planetary Nebulae II: From Origins to Microstructures, ed. J. H. Kastner, N. Soker, & S. Rappaport (San Francisco: ASP), 71
Soker, N., Rappaport, S., & Harpaz, A. 1998, ApJ, 496, 833
Sorensen, P., & Pollacco, D. 2004, in ASP Conf. Ser. 313, Asymmetrical Planetary Nebulae III: Winds, Structure, and the Thunderbird, ed. M. Meixner et al. (San Francisco: ASP), 515
Stasińska, G., Górny, S. K., & Tylenda, R. 1997, A&A, 327, 736
Stellingwerf, R. F. 1978, ApJ, 224, 953
Tylenda, R., Acker, A., Raytchev, B., Stenholm, B., & Gleizes, F. 1991a, A&AS, 89, 77
Tylenda, R., Stasińska, G., Acker, A., & Stenholm, B. 1991b, A&A, 246, 221
Weidemann, V. 1989, A&A, 213, 155
Welch, C. A., Frank, A., Pipher, J. L., Forrest, W. J., & Woodward, C. E. 1999, ApJ, 522, L69
Zhang, C. Y., & Kwok, S. 1993, ApJS, 88, 137
Zuckerman, B., & Aller, L. H. 1986, ApJ, 301, 772

GROUND-BASED OBSERVATION OF ASTEROID SAMPLE RETURN MISSION TARGET. S. Nishihara[1,2], M. Abe[1], K. Kitazato[1, 2], Y. Sarugaku[1,2], D. Kuroda[3], S. Hasegawa[1], and D. Kinoshita[4]. [1]Institute of Space and Astronautical Science, Japan Aerospace Exploration Agency, 3-1-1 Yoshinodai, Sagamihara, Kanagawa 229-8501, Japan (nisihara@planeta.sci.isas.jaxa.jp), [2]Graduate School of Science, The University of Tokyo, [3]Department of Space and Astronautical Science, The Graduate University for Advanced Studies, [4] Institute of Astronomy, National Central University.

Introduction: One of the important goals in the study of compositional characterization of asteroids is to understand the relationship between asteroids and meteorites. The asteroids are classified into some groups with similar spectral characteristics. The Japanese sample return mission, HAYABUSA, the spacecraft arrived at its exploration target, near Earth asteroid (25143) Itokawa this fall. The taxonomic type of Itokawa is S-type, and the spectrum of this type asteroid is similar to that of the ordinary chondrites[1].

The purpose of our observation is to obtain the information about taxonomic type and rotational status of the candidate target of the next asteroid sample return mission (post-HAYABUSA mission). This information is useful for mission targets selection and helpful for raising the technical feasibility of the exploration. Our goal is to find some primordial type asteroid, C-type and D-type, in our candidate objects. Considering several mission plans, we chose 287 asteroids from about 3700 NEAs as the candidate objects of the post-HAYABUSA mission. As the taxonomic types of 238 candidates are unknown, we have performed the colorimetric observations in order to obtain its taxonomic type information.

Observations and Data reductions: We have observed 23 near-Earth asteroids (NEAs) during 2003-2005, using the 1.05-m Kiso Schmidt telescope with 2kCCD in Japan, and the Lulin One-meter Telescope with PI1300B or AP8 in Taiwan. The observational log is summarized in Table 1. We made multicolor photometry at clear-stable nights, using broadband filter, B, V, R, and I. Figure 1 is the transmission characteristics of each filters. As the filter systems of each observatory are slightly different, we have to convert our result from each instrumental system into the standard system, in order to compare them with those obtained at other instrumental system. For this purpose, we observed some standard stars listed in [2] Landolt (1992) for each photometric night. We define the transformation equations as

$$V = a_v v - b_v X - c_v r + d_v$$
$$B = a_b b - b_b X - c_b V + d_b$$
$$R = a_r r - b_r X - c_r V + d_r$$
$$I = a_i i - b_i X - c_i V + d_i$$

where *V, B, R, I* are the standard magnitudes, *v, b, r, I* are the instrumental magnitudes, a_{band}, b_{band}, c_{band}, d_{band} are the transmission coefficients.

Since the brightness of the asteroid changes with its spin rotation, we set the observation sequence as R-V-R-I-R-B-R in order to ensure color difference even where the brightness was changed. Furthermore, in some cases, we obtained the information of its spin status from the R-band lightcurves. Figure 2 is the example of (11284) Belenus taken on 2005 Nov. 25 at Lulin Observatory.

Classification: Our objects were classified by comparing with ECAS dataset[3] and SMASS dataset[4][5]. Only from our BVRI color information, we could not judge the delicate characteristics of asteroidal type. We classified our objects in broad groups, C-group, S-group, D-group, and X-group. We obtained BVRI photometry data for 15 mission candidates, and classified 14 objects in broad groups. Out of 14 candidates, 4 had previous classification, and 2 of them had also spectrum data[6][7].

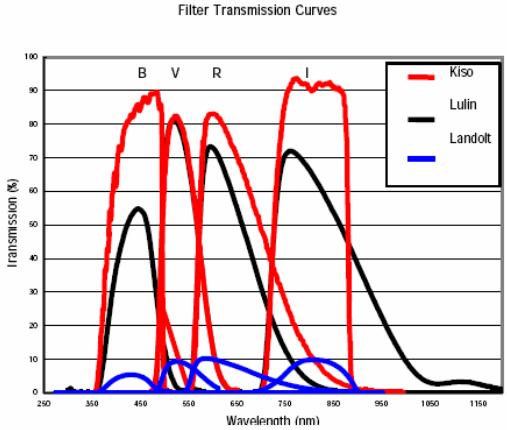

Figure 1: Filter transmission curve. The horizontal axis shows the wavelength[nm], the vertical axis gives transmission[%]. The red, black, blue lines are filter set of Kiso Observatory, Lulin Observatory, Landolt standard system, respectively.

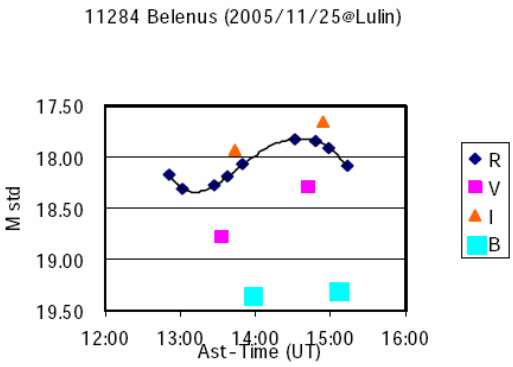

Figure 2: Observed magnitude of (11284) Belenus. The horizontal axis shows the Time (UT) in consideration of 1-way light time from the asteroid to the earth, the vertical axis gives magnitude converted to standard system. The solid line was fitted by polynomial approximation.

References: [1] Abe et al. (2002) Lunar & Planetary Science XXXIII, abstract #1666. [2] Landolt, A. U. (1992) AJ, 104, 340-371. [3] Tholen, D. J. (1984) Ph.D. thesis. [4] Bus, S. J., Binzel R. P. (2002) Icarus, 158, 146-177. [5] Binzel et al. (2004) Icarus, 170, 259-294. [6] Binzel et al. (2001) Icarus, 151, 139-149. [7] Wisniewski, W. Z. (1991) Icarus, 90, 117-122.

Table 1: Observation log. Observatory mark L: Lulin Observatory in Taiwan, K: Kiso Observatory in Japan, U: University of Hawaii 2.24-m telescope in Hawaii.

Asteroid	Date Observed (observatory)	Filter used
3361 Orpheus	2005/10/24 (K), 2005/11/28 (L)	BVRI
11284 Belenus	2005/11/25,26,27 (L)	BVRI
65803 Didymos	2003/12/1,3,4 (K), 2004/1/20 (K)	BVRI
85585 Mjolnir	2003/9/28,29,30 (K)	BVRI
98943 2001CC21	2003/9/29 (K), 2003/12/2 (K)	RVI
1989UQ	2003/926,29,30 (K)	BVRI
1999XO141	2005/8/31 (L), 2005/9/11 (L)	R
1999YB	2005/11/25,26,27 (L)	BVRI
2000QK25	2005/11/25,28 (L)	BVRI
2001FC7	2003/9/26,29,30 (K)	BVRI
2001US16	2004/4/10,11,12 (K)	RVI
2002CD	2004/4/10,11,12) (K)	RVI
2002CE10	2003/9/26,28 (K)	R
2002RX211	2005/8/29 (K), 2005/9/11 (L), 2005/11/25,26 (L)	BVRI
2002UC20	2003/12/3,4 (K), 2005/11/26 (L)	BVRI
2003AM31	2003/5/4 (U)	BVRI
2003CY18	2005/6/3 (K), 2005/9/11 (L), 2005/10/24 (K)	BVRI
2003RB	2003/9/28,29,30 (K)	BVRI
2003SD220	2003/12/1,2,3 (K)	BVRI
2004DK1	2004/4/11 (K)	RVI
2005ED318	2005/6/3 (K)	R
2005JU108	2005/8/29,31 (K)	R
2005TF	2005/11/28 (L)	BVRI

The Astrophysical Journal, 652:1390–1399, 2006 December 1

WHEN DO INTERNAL SHOCKS END AND EXTERNAL SHOCKS BEGIN? EARLY-TIME BROADBAND MODELING OF GRB 051111

N. R. Butler,[1,2] W. Li,[2] D. Perley,[2] K. Y. Huang,[3] Y. Urata,[4,5] J. X. Prochaska,[6] J. S. Bloom,[2] A. V. Filippenko,[2] R. J. Foley,[2] D. Kocevski,[2] H.-W. Chen,[7] Y. Qiu,[8] P. H. Kuo,[3] F. Y. Huang,[3] W. H. Ip,[3] T. Tamagawa,[4] K. Onda,[5] M. Tashiro,[5] K. Makishima,[4,9] S. Nishihara,[10] and Y. Sarugaku[10]

Received 2006 June 30; accepted 2006 August 15

ABSTRACT

Even with the renaissance in gamma-ray burst (GRB) research fostered by the *Swift* satellite, few bursts have both contemporaneous observations at long wavelengths and exquisite observations at later times across the electromagnetic spectrum. We present here contemporaneous imaging with the KAIT robotic optical telescope, dense optical sampling with Lulin, supplemented with infrared data from PAIRITEL and radio to gamma-ray data from the literature. For the first time, we can test the constancy of microphysical parameters in the internal-external shock paradigm and carefully trace the flow of energy from the GRB to the surrounding medium. KAIT data taken $\lesssim$1 minute after the start of GRB 051111 and coinciding with the fading gamma-ray tail of the prompt emission indicate a smooth reinjection of energy into the shock. No color change is apparent in observations beginning $\sim$1.5 minutes after the GRB and lasting for the first hour after the burst. There are achromatic flux modulations about the best-fit model at late ($t \approx 10^4$ s) times, possibly due to variations in the external density. We find that the host galaxy extinction is well fit by a curve similar to that of the Small Magellanic Cloud. Low visual extinction, $A_V \approx 0.2$ mag, combined with high column densities determined from the X-ray and optical spectroscopy ($N_{\rm H} > 10^{21}$ cm^{-2}), indicate a low dust-to-metals ratio and a possible overabundance of the light metals. An apparent small ratio of total to selective extinction ($R_V \approx 2$) argues against dust destruction by the GRB. Time constancy of both the IR/optical/UV spectral energy distribution and the soft X-ray absorption suggests that the absorbing material is not local to the GRB.

Subject headings: gamma rays: bursts — supernovae: general — telescopes — X-rays: general

Online material: color figures

1. INTRODUCTION

The *Swift* gamma-ray burst (GRB) satellite (Gehrels et al. 2004) continues to unleash a torrent of finely time- and energy-sampled photons arising from the bursts and their impact on the surrounding medium (i.e., the GRB afterglows). The X-ray Telescope (XRT) provides detailed light curves for 1–2 bursts and burst afterglows per week, allowing us to routinely view the practically uncharted first 100 s to $\sim$1 day in the life of a GRB. In the X-ray data, we see complex phenomena: unexpected rapid decays, sometimes temporally flat and apparently reenergized afterglows, and massive X-ray flares (see, e.g., Nousek et al. 2006). Unfortunately, it has proven very challenging to complement these data with an early and rapid-cadence data set at longer wavelengths. Because studies of GRB afterglows prior to *Swift* rely primarily on observations in the optical and longer wavelengths, and mostly at later times, contemporaneous observations are critical for connecting newfound insights to the large body of previous work. Correlated, broadband observations of events that exhibit extremely energetic broadband emission from the radio to the gamma ray (e.g., Fig. 1) allow us to study and potentially understand the new phenomenology and to pose answers to numerous open questions.

Optical observation of GRBs in the prompt phase and shortly thereafter are extremely rare. Of $\sim$50 optical afterglows detected prior to *Swift*, only one (GRB 990123; Akerlof et al. 1999) was detected during the prompt phase, and only a handful were detected in the first 10 minutes of the afterglow: GRB 021004 (Fox et al. 2003b), GRB 021211 (Fox et al. 2003a; Li et al. 2003a; Vestrand et al. 2004), and GRB 030418 (Rykoff et al. 2004). In the *Swift* era, the rate of early detections has jumped dramatically, thanks to rapidly communicated and tight GRB localizations from *Swift* and also due to the maturing system of ground-based robotic telescopes (e.g., $\sim$15 early detections by Robotic Optical Transient Search Experiment [ROTSE][11] alone). The Ultraviolet and Optical Telescope (UVOT) on *Swift* has the potential to match this performance, particularly with a recent prioritization of early unfiltered observations of the very red afterglows. Perhaps most impressive, the RAPTOR experiment has detected two GRBs during the prompt phase: GRB 041219 (Vestrand et al. 2005) and GRB 050820A (Vestrand et al. 2006). The prompt and contemporaneous long-wavelength emission of GRB 041219A was actually discovered at infrared (IR) wavelengths (Blake et al. 2005) with the Peters Automated Infrared Imaging Telescope (PAIRITEL; Bloom et al. 2006). Even though

[1] Townes Fellow, Space Sciences Laboratory, University of California, 7 Gauss Way, Berkeley, CA 94720-7450.
[2] Astronomy Department, University of California, 445 Campbell Hall, Berkeley, CA 94720-3411.
[3] Institute of Astronomy, National Central University, Chung-Li 32054, Taiwan.
[4] RIKEN (Institute of Physical and Chemical Research), 2-1 Hirosawa, Wako, Saitama 351-0198, Japan.
[5] Department of Physics, Saitama University, Shimo-Okubo, Sakura, Saitama 338-8570, Japan.
[6] Department of Astronomy and Astrophysics, University of California, Santa Cruz, CA 95064.
[7] Department of Astronomy and Astrophysics, University of Chicago, 5640 South Ellis Avenue, Chicago, IL 60637.
[8] National Astronomical Observatories, Chinese Academy of Sciences, Beijing 100012, China.
[9] Department of Physics, University of Tokyo, 7-3-1 Hongo, Bunkyo-ku, Tokyo 113-0033, Japan.
[10] Institute of Space and Astronautical Science, Japan Aerospace Exploration Agency, 3-1-1 Yoshinodai, Sagamihara, Kanagawa 229-8510, Japan.

[11] See http://www.rotse.net.

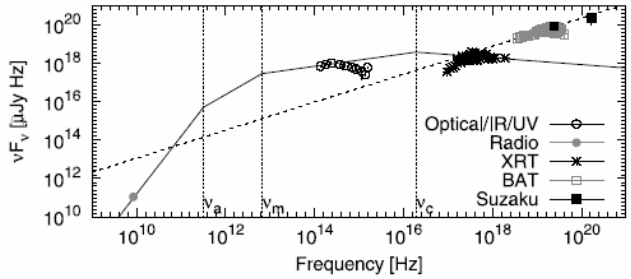

FIG. 1.—Broadband model overview, with data shown at $t = 100$ s. The afterglow data in the radio, optical, IR, UV, and X-ray are well fit by a external shock expanding into a uniform-density medium and emitting synchrotron radiation (§§ 4.1 and 4.3). The optical and X-ray data drop away from the model curve at high and low energies, respectively, due to an appreciable amount of absorption by dust and metals, respectively. Also shown are the prompt gamma-ray spectra from *Swift* BAT and *Suzaku* WAM. [*See the electronic edition of the Journal for a color version of this figure.*]

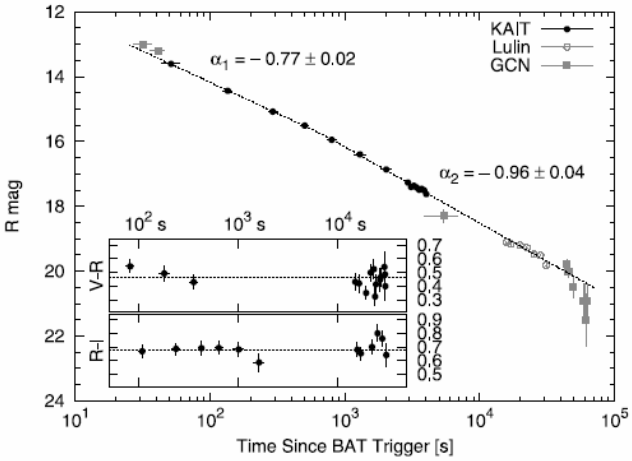

FIG. 2.—The R-band light curve and $(V - R)$, $(R - I)$ colors from KAIT and Lulin. The best-fit temporal decay indices (α) for the source flux are also shown. The unfiltered and R-band data are from the GCN (Garimella et al. 2005; Milne et al. 2005; Nanni et al. 2005; Rujopakarn et al. 2005; Rykoff et al. 2005; Sharapov et al. 2005; Smith et al. 2005). [*See the electronic edition of the Journal for a color version of this figure.*]

the Galactic extinction toward the GRB was large, GRB 041219A is the only prior burst with prompt, long-wavelength observations at multiple frequencies.

Here we present observations of GRB 051111 conducted with the robotic 0.76 m Katzman Automatic Imaging Telescope (KAIT; Filippenko et al. 2001; Li et al. 2003b, 2003a), beginning with an unfiltered exposure 43.7 s after the GRB trigger from the Burst Alert Telescope (BAT) on *Swift* and just catching the tail of the prompt emission. We obtained color information in the form of V- and I-band observations beginning just 73.7 s after the trigger. Supplemented with B-, V-, R-, and I-band observations with the Lulin One-meter Telescope; J-, H-, and K_s-band observations with PAIRITEL taken hours after the burst; and with other observations reported in the literature, we present an unrivaled and impressive broadband view of this afterglow and its early evolution.

The study of the early emission during and following a GRB is a critical step toward understanding the origin of the emission and the nature of the surrounding medium. It is widely accepted that GRBs are produced by a self-interacting relativistic outflow ("internal shocks," e.g., Fenimore et al. 1996) that heats and shocks the surrounding medium ("external shocks") to form a long-lasting afterglow at longer wavelengths (Mészáros & Rees 1997; Sari & Piran 1999). Transient emission from a "reverse shock," which propagates backward toward the central engine in the shock frame, can also be produced. Despite an early indication to the contrary from GRB 990123 (e.g., Akerlof et al. 1999), the reverse shock does not appear to be a common feature in the early optical data (see also McMahon et al. 2006). Primarily due to the larger physical size, the external shocks are expected to generate smoother light curves, and the ~10% of GRBs with smooth time histories may require only external shocks (e.g., McMahon et al. 2004).

However, the growing sample of early afterglow observations militates against such a simple interpretation. As mentioned above, the X-ray data (and also some optical data; e.g., Fox et al. 2003b; Wozniak et al. 2005) evidence shock refreshment (Rees & Mészáros 1998; Sari & Mészáros 2000; Ramirez-Ruiz et al. 2001) or continued central engine activity (Rees & Mészáros 2000; MacFadyen et al. 2001; Ramirez-Ruiz 2004; Lee & Ramirez-Ruiz 2002), which can persist for several hundred seconds or longer (e.g., Nousek et al. 2006). While its physical size is still small compared to the timescale for synchrotron cooling, the external shock can cool rapidly. Energy can be efficiently radiated from the shock at this stage (e.g., Sari et al. 1998), prior to the onset of an adiabatic evolution. Depending on the breadth of the shock shell, which depends on the duration of the period of internal shock generation, the internal shock emission can overlap with the external shock emission. Below, we use the exquisitely sampled data for GRB 051111 to disentangle the early-time emission components and also to study the dust and gas properties of the host galaxy.

2. OBSERVATIONS AND DATA REDUCTION

At 05:59:41.4 UT, *Swift* BAT triggered and localized GRB 051111 (Sakamoto et al. 2005). The 3′ radius error region from BAT enabled the rapid detection of a new optical source only 26.9 s after the trigger (Rujopakarn et al. 2005), while the burst was still in progress. A barrage of detections in the optical, UV, IR, radio, and X-ray bands followed. Figure 2 shows a snapshot of the full data set, interpolated via the modeling below to $t = 100$ s.

2.1. *Gamma- and X-Ray*

We downloaded the *Swift* BAT gamma-ray data from the *Swift* Archive.[12] The energy scale and mask weighting were established by running the `bateconvert` and `batmaskwtevt` tasks from HEAsoft 6.0.6. Spectra and light curves were extracted with the `batbinevt` task, and response matrices were produced by running `batdrmgen`. We applied the systematic error corrections to the low-energy BAT spectral data, as suggested by the BAT Digest Web site,[13] and fit the data using ISIS.[14]

The *Swift* XRT X-ray data from five follow-up observations of the GRB 051111 field were downloaded from the *Swift* Archive and reduced by running version 0.10.3 of the `xrtpipeline` reduction script from the HEAsoft 6.0.6[15] software release. From there, we bin the data in time, exclude pileup chip regions for each time interval, account for lost flux due to bad pixels, and produce spectra using custom IDL scripts (e.g., Butler 2006). The data cover the time range from 5.56 to 405.29 ks after the burst, with a total exposure (livetime) of 51.98 ks. Spectral response files are generated using the `xrtmkarf` task and the latest calibration

[12] See ftp://legacy.gsfc.nasa.gov/swift/data.
[13] See http://swift.gsfc.nasa.gov/docs/swift/analysis/bat_digest.html.
[14] See http://space.mit.edu/CXC/ISIS/.
[15] See http://heasarc.gsfc.nasa.gov/docs/software/lheasoft/.

TABLE 1
KAIT Photometry of GRB 051111

t (s)	Exposure (s)	Magnitude	σ_{Mag}	Band
43.7	15	13.60	0.02	R
73.7	15	14.54	0.02	V
99.7	15	13.57	0.02	I
124.7	20	14.43	0.02	R
156.7	45	15.16	0.03	V
212.7	45	14.21	0.02	I
268.7	45	15.08	0.02	R
324.7	60	15.66	0.02	V
395.7	60	14.69	0.02	I
470.7	60	15.51	0.02	R
578.7	120	15.04	0.02	I
734.7	120	15.94	0.02	R
892.7	240	15.49	0.02	I
1167.7	240	16.40	0.03	R
1448.7	360	16.05	0.03	I
1843.7	360	16.86	0.03	R
2873.7	120	17.27	0.05	R
3026.7	120	17.40	0.06	R
3178.7	120	17.36	0.05	R
3330.7	120	17.41	0.06	R
3486.7	120	17.49	0.06	R
3639.7	120	17.46	0.07	R
3791.7	120	17.51	0.06	R
3944.7	120	17.62	0.07	R

Notes.—The R-band magnitudes are determined for unfiltered observations (§ 2). We denote with t the elapsed time since the BAT trigger.

TABLE 2
Lulin Photometry of GRB 051111

t (hr)	Exposure (s)	Magnitude	σ_{Mag}	Band
4.2201	300	19.52	0.05	V
4.3154	300	19.12	0.04	R
4.4107	300	18.45	0.04	I
4.5071	300	20.38	0.07	B
4.6021	300	19.56	0.05	V
4.6974	300	19.15	0.03	R
4.8012	300	18.51	0.04	I
4.9154	300	20.30	0.07	B
5.0085	300	20.37	0.08	B
5.1018	300	20.25	0.07	B
5.3204	300	20.32	0.07	B
5.4157	300	19.54	0.04	V
5.5110	300	19.20	0.03	R
6.0479	300	19.76	0.05	V
6.1435	300	19.27	0.04	R
6.2387	300	18.59	0.04	I
6.4037	300	20.55	0.06	B
6.4990	300	19.89	0.06	V
6.6893	300	19.73	0.05	V
6.7846	300	20.88	0.08	B
6.8796	300	19.86	0.05	V
6.9813	300	19.47	0.05	R
7.0762	300	18.68	0.03	I
7.1799	300	20.86	0.08	B
7.2729	300	20.73	0.10	B
7.3662	300	20.88	0.10	B
7.5546	300	19.94	0.07	V
7.6479	300	19.96	0.05	V
7.7926	300	19.50	0.03	R
7.8879	300	18.78	0.04	I
8.0488	300	20.72	0.08	B
8.1421	300	21.01	0.14	B
8.2365	300	21.03	0.14	B
8.3318	300	20.25	0.10	V
8.4257	300	20.23	0.08	V
8.5193	300	20.18	0.08	V
8.6235	300	19.82	0.06	R
8.7190	300	19.21	0.06	I

Note.—We denote with t the elapsed time since the BAT trigger.

database (CALDB) files (ver. 8, 2006 April 27). The spectra are modeled using ISIS. For each spectral bin, we require a signal-to-noise ratio (S/N) of 3.5. We define S/N as the background-subtracted number of counts divided by the square root of the sum of the signal counts and the variance in the background. We define the background region as that where the number of counts in an aperture the size of the source extraction region is within 2 σ of the median background over the chip in that aperture for one contiguous follow-up observation. For the Photon Count (PC) mode data, the source aperture is a circle of radius 16 pixels.

2.2. *Optical*

The robotic 0.76 m KAIT (Filippenko et al. 2001; Li et al. 2003b, 2003a) at Lick Observatory observed GRB 051111 in a series of images automatically obtained starting at 05:60:25.2 UT (43.7 s after the BAT trigger; Li et al. 2005). The sequence includes a combination of images taken with the V and I filters, as well as some that are unfiltered (Table 1). The optical transient first identified by Rujopakarn et al. (2005) at $\alpha = 23^{h}12^{m}33\overset{s}{.}2$, $\delta = +18°22'29\overset{''}{.}1$ (J2000.0) was clearly detected in each exposure. We began B-, V-, R-, and I-band imaging (Huang et al. 2005a) of the GRB 051111 afterglow using the Lulin One-meter Telescope (Huang et al. 2005b; Urata et al. 2005) at 10:07 UT. We detected the optical afterglow clearly in each band until observations ceased at 14:42:06 UT (Table 2).

We find that the combination of the KAIT optics and the quantum efficiency of the Apogee CCD camera makes the KAIT unfiltered observations mostly mimic the R band. We determine a small color correction (Li et al. 2003b, 2003a; Riess et al. 1999) between the unfiltered and R-band photometry of 0.11 ± 0.02 mag using the $(V - R)$ and $(R - I)$ color information from the Lulin observations.

We use point-spread function (PSF) fitting through the IDL DAOPHOT[16] package to reduce our data. Only unsaturated and spherically symmetric sources within a given CCD exposure are used to model the stellar PSF for that exposure. The absolute photometric calibration for KAIT is determined using more than 10 Landolt (1992) fields observed on November 24 UT at a range of air masses. The Lulin photometry is calibrated using Landolt (1992) fields PG 0231+051, SA 92, and SA 97, and also cross-checked using the KAIT standard star observations.

2.3. *Near-IR and UV*

After initially poor transmission conditions (i.e., clouds) at Mount Hopkins, we obtained a total imaging exposure of 188 s on the field of GRB 051111 before hitting a telescope limit. In simultaneous observations with PAIRITEL (Bloom et al. 2006) we measure magnitudes of the Rujopakarn et al. (2005) transient of $J = 16.55 \pm 0.03$, $H = 15.85 \pm 0.04$, and $K_s = 15.29 \pm 0.06$ (Bloom et al. 2005), relative to the Two Micron All Sky Survey

[16] See http://idlastro.gsfc.nasa.gov.

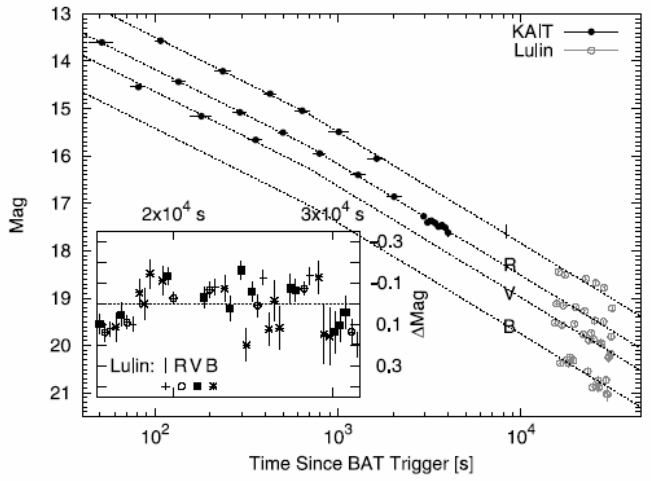

FIG. 3.—Multicolor light curve of GRB 051111 from KAIT and Lulin. The fit residuals for the Lulin data are plotted in the inset. [*See the electronic edition of the Journal for a color version of this figure.*]

(2MASS). The data were taken from 07:23:29 to 07:28:26 UT, centered 1.44 hr after the BAT trigger.

We refine the *Swift* UVOT photometry (Poole et al. 2005) in the *V*, *B*, and *U* bands by employing a tight extraction region in order to maximize the S/N (see Li et al. 2006). We find $V = 19.38 \pm 0.15$ ($t = 16,298$–$17,198$ s post BAT trigger), $B = 20.04 \pm 0.10$ ($t = 11,237$–$12,136$ s post BAT trigger), and $U = 19.81 \pm 0.12$ ($t = 10,329$–$11,229$ s post BAT trigger). These numbers are consistent with those of Poole et al. (2005) but with considerably smaller error bars. We extrapolate the Galactic extinction curve (Schlegel et al. 1998) into the UV in order to perform the fitting for the UVW1, UVM2, and UVW2 bands below.

3. FITS TO THE DATA

3.1. *Optical Light Curve and Lack of Color Change*

As shown in Figure 2, the KAIT *R*-band data are well fit by a broken power law with $t_{\rm br} = (700 \pm 260)$ s ($\chi^2/\nu = 5.61/11$). The best-fit flux decay indices are shown in Figure 2. The fit is statistically unacceptable without the break ($\chi^2/\nu = 65.15/13$, $\alpha = 0.83 \pm 0.01$). Including the Lulin *R*-band data in the fit, the model parameters do not change, but the fit quality degrades ($\chi^2/\nu = 38.9/20$). Similar fit qualities are found for the data in the *B*, *V*, and *I* bands by applying magnitude offsets to the best-fit *R*-band model ($\chi^2/\nu = 27.0/11$, 54.1/13, and 64.0/10, respectively). From the fits, we derive the following afterglow colors: $(B - R) = 0.97 \pm 0.02$, $(V - R) = 0.37 \pm 0.01$, and $(R - I) = 0.80 \pm 0.01$ mag, corrected for Galactic extinction (Schlegel et al. 1998).

The $(R - I)$ and $(V - R)$ colors, without the Galactic extinction correction, are plotted in the insets of Figure 2, and the multiband data are plotted in Figure 3, along with the fits. The KAIT and Lulin data are consistent with no color evolution, and the light-curve break is most likely achromatic. From the $(V - I)$ colors before and after the break, we derive a change in the spectral index $\delta\beta < 0.38$ (3 σ). Figure 3 displays another interesting characteristic of the data: there are strong residuals in the Lulin data with $\delta t/t \approx 0.1$ relative to the broken power-law fit, and these are correlated across spectral bands.

As we discuss further below, the PAIRITEL data, as well as the available data from the Gamma-ray bursts Coordinates Network (GCN) in the optical and UV, are consistent with the broken power-law decay, modified by dust absorption.

3.2. *Gamma- and X-Ray*

The BAT gamma-ray light curve exhibits a characteristic FRED-like ("fast rise exponential decline") time decay, with duration $T_{90} \approx 30$ s. From a wavelet analysis, we determine the start of the burst as 7.17 s prior to the BAT trigger (Fig. 6). From this point onward, we use this time as the beginning of the burst. This has the effect of increasing the initial optical decay index from 0.77 to 0.81 (Fig. 2) but does not affect any of the other results above. The 15–150 keV spectrum from the beginning of the burst to 40 s later is adequately fit by a power law with photon index $\Gamma = 1.27 \pm 0.05$ ($\chi^2/\nu = 53.65/51$). The model fluence in the 15–100 keV band is $(2.1 \pm 0.1) \times 10^{-6}$ ergs cm^{-2}. The fits are consistent with those reported by Sakamoto et al. (2005) and Krimm et al. (2005), where a modestly longer burst-time extraction region is applied.

There is a significant amount of spectral evolution, comparing the time prior to burst peak to the time postpeak. For the burst rise from 0 to 10 s, we find $\Gamma_1 = 1.11 \pm 0.07$ and $F_{15\ \rm keV} = (0.48 \pm 0.04)$ mJy ($\chi^2/\nu = 49.35/51$). For the burst decline from 10 to 40 s, we find $\Gamma_2 = 1.38 \pm 0.08$ and $F_{15\ \rm keV} = (0.31 \pm 0.03)$ mJy ($\chi^2/\nu = 41.15/45$). The photon index for 20–40 s ($\Gamma_3 = 1.4 \pm 0.1$, $\chi^2/\nu = 29.28/31$) is consistent with the 10–40 s value, indicating that this value provides a reasonable characterization for the full decline phase. The burst was also observed by the *Suzaku* Wideband All-sky Monitor (WAM; Yamaoka et al. 2006) and found to have a similar time profile as that from *Swift*, a consistent time-integrated spectral slope ($\Gamma = 1.5 \pm 0.3$), and a fluence in the 100–700 keV band of $(8.4 \pm 0.8) \times 10^{-6}$ ergs cm^{-2} (Yamaoka et al. 2005). Combining the fluence determinations from *Swift* and *Suzaku*, we find a 15–700 keV fluence of $(1.05 \pm 0.08) \times 10^{-5}$ ergs cm^{-2}. Because the peak νF_ν energy for this burst has not been measured, the bolometric fluence could be substantially larger than the 15–700 keV fluence. Assuming that all the prompt photons have been accounted for, a lower limit on the isotropic equivalent energy emitted in the host frame at $z = 1.55$ (Hill et al. 2005) is $E_{\rm iso} = 6.2 \times 10^{52}$ ergs. Here and throughout, we assume a cosmology with $(h, \Omega_m, \Omega_\Lambda) = (0.71, 0.3, 0.7)$.

The X-ray light curve in the 0.3–10.0 keV band is reasonably well fit ($\chi^2/\nu = 38.7/32$) by a power-law model with $\alpha = -1.6 \pm 0.1$. The spectrum in the same band contains 573 counts and is well fit ($\chi^2/\nu = 43.61/36$) by an absorbed power law with photon index $\Gamma = 2.3 \pm 0.2$, absorbing column $N_{\rm H} = (1.8 \pm 0.4) \times 10^{21}$ cm^{-2}, and unabsorbed flux $(5.0 \pm 0.5) \times 10^{-13}$ ergs cm^{-2} s^{-1}, for the time period 5.56–405.29 ks after the GRB. We use the corresponding average spectral flux at 1 keV, $(6.6 \pm 0.9) \times 10^{-2}$ μJy, to translate the XRT count rate to microjanskys below. The absorption is greater than the inferred Galactic value in the source direction ($N_{\rm H,Gal} = 5 \times 10^{20}$ cm^{-2}; Dickey & Lockman 1990) at 4.1 σ significance ($\Delta\chi^2 = 16.48$, for 1 additional degree of freedom). At redshift $z = 1.55$ (Hill et al. 2005), the excess column is $(7 \pm 4) \times 10^{21}$ cm^{-2}, allowing for a 20% uncertainty in the Galactic column. We find no evidence for $\gtrsim 1$ σ significant emission lines in the spectrum. These fits are consistent with the preliminary fits reported by La Parola et al. (2005).

4. DISCUSSION

4.1. *Late-Time Broadband Afterglow Modeling*

After $t \approx 10^3$ s, the broadband afterglow data are well described by the external shock synchrotron model (Paczyński & Rhoads 1993; Katz 1994; Waxman 1997; Wijers et al. 1997). We do not attempt to model the slowly decaying, early optical

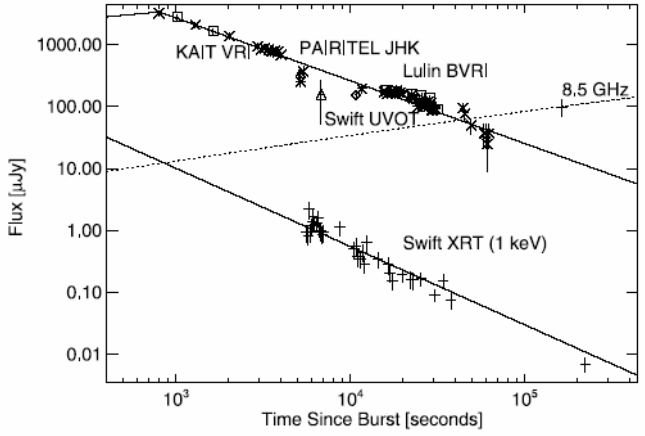

FIG. 4.—Data for $t \gtrsim 700$ s well fit by a synchrotron external shock model. The optical, UV, and IR data are scaled to R band using the best-fit synchrotron shock plus absorption model (Table 3; $A_{R,\rm obs} = 0.72$ mag; Fig. 5). All data include a 10% systematic error added in quadrature to the statistical error. The dip near 10^4 s is seen in the R-band data as well as in the UVOT data and the data from PAIRITEL (§ 4.2). We include the GCN data (Frail et al. 2005; Garimella et al. 2005; Milne et al. 2005; Nanni et al. 2005; Poole et al. 2005; Rujopakarn et al. 2005; Rykoff et al. 2005; Sharapov et al. 2005; Smith et al. 2005), in addition to the data from KAIT, PAIRITEL, Lulin, and *Swift*. All data are corrected for Galactic extinction (Schlegel et al. 1998).

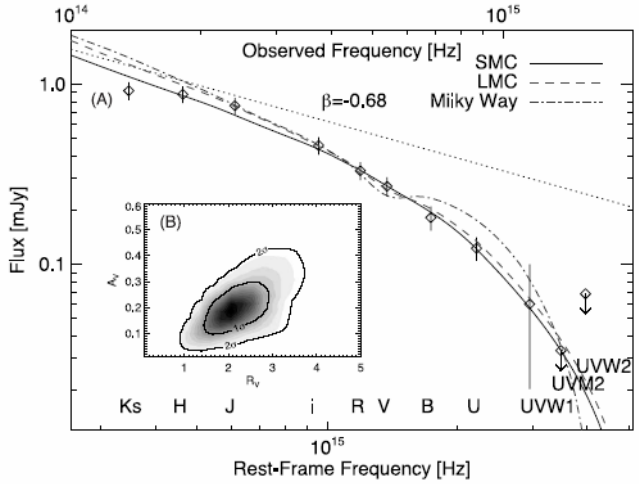

FIG. 5.—(*a*) SED for the optical, IR, and UV data interpolated to $t = 5200$ s after GRB 051111. All data are corrected for Galactic extinction (Schlegel et al. 1998). The dashed curve is a power law with (energy) index $\beta = -0.68$, the best-fit value found from the synchrotron shock modeling. The other curves represent fits of the empirical extinction models from Pei (1992) with the models labeled in the legend and discussed in § 4.2. (*b*) Posterior probability for A_V and R_V, using the Reichart (2001) model prior. The 1 and 2 σ confidence contours are overplotted. [*See the electronic edition of the Journal for a color version of this figure.*]

light curve or the achromatic (or nearly so) optical break discussed above, nor do we fit for the BAT data or the apparent fluctuations in the optical at $t \approx 6000$ s (Fig. 3) at this stage. These features are discussed below. Due to the fluctuations in the optical about the best-fit model at $t \sim 10^4$ s, we are also forced to add a 10% systematic uncertainty component in quadrature to the statistical uncertainty of each data point, in order to obtain an acceptable fit ($\chi^2/\nu = 118.1/103$, $t \geq 700$ s). Figure 4 shows the best-fit model, plotted over the radio, optical, UV, IR, and X-ray data at $t \geq 700$ s. In § 4.2, we describe the modeling of the host-frame extinction by dust, which has been taken into account (Fig. 5) in the figure so that the data in the optical, UV, and IR appear on one common curve.

Because the optical time decay is shallow and the X-ray decay is steep, we expect and observe the data to be well fit by a uniform density, interstellar medium (ISM) model. A model with $n \propto R^{-2}$, describing the expected density contours for a progenitor star with a significant wind, would exhibit a synchrotron cooling break frequency ν_c that increases in frequency with time (Chevalier & Li 2000). This leads to shallower decays at high versus low energy, opposite to the behavior of the ISM model. For the constant-density model, the optical and X-ray decay indices ($\alpha_{\rm opt} = -0.96 \pm 0.04$, $\alpha_{\rm X} = -1.6 \pm 0.1$) and the X-ray energy index ($\beta_{\rm X} = -1.3 \pm 0.2$) constrain the power-law index p describing the energy distribution of synchrotron-emitting electrons: $p = 2.35 \pm 0.05$ (e.g., Sari et al. 1998). In the best-fit model, the synchrotron cooling break lies between the optical and X-ray bands during the observation. The predicted value for the optical energy index is $\beta_{\rm opt} = -0.68 \pm 0.03$.

The model contains four additional free parameters (e.g., Sari et al. 1998): η_γ, ϵ_e, ϵ_B, and n, the efficiency factor relating the shock energy to the energy released in gamma rays, the fractions of equipartition energy going into the electrons and magnetic field B, and the density n, respectively. These are constrained by the three observed radio, optical, and X-ray fluxes and by the equation describing the time evolution of the synchrotron spectral peak frequency ν_m. If we assume that the peak in the synchrotron spectrum passes through the optical band at the same time the light curve breaks ($t \approx 700$ s), as might be expected if the early optical light curve is dominated by the internal shocks, then we derive the parameters listed in Table 3. As we describe below, the prebreak optical light curve may also be due to external shocks, in which case we only have an upper limit on the passage time $t_{m,\rm opt}$ for the synchrotron peak through the optical bands. Aside from ϵ_B, the model parameters are sensitive to (and roughly linearly proportional to) $t_{m,\rm opt}$ (Table 3).

4.2. *Optical/IR/UV Spectral Energy Distribution*

A tight constraint can be placed on the optical absorption considering only the observed optical/X-ray spectral flux ratio $F_{\nu=R,\rm obs}/F_{\nu=1\ \rm keV} = 467 \pm 2$, at $t = 2 \times 10^4$ s in the observer frame. Here, the X-ray flux is corrected for absorption. Allowing for the possibility that the synchrotron cooling break (ν_c) is between the observer-frame R band, $\nu_{R,\rm obs}$, and 1 keV in the observer frame, $\nu_{1\ \rm keV}$, the observed optical to X-ray flux is (e.g., Galama & Wijers 2001)

$$\frac{F_{\nu=R,\rm obs}}{F_{\nu=1\ \rm keV}} = \left(\frac{\nu_{1\ \rm keV}}{\nu_{R,\rm obs}}\right)^{1/2-\beta_{\rm opt}} \left(\frac{\nu_c}{\nu_{R,\rm obs}}\right)^{-1/2} 10^{-0.4 A_{R,\rm obs}}, \quad (1)$$

TABLE 3
BROADBAND FIT PARAMETERS FOR CONSTANT-DENSITY ISM

Parameter	Value
$E_{\gamma,\rm iso}$	6.2×10^{52} ergs (fixed)
$D_{\rm lum}$	3.46×10^{28} cm (fixed)
z	1.55 (fixed)
η_γ	$(2.1 \pm 0.3)[t_{m,\rm opt}/(700\ \rm s)]^{1.39 \pm 0.05}$
p	2.35 ± 0.05
ϵ_e	$(0.03 \pm 0.01)[t_{m,\rm opt}/(700\ \rm s)]^{1.12 \pm 0.05}$
ϵ_B	$(0.02 \pm 0.01)[t_{m,\rm opt}/(700\ \rm s)]^{-0.11 \pm 0.15}$
n	$(0.8 \pm 0.5)[t_{m,\rm opt}/(700\ \rm s)]^{0.86 \pm 0.12}$ cm^{-3}

NOTE.—The fit in Fig. 4 uses $t_{m,\rm opt} = 700$ s for the passage of the synchrotron peak frequency through the optical.

where $A_{R,\rm obs}$ is the absorption at R band in the observer frame. The constraint on $\beta_{\rm opt}$ derived above for the constant-density model leads to $A_{R,\rm obs} < 1.35$ mag. For the wind-density medium, there cannot be a spectral break due to the rapid X-ray versus optical light-curve decline, and we have $A_{R,\rm obs} = -6.8\beta_{\rm opt} - 6.7$. This relation can only be satisfied with positive absorption if $-\beta_{\rm opt} > 1$. This is just possible in the wind scenario for $\nu_c < \nu_{R,\rm obs}$, implying $p = 1.6 \pm 0.1$ (Chevalier & Li 2000) and $A_{R,\rm obs} < 0.1$ mag. The rest-frame extinction in the V band (i.e., 5556 Å), A_V, will be a factor of a few times smaller than this, depending on the extinction law.

Figure 5*a* displays extinction-law fits to the optical/IR/UV spectral energy distribution (SED) interpolated to 5200 s. We interpolate all data using the broken power-law fit determined for the unfiltered KAIT and R-band Lulin data (Fig. 2). We choose 5200 s so that little interpolation is required for the IR or UV data. Because there is a prominent departure in the IR, optical, and UV light-curve data from the fit curve in the time interval 5×10^3–1.2×10^4 s in Figure 4 (see also Fig. 2), which can be modeled with a single magnitude offset of $\sim$0.6 mag from the power-law curve, we must include a variable offset in the SED fitting to describe the flux offset in this time interval. (Explanations for this behavior are discussed below.) In addition, we use the constraint derived above for the (unabsorbed) optical energy index $\beta_{\rm opt}$.

We begin by fitting the empirical Milky Way, Large Magellanic Cloud (LMC), and Small Magellanic Cloud (SMC) extinction curves of Pei (1992). The fits (Fig. 5*a*) yield rest-frame V-band extinction values of $A_V = 0.38 \pm 0.15$ ($\chi^2/\nu = 12.23/7$), 0.35 ± 0.08 ($\chi^2/\nu = 5.96/7$), and 0.23 ± 0.07 ($\chi^2/\nu = 4.32/7$) mag, respectively. The excellent fit of the SMC model and the poor fit of the Galactic extinction model point toward a weak 2175 Å dust "bump" and an increased level of far-UV extinction relative to that found in the Galaxy. In addition, we fit the data using the general, eight-parameter family of models from Fitzpatrick (1999), focusing on variations in A_V and the ratio of total to selective extinction, $R_V = A_V/E(B-V)$. In order to fold in prior knowledge of physically realistic values for R_V while not suppressing possible variations in the other parameters describing the extinction curve (e.g., the magnitude of the dust bump, which we marginalize over), we exploit the Reichart (2001) prior. The best-fit extinction curve has $A_V = 0.2 \pm 0.1$ mag, in agreement with the SMC value determined above, and $R_V = 2.0 \pm 1.0$ ($\chi^2/\nu = 4.9/6$). The model extinction at R band in the observer frame is $A_{R,\rm obs} = 0.7 \pm 0.1$ mag, consistent with the value derived above from the optical/X-ray flux ratio alone. Finally, we note that the extinction curve of Calzetti et al. (2000) provides a poor fit ($\chi^2/\nu = 9.42/6$, with best-fit $A_V = 0.24$ mag, $R_V = 2.0$).

Standard Galactic dust has $R_V = 3.1$ (Sneden et al. 1978), and the low inferred R_V (see also, e.g., Krisciunas et al. [2000] for the appearance of such values in the SEDs of supernovae) implies a dust grain distribution skewed toward fine grain sizes. The posterior probability contours in Figure 5*b* show $A_V < 0.45$ mag (2 σ). Larger values of $A_V \approx \beta_{\rm opt} \approx 3$ mag are possible if we relax the constraint on $\beta_{\rm opt}$ and allow positive values; however, these models are inconsistent with the temporal decay observed in the light curve and cannot produce the observed optical/X-ray flux ratio. For the wind-density medium, which is excluded by the rapid X-ray versus slow optical flux decay unless the early X-ray light curve is actually dominated by low-level flaring, the spectral slope can be as shallow as $\beta_{\rm opt} = -0.3$ (ν_c above the X-ray band, in conflict with the constraint derived above from the optical/X-ray flux ratio). But this has little effect on the inferred A_V, and we find $A_V < 0.5$ mag (2 σ).

Both the SED fits and the optical/X-ray flux ratio demand a considerably smaller dust column than we infer from the soft X-ray absorption (§ 3.2) or from detailed modeling of the GRB 051111 optical spectrum. The Galactic $N_{\rm H}$-A_V relation (Predehl & Schmitt 1995) and the observed X-ray column imply $A_V = 4 \pm 2$ mag. (One caveat here is that XRT low-energy calibration efforts are ongoing.)[17] This indicates that the ISM exhibits a low dust-to-gas ratio, similar to the SMC, which is $\sim$8 times smaller than Galactic (Bouchet et al. 1985; Pei 1992). Another contributing factor could be an overabundance of the light metals (which dominate the opacity at soft X-ray wavelengths; Morrison & McCammon 1983), as also suggested by optical spectroscopy in the case of GRB 050401 (Watson et al. 2006). Similar to GRB 050401, the Keck HIRES spectrum of GRB 051111 (Prochaska et al. 2005; Penprase et al. 2006; Prochaska 2006) exhibits strong absorption lines in the trace element Zn [implying $\log(N_{\rm H,gas}) = 21.2 \pm 0.2$, for solar metallicity], which combines with the inferred light-metal column from the X-ray data to imply a factor of $4.0^{+4.0}_{-2.6}$ overabundance in the multiple-α elements relative to the Fe-group elements. Because of the saturation of the Zn absorption in the Watson et al. (2006) GRB 050401 spectrum and because Zn is only a trace element and does not contribute directly to the opacity (e.g., at X-ray wavelengths), this possibility should be approached cautiously.

In a separate paper, we plan to study in more detail the X-ray absorption in this burst relative to the absorption properties determined from the optical spectroscopy. From the metal abundances inferred from the GRB 051111 Keck spectrum (e.g., Si/Fe or Zn/Fe), we find evidence that the gas is highly depleted by dust. There is also marginal evidence that the light-metal column [in gas form, $\log(N_{\rm H,gas}) = 21.0^{+0.7}_{-0.5}$, from $\log(N_{\rm Si^+}) = 16.6^{+0.7}_{-0.5}$] may be a factor of $\sim$10 smaller than that inferred from the X-ray data. It is not clear how these column densities are to be reconciled with the constraints imposed by the optical and X-ray SED and the soft X-ray absorption. The Keck spectrum shows, for example, $N_{\rm Si^{++}} < N_{\rm Si^+}$, which argues against an explanation in terms of a significant ionization of the column. The large X-ray column is probably not significantly due to intervening systems [a Mg II absorber in the optical spectrum at $z = 1.189$ only contributes $\log(N_{\rm H}) \approx 19.5$].

4.3. *External Shock Origin for the Early Optical Light Curve and GRB?*

From the optical colors, we derive above a stringent constraint on the change in the spectral slope across the break at $t \approx 700$ s, which excludes an explanation based on a passage through the spectral bands of the synchrotron cooling break (yielding $\Delta\beta = 0.5$; e.g., Sari et al. 1998). The most commonly invoked cause of achromatic breaks—flux decrements due to finally viewing the edge of the sideways-expanding GRB jet (e.g., Rhoads 1999)—is ruled out here by the mildness of the break ($\Delta\alpha = 0.19 \pm 0.04$) and by the extremely slow optical fade after the break. Another possible explanation, which grafts directly onto the $t > 700$ s solution discussed above, is that the density prior to the break is increasing with radius. A decreasing density, as for a wind medium (e.g., Rykoff et al. 2004), does not work because the flux increase due to the decreasing optical absorption

[17] See http://swift.gsfc.nasa.gov/docs/swift/analysis/xrt_digest.html.

is overcompensated by the decrease in synchrotron flux with radius. We would also expect to see a strong color change due to the changing absorbing column. For the increasing-density model, the absorbing matter close to the burst is unimportant, and there is little expected evolution in the absorption with time.

The prebreak decay is shallower by $\Delta\alpha = s/(8 + 2s)$, for a density rising as $n \propto R^s$ and $s = 4 \pm 2$. This is because the flux between the synchrotron peak frequency and the cooling break is proportional to the synchrotron peak frequency $\nu_m^{(p-1)/2}$ times the peak flux F_m (e.g., Sari et al. 1998). The frequency ν_m is independent of s, while $F_m \propto t^{s/(8+2s)}$ (e.g., Chevalier & Li 2000; Sari et al. 1998). The implied increase in density from $t \approx 30$ to 10^3 s is a factor of $\sim$5. Such a picture could potentially describe the prompt emission via the same external shock that later generates the afterglow. An external shock explanation for the prompt emission is motivated superficially by the apparent smoothness of the GRB (see, e.g., McMahon et al. 2004). Minimally, the model must be able to reproduce the extremely hard GRB spectrum, with $-\beta_\gamma \approx 0.3$–$0.5$ extending to $E \approx 1$ MeV. During the Blandford & McKee (1976) evolution stage when the fireball expands adiabatically, neither the synchrotron peak frequency (ν_m) nor the synchrotron cooling frequency (ν_c) can decrease more rapidly than $t^{-3/2}$ and go from such a high value at $t \approx 10$ s to the derived values above at $t \approx 10^3$ s. However, prior to this, during the fireball deceleration phase when the Lorentz factor Γ is expected to be roughly constant, the cooling frequency will decrease very rapidly, $\nu_c \propto t^{-2-3s/2}$. Our fits of this model, however, with an initial Lorentz factor $\Gamma_0 \approx 700$ (e.g., Mészáros & Rees 1997) for $t < t_d = 10$ s (Fig. 6), show that the external shocks that generate the optical flux underproduce gamma rays by a factor of $\sim$10. Synchrotron self-Compton emission cannot help due to that mechanism's inefficiency at small ϵ_e (Sari & Esin 2001). A more careful calculation of the expected GRB flux from the Blandford & McKee (1976) solution (e.g., Granot et al. 1999), with modifications to the standard synchrotron spectrum to possibly account for the harder GRB versus optical spectrum, is beyond the scope of this paper.

4.4. *Energy Injection*

Refreshed shocks offer a plausible and perhaps better-traveled explanation (e.g., Nousek et al. 2006) for the flat early light curve. Figure 6 shows the external shock model discussed above, but with the addition of a changing shock energy $E \propto t^a$ for $t < t_{\rm br}$. For a slow-cooling, constant-density synchrotron model between ν_m and ν_c, the light curve drops as $t^{a(p+3)/4+\alpha}$ (Sari & Mészáros 2000), where $\alpha = 3(1 - p)/4$ is the decay index without energy injection (e.g., Sari et al. 1998). We derive $a = 0.20 \pm 0.05$. Between 60 and 700 s, the shock energy increases by $\sim$60%. If the energy injection is due to a changing luminosity of the long-lasting central engine (Rees & Mészáros 2000; MacFadyen et al. 2001; Ramirez-Ruiz 2004; Lee & Ramirez-Ruiz 2002), the luminosity goes as $t^{-0.8\pm0.1}$, which may be challenging for the progenitor models (e.g., MacFadyen et al. 2001). If instead the central engine generated a flow with a power-law distribution of Lorentz factors Γ, with the slower shells of material gradually catching up to the shock, we find $M(\Gamma) \propto \Gamma^{-1.6\pm0.1}$ (Rees & Mészáros 1998; Sari & Mészáros 2000; Ramirez-Ruiz et al. 2001).

In the constant-density case, the optical flux is more sensitive to the energy injection than is the X-ray flux (by a factor $\Delta\alpha = a/4$; e.g., eq. [2] in Nousek et al. [2006]). If X-ray data were available for GRB 051111 during the energy injection episode, we could therefore verify and possibly better test the scenario. Long-wavelength observations are particularly important for testing the claims of strong energy injection episodes ($\Delta\alpha \approx 1$), inferred from the X-ray data alone (Nousek et al. 2006).

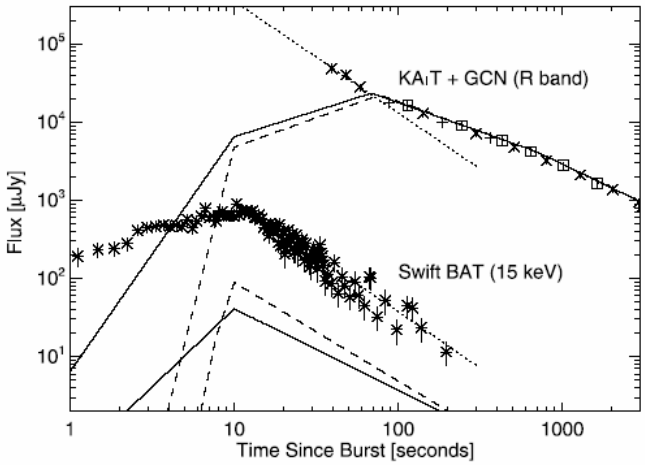

FIG. 6.—Early optical and prompt gamma-ray data fit with two variations on the external shock model: energy injection prior to $t = 700$ s with $E_{\rm sh} \propto t^{0.2}$ (*solid lines*) and an increasing density $n \propto R^4$ prior to $t = 700$ s (*dashed lines*). Due to an assumed constant initial Lorentz factor $\Gamma_0 = 700$, all curves rise prior to the estimated deceleration time $t_d = 10$ s. Neither model reproduces the strong gamma-ray flux. The best-fit power law for the prompt light-curve decline ($F_\gamma \propto t^{-1.4\pm0.1}$) is shown as a dotted line and is also scaled by a factor of 350 to match the first three optical data points. Here, we assume that the synchrotron peak frequency crosses the *R*-band central frequency at $t_0 = 70$ s (e.g., Table 3), which is an upper limit. We include the GCN data (Milne et al. 2005; Rujopakarn et al. 2005), in addition to the data from KAIT and *Swift*. All data are corrected for Galactic extinction (Schlegel et al. 1998). The optical data are shown mapped in frequency to the *R* band using the best-fit shock plus absorption model (Table 3; $A_{R,\rm obs} = 0.72$ mag; Fig. 5).

4.5. *The Optical Flux as Reprocessed Prompt Emission*

Similar to what was found above for the increasing-density model, the GRB flux at 15 keV in the energy injection scenarios is $\sim$10 times brighter than the expected flux from the external shock (solid line in Fig. 6). There is a possible steepening of the light-curve decay near $t \approx 60$ s apparent from ROTSE (Rujopakarn et al. 2005), Super-LOTIS (Milne et al. 2005), and the first KAIT observation (Fig. 2). This early flux decline is too steep, even assuming that energy injection has not yet begun to occur at this epoch. These three data points therefore suggest that the earliest optical flux is dominated by emission from the GRB.

The dotted curve in Figure 6 shows a power-law fit to the gamma-ray data overplotted on the optical. The implied broadband slope is $\beta_{\rm opt-\gamma} = -0.7$, consistent with the afterglow spectral slope in the optical but marginally inconsistent with the prompt gamma-ray spectral slope (§ 3.2). If there is a time delay for the reprocessing of the gamma-ray photons as has recently been proposed (Vestrand et al. 2006), this is a coincidence, and the broadband slope could easily be consistent with the gamma-ray spectral slope. In any case, for this and the rising-density model discussed above, the synchrotron peak frequency passes through the optical quite early ($t \lesssim 60$ s), implying a very inefficient transfer of the shock energy to the synchrotron-emitting electrons (Table 3), which may also be true for the prompt emission.

4.6. *Light-Curve Variability*

The optical light curve at $t \gtrsim 10^4$ s (Fig. 3, *inset*; § 3.1) and the optical/IR/UV light curve in the range 5×10^3–1.2×10^4 s show evidence for residual variability at the $\gtrsim$30% level, with

$dt/t \approx 0.1$. There is little evidence for spectral change during the variability. Such variability may be common and has been seen previously for well-sampled GRB afterglows. The light curve of GRB 021004 (Shirasaki et al. 2002) displayed several prominent bumps (Bersier et al. 2003; Mirabal et al. 2003; Fox et al. 2003b). The exquisitely sampled light curve of GRB 030329 (Lipkin et al. 2004; Vanderspek et al. 2003) displayed prominent departures from a broken power-law fade, even when the underlying supernova emission was subtracted away (Bersier et al. 2003).

Nakar et al. (2003) explore several possible explanations for the variability in GRB 021004 and find that an explanation in terms of refreshed shocks, a nonuniform (or "patchy") GRB jet, or variations in the external density (see also Wang & Loeb 2000; Dai & Lu 2002; Lazzati et al. 2002) are all possible. Granot et al. (2003) carry out a similar analysis for GRB 030329 and suggest that density variations are unlikely to be responsible for the optical variability due to the apparent passage of the synchrotron cooling break through the passband (e.g., Bersier et al. 2003). Late-time variability after an apparent jet break also argues against the patchy jet model, although that model could still describe the variability observed at earlier times.

For GRB 051111, the variability occurs during the phase ($t \gtrsim 700$ s) when the afterglow appears to be well described by external shocks. We believe that this favors an explanation in terms of density variation in the surrounding medium. Because the X-ray data are not expected to be affected by small variations in the density, this explanation is backed up by the quality of the X-ray fit with a single temporal power law, although the X-ray error bars are ~30%. Recently, Guidorzi et al. (2005) argue that density enhancements can explain an achromatic optical light-curve bump in data taken 3 minutes after GRB 050502A. More finely sampled data, with broad spectral coverage, will be required to pin down the true source of this variability in GRB afterglows.

5. CONCLUSIONS

We have presented a thorough analysis of the rich broadband data available for *Swift* GRB 051111, with a focus on the early, multiband optical data from KAIT and Lulin. The optical data prior to $t \approx 700$ s show a very flat decline, with little or no evidence for a color change as compared to the data after $t \approx 700$ s. The data at $t \gtrsim 1$ minute to several hours after the GRB are well fit using a simple, modified external shock model with absorption by gas and dust. The modeling entails energy injection or a rapidly increasing density profile with radius, prior to the break time. At later times there are large ($\gtrsim$30%), possibly achromatic modulations in the optical, IR, and UV about the best-fit model. The modulations appear to be common in well-studied optical afterglows, yet their origin remains mysterious.

The increasing-density model may allow for an external shock explanation of both the prompt gamma-ray and later emission. Such an increase in density might be expected if a supernova (SN) occurred prior to the GRB, as in the "supranova" model (Vietri & Stella 1998). However, the simultaneity of GRBs and SNe in the nearby, well-studied cases (GRB 060218/SN 2006aj, GRB 980425/SN 1998bw, GRB 031203/SN 2003lw) argues against this possibility.

On the other hand, slowly declining light curves in the X-ray band are common and are thought to be due to shock refreshment (e.g., Nousek et al. 2006), and the GRB 051111 observations from KAIT show that this emission can also dominate the optical light curve at early times. In fact, the optical light curve for this event, which shows a rapid early decline, followed by a leveling off and then a moderate decline typical of those found in the past and modeled with external shocks, appears quite similar to the "canonical" behavior observed in the X-ray band and reported by Nousek et al. (2006). Perhaps there is a canonical optical afterglow behavior, too. (As a counterpoint, the early optical behavior reported for GRB 060206 [Monfardini et al. 2006; Stanek et al. 2006] and GRB 060210 [Stanek et al. 2006] appears quite different from that here.)

An important feature of the GRB 051111 optical afterglow is the lack of a turnover in the optical decay rate at early times. We do not detect the peak in the synchrotron spectrum passing through the optical bands. Consonant with a lower than average X-ray flux at late times, this leads to a low value for the fraction (assuming constant equipartition) of shock kinetic energy winding up in the synchrotron-emitting electrons, $\epsilon_e \lesssim 0.3\%$. Such a low value for ϵ_e is uncommon, but not unheard of, in GRBs (see, e.g., Panaitescu & Kumar 2002). The very low value may indicate a wider diversity than previously suspected in the microphysical parameters from GRB to GRB (see also Berger et al. 2003). Aside from the low ϵ_e value, the derived external shock parameters are comparable to those previously found.

It is important to stress that whether we find $\epsilon_e \approx 0.3\%$ or $\approx$3% depends on the deconvolution of the early data into prompt internal shock and afterglow external shock components. Our favored smaller ϵ_e arises if the synchrotron peak frequency has passed through the optical well before the break at $t \approx 700$ s, in which case mild energy reinjection into the shock can explain the gradually decaying light curve. To get the larger ϵ_e value, the light curve prior to $t \sim 700$ s must be dominated by the GRB and not by the external shocks that dominate after $t \sim 700$ s. Otherwise, the early light curve would be rising rather than declining. In any case, reverberations of the prompt emission reprocessed into optical radiation (e.g., Vestrand et al. 2006) appear to be required to explain the earliest few optical data points for GRB 051111. It does not appear to be necessary to invoke reverse-shock emission (e.g., Akerlof et al. 1999; Li et al. 2003a), which is expected to produce time decays more rapid than those observed.

The absorption at IR, optical, and UV wavelengths in the observer frame is well fit by an SMC extinction curve. Little evidence for the 2175 Å dust "bump" and an excellent fit of the SMC extinction profile are common features in optical GRB afterglow spectra (e.g., Vreeswijk et al. 2004; Jakobsson et al. 2003; Savaglio & Fall 2004; Watson et al. 2006). Combined with the soft X-ray absorption measurement, there is an implied low dust-to-gas ratio and a possible overabundance of the light metals relative to the Fe-group metals. This has also been observed for GRB 050401 (Watson et al. 2006). The light-metal overabundance works against a direct association with an SMC-like environment, because the SMC has a metallicity ~1/10 times solar (Pei 1992).

The SED fitting also implies a low ratio of total to selective extinction, $R_V \approx 2$. This is a clue that the absorbing medium exhibits unusual dust properties. The work of Galama & Wijers (2001) establishing large typical N_H/A_V values has led to suspicions that GRBs could destroy dust out to distances $R \approx 20$ pc (see also Waxmann & Draine 2000; Fruchter et al. 2001; Draine & Hao 2002; Perna & Lazzati 2002; Perna et al. 2003). The small dust grains are preferentially destroyed, creating a flat (or "gray") extinction curve (Galama & Wijers 2001; Savaglio & Fall 2004; Stratta et al. 2005). A small R_V, however, suggests small dust grains are dominant, and our SED is very curved. These facts argue against the GRB playing a direct role in defining the extinction properties. The unchanging optical color

implies that the absorbing column is not local to the GRB (i.e., $R \gtrsim 0.1$ pc) and may be associated with a nearby giant molecular cloud or the GRB host galaxy. Time-resolved spectroscopy in the optical and X-ray bands is of utmost importance for answering these questions.

For GRB 051111, as for a few other *Swift* events for which ground-based observers have been fortunate enough to capture early data, there is an emerging complicated interplay between the GRB and the subsequent shocking of the external medium. It is critical that more long-wavelength data be taken and published for other GRBs in order to facilitate modeling similar to that performed above. Only with such a disentangling of the competing emission processes can we hope to answer open questions regarding which shock components are truly the most important and what microphysical parameters define the shocks and characterize the transition from internal to external shocks.

N. B. gratefully acknowledges support from a Townes Fellowship at the University of California Berkeley Space Sciences Laboratory, as well as partial support from J. S. B. and A. V. F. The work of A. V. F.'s group is supported by NASA *Swift* grants NNG05GF35G and NNG06GI86G. J. S. B., J. X. P., and H.-W. C. are partially supported by NASA *Swift* grant NNG05GF55G. KAIT and its ongoing research were made possible by generous donations from Sun Microsystems, Inc., the Hewlett-Packard Company, AutoScope Corporation, Lick Observatory, the National Science Foundation, the University of California, the Sylvia & Jim Katzman Foundation, and the TABASGO Foundation. This work is partly supported by grants NSC 94-2752-M-008-001-PAE, NSC 94-2112-M-008-002, and NSC 94-2112-M-008-019. Y. U. acknowledges support from the Japan Society for the Promotion of Science (JSPS) through JSPS Research Fellowships for Young Scientists.

REFERENCES

Akerlof, C., et al. 1999, Nature, 398, 400
Berger, E., Kulkarni, S. R., & Frail, D. A. 2003, ApJ, 590, 379
Bersier, D., et al. 2003, ApJ, 584, L43
Blake, C. H., et al. 2005, Nature, 435, 181
Blandford, R. D., & McKee, C. F. 1976, Phys. Fluids, 19, 1130
Bloom, J. S., et al. 2005, GCN Circ. 4256, http://gcn.gsfc.nasa.gov/gcn3/4256.gcn3
———. 2006, in ASP Conf. Ser. 351, Astronomical Data Analysis Software and Systems XV, ed. C. Gabriel et al. (San Francisco: ASP), 751
Bouchet, P., et al. 1985, A&A, 149, 330
Butler, N. 2006, ApJ, sumbitted (astro-ph/0604083)
Calzetti, D., et al. 2000, ApJ, 533, 682
Chevalier, R. A., & Li, Z.-Y. 2000, ApJ, 536, 195
Dai, Z. G., & Lu, T. 2002, ApJ, 565, L87
Dickey, J. M., & Lockman, F. J. 1990, ARA&A, 28, 215
Draine, B. T., & Hao, L. 2002, ApJ, 569, 780
Fenimore, E. E., Madras, C. D., & Nayakshin, S. 1996, ApJ, 473, 998
Filippenko, A. V., et al. 2001, in ASP Conf. Ser. 246, Small-Telescope Astronomy on Global Scales, ed. W. P. Chen, C. Lemme, & B. Pacyński (San Francisco: ASP), 121
Fitzpatrick, E. L. 1999, PASP, 111, 63
Fox, D. W., et al. 2003a, ApJ, 586, L5
———. 2003b, Nature, 422, 284
Frail, D. A., et al. 2005, GCN Circ. 4270, http://gcn.gsfc.nasa.gov/gcn3/4270.gcn3
Fruchter, A. S., Krolik, J. H., & Rhoads, J. S. 2001, ApJ, 563, 597
Galama, T. J., & Wijers, R. A. M. J. 2001, ApJ, 549, L209
Garimella, K., et al. 2005, GCN Circ. 4257, http://gcn.gsfc.nasa.gov/gcn3/4257.gcn3
Gehrels, N., et al. 2004, ApJ, 611, 1005
Granot, J., Nakar, E., & Piran, T. 2003, Nature, 426, 138
Granot, J., Piran, T., & Sari, R. 1999, ApJ, 513, 679
Guidorzi, C., et al. 2005, ApJ, 630, L121
Hill, G., et al. 2005, GCN Circ. 4255, http://gcn.gsfc.nasa.gov/gcn3/4255.gcn3
Huang, F. Y., et al. 2005a, GCN Circ. 4258, http://gcn.gsfc.nasa.gov/gcn3/4258.gcn3
Huang, K. Y., et al. 2005b, Nuovo Cimento C, 28, 731
Jakobsson, P., et al. 2003, A&A, 408, 941
Katz, J. I. 1994, ApJ, 422, 248
Krimm, H., et al. 2005, GCN Circ. 4260, http://gcn.gsfc.nasa.gov/gcn3/4260.gcn3
Krisciunas, K., et al. 2000, ApJ, 539, 658
Landolt, A. U. 1992, AJ, 104, 340
La Parola, V., et al. 2005, GCN Circ. 4261, http://gcn.gsfc.nasa.gov/gcn3/4261.gcn3
Lazzati, D., et al. 2002, A&A, 396, L5
Lee, W. H., & Ramirez-Ruiz, E. 2002, ApJ, 577, 893
Li, W., et al. 2003a, ApJ, 586, L9
———. 2003b, PASP, 115, 844
———. 2005, GCN Circ. 4254, http://gcn.gsfc.nasa.gov/gcn3/4254.gcn3
Li, W., et al. 2006, PASP, 118, 37
Lipkin, Y. M., et al. 2004, ApJ, 606, 381
MacFadyen, A. I., et al. 2001, ApJ, 550, 410
McMahon, E., Kumar, P., & Panaitescu, A. 2004, MNRAS, 354, 915
McMahon, E., Kumar, P., & Piran, T. 2006, MNRAS, 366, 575
Mészáros, P., & Rees, M. J. 1997, ApJ, 476, 232
Milne, P., et al. 2005, GCN Circ. 4252, http://gcn.gsfc.nasa.gov/gcn3/4252.gcn3
Mirabal, N., et al. 2003, ApJ, 595, 935
Monfardini, A., et al. 2006, ApJ, 648, 1125
Morrison, R., & McCammon, D. 1983, ApJ, 270, 119
Nakar, E., Piran, T., & Granot, J. 2003, NewA, 8, 495
Nanni, D., et al. 2005, GCN Circ. 4298, http://gcn.gsfc.nasa.gov/gcn3/4298.gcn3
Nousek, J. A., et al. 2006, ApJ, 642, 389
Paczyński, B., & Rhoads, J. 1993, ApJ, 418, L5
Panaitescu, A., & Kumar, P. 2002, ApJ, 571, 779
Pei, Y. C. 1992, ApJ, 395, 130
Penprase, B. E., et al. 2006, ApJ, 646, 358
Perna, R., & Lazzati, D. 2002, ApJ, 580, 261
Perna, R., et al. 2003, ApJ, 585, 775
Poole, T. S., et al. 2005, GCN Circ. 4263, http://gcn.gsfc.nasa.gov/gcn3/4263.gcn3
Predehl, P., & Schmitt, J. H. M. M. 1995, A&A, 293, 889
Prochaska, J. X. 2006, ApJ, 650, 272
Prochaska, J. X., et al. 2005, GCN Circ. 4271, http://gcn.gsfc.nasa.gov/gcn3/4271.gcn3
Ramirez-Ruiz, E. 2004, MNRAS, 349, L38
Ramirez-Ruiz, E., Merloni, A., & Rees, M. J. 2001, MNRAS, 324, 1147
Rees, M. J., & Mészáros, P. 1998, ApJ, 496, L1
———. 2000, ApJ, 545, L73
Reichart, D. E. 2001, ApJ, 553, 235
Rhoads, J. 1999, ApJ, 525, 737
Riess, A. G., et al. 1999, AJ, 118, 2675
Rujopakarn, W., et al. 2005, GCN Circ. 4247, http://gcn.gsfc.nasa.gov/gcn3/4247.gcn3
Rykoff, E. S., et al. 2004, ApJ, 601, 1013
———. 2005, GCN Circ. 4251, http://gcn.gsfc.nasa.gov/gcn3/4251.gcn3
Sakamoto, T., et al. 2005, GRB Circ. 4248, http://gcn.gsfc.nasa.gov/gcn3/4248.gcn3
Sari, R., & Esin, A. A. 2001, ApJ, 548, 787
Sari, R., & Mészáros, P. 2000, ApJ, 535, L33
Sari, R., & Piran, T. 1999, ApJ, 520, 641
Sari, R., Piran, T., & Narayan, R. 1998, ApJ, 497, L17
Savaglio, S., & Fall, S. M. 2004, ApJ, 614, 293
Schlegel, D. J., Finkbeiner, D. P., & Davis, M. 1998, ApJ, 500, 525
Sharapov, D., et al. 2005, GCN Circ. 4307, http://gcn.gsfc.nasa.gov/gcn3/4307.gcn3
Shirasaki, Y., et al. 2002, GCN Circ. 1565, http://gcn.gsfc.nasa.gov/gcn3/1565.gcn3
Smith, I. A., et al. 2005, GCN Circ. 4267, http://gcn.gsfc.nasa.gov/gcn3/4267.gcn3
Sneden, C., et al. 1978, ApJ, 223, 168
Stanek, K. Z., et al. 2006, ApJ, submitted (astro-ph/0602495)
Stratta, G., et al. 2005, A&A, 441, 83
Urata, Y., et al. 2005, Nuovo Cimento C, 28, 775
Vanderspek, R., et al. 2003, GCN Circ. 1997, http://gcn.gsfc.nasa.gov/gcn3/1997.gcn3
Vestrand, W. T., et al. 2004, Astron. Nachr., 325, 549
———. 2005, Nature, 435, 178
———. 2006, Nature, in press (astro-ph/0605472)
Vietri, M., & Stella, L. 1998, ApJ, 507, L45

Vreeswijk, P. M., et al. 2004, A&A, 419, 927
Wang, X., & Loeb, A. 2000, ApJ, 535, 788
Watson, D., et al. 2006, ApJ, 652, 1011
Waxman, E. 1997, ApJ, 485, L5
Waxman, E., & Draine, B. T. 2000, ApJ, 537, 796
Wijers, R. A. M., Rees, M. J., & Mészáros, P. 1997, MNRAS, 288, L51
Wozniak, P. R., et al. 2005, ApJ, 627, L13
Yamaoka, K., et al. 2005, GCN Circ. 4299, http://gcn.gsfc.nasa.gov/gcn3/4299.gcn3
———. 2006, Proc. SPIE, submitted

THE ASTROPHYSICAL JOURNAL, 654:L25–L28, 2007 January 1

MULTICOLOR SHALLOW DECAY AND CHROMATIC BREAKS IN THE GRB 050319 OPTICAL AFTERGLOW

K. Y. HUANG,[1] Y. URATA,[2,3] P. H. KUO,[1] W. H. IP,[1] K. IOKA,[4] T. AOKI,[5] C. W. CHEN,[1] W. P. CHEN,[1] M. ISOGAI,[5] H. C. LIN,[1] K. MAKISHIMA,[3,6] H. MITO,[5] T. MIYATA,[5] Y. NAKADA,[5] S. NISHIURA,[7] K. ONDA,[2] Y. QIU,[8] T. SOYANO,[5] T. TAMAGAWA,[3] K. TARUSAWA,[5] M. TASHIRO,[2] AND T. YOSHIOKA[9]

Received 2006 June 12; accepted 2006 November 9; published 2006 December 7

ABSTRACT

Multiwavelength observations of the optical afterglow of GRB 050319 were performed from 1.31 to 9.92 hr after the burst. Our *R*-band light curves, combined with other published data, can be described by the smooth broken power-law function, with $\alpha_1 = -0.84 \pm 0.02$ to $\alpha_2 = -0.48 \pm 0.03$, 0.04 days after the gamma-ray burst. The optical light curves are characterized by shallow decays—as was also observed in the X-rays—which may have a similar origin, related to energy injection. However, our observations indicate that there is still a puzzle concerning the chromatic breaks in the *R*-band light curve (at 0.04 days) and the X-ray light curve (at 0.004 days) that remains to be solved.

Subject heading: gamma rays: bursts

On-line material: machine-readable table

1. INTRODUCTION

The gamma-ray burst (GRB) afterglow as perceived in the X-ray, optical, and radio wavelengths is now understood to be the result of the collision between relativistic ejecta from the gamma-ray bursts and the interstellar medium (ISM). A comparison of afterglow light curves obtained at different wavelengths gives us important information about the surrounding ISM environment and the interaction processes. Such analyses can also provide essential input for theoretical models. Recently, the pace of this type of activity has quickened significantly, stimulated by the capabilities of the quick response and accurate localization of GRBs by the *Swift* satellite (Gehrels et al. 2004). This has meant that the number of GRB optical afterglow detections in the first several hours after a GRB by ground-based telescopes has recently increased significantly. It is interesting to note that the observations by *Swift* of the early X-ray emissions from a number of GRBs reveal a canonical behavior. The X-ray light curves can be divided into three distinct power-law segments (Nousek et al. 2006). Some X-ray and optical observations show that the evolution of both light curves changes at the same time (Blustin et al. 2006; Rykoff et al. 2006); however, chromatic breaks were also found in some cases (Fan & Piran 2006; Panaitescu et al. 2006). The nature of the afterglow early breaks in the light curves is thus uncertain. A detailed comparison of changes in the evolution of the optical, radio, and X-ray light curves should therefore be very interesting. This kind of physical study demands both a well-coordinated observational program and careful data analysis. We use GRB 050319, which has comprehensive observational coverage in both the X-ray and optical wavelengths and may be used as just such an example.

GRB 050319 was detected by the Burst Alert Telescope (BAT) on board the *Swift* satellite on 2005 March 19 at 09:31:18.44 UT (Krimm et al. 2005). However, a reanalysis of the BAT data showed two flares, indicating that GRB 050319 had already started 137 s before the trigger. The 15–350 keV fluence for the entire burst duration of $T_{90} = 149.6 \pm 0.7$ s has been estimated to be 1.6×10^{-6} ergs cm^{-2}. The X-ray emission of GRB 050319 after the burst was monitored by the *Swift* X-Ray Telescope (XRT) from 225 s to 28 days.[10] Two breaks in the emission curves were found (Cusumano et al. 2006). The initial sharp decline can be described by a power law with an index of $\alpha_1 = -5.53 \pm 0.67$ to be followed by $\alpha_2 = -0.54 \pm 0.04$ about 0.004 days after the burst. The unusually flat decline in the second part might have been caused by continuous energy injection. At about 0.313 days after the burst, the power-law index changed to $\alpha_3 = -1.14 \pm 0.2$, which can be readily explained as a jet break or a reduction in the energy injection (Cusumano et al. 2006; Zhang et al. 2006).

The early optical afterglow emission at 230 s was observed by the UV/Optical Telescope (UVOT) on *Swift* (Mason et al. 2006) and by two ground-based robotic telescopes, ROTSE-III (Robotic Optical Transient Search Experiment; Quimby et al. 2006) and RAPTOR (Rapid Telescopes for Optical Response; Woźniak et al. 2005). The best single–power-law fit of unfiltered data from ROTSE-III and RAPTOR indicates that $\alpha = -0.854 \pm 0.014$. A number of optical observatories have joined the follow-up observations (Yoshioka et al. 2005; Torii 2005; Sharapov et al. 2005a, 2005b; George et al. 2006; Misra et al. 2005; Kiziloglu et al. 2005; Greco et al. 2005). The spectral measurements of the afterglow by the Nordic Optical Telescope (NOT) indicate the redshift $z = 3.24$ of this event (Jakobsson et al. 2006).

2. OBSERVATIONS AND ANALYSIS

After receiving the GRB alert message from *Swift* and after the afterglow position was reported by Quimby et al. (2006), the Target-of-Opportunity procedures of the East-Asia GRB

[1] Institute of Astronomy, National Central University, Chung-Li, Taiwan; d919003@astro.ncu.edu.tw.
[2] Department of Physics, Saitama University, Shimo-Okubo, Sakura, Saitama, Japan.
[3] RIKEN, Hirosawa, Wako, Saitama, Japan.
[4] Department of Physics, Kyoto University, Kyoto, Japan.
[5] Kiso Observatory, Institute of Astronomy, University of Tokyo, Mitake-mura, Kiso-gun, Nagano, Japan.
[6] Department of Physics, University of Tokyo, Hongo, Bunkyo-ku, Tokyo, Japan.
[7] Department of Astronomy and Earth Sciences, Tokyo Gakugei University, Koganei, Tokyo, Japan.
[8] National Astronomical Observatories, Chinese Academy of Sciences, Beijing, China.
[9] Department of Physics, Nagoya University, Furo-cho, Chikusa, Nagoya, Aichi, Japan.

[10] The burst time in the article is 09:29:01.44 UT, 137 s before the BAT trigger.

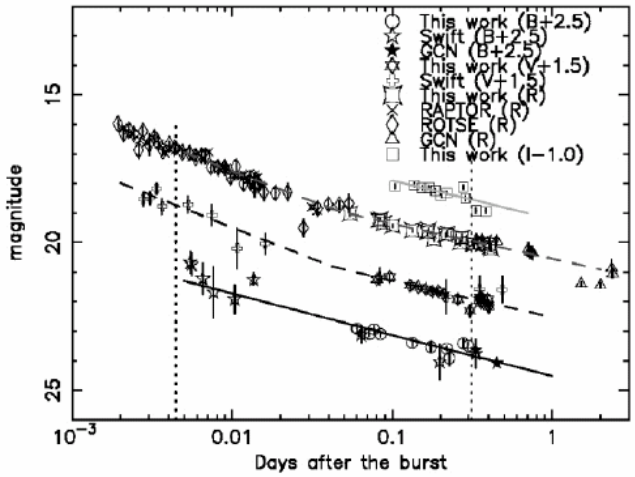

FIG. 1.—Optical light curves of GRB 050319. The solid lines present the best fit by the single power-law model ($F \propto t^{\alpha}$) for the B band ($\alpha = -0.56 \pm 0.06$) and the I band ($\alpha = -0.52 \pm 0.15$). The dashed line indicates the best fit by the smooth broken power law (eq. [1]) with the V band ($\alpha_1 = -0.87 \pm 0.21$, $\alpha_2 = -0.49 \pm 0.05$, $t_b = 0.042 \pm 0.058$ days) and the R band ($\alpha_1 = -0.84 \pm 0.02$, $\alpha_2 = -0.48 \pm 0.03$, $t_b = 0.046 \pm 0.008$ days). The dotted lines represent the break times of X-ray afterglows 0.004 and 0.31 days after the burst. The two breaks were not found in X-ray observations, but a mild break seems to exist in the V- and R-band light curves.

Follow-up Observation Network (EAFON; Urata et al. 2005) were immediately carried out. A series of multiband follow-up observations were successfully performed by the 1.05 m Schmidt telescope of the Kiso Observatory in Japan and the Lulin One-meter Telescope (LOT) in Taiwan. Photometric B and R images were obtained at the Kiso site with a 2K × 2K CCD camera (Urata et al. 2005) between 0.055 and 0.326 days after the burst. A number of parallel B, V, R, and I images were obtained by LOT with a PI1300 CCD camera (Kinoshita et al. 2005) from 0.080 to 0.413 days after the burst.

The standard routine included bias subtraction and dark subtraction; flat-field corrections were employed with the appropriate calibration data needed to process the data using IRAF. The signal-to-noise ratio was improved by combing the LOT B-band data with median filtering. The DAOPHOT package (Stetson 1987) was then used to perform point-spread function (PSF) fitting for the GRB images. Four field stars were used to create a PSF model that was applied to the optical afterglow of each GRB image. For absolute photometric calibration, we used calibrated data of the GRB field obtained by Henden (2005). The photometric error and the systematic calibration error were included in the magnitude error estimation.[11]

3. RESULTS

3.1. *Light Curve*

Figure 1 shows the multiband light curves of the GRB 050319 afterglow. Besides our B-, V-, R-, and I-band data (Table 1), we also included the R-band measurements from ROTSE-III (Quimby et al. 2006), RAPTOR (Woźniak et al. 2005), and several GRB Coordinates Network (GCN) reports (Greco et al. 2005; Kiziloglu et al. 2005; Misra et al. 2005; Sharapov et al. 2005a, 2005b). In addition, we also made use of several B- and V-band measurements taken with the *Swift* UVOT (Mason et al. 2006). The GCN R-band points were recalibrated using the GRB 050319 field stars reported by Henden (2005), so they could be plotted on the same magnitude scale. The magnitude differences between the photometric field stars in Henden (2005) and the USNO-A2.0 and USNO-B1.0 stars are +0.18 and −0.22 mag, respectively. We remeasured the reference stars from Greco et al. (2005) from the LOT R-band images and obtained the average magnitudes and rms errors.

[11] The errors in this article were quoted for a 68% (1 σ) confidence level.

TABLE 1
GRB 050319 OPTICAL AFTERGLOW PHOTOMETRY

Days after GRB[a]	Filter	Magnitude[b]	Site
0.05443	R	19.01 ± 0.08	Kiso
0.06023	B	20.42 ± 0.13	Kiso
0.08037	V	19.75 ± 0.07	Lulin
0.10439	I	19.09 ± 0.07	Lulin
0.27821	B	20.92 ± 0.12	Kiso
0.33424	I	19.91 ± 0.09	Lulin
0.40097	V	20.68 ± 0.12	Lulin
0.41346	R	20.20 ± 0.07	Lulin

NOTE.—Table 1 is published in its entirety in the electronic edition of the *Astrophysical Journal*. A portion is shown here for guidance regarding its form and content.

[a] The burst time is 2005 March 19, UT 09:29:01.44.

[b] The magnitudes are not corrected for Galactic extinction.

After fitting the B-, V-, R-, and I-band light curves to a single–power-law expression $F \propto t^{\alpha}$, where α is the index and t is the time after the burst, we get $\alpha = -0.56 \pm 0.06$ ($\chi^2/\nu = 2.90$ for $\nu = 19$) for the B band, $\alpha = -0.65 \pm 0.03$ ($\chi^2/\nu = 2.60$ for $\nu = 27$) for the V band, $\alpha = -0.59 \pm 0.01$ ($\chi^2/\nu = 5.3$ for $\nu = 97$) for the R band, and $\alpha = -0.52 \pm 0.15$ ($\chi^2/\nu = 7.7$ for $\nu = 9$) for the I band. This single–power-law fitting indicates that these light curves, obtained with different filters, have a similar power-law decay even though the reduced χ^2 values are relatively large.

Since the data sets of the V and R measurements are more complete, it is possible with following expression to attempt the fitting of the corresponding light curves with a smoothly broken power-law function:

$$F(\nu, t) = \frac{2^{1/k} F_{\nu, b}}{[(t/t_b)^{-k\alpha_1} + (t/t_b)^{-k\alpha_2}]^{(1/k)}}, \quad (1)$$

where t_b is the break time, α_1 and α_2 are the power-law indices before and after t_b, $F_{\nu, b}$ is flux at break t_b, and k is a smoothness factor. For the V band, we obtain $\alpha_1 = -0.87 \pm 0.21$, $\alpha_2 = -0.49 \pm 0.05$, $t_b = 0.042 \pm 0.058$ days, and $k = -30$ ($\chi^2/\nu = 1.48$ for $\nu = 24$). For the R band, we obtain $\alpha_1 = -0.84 \pm 0.02$, $\alpha_2 = -0.48 \pm 0.03$, $t_b = 0.046 \pm 0.008$ days, and $k = -21$ ($\chi^2/\nu = 2.24$ for $\nu = 90$). This result implies a mild break in both the V- and R-band light curves at around 0.04 days after the occurrence of the GRB.

Taking $t_b = 0.04$ days, we fit the data in the B and I bands to a respective power law before and after the break. In this manner, we find $\alpha_1 = -0.79 \pm 0.09$ ($\chi^2/\nu = 1.09$ for $\nu = 7$); $\alpha_2 = -0.36 \pm 0.05$ ($\chi^2/\nu = 1.23$ for $\nu = 9$) for the B band, and $\alpha_2 = -0.52 \pm 0.15$ ($\chi^2/\nu = 7.7$ for $\nu = 9$) for the I band. The best-fit parameters for the B, V, R, and I bands are summarized in Table 2. Our results show not only the clear presence of mild breaks in the V- and R-band light curves but a flattening trend after the break. Furthermore, our R-band slope before the break ($\alpha \sim -0.84$) is in agreement with the corresponding value derived by Quimby et al. (2006) for the interval between 0.0019 and 0.05 days after the burst.

3.2. *Color and Spectral Flux Distribution*

Our multiwavelength observations indicate that median colors between 0.07 and 0.35 days are $V - R = 0.45 \pm 0.11$, $R -$

TABLE 2
FITTING RESULTS OF THE GRB 050319 LIGHT CURVES

Filter	α_1	α_2	t_b (days)
B	-0.79 ± 0.09	-0.36 ± 0.05	...
V	-0.87 ± 0.21	-0.49 ± 0.05	0.042 ± 0.058
R	-0.84 ± 0.02	-0.48 ± 0.03	0.046 ± 0.008
I	...	-0.52 ± 0.15	...

NOTE.—The B- and I-band data were fitted by a respective power-law model ($F \propto t^{\alpha}$) before and after the break (t_b = 0.04 days). On the other hand, the V and R data were fitted by a smoothly broken power law (eq. [1]).

$I = 0.46 \pm 0.10$, and $B - V = 0.84 \pm 0.14$. These values have been corrected for foreground reddening of $E(B - V) = 0.011$ mag (Schlegel et al. 1998). The $V - R$ and $R - I$ colors so derived are consistent with those of the typical long GRBs (Simon et al. 2001), but the $B - V$ color is slightly redder than those of the typical long GRBs ($B - V = 0.47 \pm 0.17$). The larger $B - V$ value may imply a certain absorption effect because the redshift of GRB 050319 was determined to be 3.24 (Jakobsson et al. 2006).

The B, V, R, and I magnitudes have been further converted to fluxes using the effective wavelengths and normalizations of Fukugita et al. (1995). The effect of the Galactic interstellar extinction has been corrected. Figure 2 shows two samples of spectral energy distribution obtained by LOT 0.13 and 0.21 days after the occurrence of GRB 050319. A drop in the B-band flux at about 4380 Å can be clearly seen. We subsequently fitted the flux distribution of V, R, and I bands with a power-law function $F(\nu, t) \propto \nu^{\beta}$; here $F(\nu, t)$ is the flux at frequency ν with a certain t and β is the spectral index. We find that $\beta = -1.08 \pm 0.05$ ($\chi^2/\nu = 0.05$ for $\nu = 1$) at 0.13 days and that $\beta = -1.08 \pm 0.32$ ($\chi^2/\nu = 2.3$ for $\nu = 1$) at 0.21 days. Our result ($\beta = -1.08$ with an rms error of 0.23) is consistent with the X-ray fitting value ($\beta = -0.69 \pm 0.06$) in a 3 σ level.

With a redshift of 3.24, the Lyα absorption feature would shift into the B bandpass, causing reduction of the afterglow flux in the B band. To correct for this absorption effect, we used the formulation derived by Yoshii & Peterson (1994), in which the optical depth is a function of the observed wavelength and source redshift. With the computed optical depth in the B band, and a spectral slope of $\beta = -1.08$, we found the expected B-band magnitude after Lyα absorption to be 21.33 ± 0.05 at 0.13 days. This value compares very well with our observed value of $B = 21.26 \pm 0.17$ at 0.13 days after correction for Galactic extinction. The drop at the B band is hence fully produced by the Lyα absorption, and no spectral breaks should have taken place during our observation.

4. DISCUSSION AND SUMMARY

It is important to note that *Swift* found two breaks 0.004 and 0.313 days after the burst in the X-ray afterglow observations (Cusumano et al. 2006), but we only found a single break in our V and R light curves (see Fig. 1). In the following, since there are more data points available for the R-band data, we will focus on this. It is useful to remember that $\alpha_1 = -0.84$ and $\alpha_2 = -0.48$ at the break time of $t_b = 0.04$ days.

4.1. *Before the Optical Break* ($t < 0.04$ days)

The slope α_1 ($= -0.84$) is consistent with the typical range of $\alpha = -0.62$ to -2.3 for many well-observed GRBs. According to the standard afterglow model relating the power-law index (α) to the power-law index (p) of an electron spectrum (Zhang & Mészáros 2004; Dai & Cheng 2001), the corresponding value for $\alpha_1 = -0.84$ is $p = 2.1$, which is in agreement with the constant-density ISM model with slow cooling in which $p > 2$ for $\nu_m < \nu_{\rm opt} < \nu_c$ (ν_m is the typical frequency; $\nu_{\rm opt}$ is the optical frequency; and ν_c is the cooling frequency). In light of the XRT observations, the first break was likely caused by the transition from the tail end of the low-energy prompt emission to the afterglow phase (Zhang et al. 2006). However, it is important to note that the X-ray break at 0.004 days (where the steeper slope becomes shallow) is not accompanied by an R-band break. At the same time, the power-law decay slope in the X-ray (~ -5.53) and that in the R band (~ -0.84) are quite different. This is an indication that the behaviors of the X-ray afterglow and optical afterglow of the GRB 050319 event are different, but this also suggests that the afterglow phase already dominated the optical bands when the optical emission was first detected.

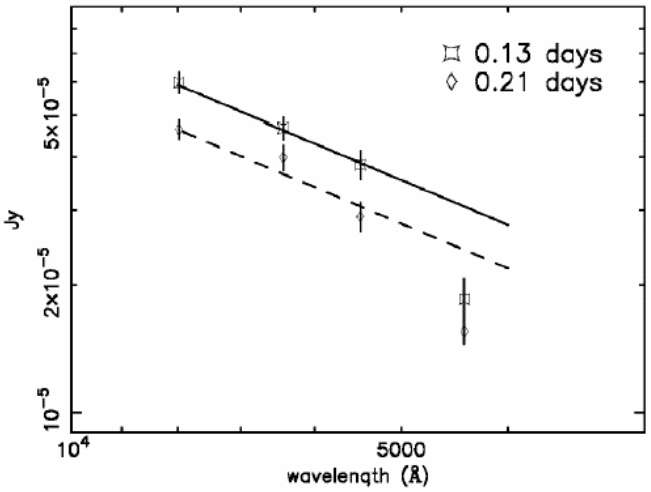

FIG. 2.—Spectral energy distribution of GRB 050319 between the V, R, and I bands 0.13 and 0.21 days after the burst (corrected for Galactic extinction). The solid and dashed lines indicate the best fit by the power-law model [$F(\nu) \propto \nu^{\beta}$], where $\beta = -1.08 \pm 0.05$ for 0.13 days and $\beta = -1.08 \pm 0.32$ for 0.21 days.

4.2. *Shallow Decay*

The power-law index becomes shallow after the break ($t_b = 0.04$ days). Neither the jet (Rhoads 1999) nor the break frequencies across the optical wavelength (Sari et al. 1998) suitably explain the break we see in the GRB 050319 light curves. As discussed before, the X-ray light curve between the two breaks 0.004 and 0.313 days after the burst is also characterized by shallow decay. Several studies indicate that such behavior is related to continuous energy injection into the ISM (Dai & Lu 1998a, 1998b; Zhang et al. 2006). For a long-lasting central engine, the energy injection rate is $\dot{E}(t) \propto t^{-q}$, with $q < 1$ (Zhang & Mészáros 2001). For slow cooling in the ISM, the temporal index can be expressed as $\alpha = [(2p - 6) + (p + 3)q]/4 = [(q - 1) + (2 + q)\beta]/2$, when $\nu_m < \nu < \nu_c$. Using this formulation, Zhang et al. (2006) obtained $q = 0.6$ and $p = 2.4$ from the X-ray observations. With $\alpha = -0.48$ and $\beta = -1.08$ from the R-band observations, we find that $q = 0.72$ and $p = 2.12$. The results not only indicate that the electron spectrum power-law index is the same before and after the break, but they also compare well with the results of Zhang et al. (2006). These results indicate that the shallow decays evidenced by both X-ray and optical afterglows could be of a similar origin, related to a continuous energy injection mechanism.

According to the energy injection model, we would also

expect an X-ray break at the time of the optical flattening break, because the onset of the energy injection should also alter the X-ray temporal index. However, such an X-ray break is not observed, which suggests that some modifications to the injection model may be needed. As mentioned in § 4.1, the X-ray break at 0.004 days was not accompanied by a break in the *R* light curve. Although a chromatic break in the X-ray was found at 0.004 days and in the optical region at 0.04 days, the light curves at both wavelengths indeed showed shallow decay after the breaks, which can be explained by the energy injection model. However, it is difficult for energy injection from 0.004 to 0.04 days to affect only high energies. This difficulty indicates that energy injection is an imperfect mechanism for explaining the shallow optical or X-ray phase associated with the GRB 050319 event.

Several models have recently been proposed to explain the shallow decay effect. Using the multiple-subjet model (Nakamura 2000), Toma et al. (2006) invoked the superposition of afterglows from many off-axis subjets. Eichler & Granot (2006) favored a combination of the tail of prompt emission model with the afterglow emissions observed from a viewing angle outside the edge of the jet. These arguments hence suggest that the multiple-subjet model and the patchy-shell model (Kumar & Piran 2000) might provide a theoretical basis for explaining the observed shallow decays in the X-ray and optical light curves. It is interesting to note that in order to sustain the shallow decay process, these models all require high gamma-ray efficiency (75%–90%); additional mechanisms such as prior activity (Ioka et al. 2006) and time-dependent shock generation (Fan & Piran 2006) have also been proposed. Comprehensive multiwavelength observations, such as those reported here, provide us with important ways to improve these models.

Finally, the second break in the X-ray emissions (~0.313 days) has been interpreted as being due to an unusual flat jet break (Cusumano et al. 2006); however, Zhang et al. (2006) provided an alternate explanation, a sudden cessation of the energy injection. In both interpretations, the corresponding break should appear in both the X-ray and optical light curves. This effect cannot be clearly identified in our measurements until 0.413 days after the burst. The lack of data for the subsequent time interval could lead to uncertainty in the power-law fitting. We thus cannot fully exclude the existence of a second break in the optical light curves. However, Panaitescu et al. (2006) have studied several afterglows. They found the shallow power-law decay evidenced by the X-ray emissions to steepen about 0.04–0.17 days after the burst, although there was no accompanying break found in the optical range. They suggest that such chromatic X-ray breaks may be common. The chromatic breaks (e.g., the shallow X-ray phase becomes steeper, with no accompanying optical break) may be caused by differences in the X-ray and optical outflow (Panaitescu et al. 2006) or by changes in the typical electron energy parameters (the so-called microphysical parameters) at the end of energy injection (Panaitescu 2006).

In summary, our analysis of the optical multiwavelength observations of GRB 050319 compared with the X-ray observations from *Swift* found the following major results:

1. The *B*, *V*, *R*, and *I* band light curves displayed unusual shallow decays.
2. The *R* light curve can be described by a smooth broken power-law function; $\alpha_1 \sim -0.84$ becomes shallow ($\alpha_2 \sim -0.48$) 0.04 days after the occurrence of the GRB.
3. The shallow decay observed in the X-ray and optical light curves may have a similar origin related to energy injection. However, our observations indicate that a major puzzle remains concerning the chromatic breaks in the *R*-band light curve (at 0.04 days) and the X-ray light curve (at 0.004 days).
4. Our calculations revealed that the drop in spectral energy distribution was fully caused by a shift in the Lyα absorption to the *B* bandpass at $z = 3.24$.

We thank the referee for his/her valuable advice. This work is supported by NSC 95-2752-M-008-001-PAE, NSC 95-2112-M-008-021, the Japan Society for the Promotion of Science (JSPS) Grant-in-Aid for Young Scientists (B) 18740147, and JSPS Research Fellowships for Young Scientists (Y. U.).

REFERENCES

Blustin, E., et al. 2006, ApJ, 637, 901
Cusumano, G., et al. 2006, ApJ, 639, 316
Dai, Z. G., & Cheng, K. S. 2001, ApJ, 558, L109
Dai, Z. G., & Lu, T. 1998a, A&A, 333, L87
———. 1998b, Phys. Rev. Lett., 81, 4301
Eichler, D., & Granot, J. 2006, ApJ, 641, L5
Fan, Y., & Piran, T. 2006, MNRAS, 369, 197
Fukugita, M., Shimasaku, K., & Ichikawa, T. 1995, PASP, 107, 945
Gehrels, N., et al. 2004, ApJ, 611, 1005
George, K., Banerjee, D. P. K., Chandrasekhar, T., & Ashok, N. M. 2006, ApJ, 640, L13
Greco, G., Bartolini, C., Guarnieri, A., Piccioni, A., Ferrero, P., & Bruni, I. 2005, GCN Circ. 3142, http://gcn.gsfc.nasa.gov/gcn/gcn3/3142.gcn3
Henden, A. 2005, GCN Circ. 3454, http://gcn.gsfc.nasa.gov/gcn/gcn3/3454.gcn3
Ioka, K., Toma, K., Yamazaki, R., & Nakamura, T. 2006, A&A, 458, 7
Jakobsson, P., et al. 2006, A&A, 460, L13
Kinoshita, D., Chen, C.-W., Lin, H.-C., Lin, Z.-Y., Huang, K.-Y., Chang, Y.-S., & Chen, W.-P. 2005, Chinese J. Astron. Astrophys., 5, 315
Kiziloglu, U., et al. 2005, GCN Circ. 3139, http://gcn.gsfc.nasa.gov/gcn/gcn3/3139.gcn3
Krimm, H., et al. 2005, GCN Circ. 3119, http://gcn.gsfc.nasa.gov/gcn/gcn3/3119.gcn3
Kumar, P., & Piran, T. 2000, ApJ, 535, 152
Mason, K. O., et al. 2006, ApJ, 639, 311
Misra, K., Kamble, A. P., & Pandey, S. B. 2005, GCN Circ. 3130, http://gcn.gsfc.nasa.gov/gcn/gcn3/3130.gcn3
Nakamura, T. 2000, ApJ, 534, L159
Nousek, J. A., et al. 2006, ApJ, 642, 389
Panaitescu, A. 2006, preprint (astro-ph/0607396)
Panaitescu, A., Mészáros, P., Burrows, D., Nousek, J., O'Brien, P., & Willingale, R. 2006, MNRAS, 369, 2059
Quimby, R. M., et al. 2006, ApJ, 640, 402
Rhoads, J. E. 1999, ApJ, 525, 737
Rykoff, E., et al. 2006, ApJ, 638, L5
Sari, R., Piran, T., & Narayan, R. 1998, ApJ, 497, L17
Schlegel, D. J., Finkbeiner, D. P., & Davis, M. 1998, ApJ, 500, 525
Sharapov, D., et al. 2005a, GCN Circ. 3124, http://gcn.gsfc.nasa.gov/gcn/gcn3/3124.gcn3
———. 2005b, GCN Circ. 3140, http://gcn.gsfc.nasa.gov/gcn/gcn3/3140.gcn3
Simon, V., Hudec, R., Pizzichini, G., & Masetti, N. 2001, A&A, 377, 450
Stetson, P. B. 1987, PASP, 99, 191
Toma, K., Ioka, K., Yamazaki, R., & Nakamura, T. 2006, ApJ, 640, L139
Torii, K. 2005, GCN Circ. 3121, http://gcn.gsfc.nasa.gov/gcn/gcn3/3121.gcn3
Urata, Y., et al. 2005, Nuovo Cimento, 28, 775
Woźniak, P. R., Vestrand, W. T., Wren, J. A., White, R. R., Evans, S. M., & Casperson, D. 2005, ApJ, 627, L13
Yoshii, Y., & Peterson, B. A. 1994, ApJ, 436, 551
Yoshioka, T., et al. 2005, GCN Circ. 3120, http://gcn.gsfc.nasa.gov/gcn/gcn3/3120.gcn3
Zhang, B., & Mészáros, P. 2001, ApJ, 552, L35
———. 2004, Int. J. Mod. Phys. A, 19, 2385
Zhang, B., et al. 2006, ApJ, 642, 354

Astronomy & Astrophysics manuscript no. 2005ud˙aa˙20070110
January 10, 2007

Surface heterogeneity of 2005 UD from photometric observations

Daisuke Kinoshita[1], Katsuhito Ohtsuka[2], Tomohiko Sekiguchi[3], Jun-ichi Watanabe[3], Takashi Ito[3], Hideyoshi Arakida[4], Toshihiro Kasuga[3], Seidai Miyasaka[5], Ryosuke Nakamura[6], Hung-Chin Lin[1]

[1] Institute of Astronomy, National Central University, 300 Jhongda Rd., Jhongli, Taoyuan, 32001, Taiwan
e-mail: kinoshita@astro.ncu.edu.tw
[2] Tokyo Meteor Network, 1-27-5 Daisawa, Setagaya, Tokyo, 155-0032, Japan
[3] National Astronomical Observatory of Japan, 2-21-1 Osawa, Mitaka, Tokyo, 181-8588, Japan
[4] Waseda University, 1-6-1 Nishi-Waseda, Shinjuku, Tokyo, 169-8050, Japan
[5] Tokyo Metropolitan Government, 2-8-1 Nishi-Shinjuku, Shinjuku, Tokyo, 163-8001, Japan
[6] Grid Technology Research Center, National Institute of Advanced Industrial Science and Technology, Central 2, 1-1-1 Umezono, Tsukuba, Ibaraki, 305-8568, Japan

Received August 24, 2006; accepted November 28, 2006

ABSTRACT

Context. The recently discovered Apollo-type near-Earth asteroid 2005 UD has been suggested to be a fragment of (3200) Phaethon.
Aims. To test this hypothesis, we carried out photometric observations of 2005 UD using the 1-m telescope at Lulin Observatory.
Methods. Multi-color photometry was used to compare the surface properties of (3200) Phaethon and 2005 UD. Surface-color variation due to the rotation was also examined.
Results. The time-resolved differential photometry showed clear brightness variation, and the lightcurve was fitted with a rotation period of 5.23 hours and an amplitude of 0.44 mag. Using this rotational lightcurve, we derived the surface colors of 2005 UD. The surface of 2005 UD exhibits colors similar to those of F- and B-type asteroids, which is consistent with (3200) Phaethon. Furthermore, the $(R-I)$ color of 2005 UD shows variation during the rotation of the body.
Conclusions. The similarity of surface colors between (3200) Phaethon and 2005 UD observationally supports the hypothesis that 2005 UD is likely to be a fragment of (3200) Phaethon. A simple explanation for the inhomogeneity of the surface is that we see the surface and subsurface of the precursor object. Another explanation is the topographical structure that such as a large crater causes on this heterogeneous surface.

Key words. Minor planets, asteroids - Comets: general - Meteors, meteoroids - Techniques: photometric

1. Introduction

An Apollo-type near-Earth asteroid, (3200) Phaethon (= 1983 TB), was discovered by the InfraRed Astronomical Satellite (IRAS) in October 1983 (Green & Kowal 1983). Although the appearance of (3200) Phaethon is asteroidal, its orbit is highly eccentric with $e = 0.89$, like those of comets. In addition, (3200) Phaethon is a strong candidate for the Geminid meteor stream (Whipple 1983; Gustafson 1989; Williams & Wu 1993), so it is regarded as one of the most likely dormant cometary nuclei, whose cometary activity is sporadic, or as extinct cometary nuclei whose activity has already stopped. Many attempts have been made to detect the faint coma of this object (Cochran & Barker 1984; Chamberlin et al. 1996; Hsieh & Jewitt 2005). No cometary activity has been observed yet; therefore, (3200) Phaethon seems to be one of the most peculiar and enigmatic objects in the solar system.

On October 22, 2005, an Apollo-type, near-Earth asteroid was discovered by the Catalina Sky Survey, and the provisional designation of 2005 UD was given to this object (McNaught et al. 2005). Ohtsuka et al. (2005) immediately pointed out that 2005 UD was probably the parent body of the daytime Sextantids meteor stream, based on the orbital similarity. Thus, 2005 UD is very likely a large member of the Phaethon-Geminid stream complex. Furthermore, Ohtsuka et al. (2006) performed both forward and backward 10,000-yr numerical integrations of the Kustaanheimo-Stiefel (K-S) regularized equation of motion (Arakida & Fukushima 2000, 2001) for (3200) Phaethon and 2005 UD. The results of this numerical work show quite similar evolutional behaviors along with the time shift by ~ 4600-yr; hence, they suggest that both bodies are dynamically related and 2005 UD is most likely a km-sized fragment of (3200) Phaethon. Ohtsuka et al. (2006) also point out that fragmentation processes are important in forming the complex meteor stream.

Very recently, Jewitt and Hsieh (2006) have reported their analysis of the photometric observation of 2005 UD. The results of their broadband multi-color photometry support the possible dynamical association between 2005 UD and (3200) Phaethon. The mass-loss rate from 2005 UD, based on the point-spread function (PSF) fitting, is found to be very small or negligible. They also mention that a mainbelt comet (MBC) could be a possible origin of (3200) Phaethon and 2005 UD, although testing their idea currently does not seem to be easy.

We carried out observational studies of 2005 UD. The primary aim of our observations was to verify the dynamical relationship between (3200) Phaethon and 2005 UD through the similarity of surface physical properties. If 2005 UD exhibited photometric properties similar to those of (3200) Phaethon, we can confirm prior research by providing another strong piece of evidence for their genetic relationship. Second, we tried to detect the surface color variation of 2005 UD. Ohtsuka et al.

Send offprint requests to: Kinoshita Daisuke

(2006) concluded 2005 UD is very likely a km-order fragment from (3200) Phaethon from the standpoint of dynamics; therefore, there may be non-uniformity of photometric properties if the fresh materials are exposed elsewhere on the surface. This sort of exposed fresh materials may create color variations during the rotation of the body.

We briefly introduce our observations, data analysis procedures, and results in Sec. 2. We give the discussion in Sec. 3 and summarize our results in Sec. 4.

2. Observation, analysis, and results

Photometric observations of 2005 UD were carried out at Lulin Observatory operated by the Institute of Astronomy, National Central University in Taiwan. The Lulin Observatory sits on the peak of Mount Lulin (120°52′25″E, 23°28′7″N, H = 2862-m) in the central region of Taiwan. We used the Princeton Inc. CCD (charge coupled device) camera, PI1300B, with the Cassegrain focus (F/8.0) of the 1-m telescope to obtain imaging data. The pixel scale of this system is 0.516 arcsec per pixel, and it is spatially well-sampled at the typical seeing size of stellar FWHM (full width at half maximum), ~ 1.5 arcsec. The number of pixels of the CCD is 1340 × 1300, and the resultant field-of-view is 11.5 × 11.2 arcmin. The cooling temperature of the CCD is set to -50°C, and this is achieved by both thermoelectric cooling and water circulation. The filter set is based on the Bessel system. More detailed specifications and performances of the instrument have been reported by Kinoshita et al. (2005).

The data was acquired on six nights from 31 October to 5 November 2005. At the time of observations, the heliocentric distance of the object ranged from 1.36 to 1.42 AU, and its geocentric distance ranged from 0.51 to 0.62 AU. The apparent motion of 2005 UD is relatively large and non-sidereal tracking was used for this target. We used *BVRI* filters to measure the surface colors of 2005 UD for taxonomic study and color variation. To minimize the rotational effect, observations were done in *R-B-R-V-R-I-R* sequences. This sequence of observation at least secured the rotational lightcurve when the sky condition was unstable. The exposure time was set to 180 sec for the *R*-band, and 300 sec for other bands. When the sky was photometric, standard stars from the list provided by Landolt (1992) were observed during the night. Photometric standard stars were carefully selected to cover wide ranges of airmass and colors for accurate correction of atmospheric and instrumental signatures. The number of Landolt fields we obtain was typically 20 per night, and this gave about 50-70 measurements of photometric standards. The flatfield frames were obtained using the twilight sky, both in the evening and morning.

The dark subtracting and flatfielding were applied in the standard manner using an image-analysis software package NOAO IRAF. Then, plate constants were refined by WCSTools (Mink 2002) for astrometric measurements. By including our 183 astrometric positions and the newly found precovery positions in 1982 and 2001, hence three oppositions until now, Nakano (2005) improved the orbit of 2005 UD.

2.1. Differential Photometry and Rotational Lightcurve

Differential photometry was performed using *R*-band images. We used Lomb's algorithm for unevenly sampled data (Press et al. 1992) to extract the periodicity from relative magnitudes of 2005 UD. Ten field stars are selected as references. To combine measurements from different nights, we corrected the effect of the heliocentric and geocentric distance of the target. The change in the phase angle is about 0.2 degree during our observations, so was ignored. The Lomb periodogram for 2005 UD is shown in Fig. 1. The periodogram exhibits the maximum at a period of 2.6155 hours. Considering the lightcurve is due to the rotation of the irregularly shaped body, double the obtained periodicity 5.2310 hours is the actual rotational period. Fig. 2 is the phase curve assuming the periodicity of 5.2310 bf hours. Jewitt and Hsieh (2006) utilized the phase dispersion minimization (PDM) method to obtain the rotational period of 5.2492 hours, which is quite close to ours.

The lower limit of the axis ratio of 2005 UD is calculated from the amplitude of the lightcurve, assuming that the variability comes entirely from the elongated shape of the object. The amplitude of the lightcurve is 0.44 ± 0.02 mag, which implies the lower limit of the axis ratio of 1.50 from the relation

$$\frac{a}{b} > 10^{0.4\Delta m}, \tag{1}$$

where a/b is the axis ratio of primary and secondary axes, and Δm is the amplitude of the lightcurve. Assuming 2005 UD has a weakly connected rubble-pile structure, we can set the lower limit of the bulk density (Jewitt & Sheppard 2002; Ortiz et al. 2006). Giving the simple shape model of a Jacobi ellipsoid with an axis ratio of a/b = 1.50, and the rotation period of 5.2310 hours, the critical density of 2005 UD is estimated as 1.5×10^3 $kg\,m^{-3}$ by referring to the table in Chandrasekhar (1969). This lower limit implies an asteroidal picture for the bulk properties of 2005 UD, rather than the cometary picture. The amplitude of the lightcurve, axis ratio, and critical density agrees well with values reported by Jewitt and Hsieh (2006).

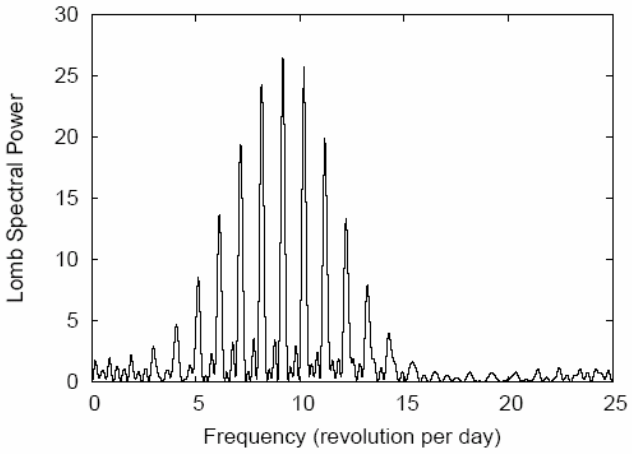

Fig. 1. The Lomb periodogram of 2005 UD. The highest peak corresponds to the period of 2.6155 hours.

2.2. Multi-color photometry

The multi-color photometry was performed with *B*, *V*, *R*, and *I* filters. The transformation coefficients were estimated using the "photcal" package of NOAO IRAF. We defined transformation equations as

$$B_{std} = B_{inst} + Z_B - k'_B X + C_B(B-V), \tag{2}$$
$$V_{std} = V_{inst} + Z_V - k'_V X + C_V(B-V), \tag{3}$$
$$R_{std} = R_{inst} + Z_R - k'_R X + C_R(V-R), \tag{4}$$
$$I_{std} = I_{inst} + Z_I - k'_I X + C_I(V-I), \tag{5}$$

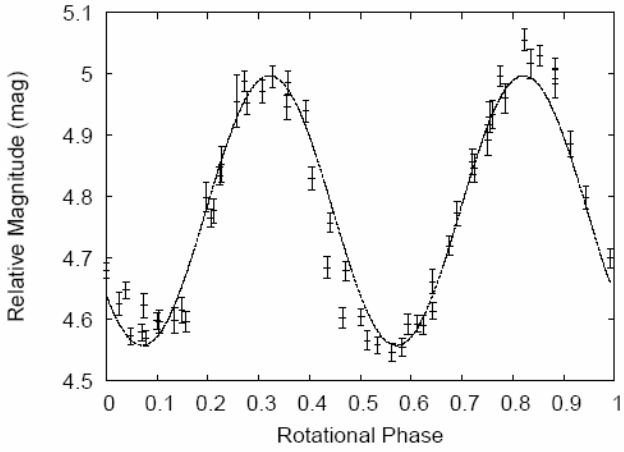

Fig. 2. The rotational phase curve of 2005 UD assuming periodicity of 5.2310 hours is shown. The dotted curve is the simple sinusoidal fit to the data. The fitted amplitude is 0.45 ± 0.02 mag.

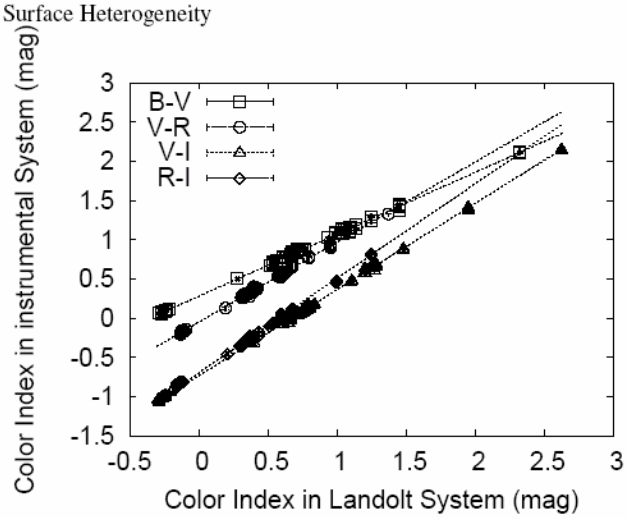

Fig. 3. Landolt colors and the atmospheric-extinction-corrected instrumental colors of Landolt photometric standards are plotted for $(B-V)$, $(V-R)$, $(V-I)$, $(R-I)$. The dotted straight lines are the least-square fit to the data. The data were obtained on November 3, 2005.

where B_{std}, V_{std}, R_{std}, I_{std} are the standard magnitudes, B_{inst}, V_{inst}, R_{inst}, I_{inst} are the instrumental magnitudes, Z_B, Z_V, Z_R, Z_I are photometric zero points, k'_B, k'_V, k'_R, k'_I are the first-order extinction coefficients, C_B, C_V, C_R, C_I are the color terms, and X is the airmass. The second-order extinction coefficients are found to be small on clear nights from our previous observations, so are neglected for this study. The transformation coefficients obtained on November 3, 4, and 5, 2005 are summarized in Table 1. These values are in good agreement with those reported by Kinoshita et al. (2005). The color conversions between the instrumental system and the Landolt system are also performed. Fig. 3 shows an example result of the color-color conversion. The data points are fitted by straight lines. We used the following formulae,

$$(B-V) = c_{B-V} \times (b-v) + z_{B-V}, \quad (6)$$
$$(V-R) = c_{V-R} \times (v-r) + z_{V-R}, \quad (7)$$
$$(V-I) = c_{V-I} \times (v-i) + z_{V-I}, \quad (8)$$
$$(R-I) = c_{R-I} \times (r-i) + z_{R-I}, \quad (9)$$

where capital letters refer to the Landolt system and lower-case letters refer to the instrumental system. The coefficients c_{B-V}, c_{V-R}, c_{V-I}, c_{R-I}, z_{B-V}, z_{V-R}, z_{V-I}, and z_{R-I} are constants, and they are listed in Table 2. These values are also consistent with those reported by Kinoshita et al. (2005).

Table 1. The transformation coefficients on 3, 4, 5, November 2005.

	03/Nov/2005	04/Nov/2005	05/Nov/2005
Z_B	+22.77 ± 0.03	22.85 ± 0.01	22.83 ± 0.01
k_B	0.15 ± 0.02	0.18 ± 0.01	0.17 ± 0.01
C_B	+0.12 ± 0.01	+0.15 ± 0.01	+0.14 ± 0.01
Z_V	+23.08 ± 0.03	23.14 ± 0.01	23.11 ± 0.01
k_V	0.08 ± 0.02	0.10 ± 0.01	0.09 ± 0.01
C_V	−0.09 ± 0.01	−0.07 ± 0.01	−0.06 ± 0.01
Z_R	+23.04 ± 0.03	23.09 ± 0.01	23.05 ± 0.01
k_R	0.06 ± 0.02	0.07 ± 0.01	0.08 ± 0.01
C_R	−0.13 ± 0.02	−0.11 ± 0.01	−0.08 ± 0.01
Z_I	+22.37 ± 0.03	22.38 ± 0.01	22.36 ± 0.02
k_I	0.05 ± 0.02	0.04 ± 0.01	0.03 ± 0.01
C_I	+0.02 ± 0.01	+0.04 ± 0.01	+0.04 ± 0.01

Table 2. The coefficients of conversions between the Landolt colors and the instrumental colors, where the numbers in parentheses are errors of the fit.

	3/Nov/2005	4/Nov/2005	5/Nov/2005
c_{B-V}	1.270 (0.006)	1.264 (0.005)	1.266 (0.004)
z_{B-V}	-0.366 (0.005)	-0.359 (0.004)	-0.357 (0.003)
c_{V-R}	0.980 (0.005)	0.980 (0.004)	0.978 (0.004)
z_{V-R}	0.047 (0.002)	0.049 (0.002)	0.048 (0.002)
c_{V-I}	0.920 (0.003)	0.906 (0.002)	0.909 (0.003)
z_{V-I}	0.675 (0.002)	0.676 (0.002)	0.667 (0.002)
c_{R-I}	0.836 (0.005)	0.823 (0.005)	0.828 (0.004)
z_{R-I}	0.591 (0.002)	0.584 (0.002)	0.577 (0.002)

Using the results of the photometric calibration shown above, we derived surface colors of 2005 UD. The photometry was done using a circular aperture three times larger than FWHM. After the atmospheric extinction correction, we scaled individual *BVRI* photometric measurements to the average brightness, using the rotational phase. Then, instrumental colors were converted into the standard colors. The mean colors of 2005 UD averaged over the entire rotational lightcurve are summarized in Table 3. These mean colors are plotted in the $(B-V, V-R)$ space, together with the typical colors of major sub-groups of asteroids in Fig. 4. Similar to those of asteroids with primordial characteristics (cf. C-type and its subclasses), 2005 UD exhibits a bluish surface. From the broadband photometry, 2005 UD is most likely an F-type or B-type asteroid. Our measurements of the mean colors of 2005 UD agree with those of (3200) Phaethon (Skiff et al. 1996; Dundon 2005). This similarity in surface colors between 2005 UD and (3200) Phaethon supports the hypothesis that 2005 UD is a fragment of (3200) Phaethon. Recently, Jewitt and Hsieh (2006) has also reported the photometric measurements of 2005 UD. Their measurements of the mean colors of 2005 UD are consistent with ours.

Next, we checked the color variation during the rotation of 2005 UD. Figures 5-7 show the $(B-V)$, $(V-R)$, $(R-I)$ colors of 2005 UD at different rotational phases. In addition to our own measurements, results from Jewitt and Hsieh (2006) are also superimposed on the figures. In all three figures, there is no inconsistency between this work and Jewitt and Hsieh (2006). The $(R-I)$ color is not uniform, and the color variation is recognized

in Fig. 7, where it exhibits bluer at the rotational phase of 0.9-0.3. It is not as clear as $(R-I)$, but possible variation is seen also in $(B-V)$ in Fig. 5. No clear trend is identified for $(V-R)$. Fig. 8 shows the scaled reflectance of 2005 UD normalized at the V-band. The rotational phase is divided into four regions (0.20-0.45, 0.45-0.70, 0.70-0.95, 0.95-0.20), and reflectances are shown for each of the rotational phase regions. These four regions correspond to the first maximum, first minimum, second maximum, and the second minimum of the lightcurve. For the rotational phase between 0.45 and 0.70, the spectra of 2005 UD are as neutral as these of the Sun (Fig. 8 B). At other rotational phase regions, a slight decrease in reflectance is found at the I-band (Fig. 8 A, C, D).

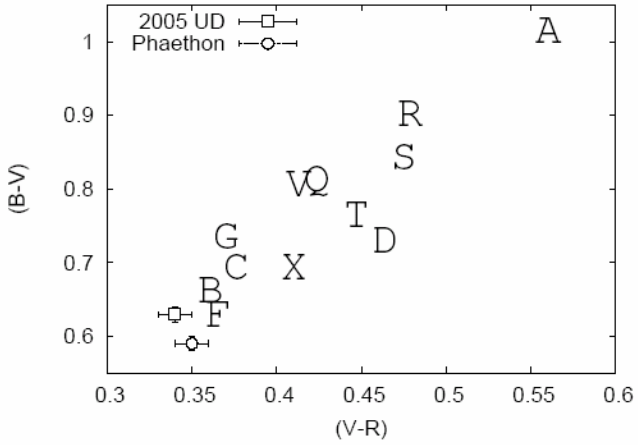

Fig. 4. The mean surface colors of 2005 UD from this work in the ($B-V$, $V-R$) two-color diagram using open squares. The result of surface color measurements of (3200) Phaethon from Dundon (2005) is also superimposed in the figure, using open circles. The capital letters denote typical colors of major sub-groups of asteroids. These values are from Dandy et al. (2003).

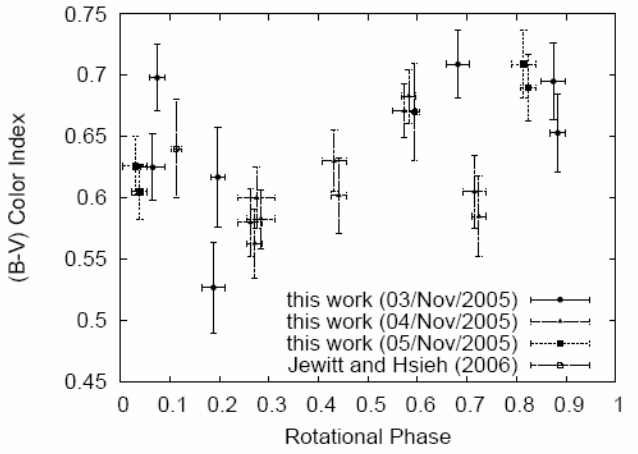

Fig. 5. The $(B-V)$ color of 2005 UD. The horizontal axis is the rotational phase. In addition to our own measurements, the results from Jewitt and Hsieh (2006) are also superimposed on the figure.

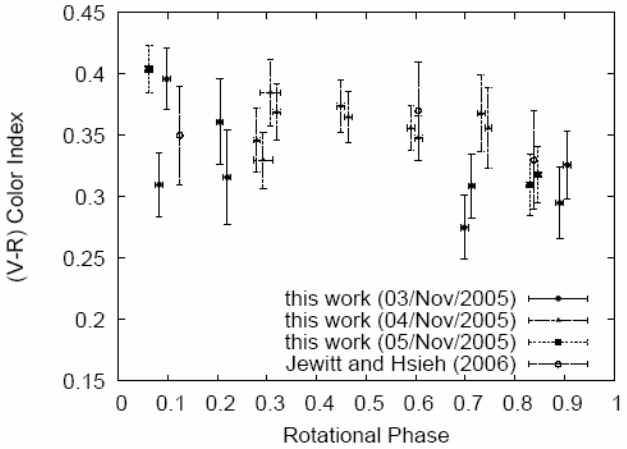

Fig. 6. Same as Figure 5, but for $(V-R)$.

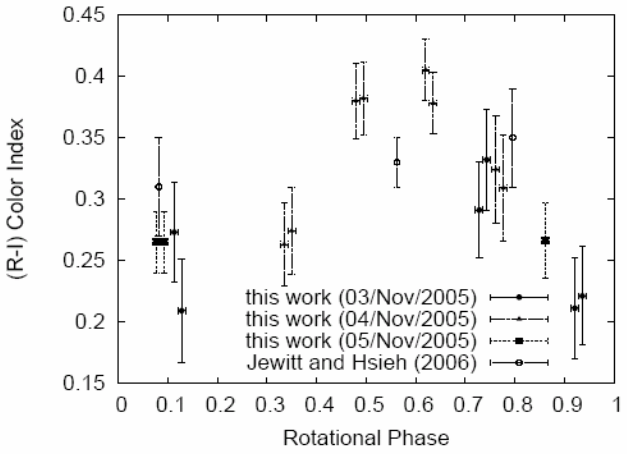

Fig. 7. Same as Fig. 5, but for $(R-I)$.

3. Discussion

The surface color of 2005 UD differs at different rotational phases. Such color variations are also found for (832) Karin, the largest member of the Karin family (Sasaki et al. 2004, Yoshida et al. 2004). The surface color heterogeneity does not seem to be rare for relatively young fragments. In the first-order approximation, the overall spectral behavior of 2005 UD is consistent with low-albedo carbonaceous asteroids.

We divide the surface of 2005 UD into two distinct areas. One is the surface of a C-type asteroid analogue with flat reflectance of mostly solar colors. The rotational phase between 0.45 and 0.70 corresponds to this area. The other is the surface of an F-type asteroid analogue with slightly bluer reflectance compared to the solar colors. The area other than the C-type analogue surface corresponds to this area. In current understanding, thermal metamorphism turns C-type asteroid materials into F-type asteroid materials. The dehydration of hydrated minerals may be the key process in this change. The surfaces of F-type asteroids are thought to experience high temperature. The temperature is high enough to dehydrate hydrated minerals, and they form anhydrous minerals after thermal metamorphism (Rivkin et al. 2002). The C-type analogue area is most likely to consist of less thermally processed materials. The main issue is the coexistence of C- and F-type materials on a single asteroid. In this

Table 3. The mean surface colors of 2005 UD.

	$B-V$	$V-R$	$R-I$	Ref.
2005 UD	0.63 ± 0.01	0.34 ± 0.01	0.30 ± 0.01	This work
2005 UD	0.66 ± 0.02	0.35 ± 0.02	0.33 ± 0.02	Jewitt et al. 2006
(3200) Phaethon	—	0.34	—	Skiff et al. 1996
(3200) Phaethon	0.59 ± 0.01	0.35 ± 0.01	0.32 ± 0.01	Dundon 2005

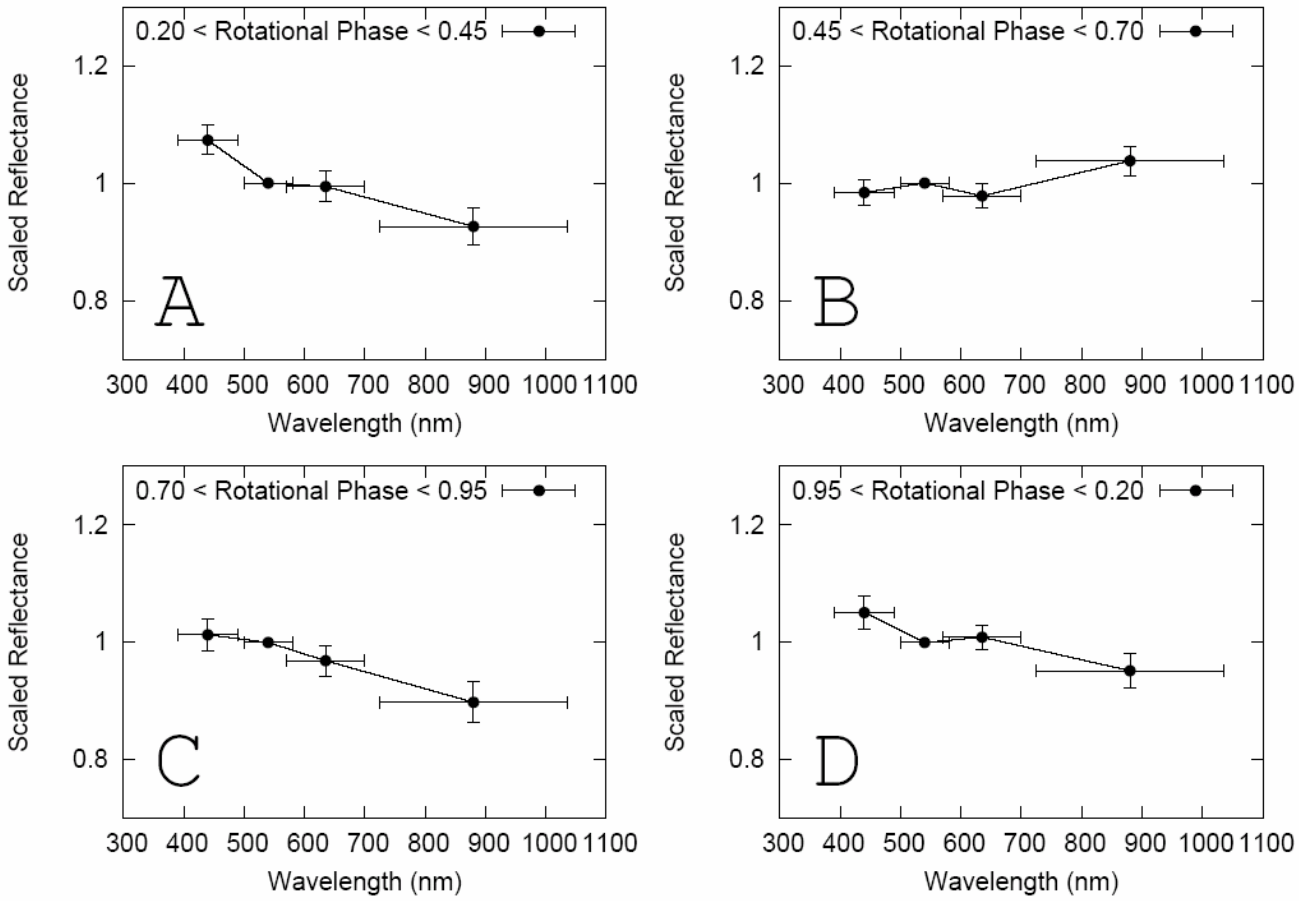

Fig. 8. Scaled reflectances normalized at the V-band of 2005 UD are shown. The rotational phase is divided into four regions (0.20-0.45, 0.45-0.70, 0.70-0.95, 0.95-0.20), and scaled reflectances are calculated for each rotational phase region. Panels A, B, C and D correspond to rotational phases of 0.20-0.45, 0.45-0.70, 0.70-0.95, and 0.95-0.20, respectively.

section, we discuss possible explanations for the surface heterogeneity of 2005 UD.

We assume the precursor object experienced fragmentation at some time in the past, after which the current (3200) Phaethon and 2005 UD were formed. If the split of the precursor object was due to the collision of two objects, part of 2005 UD may have come from the projectile. A simple explanation for the inhomogeneity of 2005 UD surface is that part of 2005 UD is from the precursor object and the rest is from the projectile. If the surface composition of the precursor object and the projectile are intrinsically different, the surface color variation of 2005 UD is easily understood. We call this the "precursor-projectile" model. The difficulty with this model is that the projectile must also be a bluish object, which is not a large population among near-Earth asteroids.

A second explanation is the combination of the alteration and resurfacing mechanism on the surface. It is widely accepted that the thermal alteration (or metamorphism) and space-weathering gradually changes the surface colors with time (ex. Sasaki et al. 2001). For asteroids of C-type and its subclasses, the thermal alteration makes the surface bluer (Hiroi et al. 1993). In addition, seismic shaking by impact or tidal distortion by planetary encounter may be mechanisms of resurfacing on 1-km or smaller sized asteroids (Saito et al. 2006), and these processes remove some portions of the altered surface layer. This resurfacing mechanism exposes the fresh materials on the surface. We call this the "alteration-resurfacing" model. The difficulty with this model is that the patchy surface may not be detected from the ground by disk-integrated photometry.

A third explanation is that we see the surface and subsurface of the precursor object on the surface of the current 2005 UD. The thermal history of the surface and subsurface of the precursor object must be different, and the current 2005 UD exhibits different surface properties on different sides. We call this the

"surface-subsurface" model. A part of the surface on 2005 UD that originated on the surface of the precursor object is likely to be covered with more anhydrous mineral. Another part of the surface that originated in the subsurface of the precursor object is probably covered with more hydrated mineral. The important factor for this model is the timescale of the alteration. If the timescale of the alteration is short enough compared to the time elapsed from the fragmentation of the precursor, no difference may be detected in the degree of alteration. Thus, this model requires that the age of 2005 UD be relatively young.

The last explanation is based on the topographical structure on the surface. A number of spacecraft explorations have revealed the existence of large craters on the surfaces of asteroids. Asteroids can support craters with sizes comparable to their diameters (Thomas 1999). The surface of an asteroid is excavated when a crater is formed so one can expect fresh materials to be exposed in the crater. We call this the "cratering-exposition" model. Similar to the discussion for the surface-subsurface model, the age of the crater must be less than the timescale of the alteration of the surface. However, the formation time of 2005 UD is less restricted for this model. The age of 2005 UD can be as old as the typical dynamical lifetime of near-Earth asteroids.

We believe that either the surface-subsurface or cratering-exposition model is more plausible to explain the surface heterogeneity of 2005 UD. To test these ideas, a combination of more observations, theoretical work, and laboratory experiments are essential. For observational study, spectroscopic monitoring covering the entire rotational phase is strongly encouraged. Time-resolved polarimetric measurements are also effective.

4. Summary

An Apollo-type near-Earth asteroid 2005 UD has been considered to be associated with the daytime Sextantids meteor stream and to be a fragment of (3200) Phaethon. To test this hypothesis, we performed photometric observations of 2005 UD using the 1-m telescope at Lulin Observatory in Taiwan to test this hypothesis. The time-resolved photometry in the R-band showed a rotational period of 5.2310 hours. The lower limit of the axis ratio $a/b \sim 1.50$ is estimated from the amplitude of the lightcurve. The lower limit of the bulk density of 2005 UD is estimated as 1.5×10^3 kg/m^3. Results of multi-color photometry show a bluish surface for 2005 UD, which is consistent with (3200) Phaethon, and this supports the hypothesis that 2005 UD is a km-sized fragment of (3200) Phaethon. Furthermore, surface colors of 2005 UD exhibit variations during the rotation of the body. This surface inhomogeneity may be associated with the fragmentation or collisional processes.

Acknowledgements. We would like to express our hearty thanks to Mr. Jun-Shiung Shih, Mr. Jing-Chuan Du, Mr. Hao-Wei Shih, and Mr. Zong-Jing Wan for their local support at Lulin Observatory. One of the authors (KD) thanks the fellowship from the Japan Society for Promotion of Science (ID: 15-1-2-02681-1) that provided partial support for this study. This work was also supported in part by the Ministry of Education of Taiwan under the "Aim for Top University Program". Authors also would like to thank Dr. Tatsuaki Okada, Prof. Sho Sasaki, and Dr. Masanao Abe for fruitful discussions at the 3rd annual meeting of AOGS in Singapore and 36th COSPAR scientific assembly in Beijing.

References

Arakida, H., Fukushima, T., 2000, AJ, 120, 3333.
Arakida, H., Fukushima, T., 2001, AJ, 121, 1764.
Chamberlin, A. B., McFadden, L.-A., Schulz, R., Schleicher, D. G., Bus, S. J., 1996, Icarus, 119, 173.
Chandrasekhar, S., 1969, in "Ellipsoidal Figures of Equilibrium", Dover Publication, ISBN 0-486-65258-0.
Cochran, A. L., Berker, E. S., 1984, Icarus, 59, 296.
Dundon, L., 2005, master thesis at University of Hawaii.
Dandy, C. L., Fitzsimmons, A., Collander-Brown, S. J., 2003, Icarus, 163, 363.
Green, S., Kowal, C., 1983, IAU Circular, 3878.
Gustafson, B. A. S., 1989, A&A, 225, 533.
Hiroi, T., Pieters, C. M., Zolensky, M. E., Lipschutz, M., 1993, Science, 261, 1016.
Hsieh, H. H., Jewitt, D., 2005, ApJ, 624, 1093.
Jewitt, D., Hsieh, H., 2006, AJ, 132, 1624.
Jewitt, D., Sheppard, S., 2002, AJ, 123, 2110.
Kinoshita, D., Chen, C.-W., Lin, H.-C., Lin, Z.-Y., Huang, K.-Y., Chang, Y.-S., Chen, W.-P., 2005, ChJAA, 5, 315.
Landolt, A. U., 1992, AJ, 104, 340.
McNaught, R. H., McGaha, J. E., Young, J., Christensen, E. J., Beshore, E. C., Garradd, G. J., Grauer, A. D., Hill, R. E., Kowalski, R. A., Larson, S. M., Tibbets, D., Hug, G., Hutsebaut, R., Jacques, C., Pimentel, E., Miles, R., Birtwhistle, P., Marsden, B. G., Minor Planet Electronic Circ., 2005-U22.
Mink, D. J., 2002, Proceedings of *Astronomical Data Analysis Software and Systems XI*, ASP Conference Proceedings, Vol. 281. Edited by Bohlender, D. A., Durand, D., and Handley, T. H., ISBN: 1-58381-124-9, pp. 169.
Nakano, S., 2005, http://www.spaceguard.or.jp/ja/mpnews/0036.html (in Japanese)
Ohtsuka, K., Sekiguchi, T., Kinoshita, D., Watanabe, J., 2005, Central Bureau Electronic Telegrams, 283.
Ohtsuka, K., Sekiguchi, T., Kinoshita, D., Watanabe, J., Ito, T., Arakida, H., Kasuga, T., 2006, A&A, 450, L25.
Ortiz, J. L., Gutierrez, P. J., Santos-Sanz, P., Casanova, V., Sota, A., 2006, A&A, 447, 1131.
Press, W., Flannery, B. P., Teukolsky, S. A., Vetterling, W. T., 1992, *"Numerical Recipes in C: The Art of Scientific Computing"*, Cambridge University Press, ISBN 0521431085.
Rivkin, A. S., Howell, E. S., Vilas, F., Lebofsky, L. A., 2002, Asteroids III, University of Arizona Press, ISBN 0-8165-2281-2, pp. 235.
Saito, J, Miyamoto, H., Nakamura, R., Ishiguro, M., Michikami, T., Nakamura, A. M., Demura, H., Sasaki, S., Hirata, N., Honda, C., Yamamoto, A., Yokota, Y., Fuse, T., Yoshida, F., Tholen, D. J., Geskell, R. W., Hashimoto, T., Kubota, T., Higuchi, Y., Nakamura, T., Smith, P., Hiraoka, K., Honda, T., Kobayashi, S., Furuya, M., Matsumoto, N., Nemoto, E., Yukishita, A., Kitazato, K., Dermawan, B., Sogame, A., Terazono, J., Shinohara, C., Akiyama, H., 2006, Science, 312, 1341.
Sasaki, S., Nakamura, K., Hamabe, Y, Kurahashi, E., Hiroi, T., 2001, Nature, 410, 555.
Sasaki, T., Sasaki, S., Watanabe, J., Sekiguchi, T., Yoshida, F., Kawakita, H., Fuse, T., Takato, N., Dermawan, B., Ito, T., 2004, ApJ, 615, L161.
Skiff, B. A., Buie, M. W., Bowell, E., 1996, BAAS, 28, 1104.
Thomas, P. C., 1999, Icarus, 142, 89.
Whipple, F. L., 1983, IAU Circular, 3881.
Williams, I. P., Wu, Z., 1993, MNRAS, 262, 231.
Yoshida, F., Dermawan, B., Ito, T., Sawabe, Y., Haji, M., Saito, R., Hirai, M., Nakamura, T., Sato, Y., Yanagisawa, T., Malhotra, R., 2004, PASJ, 56, 1105.

A&A 450, L25–L28 (2006)
DOI: 10.1051/0004-6361:200600022

Astronomy & Astrophysics

Apollo asteroid 2005 UD: split nucleus of (3200) Phaethon?

K. Ohtsuka[1], T. Sekiguchi[2], D. Kinoshita[3], J.-I. Watanabe[2], T. Ito[2], H. Arakida[2], and T. Kasuga[4]

[1] Tokyo Meteor Network, Daisawa 1–27–5, Setagaya-ku, Tokyo 155–0032, Japan
e-mail: ohtsuka@jb3.so-net.ne.jp
[2] National Astronomical Observatory of Japan, Osawa 2–21–1, Mitaka, Tokyo 181–8588, Japan
[3] Institute of Astronomy, National Central University, 300 Jhongda Rd, Jhongli, Taoyuan 32001, Taiwan
[4] The Graduate University for Advanced Studies, Osawa 2–21–1, Mitaka, Tokyo 181–8588, Japan

Received 14 December 2005 / Accepted 7 March 2006

ABSTRACT

Context. The recently discovered Apollo asteroid 2005 UD is the most likely candidate for being a large member of the Phaethon-Geminid stream Complex (PGC).
Aims. Detecting more complex members like this should clarify the formation and evolution of the PGC.
Methods. Our backward and forward (±10 000-yr) integration of the Kustaanheimo-Stiefel regularized equation of motion revealed that the orbital evolutions of Apollo asteroids (3200) Phaethon and 2005 UD show a similar profile, time-shifting by ~4600 yr.
Results. Within the PGC, this time shift is rather large against the time-lag of 220 yr for Phaethon-Geminids and ~3900 yr between Phaethon-Sextantids, although much smaller than that of ~19 000 yr between Phaethon-Canis Minorids.
Conclusions. This is a km-order object, hence may be a split nucleus of Phaethon. Besides, the orbital parameters of 2005 UD and the Sextantids are in good agreement along with the time-lag of 100 yr. Therefore, the Sextantid meteor shower seems to be associated more closely with 2005 UD than Phaethon.

Key words. minor planets, asteroids – methods: numerical – meteors, meteoroids

1. Introduction

Apollo asteroid (3200) Phaethon (=1983 TB) is probably one of the dormant or extinct cometary nuclei from the point of view of the parent of the Geminid meteor stream (Whipple 1983; Ryabova 2001 etc.). In fact, the total mass of the Geminid meteor stream is comparable to those of other major meteor streams of cometary origin (Jewitt 2004). The current orbital parameters of Phaethon are: semimajor axis (a) ~1.27 AU (astronomical unit); eccentricity (e) ~ 0.89, thus perihelion distance (q) ~ 0.14 AU along with inclination (i) ~ 22°; however, it has a shorter orbital period of 1.43 yr than any known short-period comets.

Before the discovery of Phaethon in 1983, likely multi-meteor showers, an association between the Geminids, the Sextantids, and the Canis Minorids, had already been pointed out by Nilsson (1964), Cook (1973), and Kresáková (1974). After the discovery, Babadzhanov & Obrubov (1987, 1992) simulated the long-term orbital motion of Phaethon, stably changing with a long-period perturbation cycle of ~40 000 yr. Then a large-amplitude q-i oscillation arises, with a period equal to half the cycle, i.e. ~20 000 yr, during which the argument of the perihelion (ω) changes by ~180°. Babadzhanov & Obrubov also found that Phaethon regularly becomes an Earth-crosser over such a long-term history; consequently they predicted the occurrences of four meteor showers originating in Phaethon at four different nodal points. After all, Babadzhanov & Obrubov (1993) successfully reconciled their theoretical meteor shower model with observations. These associated meteor showers are currently observable: Geminids (shower maximum on December 14) and (day time) Sextantids (max. Oct. 2) as active meteor showers; Canis Minorids (max. Dec. 10) and (day time) δ Leonids (max. Oct. 5?) as rather weak ones. Therefore, the detection of such multi-meteor showers should be strongly evident in the formation of the Phaethon-Geminid stream Complex (hereafter, called PGC), probably formed during Phaethon's active cometary phase long ago. A stream complex formation is considered to be dust particles, released at near perihelion every return from a short-period comet with stable, rather than chaotic, cyclic long-term orbital evolutions, moving away from the comet as time goes by. Eventually, the dust particles should be distributed in and around entire space, drawn by such cyclic orbital changes of cometary motion under planetary perturbations and nongravitational effects. Evidence of the Geminid fireball activities of medieval times (Astapovich & Terentjeva 1968) should also support such a spatial spread of PGC.

Although a number of attempts to obtain signs of Phaethon's cometary activity have been carried out, no trace of cometary activities has been detected yet (e.g., Hsieh & Jewitt 2005; Kraemer et al. 2005). The spectral feature of Phaethon is rather bluish, i.e., classified in Tholen's

Table 1. Orbital parameters of (3200) Phaethon and 2005 UD (equinox J2000).

Object	(3200) Phaethon		2005 UD
osculation epoch (TT)	2005 Aug. 18.0	−2581 Aug. 18.0	2005 Aug. 18.0
mean anomaly M	115°.81866	117°.04318	353°.33143
perihelion distance q (AU)	0.1398186	0.1534601	0.1629124
semimajor axis a (AU)	1.2713838	1.2737898	1.2747596
eccentricity e	0.8900265	0.8795248	0.8722015
argument of perihelion ω	321°.99112	207°.64364	207°.46774
longitude of ascending node Ω	265°.41395	22°.12450	19°.84550
inclination i	22°.17403	28°.32959	28°.74946
# of observations	1496		287
arc (oppositions)	1983–2005 (19)		Oct. 22–Nov. 17
RMS residual	0″.58		0″.25
absolute mag. H	14.5		17.5
reference	JPL	this work	Nakano (2005)

taxonomy of F-type, as opposed to those of typical cometary nuclei being slightly reddish in general (Tholen 1985; Luu & Jewitt 1990; Binzel et al. 2004 etc.). The absolute magnitude (H) and the albedo are 14.5 and 0.11 (e.g., Harris 1998), respectively, which is equivalent to a diameter of ∼5 km. Other orbital and physical data for Phaethon are summarized on the "Near Earth Objects Dynamic Site" (`http://131.114.72.13/cgi-bin/neodys/neoibo`) and "Database of Physical and Dynamical Properties of Near-Earth Asteroids" (`http://earn.dlr.de/nea/003200.htm`).

According to the orbital study by Ohtsuka et al. (1997), Phaethon approaches the Sun up to 27 $R_\odot$ (solar radius), i.e., ∼0.126 AU, in the minimum-q phase ∼1900 yr ago. Considering its low albedo, the sunny-side surface should be heated over 1000 K, at which temperature the phyllosilicates in CI and CM chondrites decompose into olivine, magnetite and anhydrite, etc. (e.g., Nozaki et al. 2006), and the chondritic dust particles may be destroyed (e.g., Mann et al. 2004). Indeed, F-type asteroids, like Phaethon, are regarded as being anhydrous and thermally metamorphosed (Hiroi et al. 1993; Rivkin et al. 2002), and the Geminid meteoroids experienced a thermal history, probably due to the Sun (Halliday 1988; Kasuga et al. 2005). Moreover, a solar thermal stress seems to be a trigger, not only to generate a meteor-stream complex, but also to split and disintegrate a comet such as the 96P/Machholz-Quadrantid stream complex including the near-sun (i.e., sunskirting) Marsden and Kracht comet groups detected by the space-borne coronagraph, SOHO/LASCO (Ohtsuka et al. 2003; Sekanina & Chodas 2005). Their minimum q reaches up to ∼6 $R_\odot$, then their surface temperature rises at least 1.5 times higher than that of Phaethon. The other sunskirters, Meyer and Kracht II comet groups, along with q of 8–12 $R_\odot$ (Meyer 2003; Hoffman & Marsden 2005; Hönig 2005), would also accompany their complex streams. Therefore, the formation of the PGC may imply the existence of some large members as a split cometary nucleus or fragments among the PGC.

We have long believed our working hypothesis mentioned above, and have been searching for large PGC members. Finally, we found a candidate: a recently discovered Apollo asteroid, 2005 UD.

2. Orbital evolution of Phaethon

In the first stage of stream-complex formation, the orbital energy (a^{-1}) of released meteoroids, fragments, and split nuclei from the parent comet must become slightly different from that of the parent. This results in differences in their evolutional rates. The time-lags (hereafter, called Δt) between orbital evolutions of the parent comet and released matter should be longer with time. Therefore, a large PGC member, if there are any, should be in orbital similarity with Phaethon, shifting by Δt.

As preliminary work for a PGC survey (mentioned in the next chapter) and for determining the Δt of Phaethon with unknown potential PGC members, first of all, we have begun with the orbital evolution of Phaethon. We performed here the backward and forward numerical integration of the KS (Kustaanheimo-Stiefel) regularized equation of motion (cf. Arakida & Fukushima 2000, 2001) over the term of 10 000 BC to 10 000 AD (JDT −1 931 503.5 to JDT 5 373 520.5), applying the 12th-order Adams method in double precision with a step size of 0.5 day. We have confirmed that the results of the numerical integration did not significantly change, even when we adopted smaller step size or when we used other integration methods such as the extrapolation method. The initial orbital data of Phaethon at osculation epoch 2005 Aug. 18.0 TT = JDT 2 453 600.5 were taken from "JPL's HORIZONS System" (`http://ssd.jpl.nasa.gov/horizons.html`), as listed in Table 1. All the major planets from Mercury through Pluto were included as perturbing bodies, in which the mass of the moon was added to that of the Earth, and the barycenter of their masses was taken as Earth's position. The coordinates of the major planets were taken from the JPL Planetary and Lunar Ephemeris DE408.

3. Survey

3.1. Process

We surveyed whether there are the large PGC members or not among "the List of Apollo Minor Planets"

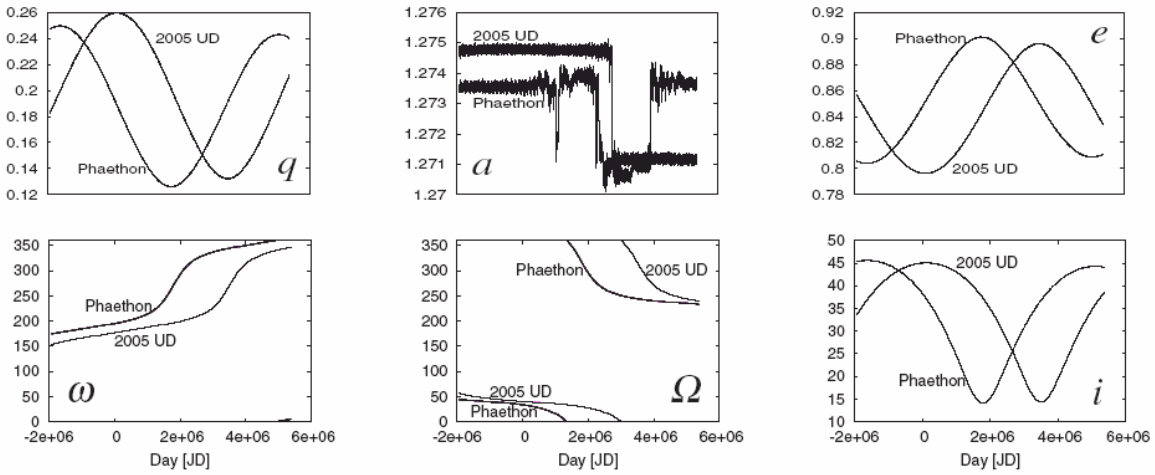

Fig. 1. Orbital evolutions of (3200) Phaethon (thick line) and 2005 UD (thin line), where six graphs show: perihelion distance q in AU (*upper left*); semimajor axis a in AU (*upper center*); eccentricity e (*upper right*); argument of perihelion ω in degree (*lower left*); longitude of ascending node Ω in degree (*lower center*); and inclination i in degree (*lower right*). The abscissa of all is time in Julian Terrestrial Date (JDT).

(`http://cfa-www.harvard.edu/iau/mpc.html`) and latest MPECs (Minor Planet electric circulars).

As of 2005 November 3, a total of 1758 Apollo asteroids are recorded in the database, among which we directed our attention to 62 Apollos with $q < 0.3$ AU, since q of Phaethon has never been beyond 0.26 AU in our orbital computation. We applied here the following three criteria as the retrieving engine for our survey: the first criterion is traditional $D_{\rm SH}$ (Southworth & Hawkins 1963), since in investigating the orbital similarity between two bodies, e.g., comet/asteroid and meteors, we often use $D_{\rm SH}$. Thus, we traced such a large PGC member on the basis of the Phaethon's orbital evolution from the integration. For each Apollo, we found the minimum $D_{\rm SH}$ between it and Phaethon, as Phaethon's orbit evolves. When this minimum value of $D_{\rm SH}$ is below 0.15, this means that Phaethon and the given Apollo are within the probable association range.

The second and third criteria are C_1 and C_2 integrals for the candidate selected by $D_{\rm SH}$. They were derived by Moiseev (1945) and Lidov (1961), respectively, given as:

$$C_1 = \left(1 - e^2\right)\cos^2 i, \tag{1}$$

$$C_2 = e^2\left(0.4 - \sin^2 i \, \sin^2 \omega\right). \tag{2}$$

These integrals describe the secular orbital variations well. Babadzhanov & Obrubov (1987, 1992) demonstrated that both C_1 and C_2 integrals are almost invariant in their 20 000-yr backward integration of Phaethon's orbit: ~0.18 and ~0.27, respectively. Therefore, C_1 and C_2 integrals should also be useful criteria to distinguish a PGC member.

3.2. Detection of the candidate: Apollo asteroid 2005 UD

By these procedures, we finally detected a candidate large PGC member, "Apollo asteroid 2005 UD", recently discovered in the Catalina sky survey on 2005 October 22 (MPEC 2005–U22). The orbital elements at epoch 2005 Aug. 18.0 TT = JDT 2 453 600.5, listed along with Phaethon in Table 1, were taken from Nakano's (2005) solution, based on 287 positions during an arc of 2005 October 22 to November 17 (27 days) with a rms residual of $0''.25$. $H \sim 17.5$ corresponds to a km-order size object. Among these observations, a total of 183 positions along with multi-color measurements were carried out by one of the authors, D. Kinoshita, at Lulin Observatory (1.0-m reflector $f/8.0$ + CCD) from 2005 October 31 to November 5, when no cometary feature was detected. His results will be published elsewhere as a journal paper.

The current orbital parameters of 2005 UD match those of Phaethon in 2582 BC strikingly well, thus $\Delta t \sim 4600$ yr. Their $D_{\rm SH}$ is minimum at only 0.04, slightly larger compared with the well-established Phaethon-Geminids association of 0.02 (based on the data by Ohtsuka et al. 1997). The C_1 and C_2 parameters of 2005 UD fit those of Phaethon: 0.184 and 0.267, respectively.

Subsequently, using Nakano's data, we also integrated the orbital motion of 2005 UD using the same method as we applied to Phaethon in order to trace both dynamical behaviors of Phaethon and 2005 UD. The solutions of the orbital evolution for both objects are represented in Fig. 1. Phaethon and 2005 UD often closely encounter the terrestrial planets, however, neither of the orbital parameters look chaotic, but rather regular. It is also easy to understand that both orbital evolutions show similar profiles along with quasi-sinusoidal changes, shifting by $\Delta t \sim 4600$ yr.

4. Concluding remarks

We found that Apollo asteroid 2005 UD is the most likely candidate for a large member of the PGC. This is a km-order object, hence may be a split nucleus of Phaethon. We confirmed Δt between Phaethon and 2005 UD ~ 4600 yr, which is rather large as against Δt, being 220 yr for the

Table 2. 2005 UD, (3200) Phaethon, and the Sextantids (Sekanina 1976) at almost the same evolutional phase.

Object	Epoch (TT)	M	q (AU)	e	ω (2000.0)	Ω	i
2005 UD	1867 Aug. 18	36°.615	0.16570	0.87002	206°.356	20°.930	29°.519
Phaethon	−2688 Aug. 18	329°.118	0.15538	0.87800	206°.759	22°.996	28°.956
Sextantids	1969 Oct. 9	38°.0	0.172	0.816	212°.3	15°.8	31°.1

Phaethon-Geminids association and ∼3900 yr between the Phaethon-Sextantids (Ohtsuka et al. 1997), although much smaller than that of ∼19 000 yr between the Phaethon-Canis Minorids (Babadzhanov & Obrubov 1987). Ohtsuka et al. (1997) simply regard Δt of the orbital evolutions between Phaethon and presently observable associated meteor streams as an indicator of the meteor stream's age. Ohtsuka et al. also hypothesized that the larger Δt means an older age of the meteor stream and more dispersive spatial number density of the meteoroid stream. Really, the hourly rates, i.e., spatial number density of the meteoroid particles, for Geminids, Sextantids, and Canis Minorids are 60, 20, and 2 at most, respectively (Kresáková 1974; Ohtsuka et al. 1997). This suggests that the meteoroid particles are not uniformly distributed over the PGC. Of particular interest should be the relation between 2005 UD and the Sextantids. The orbital parameters of 2005 UD and the Sextantids, picked out by Sekanina (1976) among the Harvard (Havana) radio meteor orbit data, are currently in good agreement. As presented in Table 2, their Δt is only 100 yr, then $D_{\rm SH}$ is minimum at 0.08, while Δt between the Phaethon-Harvard Sextantids amounts to ∼4700 yr, along with somewhat larger $D_{\rm SH} = 0.10$. Therefore, the Sextantid meteor shower seems to be associated more closely with 2005 UD than with Phaethon, judging from Δt and $D_{\rm SH}$.

Another astronomical curiosity is to estimate the splitting time of 2005 UD from Phaethon. Both the dynamical behaviors are closely related with each other. However, Δt does not become much larger with time, since there is an imperceptible difference between the two evolutional rates. Such a tendency may cause us difficulty in estimating the splitting time on the basis of our rather short-term orbital solution. In addition, the semimajor axes may have small random changes (similar to those shown in Fig. 1) as a result of perturbations from the terrestrial planets in the long term, and the changes in semimajor axes could then cause changes in precession rates. This problem may be resolved by future work based on further long-term orbital studies.

Acknowledgements. The authors are grateful to Dr. David J. Asher for his constructive comments as the reviewer. Thanks are also due to Prof. Hiroshi Nakai for providing us with useful and detailed information on JPL's Development Ephemeris, DE408. Detailed and constructive review by Yolande McLean has considerably improved the English presentation of this paper. Numerical computations were carried out on a general common use computer system at the Astronomical Data Analysis Center, ADAC, of the National Astronomical Observatory of Japan.

References

Astapovich, I. S., & Terentjeva, A. K. 1968, in Physics and Dynamics of Meteors, ed. L. Kresak, & P. M. Millman (Dordrecht: D. Reidel), 308
Arakida, H., & Fukushima, T. 2000, AJ, 120, 3333
Arakida, H., & Fukushima, T. 2001, AJ, 121, 1764
Babadzhanov, P. B., & Obrubov, Yu. V. 1987, Publ. Astron. Inst. Czechosl., 2, 141
Babadzhanov, P. B., & Obrubov, Yu. V. 1992, Celest. Mech. Dyn. Astron., 54, 111
Babadzhanov, P. B., & Obrubov, Yu. V. 1993, Astron. Vest., 27, 110
Binzel, R. P., Rivkin, A. S., Stuart, J. S., et al. 2004, Icarus, 170, 259
Cook, A. F. 1973, in Evolutionary and Physical Properties of Meteoroids, ed. C. L. Hemenway, P. M. Millman, & A. F. Cook, NASA SP–319, 183
Halliday, I. 1988, Icarus, 76, 279
Harris, A. W. 1998, Icarus, 131, 291
Hiroi, T., Pieters, C. M., Zolensky, M. E., et al. 1993, Science, 261, 1016
Hoffman, T., & Marsden, B. G. 2005, Sky & Tel., Aug., 32
Hönig, S. F. 2006, A&A, 445, 759
Hsieh, H. H., & Jewitt, D. C. 2005, ApJ, 624, 1093
Jewitt, D. C. 2004, in Comets II, ed. M. C. Festou, H. U. Keller, & H. A. Weaver (Tucson: Univ. Arizona), 659
Kasuga, T., Watanabe, J., & Ebizuka, N. 2005, A&A, 438, L17
Kraemer, K. E., Lisse, C. M., Price, S. D., et al. 2005, AJ, 130, 2363
Kresáková, M. 1974, Bull. Astron. Inst. Czechosl., 25, 20
Lidov, M. L. 1961, Iskusstvennie Sputniki Zemli, 8, 5
Luu, J. X., & Jewitt, D. C. 1990, AJ, 99, 1985
Mann, I., Kimura, H., Biesecker, D. A., et al. 2004, Space Sci. Rev., 110, 269
Meyer, M. 2003, Int. Comet Quart., 25, 115
Moiseev, N. D. 1945, Trudy Gosudarstvennogo Astron. Inst. P.K. Shternberga, 15, 75
Nakano, S. 2005, Apollo asteroid 2005 UD, `http://www.oaa.gr.jp/~muramatu/mp/2005ud.htm`
Nilsson, C. S. 1964, Aust. J. Phys., 17, 158
Nozaki, W., Nakamura, T., & Noguchi, T. 2006, M&PS, in press
Ohtsuka, K., Shimoda, C., Yoshikawa, M., & Watanabe, J. 1997, EM&P, 77, 83
Ohtsuka, K., Nakano, S., & Yoshikawa, M. 2003, PASJ, 55, 321
Rivkin, A. S., Howell, E. S., Vilas, F., et al. 2002, in Asteroids III, ed. W. F. Bottke Jr. et al. (Tucson: Univ. Arizona), 235
Ryabova, G. O. 2001, in Proc. of Meteoroids 2001 Conf., ed. B. Warmbein, ESA SP–495 (Noordwijk: ESTEC), 77
Sekanina, Z. 1976, Icarus, 27, 265
Sekanina, Z., & Chodas, P. W. 2005, ApJS, 161, 551
Southworth, R. B., & Hawkins, G. S. 1963, Smithon. Contr. Ap., 7, 261
Tholen, D. J. 1985, IAU Circ., 4034
Whipple, F. L. 1983, IAU Circ., 3881

The merging structure of Abell S0721

Pei-Li Ho[a,b] and Lin-Wen Chen[b]

[a]*Astronomical Observatory, Central Weather Bureau, No. 64, Gongyuan Road, Taipei, Taiwan 10048, R.O.C.*
[b]*Department of Earth Sciences, National Taiwan Normal University, Taipei, Taiwan, R.O.C.*

Abstract

We present the correlation analyses of the central region of Abell S0721 by using the images taken by one-meter telescope at Lulin Observatory (LOT), as well as galaxy sample compiled from NASA Extragalactic Database (NED) and the ROSAT All Sky Survey (RASS) data. The correlation analysis of galaxy distributions between the member galaxies compiled from NED and the flux-limited galaxy samples imaged by LOT shows the distributions of galaxies in both datasets are similar. This result assures that the galaxy sample from NED is not biased by the sample selection for redshift measurement, and the previous dynamics analyses based on this galaxy sample are reliable. Furthermore, the correlation analysis between the optical structure and X-ray emission shows that two nearby X-ray clumps (of which one has been suggested as a cluster, and the other is still without optical identification) are likely related to galaxy group separately, and these two groups are probably merging with each other. These results provide additional evidence to support the possibility that S0721 is under merging.

1. Introduction

Abell S0721 is a poor cluster in the Shapley Supercluster, our recent work based on galaxy data with measured velocity from NED and survey data from ROSAT All Sky Survey (RASS) and NRAO VLA Sky Survey (NVSS, Condon et al. 1998) catalogues together show that S0721 is probably a cluster merger at its early stage (Ho and Chen, 2006).

To further check whether the galaxy data compiled from NED is biased by sample selection for redshift measurement and to investigate the connection of merging and the activity of member galaxies in detail, a 2-color photometric study is required. The photometric observations in R and B bands were taken on 2006 March 3 by Lulin One-meter Telescope (LOT). Here we use the images taken by LOT to carry out correlation analyses with the galaxy sample compiled from NED and the X-ray data from RASS.

2. Data

2.1 X-ray

The X-ray images from RASS III dataset are compiled from the ROSAT data archive (http://www.xray.mpe.mpg.de/cgi-bin/rosat/data-browser), the resolution of the images is 45"and the mean exposure time of our target region is about 320 sec. To reduce the Galactic contaminations, only the RASS image in the 0.5—2.4 keV band is used.

2.2 Optical

Optical images in both R and B bands were taken on 2006 March using the Lulin One-Meter Telescope with the PI1300B CCD (Kinoshita, 2005). The field of view is 11.5′×11.2′ with *f*/8. The limiting magnitude is about 19 in R and 20 in B with 450 and 600 seconds exposure time for R and B, respectively.

3. Result and Discussion

To check whether the dataset of galaxies with measured redshift compiled from NED is biased due selection effect for redshift measurement, the images of S0721 central region (11.5′×11.2′) in R and B are superposed with the contours of the member galaxy density, as shown in Fig.1. In this figure, two groups of galaxies are clearly shown in both cases, except a little offset for the group in the lower-right, the galaxy distribution patterns are almost consistent. As a result, this indicates that the sample selection bias of the galaxy sample compiled from NED is insignificant, and therefore our previous dynamics analyses based on this data sample are reliable.

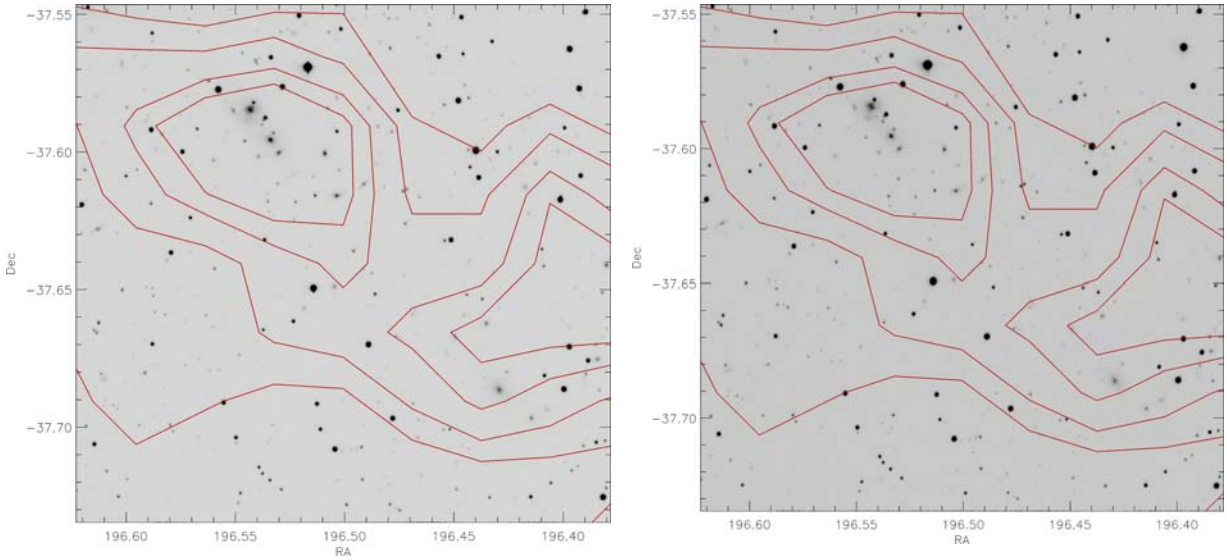

Fig. 1. The images of S0721 central region (11.5′×11.2′) in R (left) and B (right) bands observed by the LOT are superposed with the contours of surface number density of member galaxies, the contour levels are 3, 5, 8, 10σ.

For the correlation analysis between optical structure and X-ray emission, the image of S0721 central region in R is superposed with the contours of X-ray count rate density (background corrected) in the 0.5—2.4 keV band, and the positions of four X-ray sources detected by the RASS observation (Voges et al., 1999) are also labeled (see Fig. 2). In this figure, the distribution of galaxies and X-ray emission are in a similar elongated structure with same alignment. As to the X-ray clumps in this region, only one listed in the RASS Bright Source Catalogue (BSC) has been suggested as a cluster (Zimmermann et al., 2001), which is likely related to the galaxy group in the lower-right region. In addition, one X-ray clump listed in the RASS Faint Source Catalogue (FSC) seems to relate to the other galaxy group in the north-east, the offset between the group and the clump is probably caused by the velocity difference of galaxies and hot gas during its merging with other group.

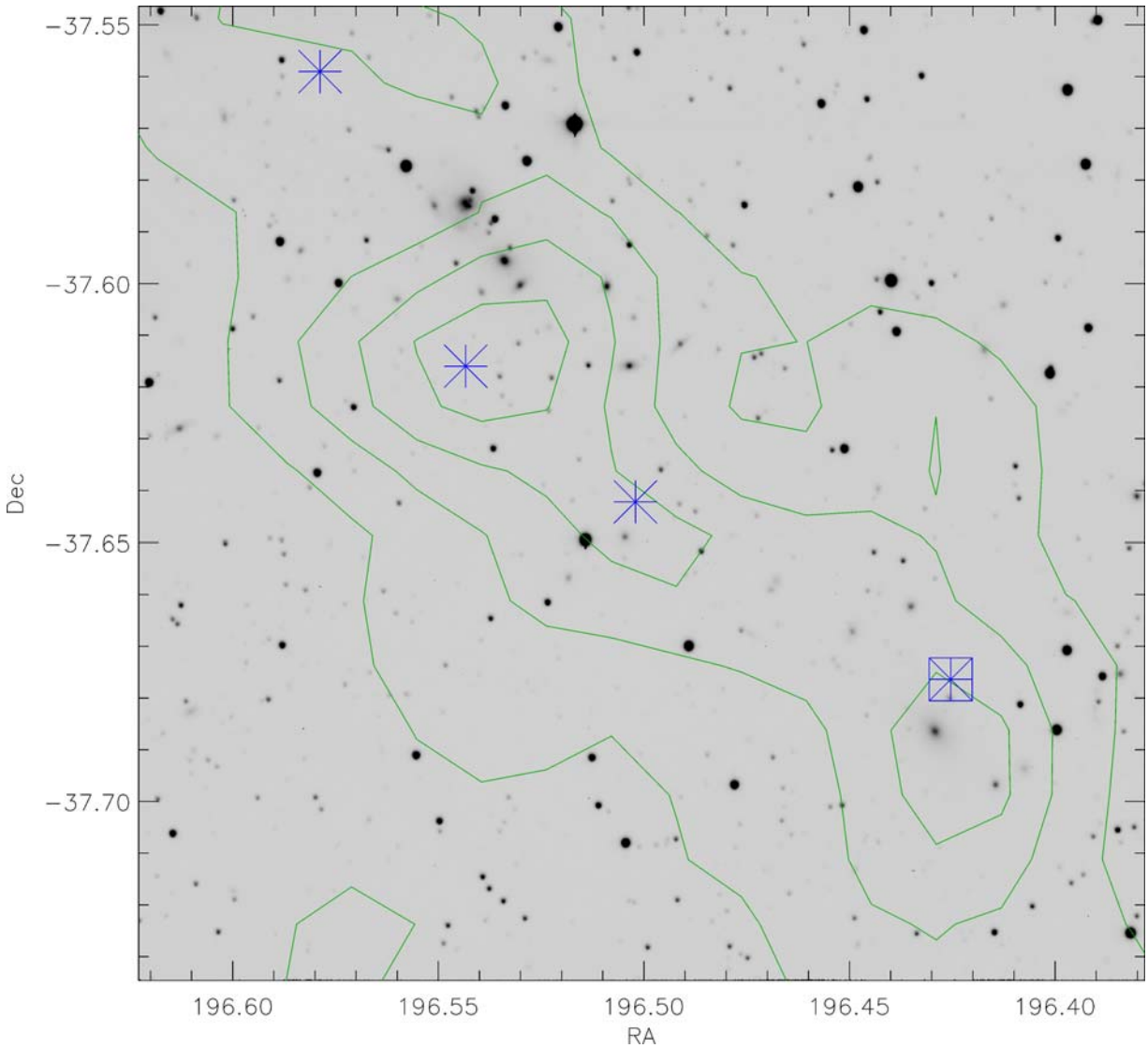

Fig. 2. The image of S0721 central region in R band observed by the LOT is superposed with the contours of X-ray count rate density (background subtracted). The contour levels are 3, 5, 7, 9 σ. The blue asterisks represent the positions of X-ray sources listed in the RASS FSC, and asterisk+square represents the source listed in the RASS BSC.

4. Summary

The correlation analyses in this report indicate that: 1) the galaxy sample with redshift compiled from NED is reliable in dynamics analyses; 2) two X-ray clumps are likely related to galaxy groups, and they are possibly merging with each other.

References

Condon, J. J. et al. 1998, AJ. 115, 1693-1716
Ho, P.-L., Chen, L.-W., 2006, 36th COSPAR Scientific Assembly, Beijing.
Kinoshita, D. et al., 2005, ChJAA, 5, 315
Voges, W. et al., 1999, A&A, 349, 389
Zimmermann, H.-U. et al., 2001, A&A, 378, 30

Acknowledgments

We thank Ting-Chang Yang at Lulin Observatory for the help in photometric observations. We also thank the ROSAT team at MPE for making the RASS X-ray data become available. This work has made use of the NASA Extragalactic Database NED.

Ground-based observation of asteroid sample return mission target.

M. Abe(JAXA), K. Kitazato(JAXA), Y. Sarugaku(JAXA), S. Nishihara(JAXA),
D. Kuroda(JAXA), D. Kinoshita(NCU), F. Yoshida(NAOJ), and W.-H. Ip(NCU)

Introduction: One of the important goals in the study of compositional characterization of asteroids is to understand the relationship between asteroids and meteorites. The asteroids are classified into some groups with similar spectral characteristics. The Japanese sample return mission, HAYABUSA, the spacecraft explored its target, near Earth asteroid (25143) Itokawa. The taxonomic type of Itokawa is S-type, and the spectrum of this type asteroid is similar to that of the ordinary chondrites [1]. The purpose of our observation is to obtain the information about taxonomic type and rotational status of the candidate target of the next asteroid sample return mission (post-HAYABUSA mission). This information is useful for mission targets selection and helpful for raising the technical feasibility of the exploration. Our goal is to find some primordial type asteroid, C-type and D-type, in our candidate objects. Considering several mission plans, we chose about 300 asteroids from NEAs as the candidate objects of the post-HAYABUSA mission. As the taxonomic types of more than 200 candidates are unknown, we have performed the colorimetric observations in order to obtain its taxonomic type information.

Observations and Data reductions: We have observed 14 near-Earth asteroids (NEAs) during December 2005 – December 2006, using the 1.05-m Kiso Schmidt telescope with 2kCCD in Japan, and the Lulin One-meter Telescope with PI1300B in Taiwan. Including our previous results [2], 32 NEAs had been observed during 2003-2006. The observational log is summarized in Table 1. We made multicolor photometry at clear-stable nights, using broadband filter, B, V, R, and I.

Classification: We classified our objects in broad groups, C-type group, S-type group, D-type group, and X-type group. We obtained BVRI photometry data for 21 mission candidates, and classified 19 objects in broad groups. Out of 19 candidates, we found that 5 asteroids are classified in C-type group. Obtained spectra of observed C-type group asteroids are shown in Figure 1.

References: [1] Abe et al. (2002) *LPS XXXIII*, Abstract#1666. [2] Nishihara et al. (2006) *LPS XXXVII*, Abstract#2352.

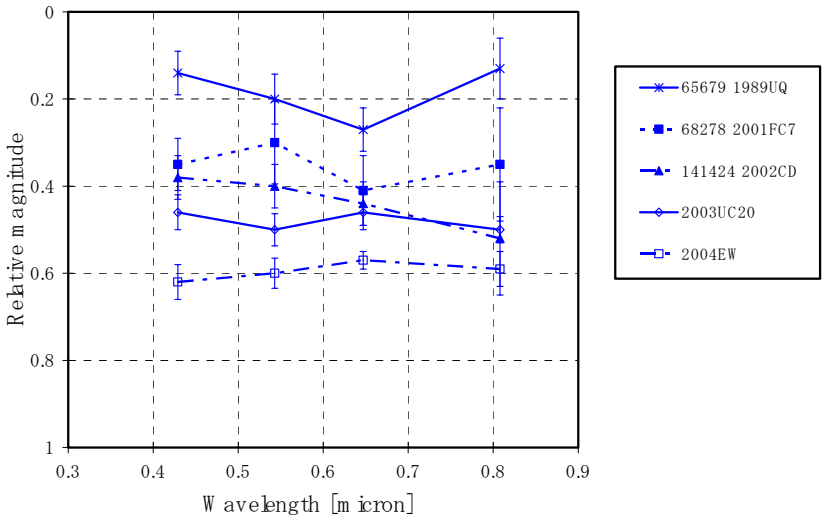

Figure 1: Obtained spectra of observed C-type group asteroids.

Table 1: Observational log. Observatory mark L: Lulin Observatory in Taiwan, K: Kiso Observatory in Japan.

Asteroid	Date Observed (observatory)	Filter used
3361 Orpheus	2005/10/14(K), 2005/11/28(L)	BVRI
5797 Bivoj	2005/10/24(K), 2005/12/22,24,26,28(K), 2006/2/4(K)	BVRI
25143 Itokawa	2001/3/26,29,31(K) 2001/4/1(K), 2001/8/22,23,24(K), 2003/12/1,2,3,4(K), 2004/1/19,20,21(K), 2004/4/10,11,12(K), 2006/11/24,25,28(K), 2006/12/18,19,20,21,22(L)	R
65679 1989UQ	2003/9/26,29,30 (K)	BVRI
65803 Didymos	2003/12/1,3,4 (K), 2004/1/20 (K)	BVRI
68278 2001FC7	2003/9/26,29,30 (K), 2006/2/4,5(K)	BVRI
68359 2001OZ31	2005/10/24(K)	RI
85585 Mjolnir	2003/9/28,29,30 (K)	BVRI
89136 2001US16	2004/4/10,11,12 (K)	RVI
98943 2001CC21	2003/9/29 (K), 2003/12/2 (K)	RVI
103066 1999XO141	2005/8/31 (L), 2005/9/11 (L)	R
11284 Belenus	2005/10/25(K), 2005/11/25,26,27(L), 2005/11/29,30(K), 2005/12/1(K)	BVRI
136618 1994CN2	2006/3/29(L)	BVRI
137799 1999YB	2005/11/25,26,27 (L), 2005/11/29,30(K)	BVRI
138404 2000HA24	2006/4/24,28,29(K)	BVRI
141018 2001WC47	2006/11/28(K), 2006/12/18,19,20,21,22(L)	BVRI
141424 2002CD	2004/4/10,11,12) (K), 2006/3/28(L)	BVRI
142348 2002RX211	2005/8/29 (K), 2005/9/11 (L), 2005/11/25,26 (L), 2005/11/30(K), 2005/12/22,24,26,28(K)	BVRI
2000QK25	2005/11/25,28 (L), 2005/11/29(K), 2005/12/14,28(K)	BVRI
2002CE10	2003/9/26,28 (K)	R
2002TD60	2006/11/24,25(K)	R
2003UC20	2003/12/3,4 (K), 2005/11/26 (L), 2006/2/5(K)	BVRI
2003CY18	2005/6/3 (K), 2005/9/11 (L), 2005/10/24 (K)	BVRI
2003RB	2003/9/28,29,30 (K)	BVRI
2003SD220	2003/12/1,2,3 (K), 2006/11/,25,28(K), 2006/12/21,22(L)	BVRI
2004DK1	2004/4/11 (K)	RVI
2004EW	2005/3/5(L), 2005/3/7,8(K), 2005/5/5 (L), 2006/3/28,29(L)	BVRI
2005ED318	2005/6/3 (K)	R
2005JU108	2005/8/29,31 (K)	R
2005TF	2005/11/30(K), 2005/12/26,27,28(K), 2006/2/5(K)	BVRI
2006GB	2006/4/25,27,28,29(K)	BVRI

Photometry on Variable Candidates from the Pisgah Survey

An-Le Chen / Taipei Astronomical Museum

In the Pisgah survey (Lopez-Morales & Clemens, 2004), two objects show interesting light variations among the 20 variable candidates. PS-1-vs0038 reveals irregular light variations but was classified by the Combined GCVS (Kholopov et al. 1998) as an "unstudied variable with rapid light changes". The amplitude of the light variation is about 0.25 mag, which is low and one of the characteristics of nova-like variable. The authors made observations with a time-resolution of 180s. Thus possible rapid variations such as flickering and QPOs may be smoothed out. An observation with better time-resolution is worth trying in order to understand its nature.

PS-6-vs0262 was classified as an EW binary. Its light curve may resemble a light curve with reflection effect. Spectroscopy and multi-colour photometry are required to examine the possibility.

I appreciated that the telescope time was allocated for this project. Unfortunately, it was heavy cloudy and rainy during the observing run. Perhaps, I could make a try in future, especially when the spectrograph is ready for observers. This certainly helps the project more.

References:

Lopez-Morales, M., Clemens, J.C., 2004, PASP, 116, 22

Photometric observations of dwarf planet and TNOs at Lulin Observatory

Hsing-Wen Lin

Rotation periods and variability amplitudes of TNOs are important characteristics of those objects. From now on, only a few rotation periods of Trans-Neptunian Objects were identified. Using 1m telescope and time-series photometry, we can measure the rotational variability and get rotation periods and variability amplitudes of TNOs. Those two information show us a path to understand some other physical properties of TNOs, like shape, density, size.

This work collaborated with Observatorio de Sierra Nevada, Spain.
We pick out 2 target, 2005 RM43 and 2005 RR43. Both of them are TNOs and the magnitude about 20.
After 3 night observations using LOT, we got about 50 snap-shot of each target.

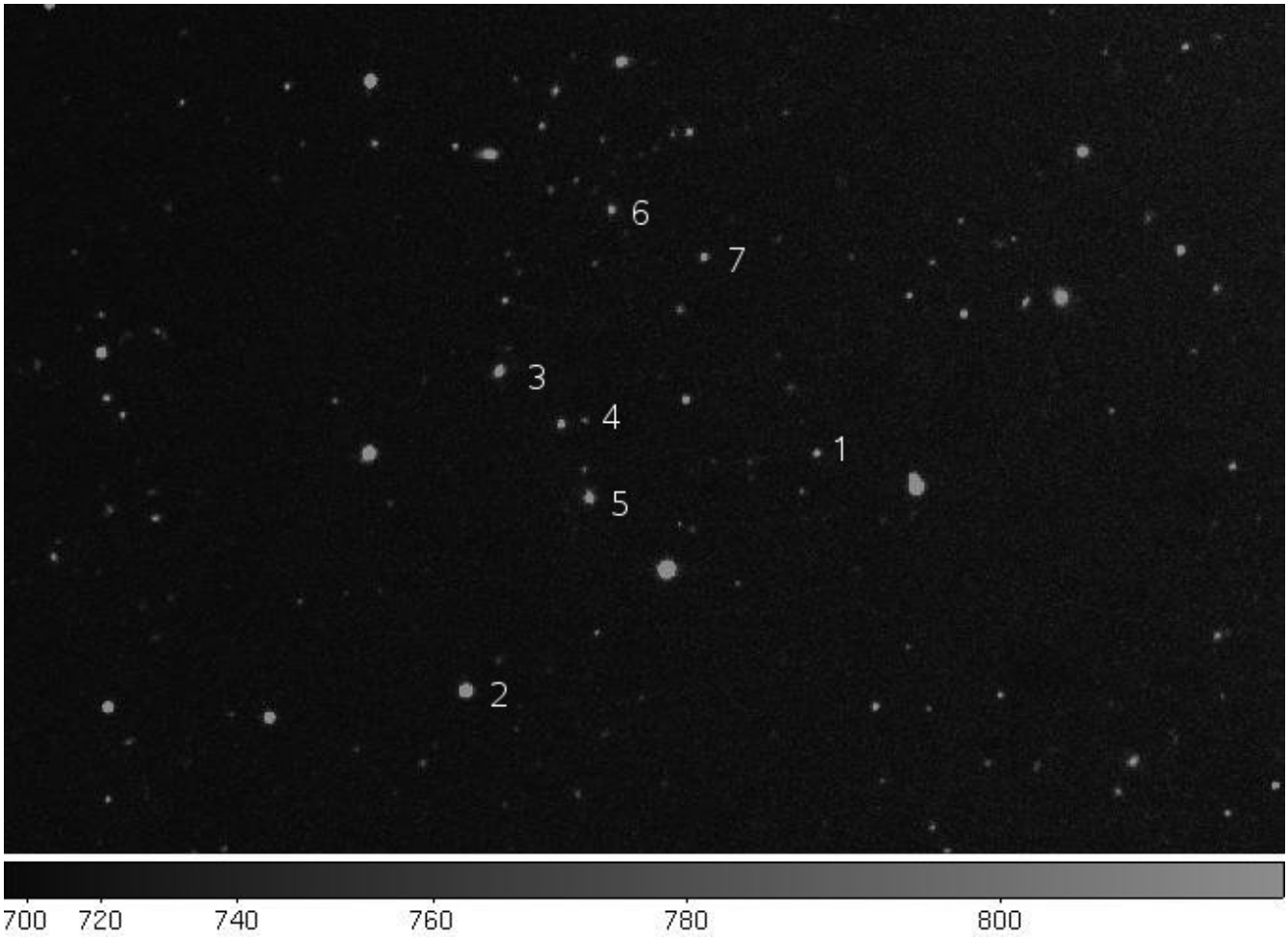

This is one of the LOT images of 2005 RM43. The TNO is locate at “1” and other marks are the positions of references.

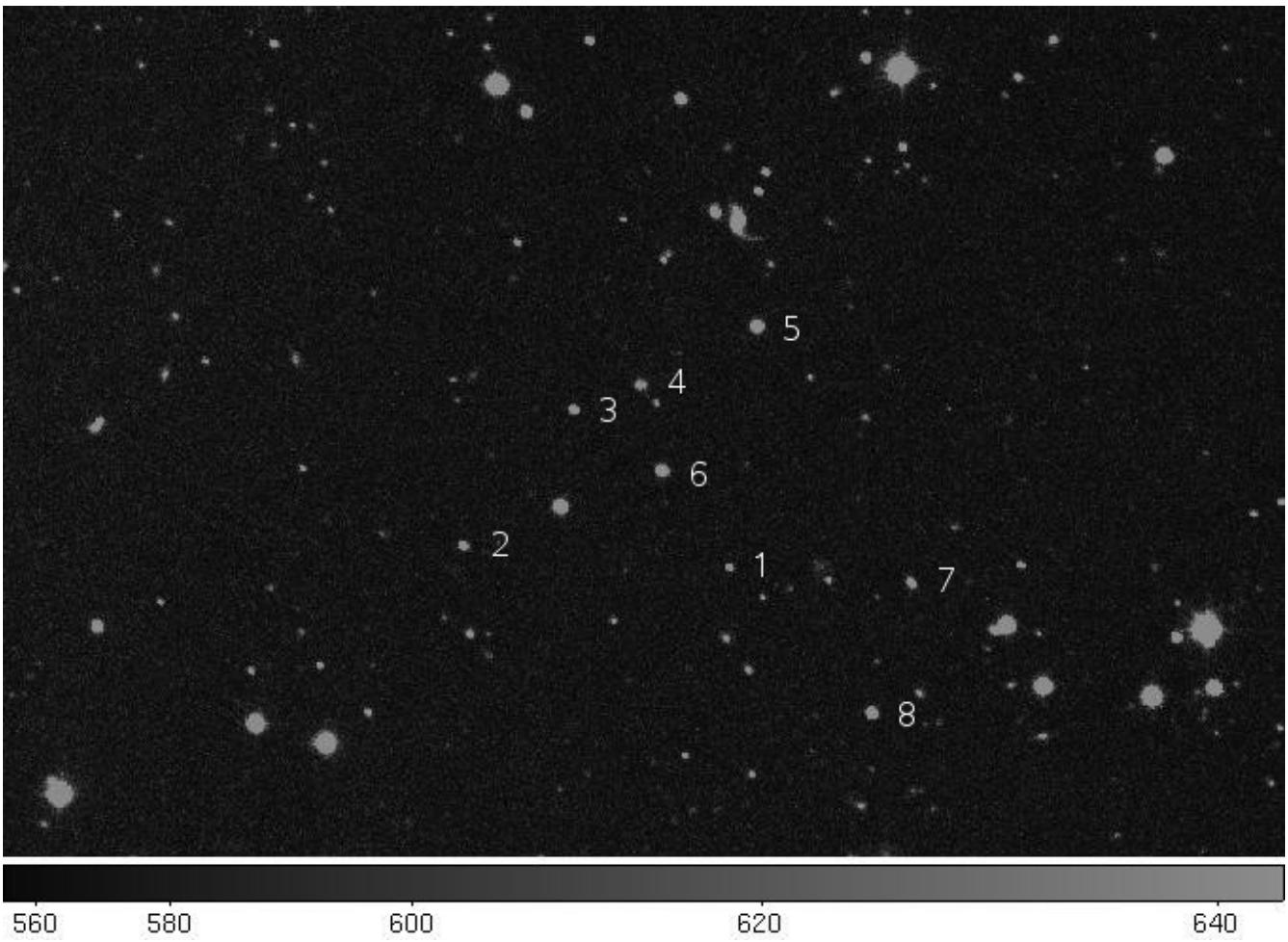

This one is for 2005 RR43.

The results are shown below:

a

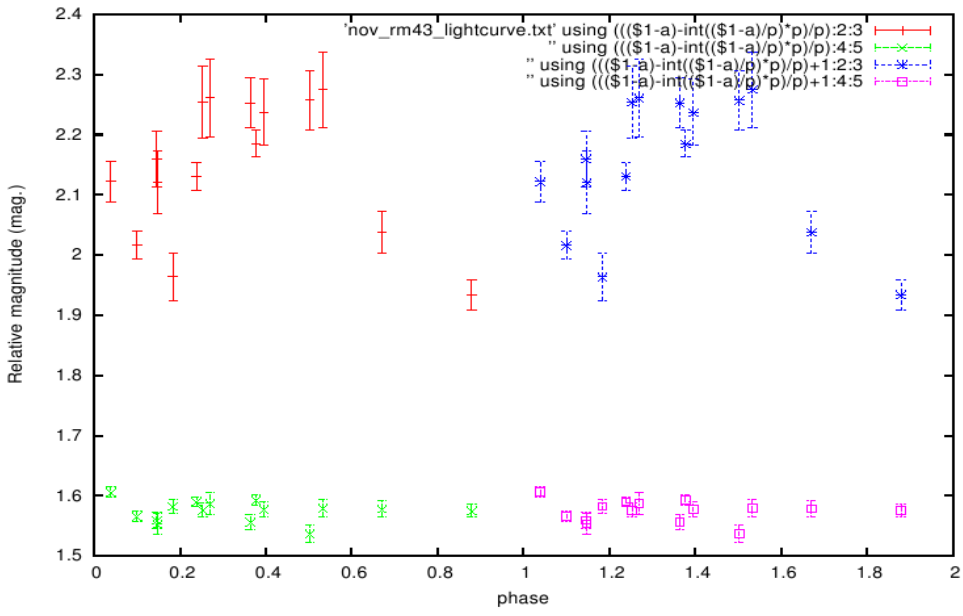

b

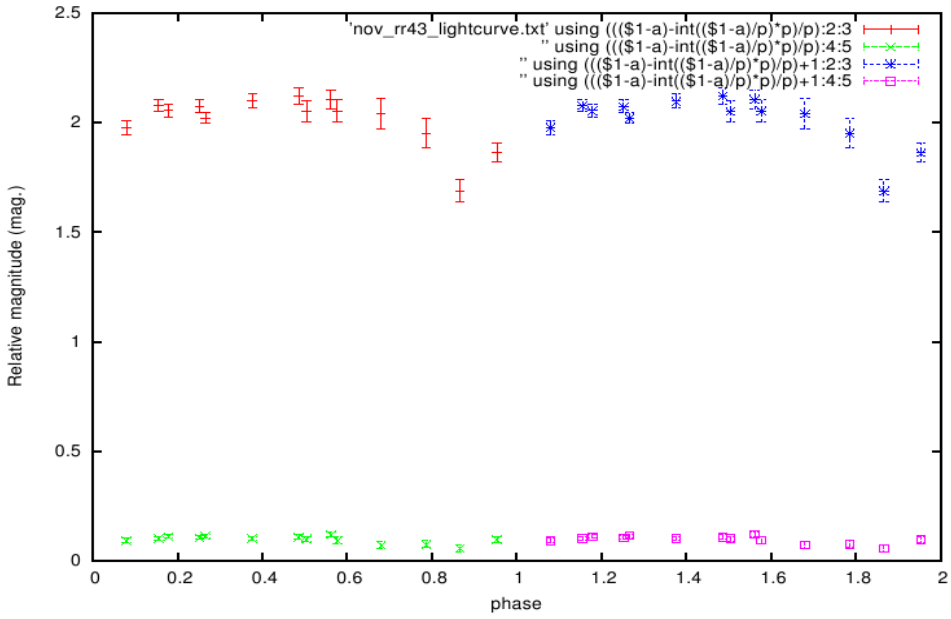

Fig. a shows the phase diagram of 2005 RM43 and Fig. b for 2005 RR43. Each figure plot two phases of variability amplitudes. References' lightcurves are shown in green and purple points. Significantly, those two TNOs have variability and the references not. That mean the variation of magnitude is not cause by weather condition.

Using those preliminary results, we find the Brightness variation are ~0.3 mag for 2005 RM43 and ~0.5 mag for 2005 RR43. And the rotation period of 2005 RM43 should be about 8 hours for 1 round, and for 2005 RR43 is about 10 hours.

Add the new results of 2007A LOT observations, we will publish this work on 2007 EGU meeting.

TAOS at Lulin in 2006

S. K. King[a] (金升光), C. Alcock[b], T. Axelrod[c], F. B. Bianco[d,b], Y. I. Byun[e], Y. H. Chang[f] (張永欣), W. P. Chen[f] (陳文屏), K. H. Cook[g], R. Dave[d], J. Giammarco[d], D. W. Kim[e], T. Lee[a] (李太楓), M. Lehner[b,d], C. C. Lin[f] (林建爭), H. C. Lin[f] (林宏欽), J. Lissauer[h], S. Marshall[i], S. Mondal[f], T. C. Nihei[d,b], I. de Pater[j], P. Protopapas[b], J. Rice[k], M. E. Schwamb[d], A. Wang[a] (汪仁鴻), S. Y. Wang[a] (王祥宇), C. Y. Wen[a] (溫志懿) and Z. W. Zhang[f] (張智威)

[a] Institute of Astronomy & Astrophysics Preparatory Office, Academia Sinica, Nankang, Taiwan, ROC
[b] Harvard-Smithsonian Center for Astrophysics, Cambridge, MA, USA
[c] Steward Observatory, University of Arizona, AZ, USA
[d] Department of Physics & Astronomy, University of Pennsylvania, PA, USA
[e] Department of Astronomy, Yonsei University, Korea
[f] Institute of Astronomy, National Central University, Chung-Li, Taiwan, ROC
[g] Institute of Geophysics & Planetary Physics, Lawrence Livermore National Laboratory, CA, USA
[h] NASA Ames Research Center, Mountain View, CA, USA
[i] Stanford Linear Accelerator Center, Stanford, CA, USA
[j] Department of Astronomy, University of California, Berkeley, CA, USA
[k]Department of Statistics, University of California, Berkeley, CA, USA

The regular long zipper data since 2004 was analyzed offline. Two predicted asteroid events were simultaneously observed by two or three TAOS telescopes successfully. Some major progresses in both hardware and software at Lulin are summarized.

1. A statistics of the long zipper observation is shown in Figure 1. The total observation time is 661.3 hours where 343.8 hours was conducted by three telescopes simultaneously during this period of time (Feb. 2005 to Dec. 2006).
2. A preliminary analysis shows no significant occultation event (see Chen 2006).
3. The predicted asteroid event of (286) Iclea was observed by telescope A/B/D on 2006 February 6. The (87) Sylvia event was observed by TAOS A & B on 2006 December 18. It was found in the Sylvia event that TYC 1947-00293-1 is really a binary system unknown before (see Figure 2 and the TAOS website for detail).
4. Focus encoders were installed in April to show the absolute focal position. Air conditions were installed in April to balance the ambient temperature. Isolation transformers were installed in June to provide better lightening protection. Both A & B got new base plate in July so that the telescopes can response well during vibration. A new auto-focus algorithm was applied in July so that a data acquisition in zipper mode can be started more efficiently. An independent wireless weather station and a more precise dew point sensor were installed in December to provide a better standard of the local weather. A new frame transfer CCD arrived in summer and will be tested soon.

TAOS Publication in 2006 (journal article, preprint, conference proceedings, thesis)

1. Early Observations in the Taiwanese-American Occultation Survey, Alcock, C. et al., 2005, BAAS, 37, 1154
2. TAOS - The Taiwanese-American Occultation Survey, Lehner, M. J. et al., 2006, Astronomische Nachrichten, 327, Issue 8, 814
3. TNO Occultation Surveys in Taiwan, King, S.-K. et al., 2006, in the 18th Rencontres de Blois on "Planetary Science: challenges and discoveries", in press
4. Search for Small Trans-Neptunian Objects by the TAOS Project, Chen, W. P. et al., 2006, in "Near Earth Objects, Our Celestial Neighbors: Opportunity and Risk" (IAU Symposium 236), in press (astro-ph/0611527)
5. Virtual Astronomical Pipelines, Dave, R. et al., 2006, in ASP Conference Series, "Astronomical Data Analysis Software and Systems XVI", edit. Shaw, R., Hill, F., and Bell, D.,

The Astronomical Society of the Pacific, San Francisco, in press
6. Photometric Analysis for KBO Occultation, Kim, D.-W., Master's thesis, Yonsei University, Korea, December, 2006
7. Probability of Stellar Occultation by Trans-Neptunian Objects, Lin, C. C. et al., 2006, Journal of Taipei Astronomical Museum, 4, 37

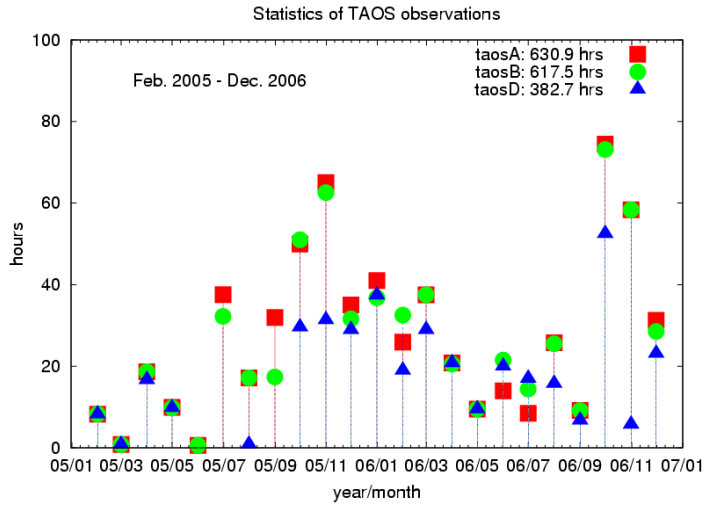

Figure 1. Statistics of TAOS observation (long zipper mode in 2005-2006) by three TAOS telescopes (figure prepared by Andrew Wang)

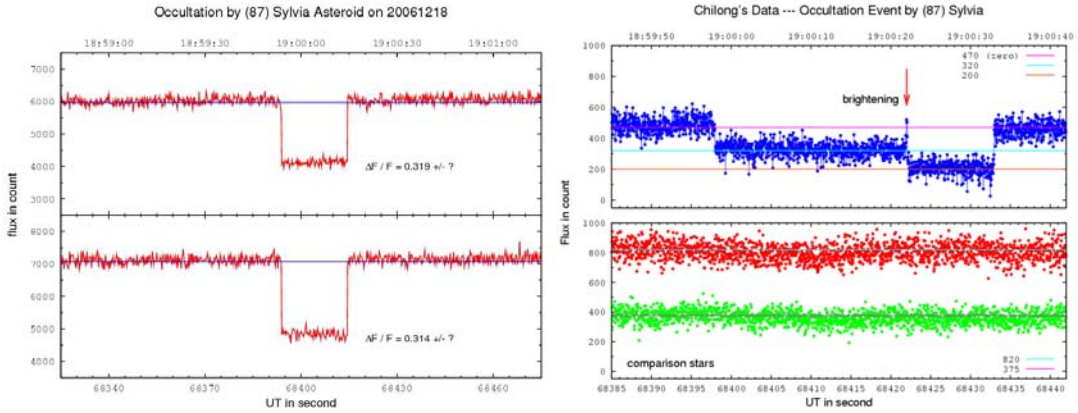

Figure 2. The light curves of the Sylvia event from the TAOS data (left) and an observation in Taichung City by Dr. Lin, C.-L. (right) showed that the background star TYC 1947-00293-1 is a previously unknown binary system. (figures provided by Kiwi Zhang)

施瓦斯曼·瓦茨曼 3 號彗星

Z.Y. Lin (林忠義), W.H. Ip (葉永烜), T.C. Yang (楊庭彰), C.S. Lin (林啓生) and H.C. Lin (林宏欽)

施瓦斯曼·瓦茨曼 3 號彗星（73P/Schwassmann-Wachmann 3），這顆短週期彗星（5.43~5.46 年 ）在 5 月 12 日左右，與地球接近至僅 0.0786AU，這個距離是自彗星 1930 年（ 由德國天文學家阿諾·施瓦斯曼（Arnold Schwassmann）和阿諾·阿瑟·瓦茨曼（Arno Arthur Wachmann）共同發現 ）發現以來第二近的距離 (0.0616AU)!

73P/S-W 3 彗星在 1995~1996 年回歸時發生巨大的爆發(從 10 月份一直持續到 11 月份)，也因於此當天文學家再度觀測此彗星時，已經發現數個 fragments 從核心分裂出來，其中有三個較大主要的部分分別被命名爲 A、B、C。

2000 年 11 月底，日本天文學家 KenIchi Kadota 再度觀測此分裂的彗星，但其中 A 已經消失，但另一個 E 卻發現，右圖一即爲所觀測到的影像。

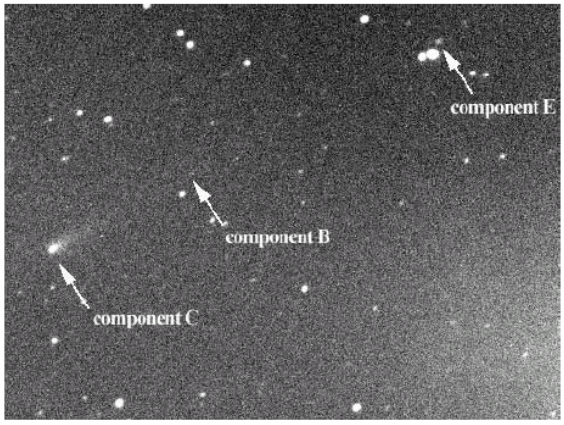

圖一：Kadota, K.利用 0.18m 的反射式望遠鏡 (f/5.5) 於 2000 年 11 月拍攝到彗星分裂的情形。

2005 年 10 月 22 日重新發現後，卻只觀測到其中的 B 和 C，E 尚未發現，可能已經消失， 不過近期所得到觀測，天文學家已經陸續發現另一個 G 核 (Tucker et al. , IAUC8679) 以及更多分裂的彗核 (H,J andL, Christensen et al. , IAUC 8685)，上圖二、即爲所觀測到的 B、C、G 核的影像以及天空中的相對位置。

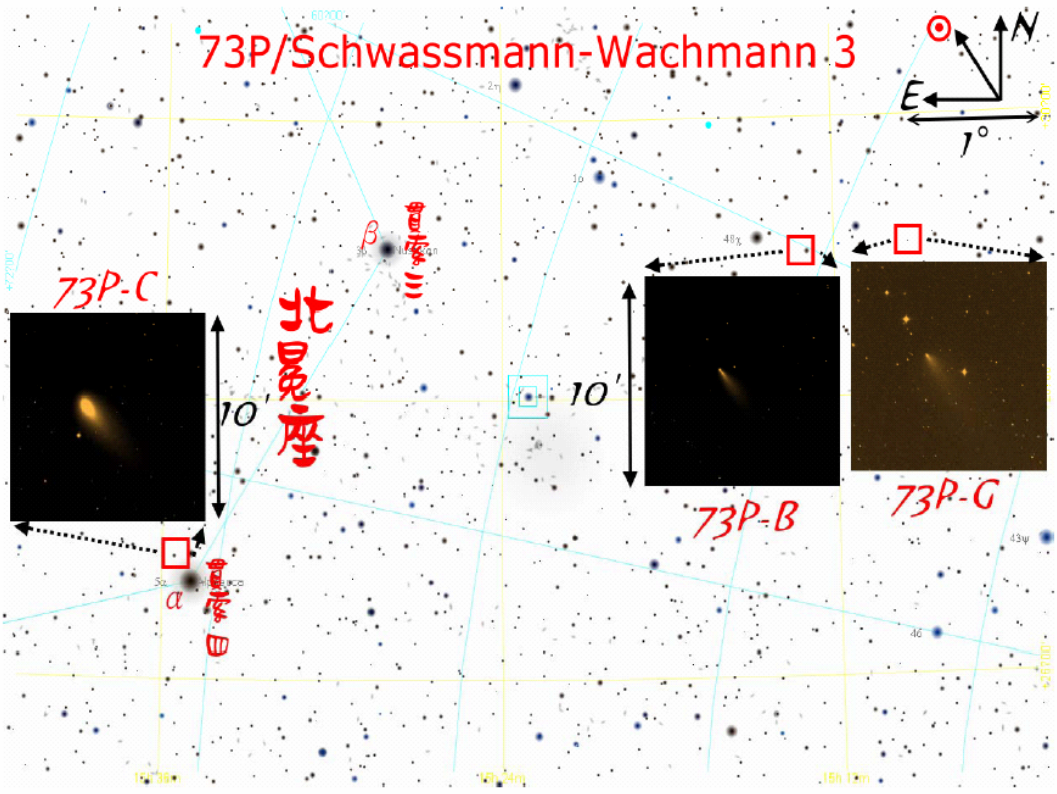

圖二：博士生林忠義利用鹿林山天文望遠鏡 (LOT) 於 2006 年 4 月所拍攝到彗星分布的情形與彗星 B 核、C 核 G 核的影像

2006 年四月初以來，隨著彗星越接近地球天文學家也發現更多彗星碎片，由各大望遠鏡觀測結果 ，這顆彗星正在持續分裂 (其中 AM 核由中央大學鹿林天文臺 RC16 望遠鏡發現) ，其中 B 核相對於其他彗核活躍得多，右圖三是 4 月中的一次分裂現象恰被鹿林天文臺拍攝到；B 核後方，可明顯的看到分裂後的碎片正逐漸遠離 B 核核心 (導致彗星分裂解體的說法不一，有的受到天體的潮汐力作用、有因本身自轉作用、有熱力作用、有的是因內部氣體壓力造成內部不穩，更有其中一個說法是它受到某種天體撞擊。過去有數顆彗星出現同樣狀況，其中較著名的有 C/1999 S4 (LINEAR)，在 2000 年 7~8 月回歸時，完全裂解消失)。

由於 73P/S-W 3 彗星太過接近地球，因此對於此彗星中的內部彗髮研究也相當顯得重要。其中又以 Comet Arclets (Coma Wings)現象較爲著名。

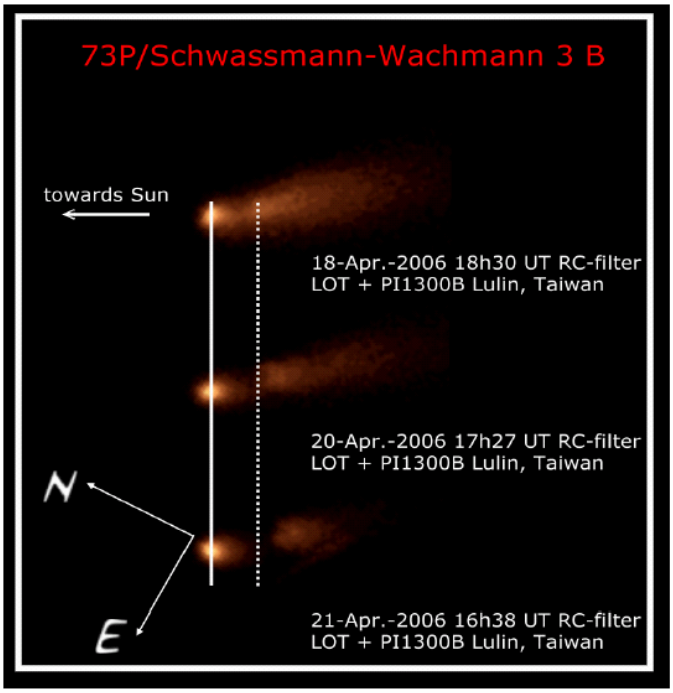

圖三：博士生林忠義於 2006 年四月中拍攝到彗星分裂的景象，其分裂的碎片與 B 核相對的距離 (投影於天空中) 分別爲 872km (4 月 18 日)、1121.5km (4 月 20 日) 和 1348km (4 月 21 日)。

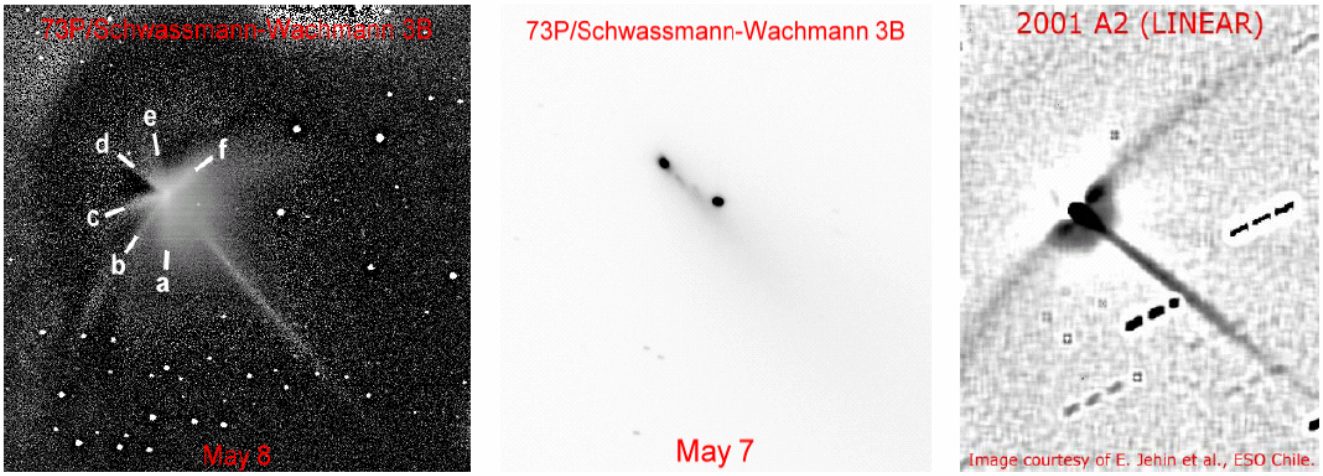

圖四：彗星圖像 (圖左) 經影像處理後發現有 Arclet 的結構，與 2001A2 (LINEAR) (圖右) 有相似的構造。圖中 爲 Arclet 現象前，發現 B 核分裂的景象。

Comet Arclets通常出現於兩個分裂核之間，而且此結構可能是由對稱的兩端組成(約有1000~10000公里)，並幾乎垂直於核與彗尾間的連線（圖四）。此結構的討論與比較（目前爲止有C/1996 B2 (Hyakutake), C/1999S4(LINEAR) , C/2001A2(LINEAR)等三顆彗星，有類似結構。）將於博士生”Activity and Morphology of Comet 73P/Schwassmann-Wachmann 3 close to its closest approach to the Earth”論文中再詳細討論。

A Study of Star Formation History of Near-by Galaxies

陳以忱
國立中央大學天文所

Hα images were obtained using the Lulin One-meter Telescope (LOT) and the affiliated H-alpha narrow band filter (See Fig 1.). R-band images are also made for continuum-subtraction. K-band images were obtained from the the Two Micron All Sky Survey (2MASS).Information on M74 and M83 transmission curve on the H-Alpha filter is presented below.

Since the weather was not good enough during the observation time to make observation of standard stars, calibration can not be done to normalize the optical / near-infrared images. However, the result of comparing the arm / inter-arm counts ratio can still be achieved. Using the ‘ARD region’ option within the Starlink GAIA package, we can define a polygon lying around each K-band arm. We then transferred the region into the H-Alpha image and calculate the average counts in both images. Dividing the average counts of the two images, we can obtain the ratios in arm and inter-arm region. The result is list as Table 2. With the result, we found H-Alpha / K ratios to be apparently higher in K-band arm than in inter-arm region, which implies that density wave triggering dominate mostly for the star-formation in spiral galaxies.

M83 (R-band)

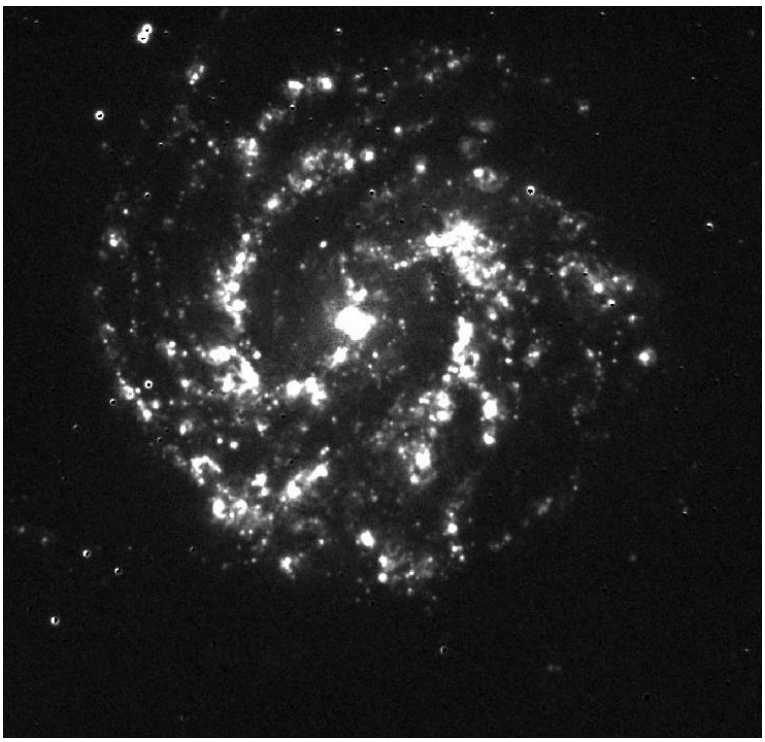

M83(subtracted H-alpha)

Discussion:

＊Some foreground stars in narrow-band images are not perfectly subtracted probably because it is almost impossible to fit the PSF perfectly for all the stars in the images. We’ re still looking for the best method to minimize errors.

＊Observation of standard stars should be made for calibration, which we can calculate the absolute magnitude of the galaxies. Using absolute magnitude, we
can determine star-formation rate of the galaxies.

＊The 2MASS images are not “deep” enough to make more accurate analysis.
It’ s necessary to use better near-infrared images.

Identification of High-Mass X-ray Binary

Huang, Kuo-Pin

X-ray binaries are composed of a normal star and a compact object. The compact object is either neutron star or black hole. Some of the stellar wind of the Be star will be captured by the companion star can cause the mass transfer in the system. When the mass fed to the compact object, it will produce X-ray. The systems will radiate characteristic infrared emission.

While the normal star is a Be star or a blue supergaint star, we call high mass X-ray binary (HMXB). The most of HMXB are in the galactic plane, LMC, and SMC. In these fields, HMXB are in general located in regions with crowded star and it is very difficult to identify the true counterparts for the HMXB via optical observations. So many optical counterpart of HMXB are unidentified. TO find the optical counterpart is an unfinished business in the study of HMXB.

We use the catalog of HMXBs (Liu et al. 2000) to search unidentified target, and select the candidate in the 2MASS data. We plot those color-color diagram of Be star ([J]-[H] verse [H]-[Ks]) in Fig1. We note that the infrared colors for these Be stars all have values very close to zero. We use this characteristics to search for counterparts for other unidentified HMXB.

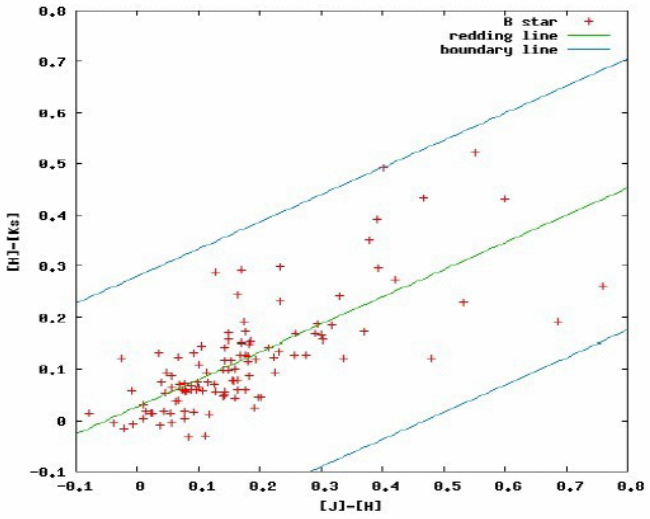

Fig 1. The color-color diagram of Be star

We select several targets to observe. The XB1954+319 is one of our target. It is our emphasis, because it's number of candidate is five. Fig 2. show position of our targets.

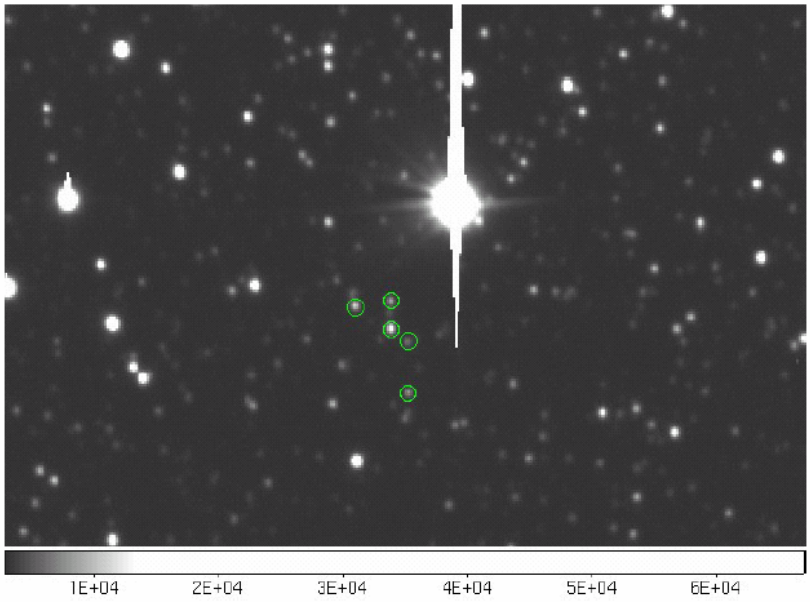

Fig 2. The five green circle is candidate of XB1954+319.

We want to plot the light curve of candidates. The least variable period of HMXB is about 17 days. So we must monitor for a long time.

During 2006 first half year, my observation time is not good. It is during Bright day. The position of this source is in Cygnus. The LOT was maintain in July to September, so I miss the best observation time for this target.

I get 12 day for proposal of LOT2006B. Because the weather is good for every observation, the useful data only eight days and I can not do standard photometry. I use differential photometric to determine the magnitude of candidates. I plot the light curve for five candidates and reference star in Fig 3.. In the Fig 3., the button picture is the light curve of reference star, others are candidate 1 to 5. The magnitude is not calibrated, so we are not sure the variation is true. The light curve of five candidates are similar the reference, so maybe those candidate are not variable star.

We can find disadvantage of our method, It can efficiency to identify the optical counterpart of our source.

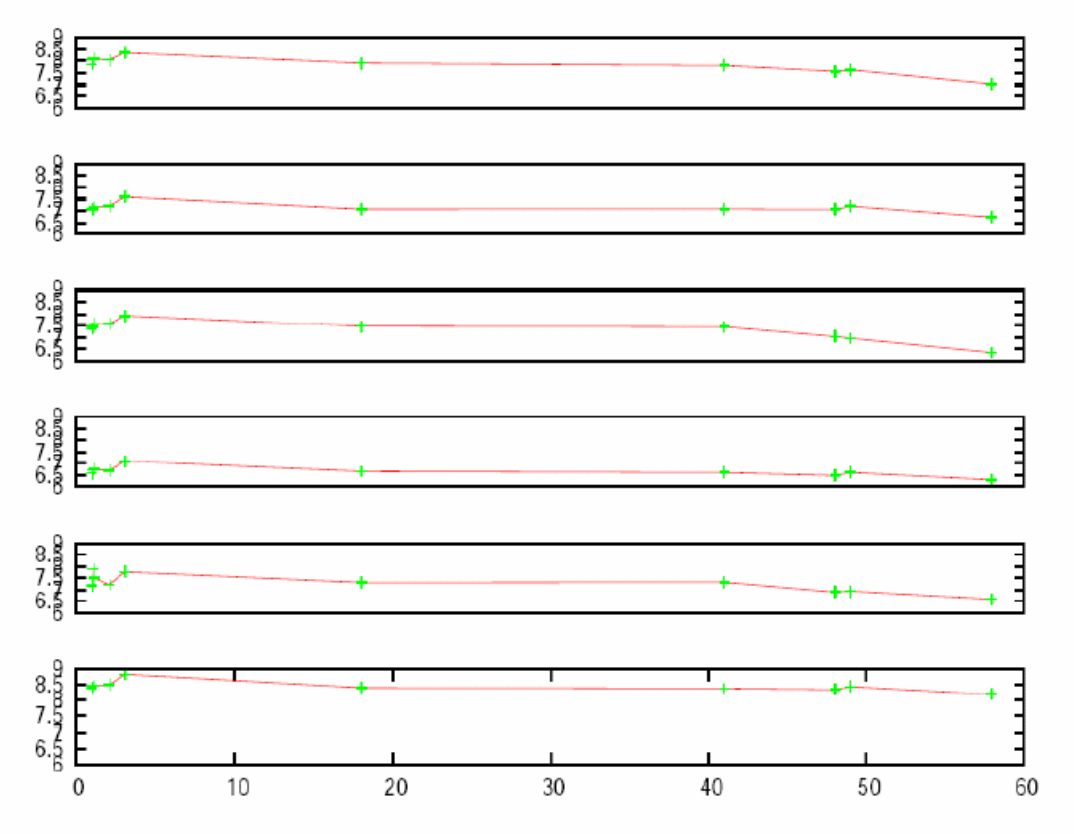
0
10
20
30
40
50
60

LELIS at Lu-Lin in 2006

LELIS : Lu-Lin Emission Line Imaging Survey

W.-H. Sun (孫維新), H.-Y. Mong (蒙宏堯), C.-C. Liu (劉治軍), K.-C. Lu（呂科智）
H.-H. Ma (馬學輝),B.-W. Wang (王斌威), Y.-W. Cheng (鄭以文)

自 2004 年起，我們在鹿林山天文台建立了一組窄波段、寬視野、多通道的星際物質巡天望遠鏡 Lu-Lin Emission Line Imaging Survey，簡稱 LELIS，在星際物質最重要的三個發射線波段 Hα、[OIII]，and [SII]，對北天作特定天體觀測及完整巡天。科學研究課題包含行星狀星雲的週邊環境、超新星遺骸的質量分佈、晚期恆星噴發物質的過程，以及近鄰巨大星系周邊低亮度的物質延伸等。

因爲本系統原先使用之 400mm/F2.8 望遠相機鏡頭光學品質不如預期，我們因此在 2006 年間，採購 PENTAX 400mm/F4.0 口徑 10 公分之廣角望遠鏡 3 組，使用原系統之前置濾鏡，並加上遠距遙控對焦裝置（Robo-Focus），得到了一套光學品質良好且運作穩定之觀測系統（請見圖一至圖三）。我們從 2006 年暑期開始，發展本系統的遠距遙控架構，並於每一組望遠鏡鏡筒上加裝弱光監控攝影機，可於觀測時確認望遠鏡之正確指向。至當年 11 月間，已可完全由中央大學遠距觀測中心控制 LELIS 系統，進行完整觀測。我們已建立由專任助理及大學部高年級生組成的觀測團隊，在中央大學科四館遠距觀測中心每天晚上進行例行觀測，我們也建立了由研究生及專任助理組成的數據處理團隊，將例行觀測所得到的數據，以系統化的方式處理分析，作爲撰寫論文的基礎。

目前的 LELIS 系統已經是自科學構想開始時的演化第三階段，每一組 PENTAX 望遠鏡，配合 ST-10XME CCD 相機，給出 2 度乘上 1.5 度的視野。因此本系統的特色，能較一般長焦望遠鏡涵蓋更大天區，同時經過多幅疊加，以及多天區拼接的方式，可以對大型天體做出有系統而規律的呈像。尤其三個波段的同步觀測能力，可以即時給出任一天體的多通道影像，進行統整分析時，很明確定出該天體的各項物理參數。隨附例圖三張，爲本系統針對大型雲氣，在不同波段所做的觀測（請見圖四至圖六）。

Figure 1. LELIS 系統初步組裝完成，包含三組短焦望遠鏡，成品字形架構，中央下方爲導星望遠鏡。

Figure 2. LELIS 系統的三組前置濾鏡，每一組包含 Hα、[OIII]，and [SII]發射譜線及連續譜兩片濾鏡。

Figure 3. LELIS 系統於圓頂內架上赤道儀，圖中可見鏡筒旁之弱光監控攝影機，以及右上方之遠距調焦裝置。

Figure 4. LELIS 系統觀測影像，NGC6990 (in H-alpha)。

Figure 5. LELIS 系統觀測影像，M42 獵戶星雲 (in H-alpha)。

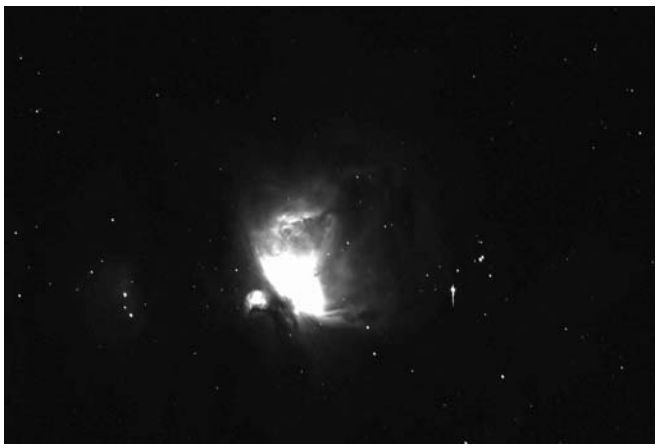

Figure 6. LELIS 系統觀測影像，M42 獵戶星雲 (in [OIII])。

超新星後續光變觀測

(The Follow-up Observations of Supernovae with Lulin Observatory)

Ting-Wan Chen (陳婷琬), Ying-Tung Chen (陳英同), Wing-Huen Ip (葉永烜),
Li-Jin Huang (黃麗錦), Lin, Hung-Chin (林宏欽), Chi-Sheng Lin (林啟生),
Hsing-Wen Lin (林省文), Kuo-Pin Huang (黃國斌), Yi-Chen Chen (陳以忱)
Institute of Astronomy, National Central University, Taiwan

Supernovae are phenomena of the end stage of life on massive stars. The energy of supernova explosion is equal to 30 hundreds million times of solar luminosity, however, the time of explosion smaller than 1 second. In average, 415 supernovae have been reported from 2001 to 2006. Amount of supernovae discovered increase with year, and they provide samples for research in property of supernovae.

We choose bright supernovae to follow-up observe, because after the maximum brightness, the magnitude decay about 0.1 every day. In average, one bright supernovae appeared every 1~2 month. To obtain BVRI light curves, we need long days (about 30 to 50 days) to observe, but not many time in one night. For this reason, we are very appreciate that LOT users and assistants assist us in observe supernovae.

We used the one-meter telescope (LOT) at Lulin to carry out follow-up observations of several supernovae in nearby galaxies. One interesting target which we have made detailed observations was SN 2006jc in UGC 4904. SN 2006jc was discovered on 10/09/2006. Rather unexpectedly, Spectra of SN 2006jc changed type from Ib (CBET 666) to Ia, because its spectrum appeared Si line (CBET 674). However, the Fred Lawrence Whipple Observatory take spectrum of SN 2006jc on 17th Oct (see figure 1). The spectrum is similar to type Ic supernova SN 1999cq. Finally it becomes a type Ib supernova, and represent a new class of former classification (Foley et al. , 2006).

We collected BVRI bands data from 10/13/2006 to 11/29/2006 (see figure 2). Note that the B-band magnitude of SN 2006jc was brighter than the other bands. We compare light curves of SN 2006jc with SN 1994I (see figure 3). We discover that the V, R, and I-band light curves are similar to each other. But the B-band light curves of SN 2006jc and SN 1994I are very different.

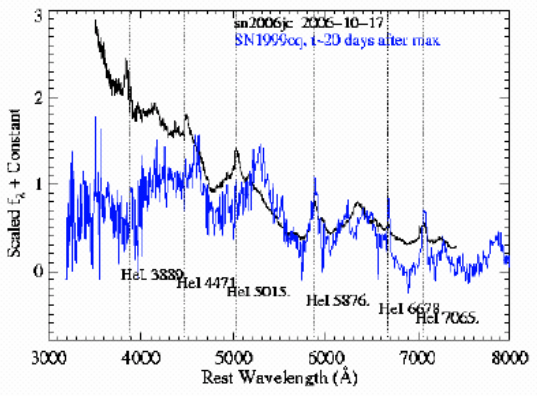

Fig. 1 Spectrum of SN 2006jc from FLWO From:http://cfa-www.harvard.edu/cfa/oir/Research/supernova/spectra/sn06jc_comp.gif

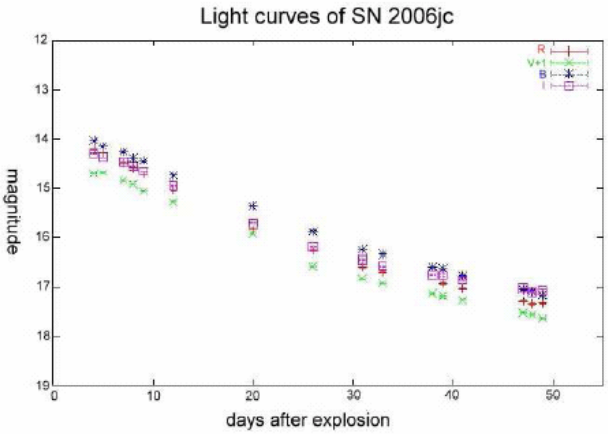

Fig. 2 B、V、R、I-band light curves of SN 2006jc obtained by LOT. B、R、I band magnitude have correction with standard stats, but V band is not.

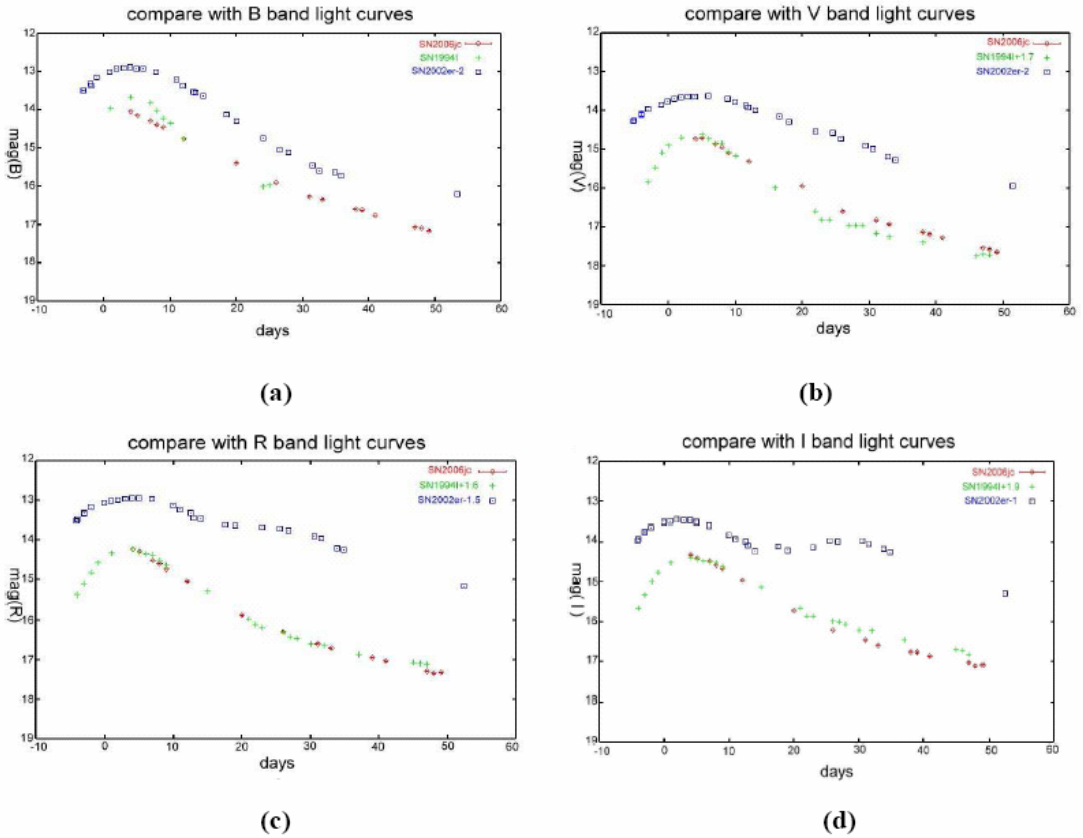

Fig. 3 are B、V、R and I light curves of SN 2006jc (red color) in comparison with SN 1994I (green color). Moreover, we compare with type Ia supernova 2002er (blue color). The data of SN 1994I are obtained from Richmond et al. (1996), and SN 2002er from G. Pignata et al. (2004). Note that the times of the maximum brightness are aligned in these figures.

The sample of Type Ib and Ic supernovae are not many, and therefore we want to use LOT to observe more data. We can understand their physical properties of supernovae themselves, and what kinds of galactic environments around progenitors.

2006 年鹿林山大氣背景站成果報告

林能暉教授 國立中央大學大氣物理研究所
李崇德教授 國立中央大學環境工程研究所
王家麟教授 國立中央大學化學系

一、前言

台灣正好位於東亞大氣污染物下風處及南亞生質燃燒傳送路徑之下風處，過去環保署雖在全國設置超過 76 個空氣品質監測站，但多為代表地區性之特性，目前仍無代表一區域型或跨洲際之觀測地點，因此在若干境外污染物傳送影響之議題上，國科會、環保署和中央大學策劃與推動鹿林山大氣背景站(Lulin Atmospheric Background Station, LABS)之建置，其設計與未來運作，則以聯合國全球大氣觀測網(Global Atmosphere Watch, GAW)規範為參考藍本。鹿林山大氣背景站地理位置優勢，作為自上游中南半島、中國南方、西太平洋夏威夷一線大氣污染監測之中繼站，相當具優勢，足以吸引國際目光，更易於推動國際合作，加入相關監測組織。

二、本年度具體成果

以下幾項為 2006 年主要成果:

1. 鹿林山國際級大氣背景站於 2005 年 9 月動工，該年 12 月竣工，已於 2006 年 4 月 13 日正式啟用，並舉辦啟用國際研討會。圖 1 為目前測站外觀。

圖 1. 鹿林山大氣背景站外觀。

2. 建立鹿林山大氣背景站之監測技術以及標準操作程序。整合降水化學、微量氣體、大氣氣膠、大氣汞、大氣輻射等主要領域專長研究者進行相關儀器功能測試和維護，目前鹿林山大氣背景站架設之儀器除了環保署空氣品質測站之標準自動觀測系統

(包括風向、風速、雨量、溫度、相對溼度、O_3、CO、UVA、UVB、PM_{10} 等監測項目)外，另有高精密 CO 連續監測儀器（ta-3000R，Trace Analytical，USA）、大氣汞監測儀(Tekran 2537A/1130/1135 Hg Monitoring Analyzer)、太陽輻射儀 (Cimel CE-318)、旋轉輻射儀 (Yankee MFR-7 Multifilter Rotating Shadowband Radiometer)、能見度儀 (PWD-22)、酸雨採樣器等監測儀器，儀器現場配置如圖 2 所示。

圖 2. 鹿林山大氣背景站儀器。

3. 完成鹿林山區域大氣污染物監測與資料分析比對。以大氣污染物的監測為例，CO 平均為 72 ppb，O_3 平均為 23.7 ppb，PM_{10} 平均為 8.7 μg m^{-3}，氣態元素汞(Gaseous Elemental Mercury, GEM)平均值為 1.77±0.66 ng m^{-3}，氣態二價汞(Reactive Gaseous Mercury, RGM)平均值為 9.04±18.99 pg m^{-3}，顆粒態汞(Particulate Mercury, PHg)平均值為 1.78±2.36 pg m^{-3}。本團隊亦藉由進行兩次背景密集觀測實驗獲得大氣污染物背景濃度值，CO 平均背景值濃度 48.8 ppb，O_3 平均背景值濃度 23.7 ppb，PM_{10} 平均背景值濃度約在 5-8 μg m^{-3}，總汞平均背景值濃度為 2.15±0.45 ng m^{-3}。

4. 本團隊在國科會、環保署和中央大學的支持下，積極推動與美國環保署、太空總署、海洋大氣總署合作，進行技術交流與資料交換。完成與美國全球光達監測網與光度輻射監測網之合作、聯繫、資料交換與分析。參與聯合國大氣褐雲國際觀測實驗(ABC)、美國太空總署亞洲生質燃燒國際觀測實驗(BASE-Asia)，以及和日本科學會-富士山的酸雨資料交換等，推動國際合作，建立國際環保外交。

5. 完成鹿林山大氣背景站中英文網頁(http://labs.org.tw)建置。

三、主要成就與貢獻

1. 鹿林山大氣背景站為具國際水準之高山大氣背景站，有助於區域性與跨洲際大氣污染傳送問題釐清，以及我國背景大氣化學基線資料之建立。

2. 藉由鹿林山大氣背景站的建置，有助於建立微量污染物的監測與分析技術。

3. 鹿林山大氣背景站合乎國際規格，且具東亞唯一之高山背景站之優勢，提供重要資訊與國際科研社群，吸引國際合作，達到國際環保外交。

四、計畫著作

林能暉、王家麟、李崇德和許桂榮，2006: 鹿林山背景站測試採樣分析與國際合作之參與及推動研究專案工作計畫，環保署。

林能暉等，2006:亞洲大氣污染物之長程輸送與衝擊研究，國科會。

郭俊江，2006: 光達及太陽輻射儀之應用: 2005 年中壢氣膠光學垂直特性及邊界層高度之變化，中央大學，碩士論文。

林建志，2006: 台灣平地與高山大氣汞之監測與比較，中央大學，碩士論文。

Wai K. M., N. H. Lin, S. H. Wang, and Y. Dokiya, 2006: Rainwater chemistry at a high-altitude monitoring station (Mt. Lulin, 2860 m) – comparison with Mt. Fuji background site, *Journal of Geophysical Research*. (in review)

鹿林巡天

葉泉志[1]，林宏欽[2]，林啓生[2]，楊庭彰[2]，張敏悌[2]，施佳佑[2]
1.中山大學環境科學與工程學院，廣州，中國大陸
2.國立中央大學天文研究所，臺灣

一、簡介

鹿林巡天開始於 2006 年 3 月，是兩岸合作進行的一個科研項目，使用鹿林天文臺的 41 釐米遠距遙控望遠鏡進行小行星的搜尋與觀測工作。望遠鏡主鏡口鏡爲 41 釐米（16 英寸），在配備減焦鏡後的視場爲 0.4 平方度，每圖元對應 1.1 角秒。在一個晴朗無月的夜晚，它可以覆蓋 20-30 平方度的天區（檢測深度 20.8 等）或 50-70 平方度的天區（檢測深度 19.3 等）。由於目前亞洲的小行星巡天項目較少，鹿林天文臺所處的地理位置也較爲獨特，鹿林巡天很好的覆蓋了全球（近地）小行星監測網的空白。

二、進展與成果

比較其他的專業巡天而言（見表 1），鹿林巡天所使用的望遠鏡口徑小、焦距長，CCD 也是使用單晶片，即使配備減焦鏡後的視場也還遠遠不到 1 平方度。因此，應該主要著眼於運行效率的提高。爲了盡可能在拉長觀測時間距離的同時覆蓋盡可能大的天區，我們使用矩陣天區交替觀測的模式來獲得觀測數據，並用自動偵測軟件進行處理，可以在半小時以內完成 10 個平方度數據的處理。我們亦自行開發了 LUSS Plan Master 等小工具，盡可能爲項目的運作提供便利。

項目	口徑	極限星等（等）	曝光時間（秒）	平均覆蓋能力（平方度/晚）	單幀視場（平方度）
LINEAR [704]	1.0-m x 2	19.5	5-7	~2000 x 2	~1
NEAT [644]	1.2-m	21.0	60	~600	~20
Spacewatch [691]	0.9-m	22.5	120	50-70	~4
CSS [703]	0.68-m	20.0	20	~1000	7.6
Siding Spring [E12]	0.5-m	19.5	n.a.	~600	~4
Mt. Lemmon [G96]	1.5-m	22.5	n.a.	100-200	0.8
LONEOS [699]	0.59-m	19.5	45	~300	8.3
LUSS [D35]	0.41-m	21.0	90	~20	0.4

表 1：鹿林巡天與其他專業巡天的比較

從 2006 年 3 月 5 日至 2007 年 3 月 5 日，我們進行了 188 個觀測夜的觀測，共發現擁有發現權的新目標 288 顆，平均每個觀測夜發現 1.5 顆新天體，其中新小行星 285 顆，其他目標 3 顆（均爲 73P 彗星的碎片）；在新發現小行星中，226 顆已經得到軌道，182 顆的軌道已經初步確定（觀測時長大於 30 天），115 顆已經在多次回歸得到觀測，79 顆在多次回歸觀測中仍然保持主要編號(principal designation)，6 顆已經得到永久編號和命名權；協助國外同行確認新的重要天體（近地小行星、彗星等）24 顆，其中包括 4 顆新的潛在危險小行星(Potential Hazardous Asteroid, PHA)和 5 顆新彗星；上報已被採納和分類的觀測數據 17899 條，平均每個觀測夜提供 95 條；觀測數據量在全球站臺中排名第 11，觀測到已知小行星 4829 顆，彗星 21 顆，天然衛星 1 顆；數據優良率（觀測誤差小於 3 角秒）爲 99.7%，平均誤差 0.3 角秒，在國際同行中居於前列。

由於項目對近地小行星的研究做出了一定的貢獻，項目負責人葉泉志代表鹿林巡天獲得了由行星學會(Planetary Society)頒發的 2007 年度 Gene Shoemaker NEO Grant。

三、未來展望

儘管代表下一代巡天的 Pan-STARRS 項目將於年底開始運行，但小口徑望遠鏡由於成本

低、分佈廣的優勢，仍可在小行星搜尋和觀測方面發揮很大作用。
在下一年裏，我們預計將完成鹿林巡天工作平臺的開發（葉泉志負責），它可以使得項目運作變得更有效率、更加便利。此外，鹿林巡天的高質量觀測數據也在國際天文數據中心(BADC)發表出來，可在互聯網上免費查詢及下載，希冀對其他科研項目能起到幫助作用。我們相信，在擁有更加成熟的觀測技術和更加高效的工作平臺之下，鹿林巡天可爲人類對小行星的認識作出更大貢獻。

參考文獻：
Hughes, D. W., Harris, N. W., 1994, The distribution of asteroid sizes and its significance, Planetary and Space Science, 1994-42(4), p.291-295.
Marsden, B. M., 2001, The asteroid discovery rate: historical perspective and future outlook, Abstracts of Asteroids 2001.
Ye, Q.-z., 2006, List of objects contained LUSS confirmations from Mar.2006 to Jul.2006, LUSS Electronic Circular No.37.
Tsay, W.-S., Chen, A. B.-C., Chang, K.-H., Li, H.-H., 2001, The NCU Lulin Observatory, post on WWW: http://www.lulin.ncu.edu.tw/english/history20010314.htm.
Yang, T.-C., Ye, Q.-z., Lin, H.-C., Lin, C.-S., Ip, W. H., Introduction of Lulin Sky Survey (LUSS), CAST2006, Taichung
胡瑞華，2005，40 公分遠距遙控望遠鏡，鹿林天文臺年報 2005-3，p.98-99。
葉泉志，2006，SCAP-II 運行草案
葉泉志，2007，小行星巡天
朱進、高健、關敏、楊彬，2002，小行星的搜尋和定軌，雲南天文臺台刊 2002-3，p.17-20。

工作報告

Transmission Curve Investigation for Bessell Filters (2006)

Ting-Chang Yang, Hung-Chin Lin
Version: 0.2
Date: 2006/11/21

1 Motivation

Recently, we purchased four Bessell filters from Costom Scientific Company. The daimeter of each filter is about 50mm to fit our need in the RC16 telescope optics system. We asked Thin Film Techonology Center, NCU, for the help of measuring the transmission curve of the four Bessell B, V, R, I band filters. To make a confirmation for the test results from the manufacturer, and know about more for the filters, like the uniformity of the filters.

2 Measurement

The filters had been sent to the Thin Film Technology Center in 11/10, 2006. The instrument "Hitachi U-3501 spectrometer" was chosen for the measurements (Fig. 1) [1]. The specs of the instrument are listed in Tab. 1 below. There are two dectors and two illumators equipped in the instrument for the measurement of different wavelength ranges. Thus, when switching the detectors or illumators, sometimes, there might show "edge" features in the transmission curves of the measured results. Usually, the "edges" appear near the wavelengthes around 350 nm and 850 nm in the transmission curves.

[1] The instruments could be found in the webpage of Thin Film Technology Center, NCU: `http://www.ncu.edu.tw/~tftc/lnk/service/service-meas.html`.

Table 1: Specialities of Hitachi U-3501 Spectrometer

Monochromator	Single or Double Monochromator
Wavelength Range	176-3300nm (UV-VIS-NIR)
Sampling Interval	0.01 nm
Functions	Transmittance, Absorbance, Reflectance at 5° Angle of Incidence

Figure 1: The overview of Hitachi U-3501 spectrometer (left), and the sample holder in the spectrometer (right).

3 Results

The transmission curve diagram offered by the manufacturer is shown in Fig. 2. Because the manufacturer just offers the testing results in graphic form, we can only approximately derive the wavelengthes where the maximum transmission rates occur ($\lambda_{T_{max}}$) and the corresponding maximun transmission rates (T_{max}). The evaluated values are shown in Tab. 2.

The area we chose for the measurements from the filters are in the position of the central region (noted as c), and other four corners near the filter edges. These are shown in Fig. 3. (left).

The measured results are shown. (Fig. 4 represented the transmittance near the central regions of the filters). In Fig. 5, the transmission ratio differences between different regions of the filters are shown in the diagrams. The wavelengthes with largest transmission ratio ($\lambda_{T_{max}}$) are put in the center of x-axes. Not all the filters reveal hightest transmission ratio near the central region. And there are some difference between different regions of the filters. The difference could reach up to 2 % (B filter). But there are many reasons to cause this kind of results. The calibration of the instruments, the intrinsic properities of the filters, and the man-made mistakes are all the possible factors which will affect the measurement result.

Fig. 6 is for the comparison to the manufacturer results. We can see that the trends are quite similiar in B, V, and R filter results, but there are larger bias left in the I band filter result. This maybe also caused by the problem of calibration for the instrument, different properites of the instrument or different conditions from the manufacturer's laboratory.

Table 2: $\lambda_{T_{max}}$ and T_{max} of the Sample Filters

Filter	Manufacturer		Measurement		Difference	
	$\lambda_{T_{max}}$	T_{max}	$\lambda_{T_{max}}$	T_{max}	$\Delta\lambda_{T_{max}}$	ΔT_{max}
B	427 nm	71 %	428 nm	70.322 %	1 nm	-0.68 %
V	514 nm	88 %	517 nm	87.474 %	3 nm	-0.52 %
R	595 nm	79 %	594 nm	80.658 %	-1 nm	1.66 %
I	815 nm	87 %	784 nm	93.428 %	-31 nm	6.43 %

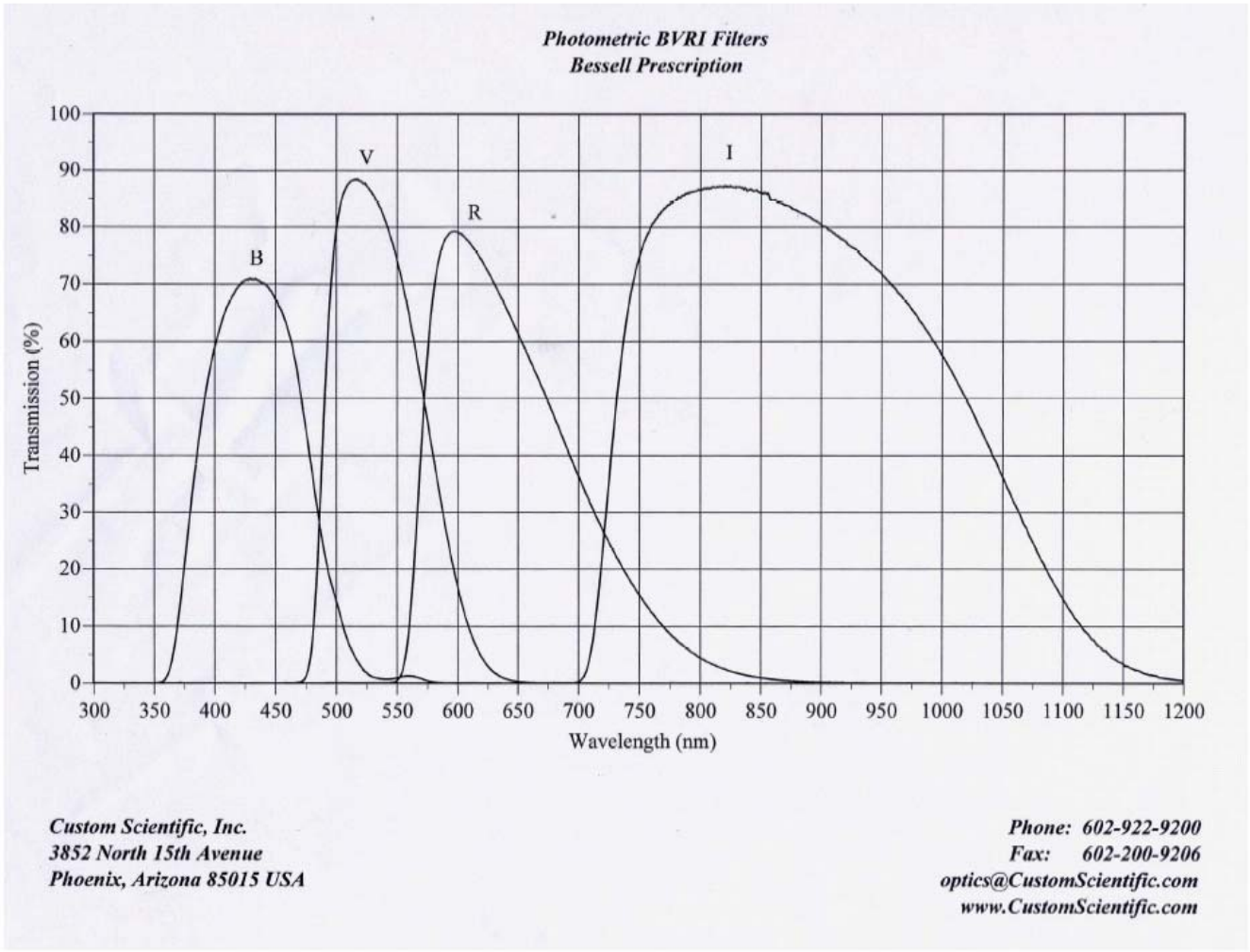

Figure 2: Transmission Curves Provided by the Manufacturer

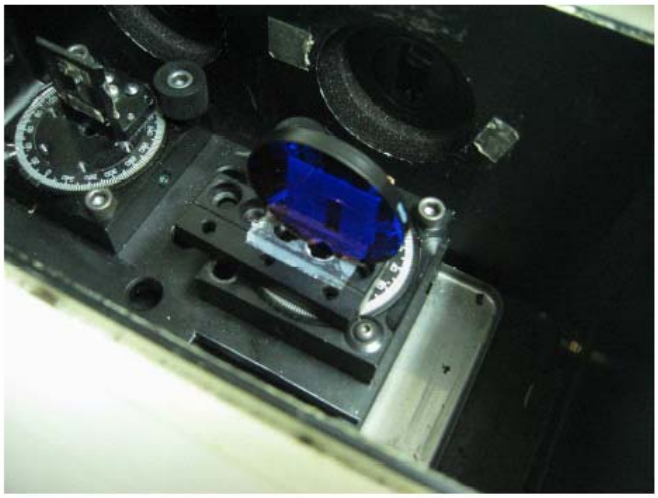

Figure 3: Left: The marked positions of the testing filter samples, there are five regions to be measured. Right: Before the measurement, the sample should be put on the holder in the stage.

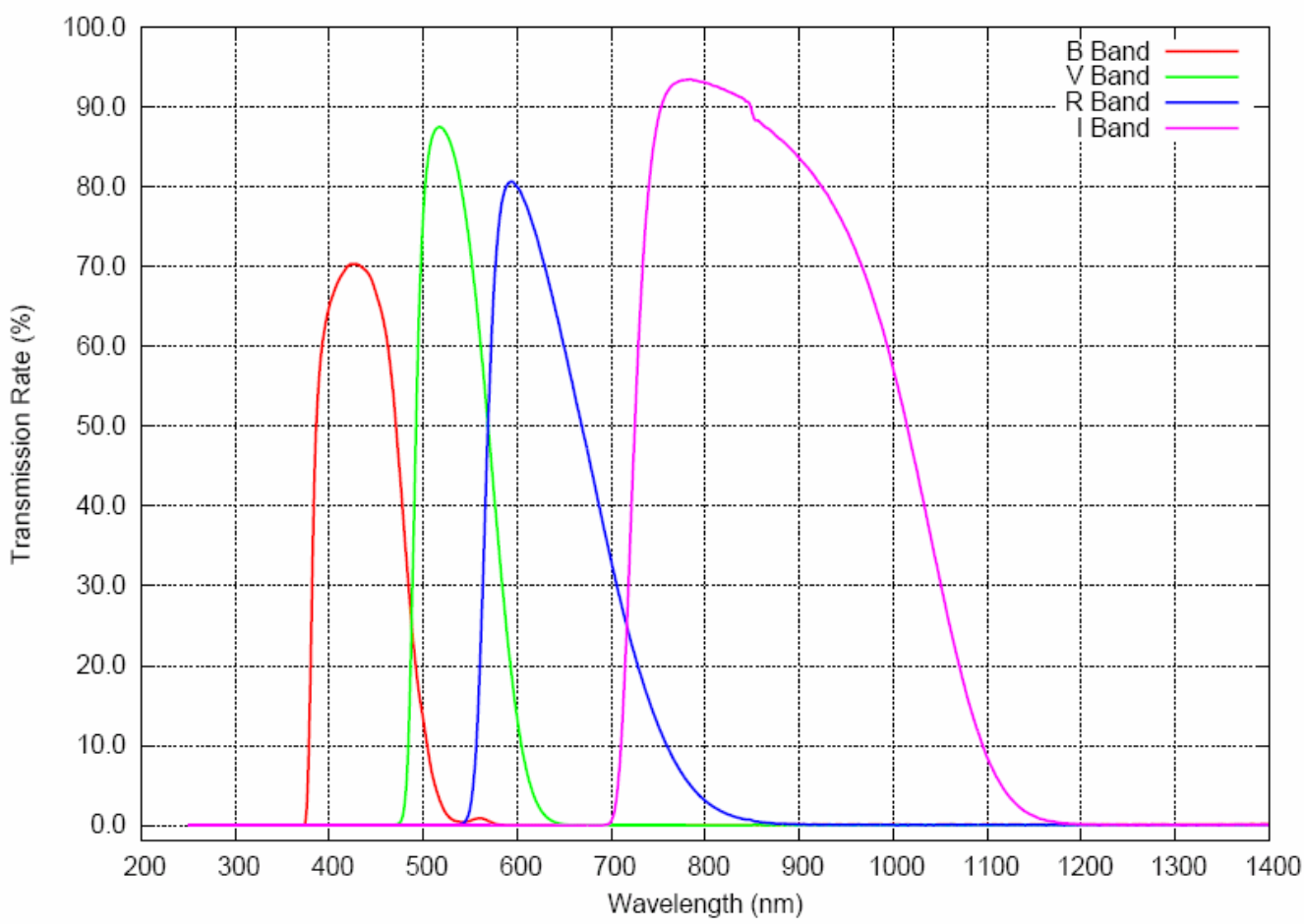

Figure 4: Transmission Curves of Filters (Central Region).

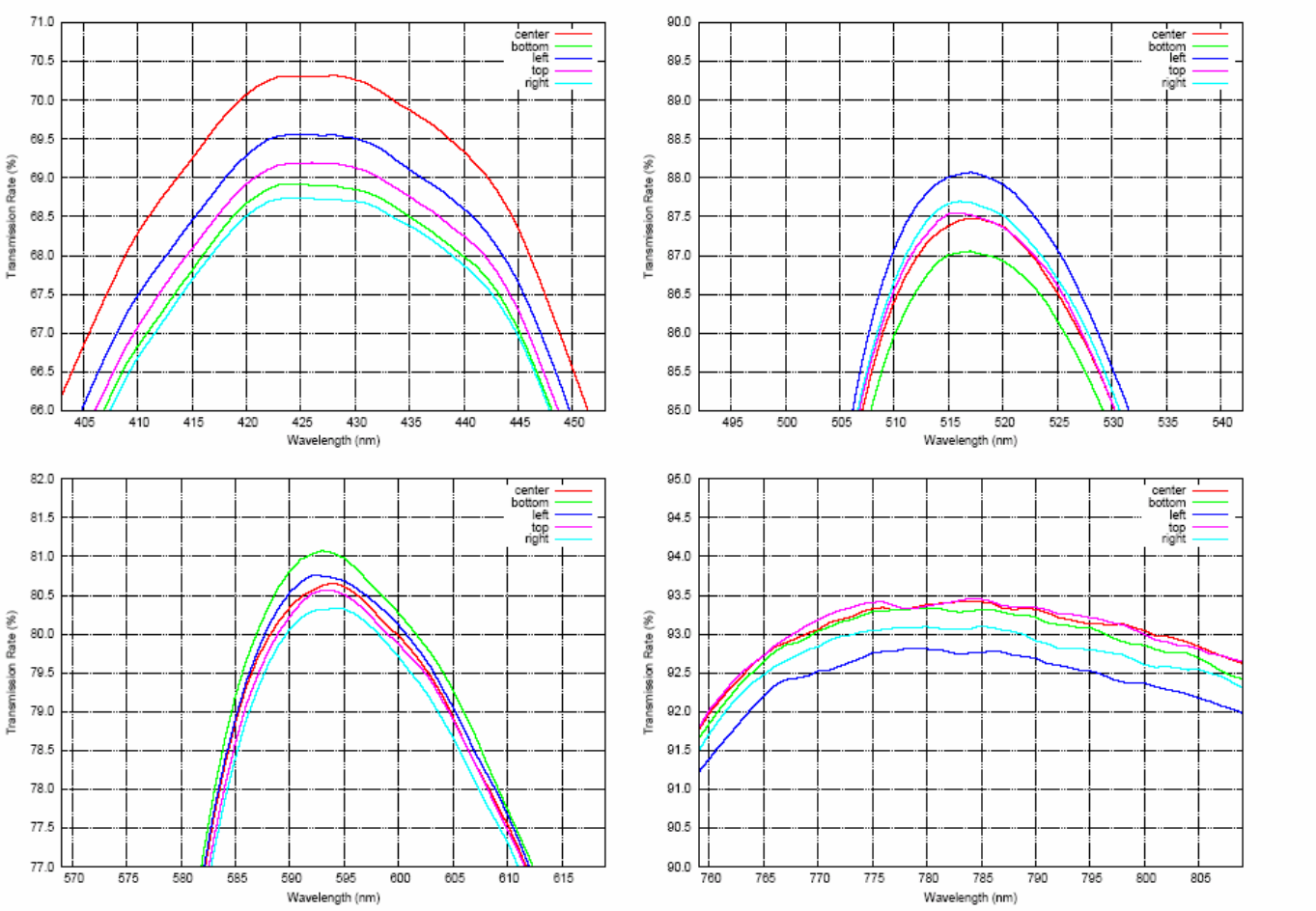

Figure 5: The Transmission Ratio Differences between Different Regions of the Filters. Top-left: B band, top-right: V band, bottom-left: R band, bottom-right: I band.

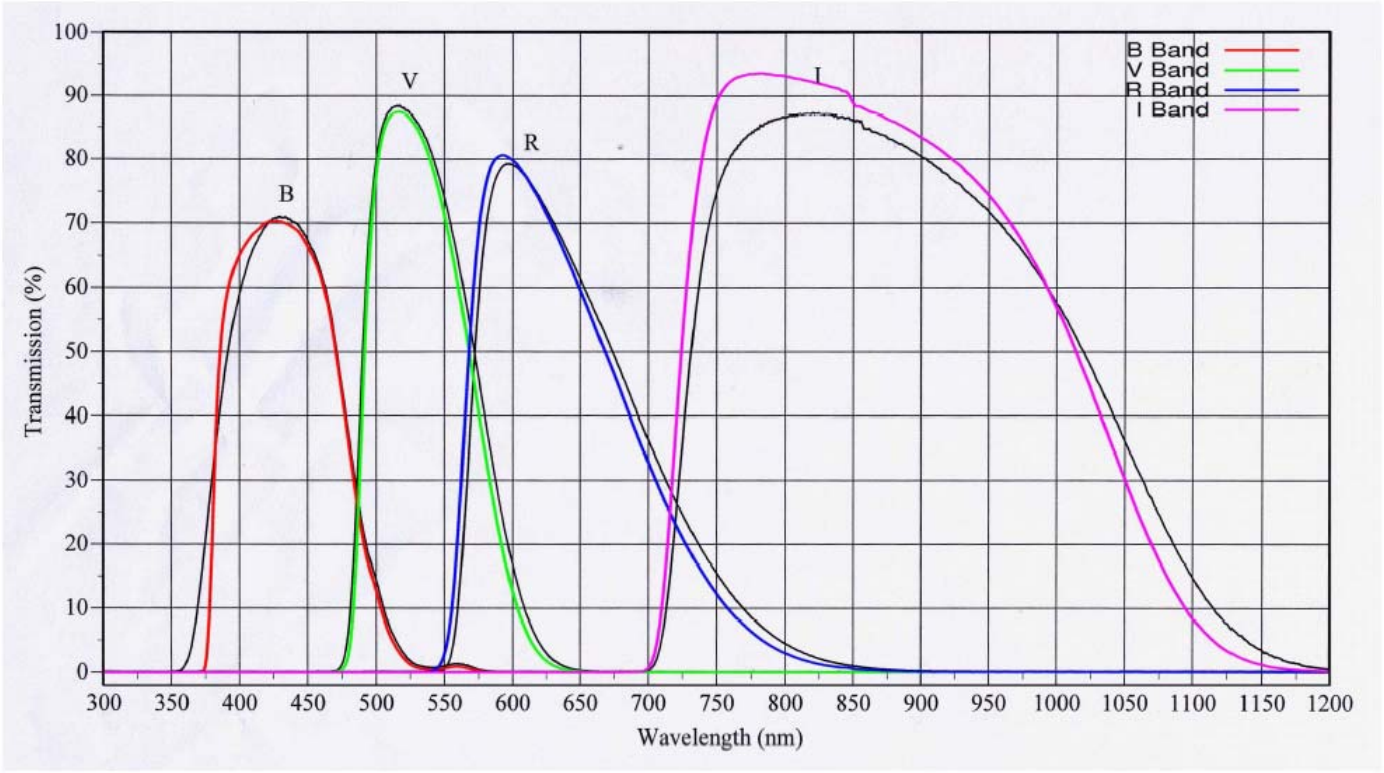

Figure 6: The Comparison of Manufacturer Provided Curves and Measured Ones

Spectrometer on LOT

Wen-Shan Hsiao, Hung-Chin Lin, Wen-Ping Chen

A duplicate Gunma Compact Spectrograph (GCS) has been installed to Lulin One-meter Telescope at the end of 2006. Two kinds of resolution are provided: low- (300gr./mm) and intermediate-resolution (1200gr./mm). Lulin Compact Spectrograph (LCS) is equipped with AP-8 CCD, and a SBIG ST-8 CCD is used to serve as slit viewer, with FOV about 5x7 arcminute. Orientation of slit is currently fixed along the north-south direction. The complete setup of equipment is shown in Fig. 1, and the view of slit monitor is shown Fig. 2. FeArNe lamp is used for wavelength calibration (Fig. 3).

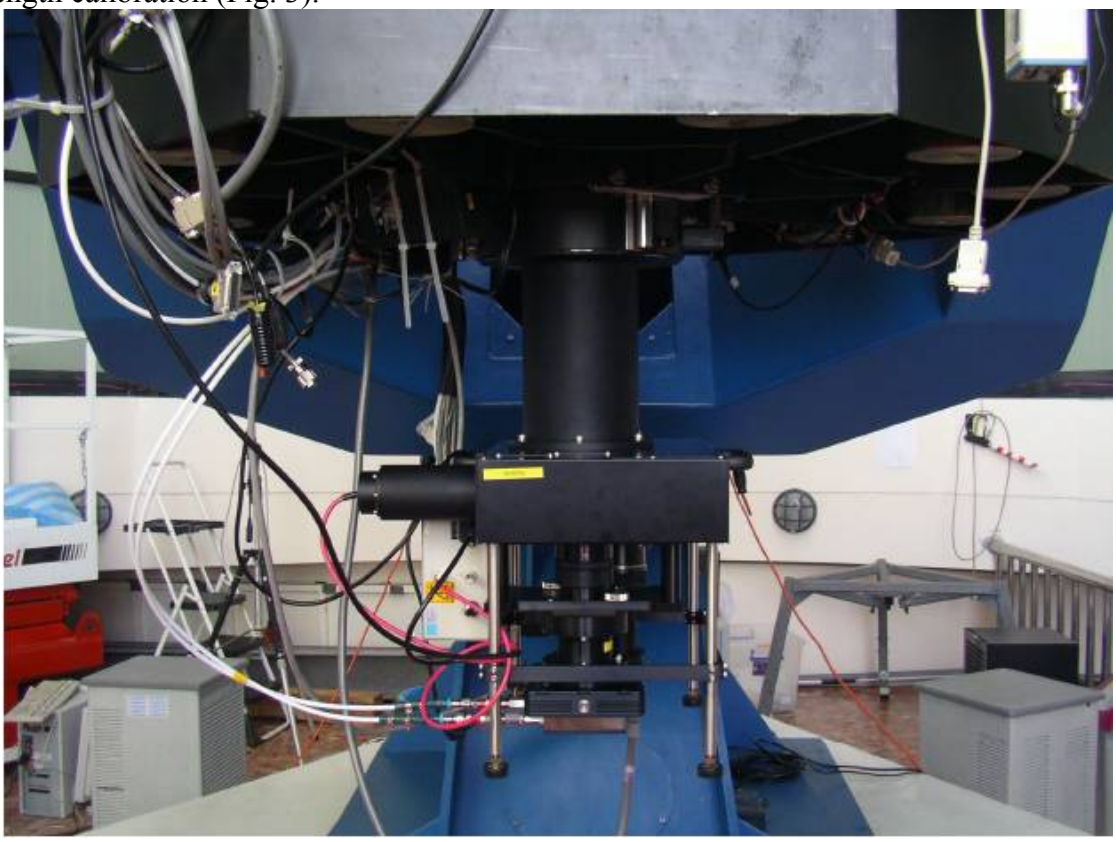

Fig. 1 LOT equipped with spectrograph.

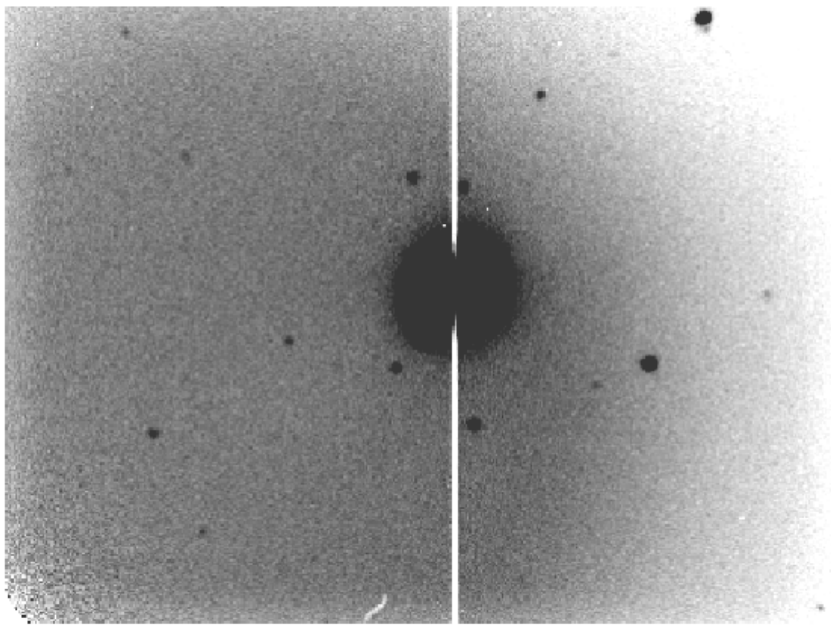

Fig. 2: NGC3242 seen in the slit monitor.

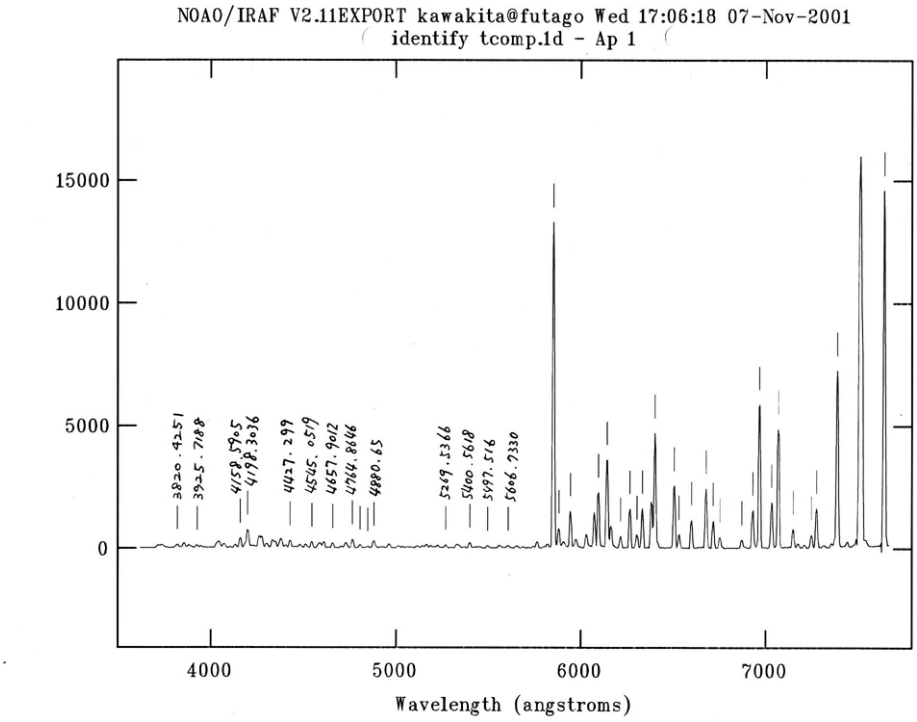

Fig. 3: Spectrum of comparison lamp.

Both dome flat and twilight flat were applied to the object, in order to examine if the results processed with these two flats are consistent. Fig. 4 and Fig. 5 are response images (could be thought as normalized flat) of dome flat and twilight flat.

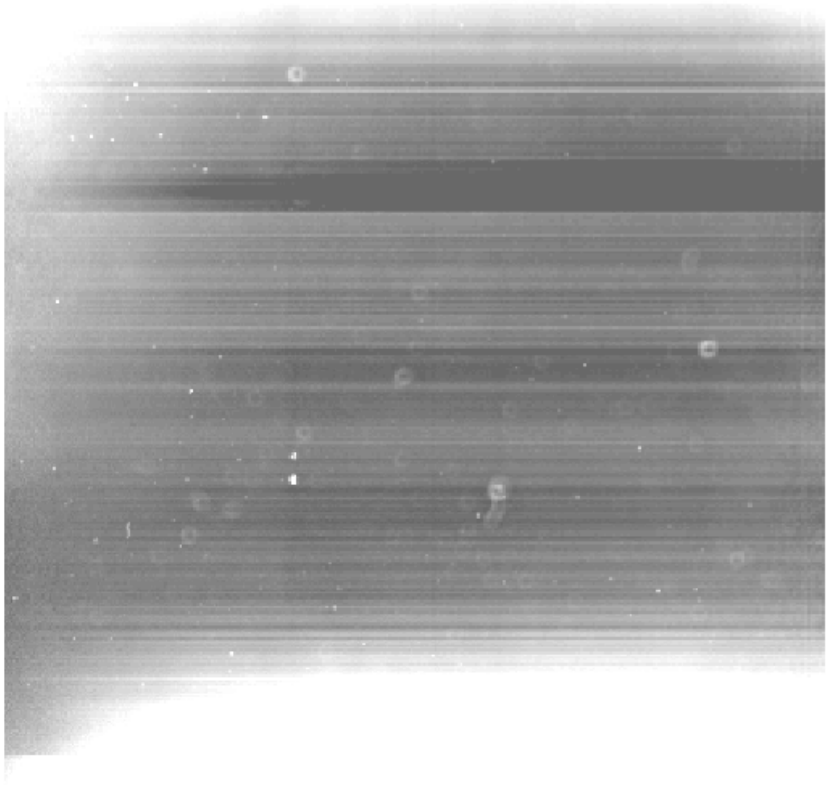

Fig. 4: Response image of dome flat.

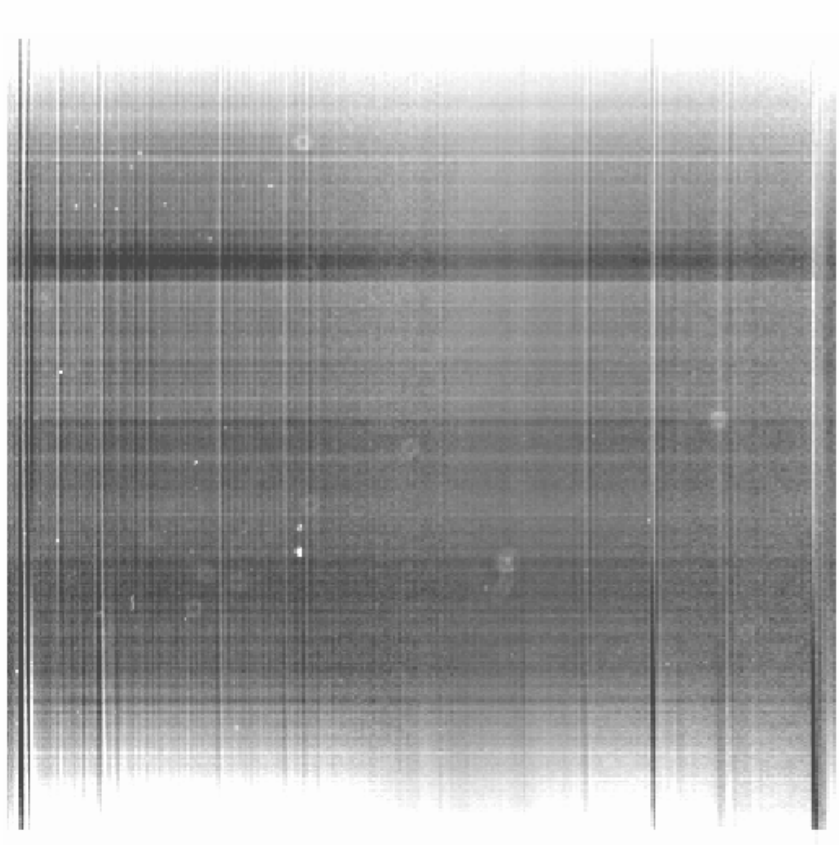

Fig. 5: Response image of twilight flat.

We took low-dispersion spectrum of Eskimo nebula (NGC2392) for the following analysis. The bright source in the center of Fig. 6 is Eskimo nebula (Vmag=10.11). We combined 2 spectra of 300-seconds and 600-seconds exposure time (with autoguiding) to

yield a better SNR spectrum. The spectrum was then bias- and dark-subtracted, and it was calibrated individually with dome flat and twilight flat. Wavelength calibration was applied with FeArNe standard lamp. The wavelength coverage is from 3900 to 7700 angstrom (about 3.7Å/pix). System sensitivity as a function of wavelength was computed from standard star HD 19445, and then we applied this result to calibrate flux of Eskimo nebula. The final results are shown in Fig. 7 and Fig. 8.

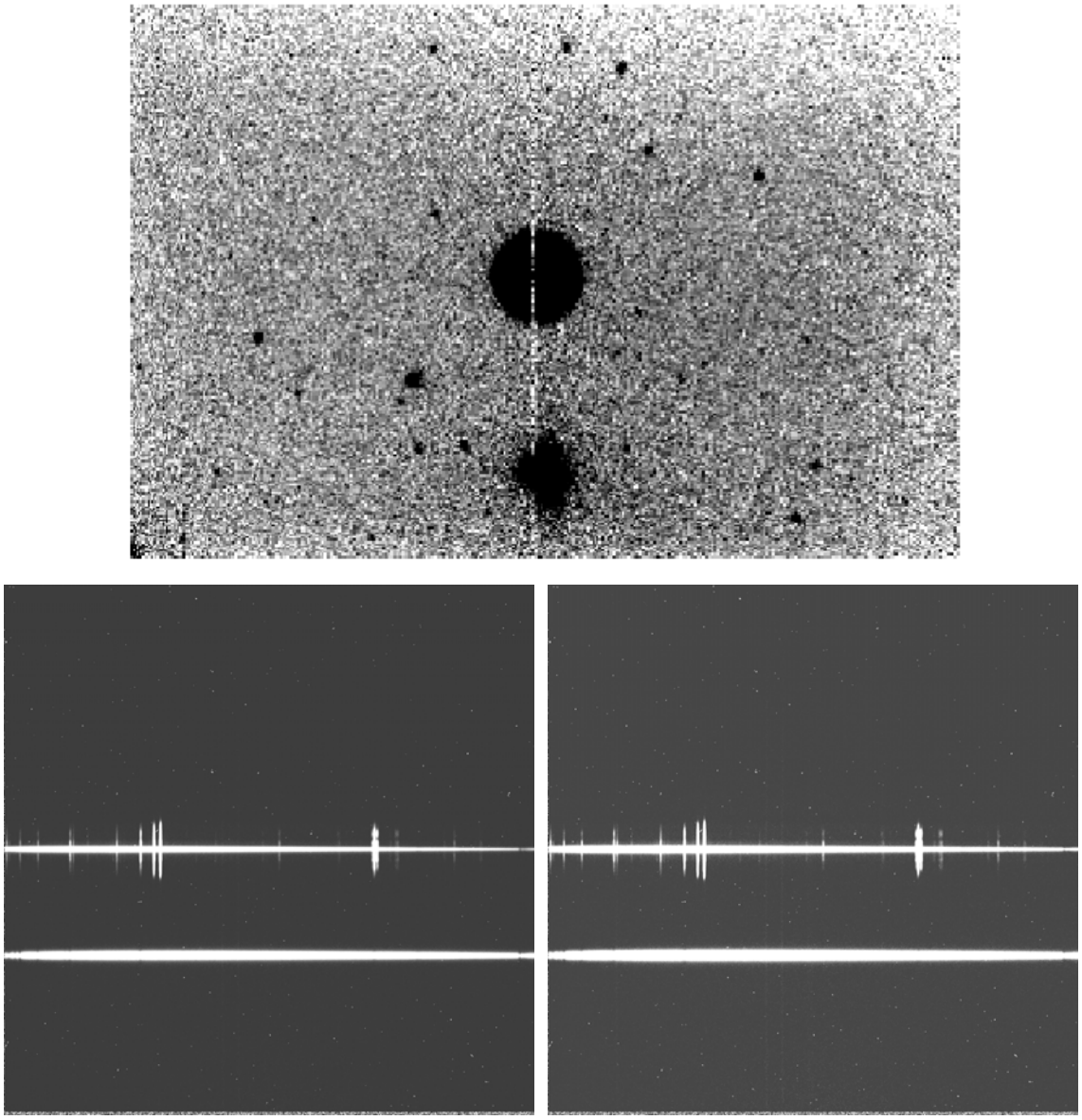

Fig. 6: Slit viewer image of Eskimo nebula (upper one), and calibrated spectra (lower-left is calibrated with dome flat, and lower-right is calibrated with twilight flat).

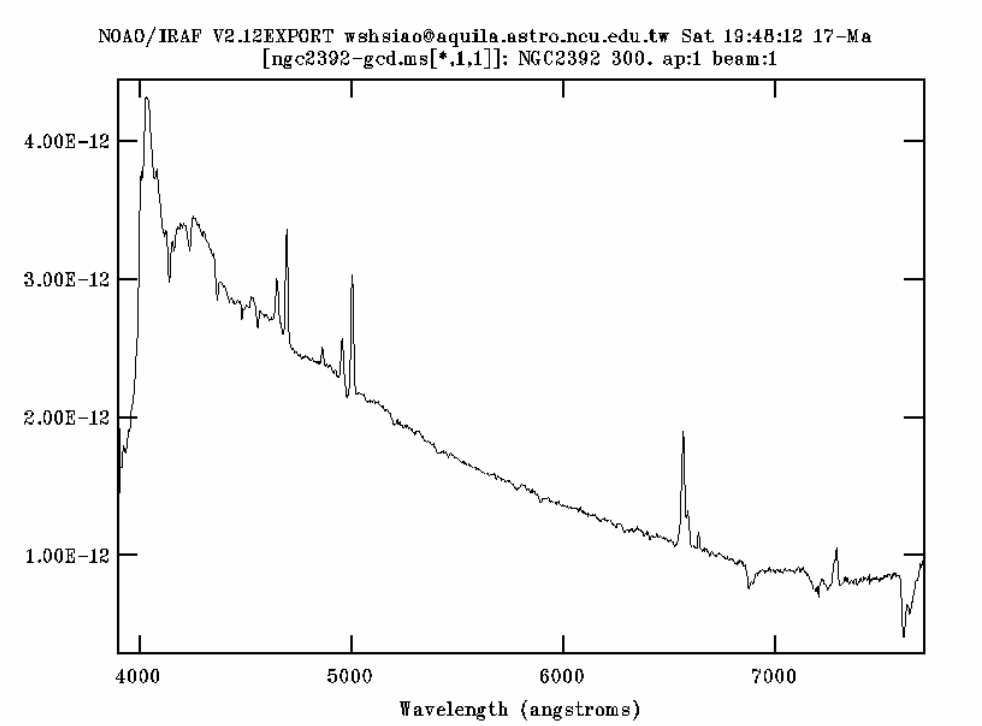

Fig. 7: Spectrum of Eskimo nebula, calibrated with dome flat.

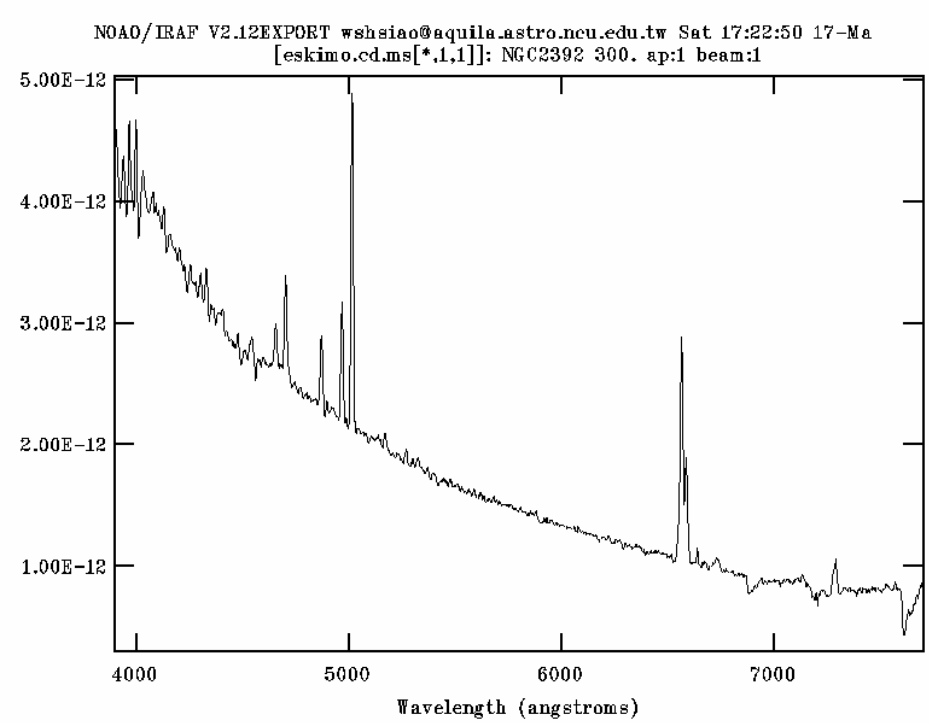

Fig. 8: Spectrum of Eskimo nebula, calibrated with twilight flat.

Many emission features, such as Hα, [OI] (5011 & 4958 Å), Hβ, MgI (4700 Å), could be identified from these low-dispersion spectra, though the intensity of some lines between these two spectra is a little bit different. The more obvious difference is the continuum at wavelength shorter than 5000 angstrom, which could be because of the slight difference of response images between dome flat and twilight flat.

Our preliminary results of the spectrograph mounted on LOT indicate that LCS serves well for the studies about line-identification and spectral-type classification. Further examinations would be done to test the behaviors of standard lamp pointing toward

different directions, to test quality of dome flat, and to get a better idea of the performance of LCS.

Below shows more spectra taken with LCS at low dispersion.

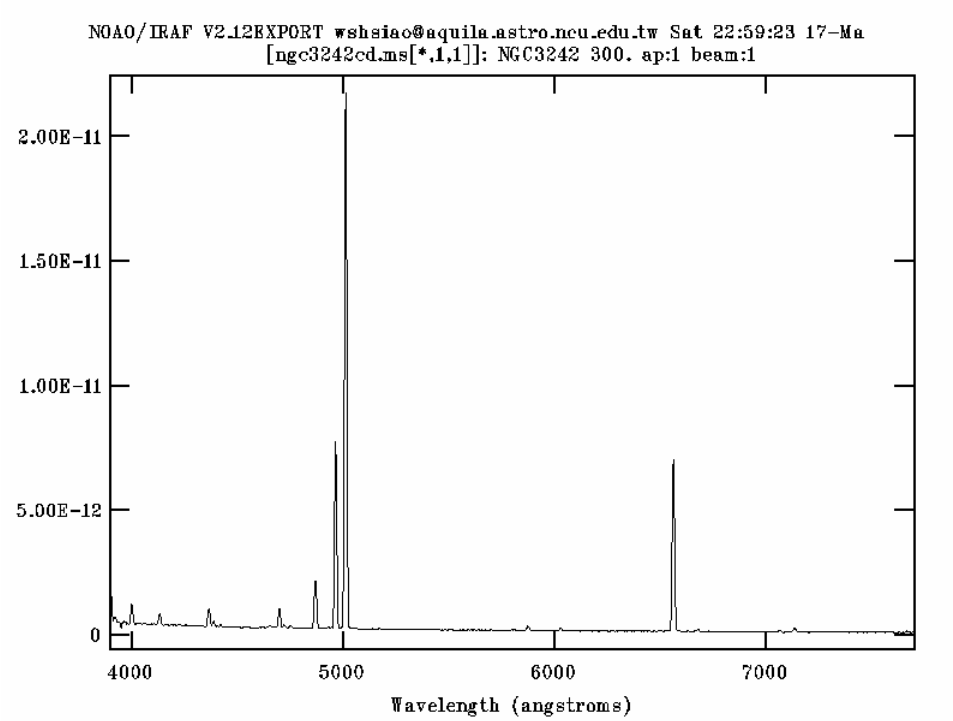

Spectrum of NGC 3242, a planetary nebula. V band magnitude is 7.0 (SIMBAD), and exposure time is 300 seconds.

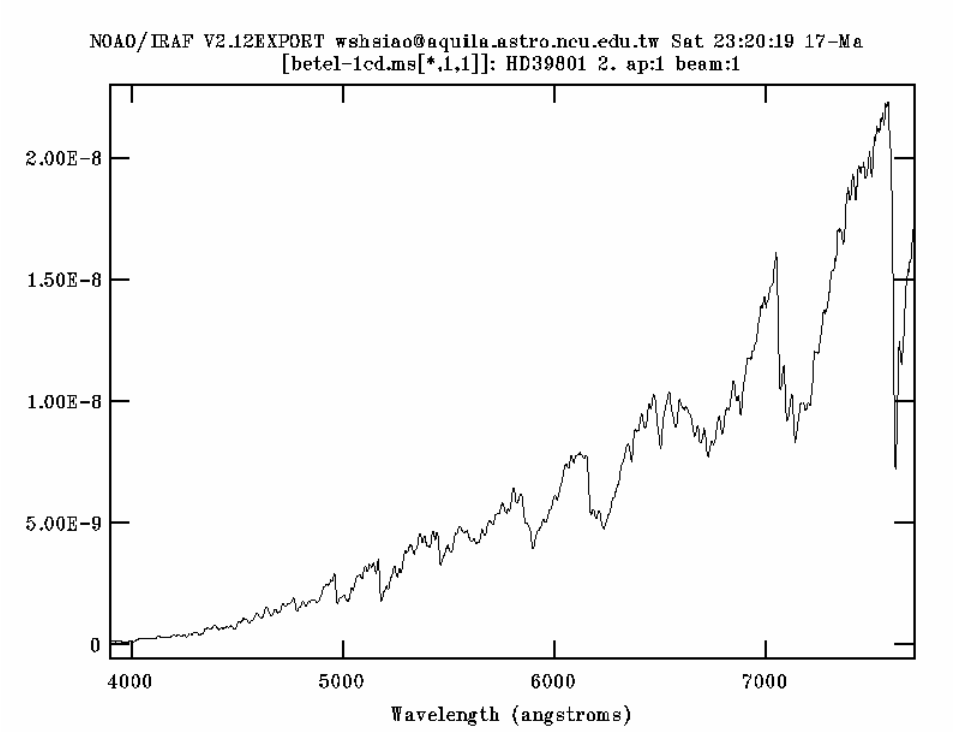

Spectrum of Betelgeuse, a M-type pulsating star. V band magnitude is 0.58 (SIMBAD). Exposure time is 2 seconds.

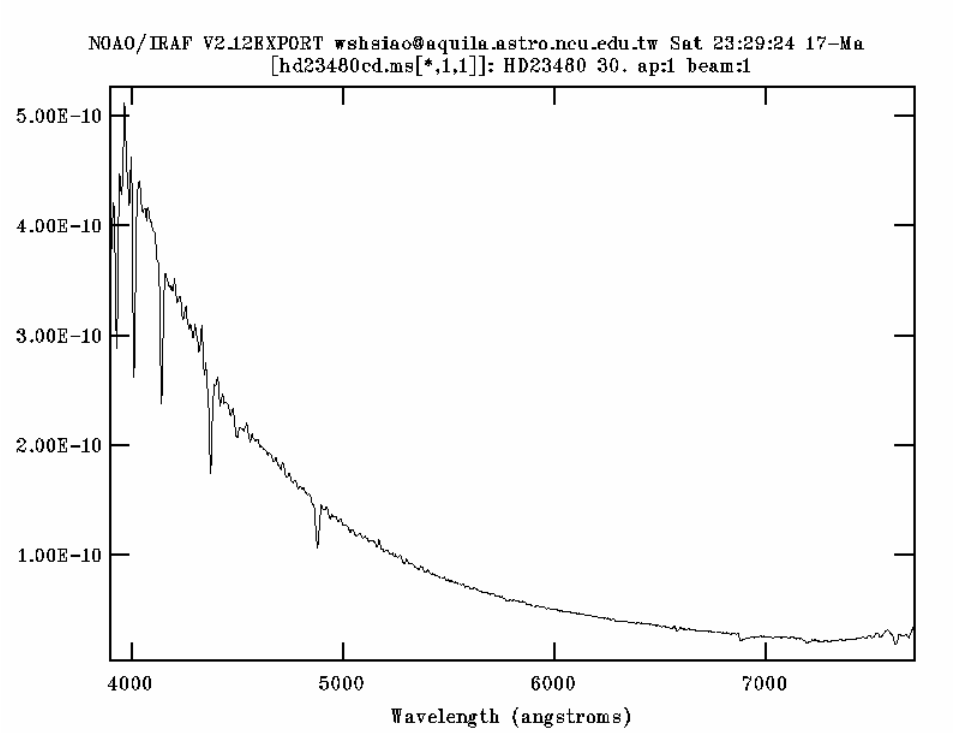

Spectrum of HD 23480, a B6-type star with V magnitude of 4.164 (SIMBAD). Exposure time is 30 seconds.

鹿林天文台 2006 年凱米颱風災害報告

林宏欽

2003 年 9 月 1-2 日杜鵑颱風來襲，最大風速每秒 34 公尺，使鹿林受創嚴重，控制中心屋頂近一半鋼瓦被掀走、屋內嚴重漏水、LOT 圓頂天窗也被掀開脫軌、對外唯一道路-玉山林道路基坍掉一半… (詳見鹿林年報 2003)。

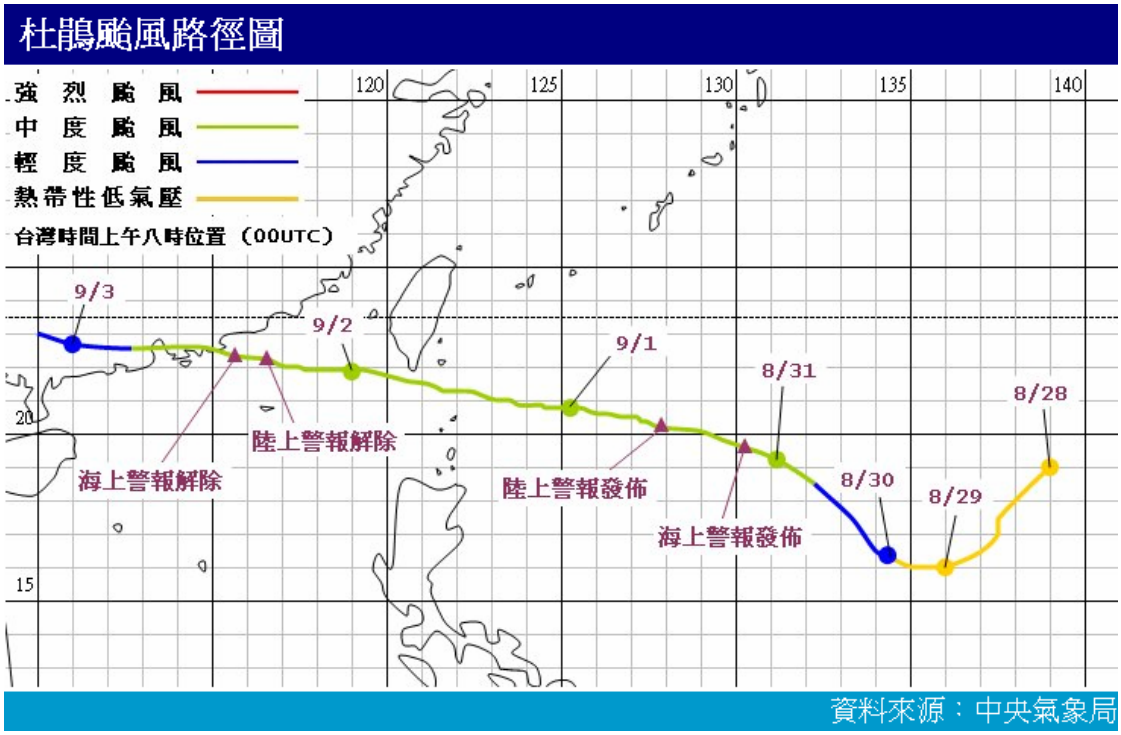

2006 年 7 月 24-25 日凱米颱風最大風速達到每秒 40 公尺，超過杜鵑颱風，鹿林再次受到嚴重考驗。

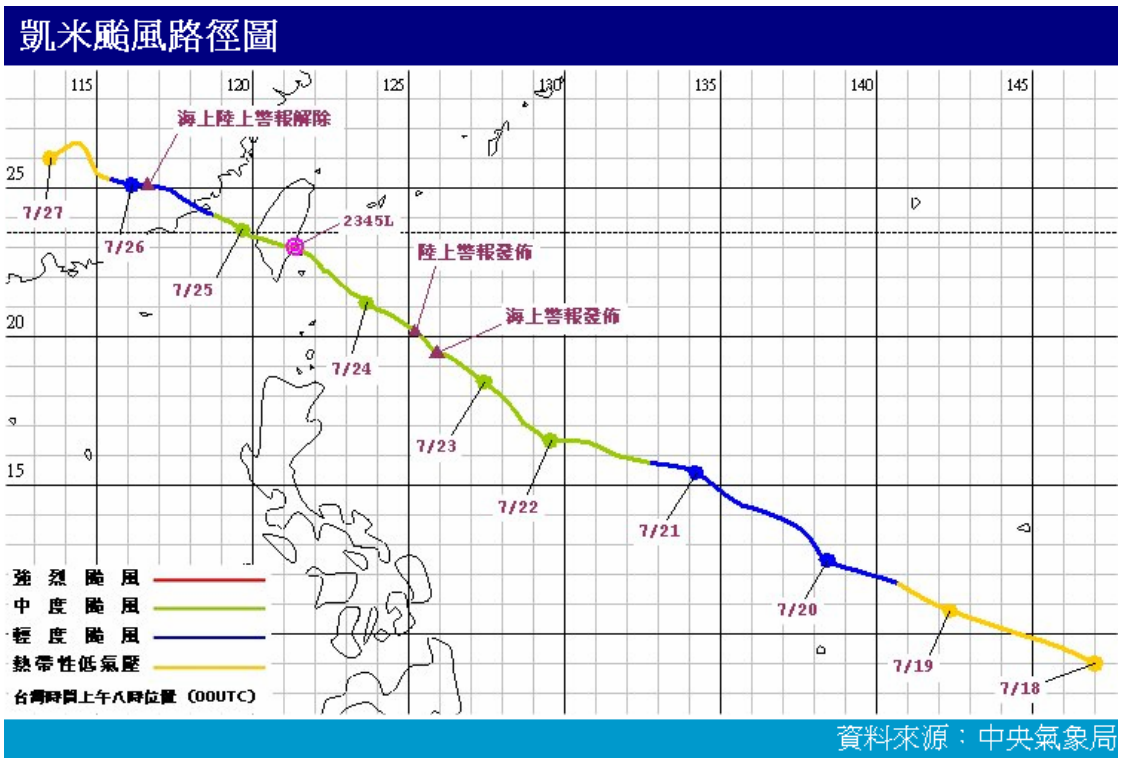

經過杜鵑颱風後的修復補強工作，當年的慘況未再出現，但仍然有防颱漏洞存在，造成損壞。駐站人員回報：經過一夜的折騰，甚至到中午都還颳風下雨，終於是稍有緩和的情勢，目前天文台內部算是還好，至於外面就比較嚴重了，但大致上算是還安全的。受損情形簡述如下

- SLT 大門被吹壞

- LOT 圓頂天窗脫軌
- LOT 圓頂耳朵鋼板被掀起

- 控制中心窗戶遮陽板多處被吹破
- 多處樹木被吹倒折斷

- 旗竿台大理石被吹壞

- 剛蓋好的環保署大氣背景站第一年就碰上鹿林有氣象紀錄(2002~)以來的強風，屋頂儀器設備被吹得東倒西歪，所幸無太大損壞

鹿林天文台氣象資料統計

楊庭彰，林宏欽，林啓生

一、前言：

一個專業的天文台，應該對氣象的資訊有充分的掌握。因爲穩定的天氣及良好的視相度是決定良好觀測資料品質的重要因素。從 2003 起，鹿林天文台的氣象資訊有了正式記錄。希望藉由資料的累積，能建立一套完整的氣象資料統計，並能從中歸納出一些結果，俾供觀測者未來選定觀測時間的參考。

二、資料來源：

中央大學鹿林天文台在 2002 年末 LOT 上線之後，爲了對天文台當地的氣候進行統計，所以在山頂的小天池旁加裝了 Campbell Weather Station（如圖），可以提供每十分鐘及每小時兩種不同時間解析度的記錄模式。此文章即是使用 Campbell Weather Station 在這三年的記錄資料所作的統計。

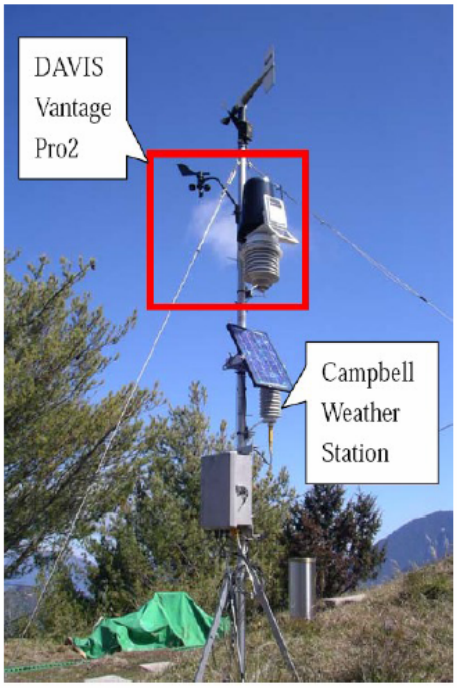

三、氣溫資料：

2003-2005 年的氣溫資料主要是由 Campbell 氣象站所記錄，資料如下：

- 2003 年氣溫資料（單位：℃）：

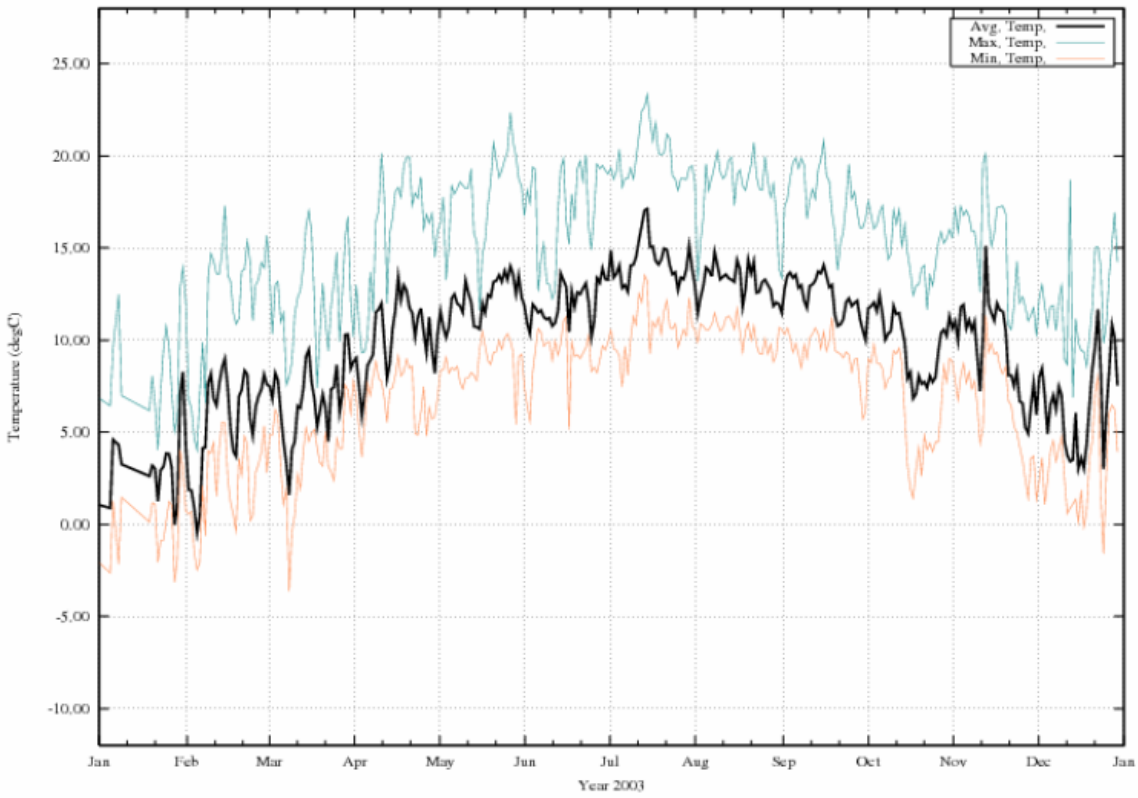

- 2004 年氣溫資料（單位：℃）：

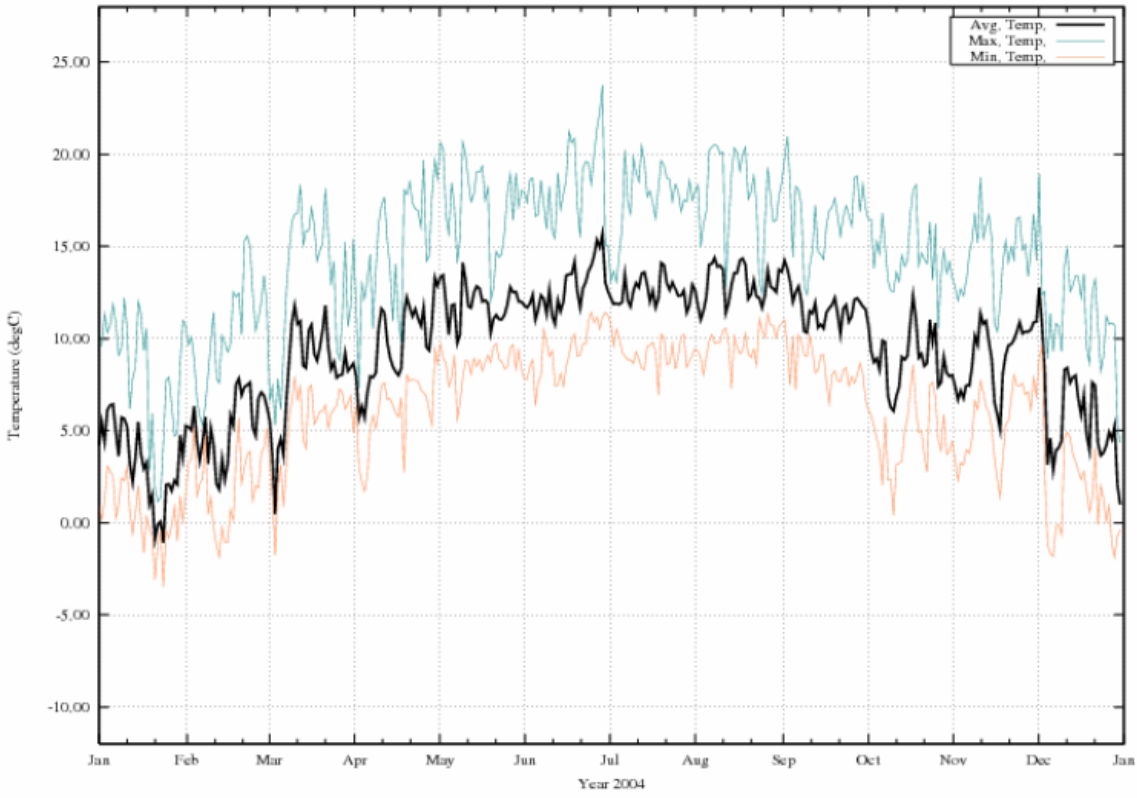

- 2005 年氣溫資料（單位：℃）：
  2005 三月份罕見的下了十年以來的大雪，所以最低溫降到了約負十度左右，爲 2003-2005 三年來的最低溫。

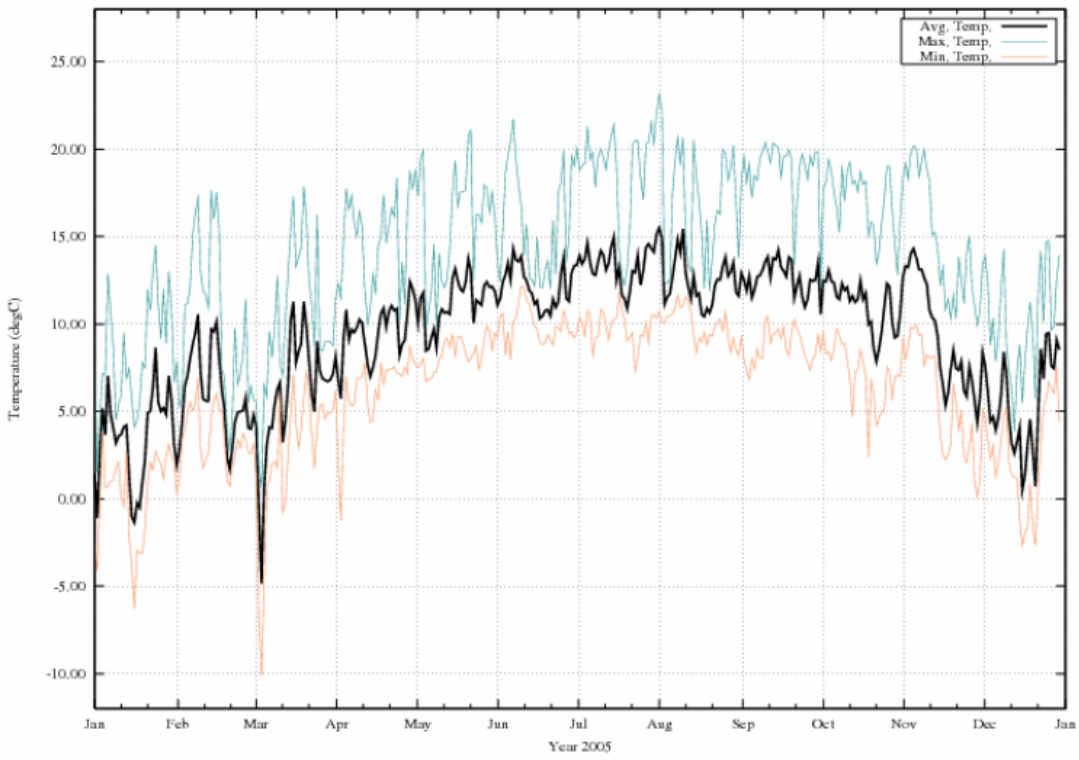

- 月均溫比較（單位：℃）：
  - 通常是每年的七月份是最熱的月份，不過也有例外，如 2004 年的 8 月份是最熱的月份。
  - 最冷的月份都是落在每年的一月份。

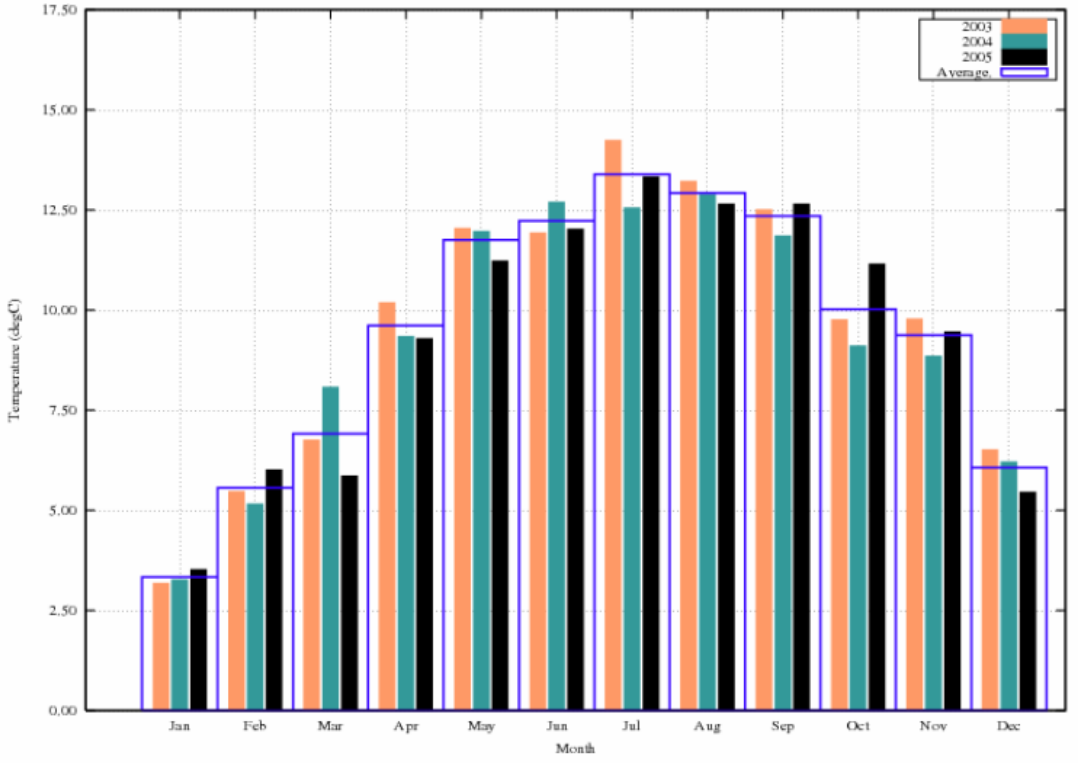

- 夜間每小時均溫比較（不同月份）（單位：℃）：

綜合 2003-2005 三年，每天 16 時到 8 時的氣溫資料，可以得出結果如下：

2003 年：

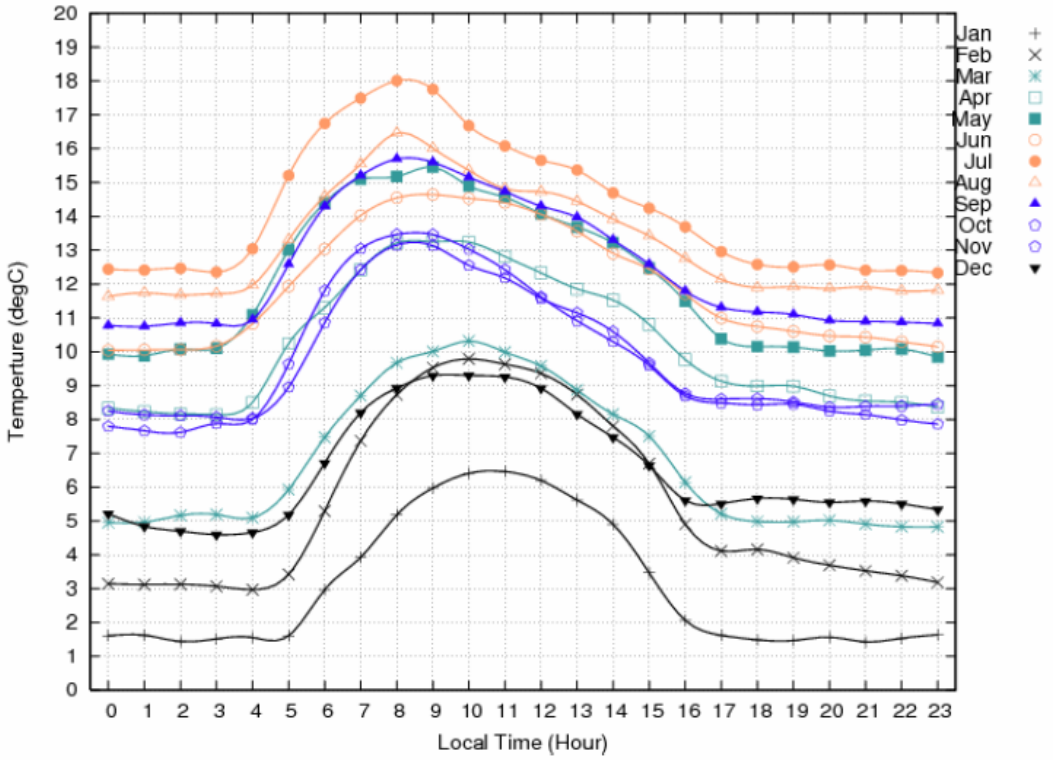

2004 年：

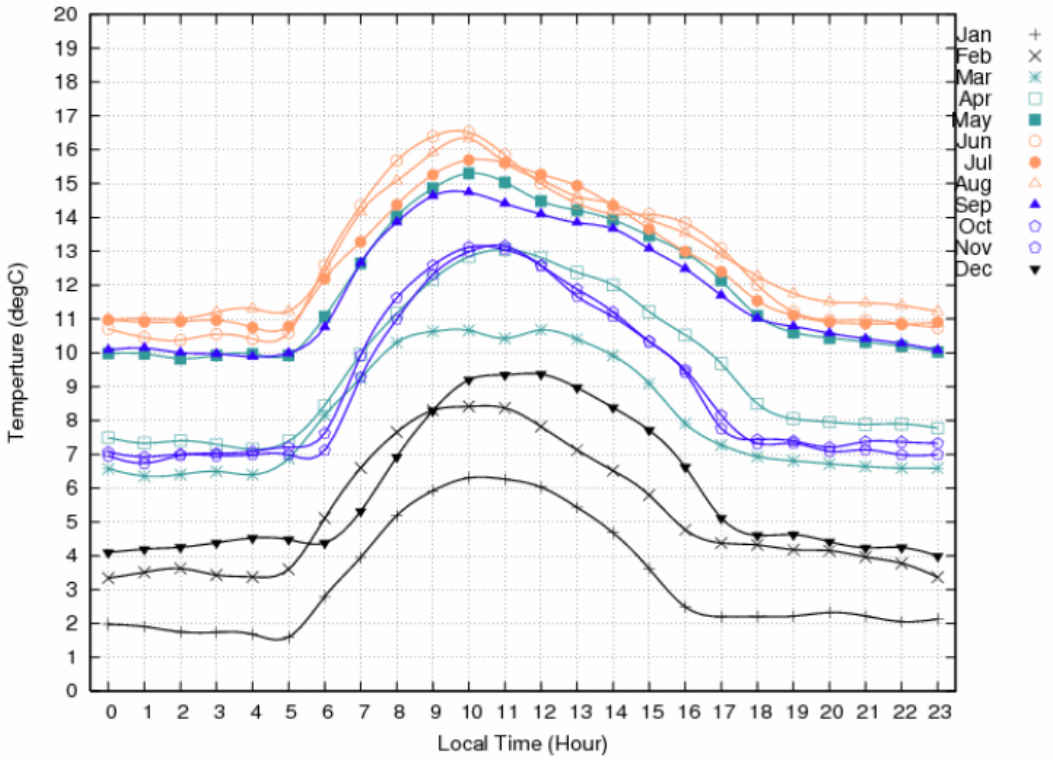

2005 年：

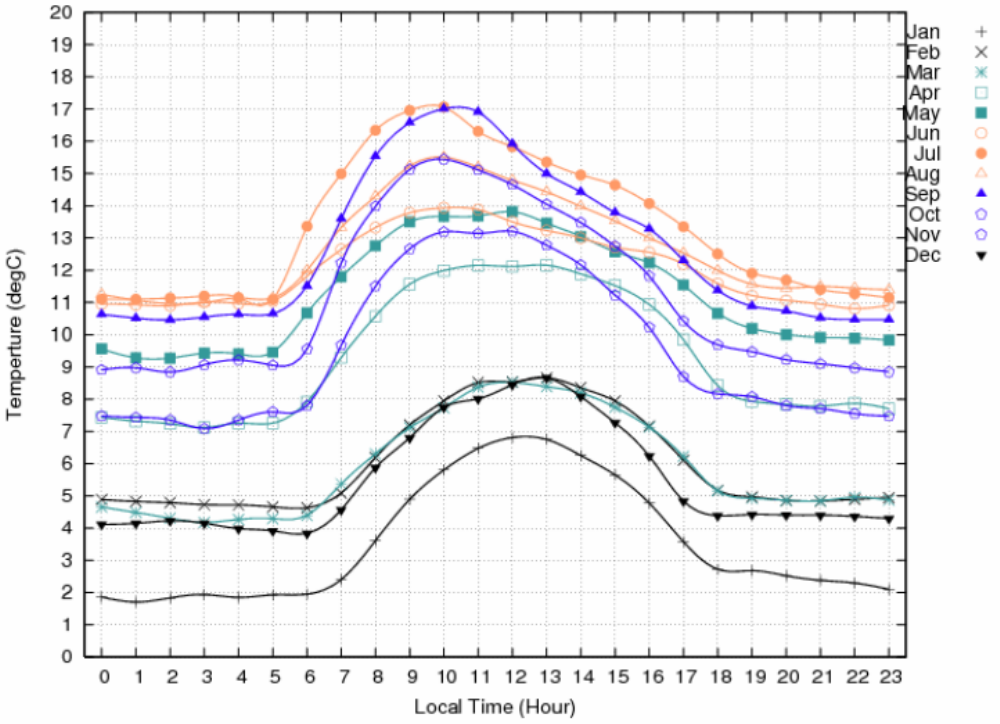

可以發現最高溫大約發生在中午或是午前時分。爲了驗證這個趨勢是否正確，所以我們也從中央氣象局拿了阿里山測站（海拔 2413.412 米）最近一個月的資料作分析，可以發現趨勢是相同的。如下圖：

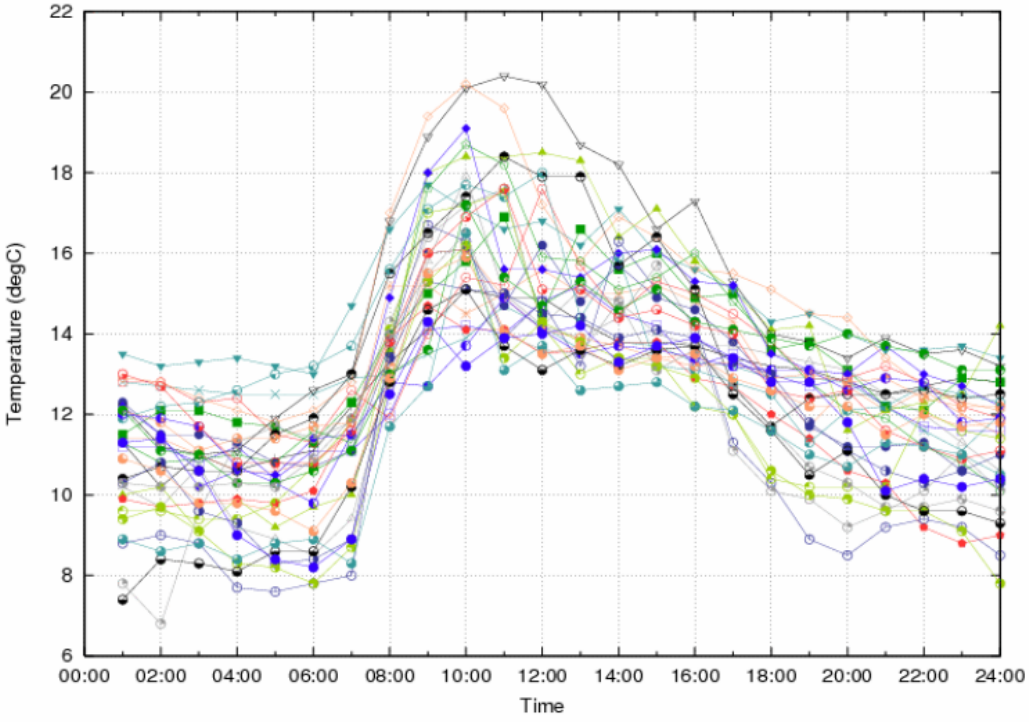

對照一下台北的資料，可以發現最高溫都市的最高溫在中午及午後附近，這點與山上的氣溫有一點小差異。在平地可能是單純[接受太陽幅射能+地面幅射能-輻散能量]爲最大值時的氣溫最高，如下圖：

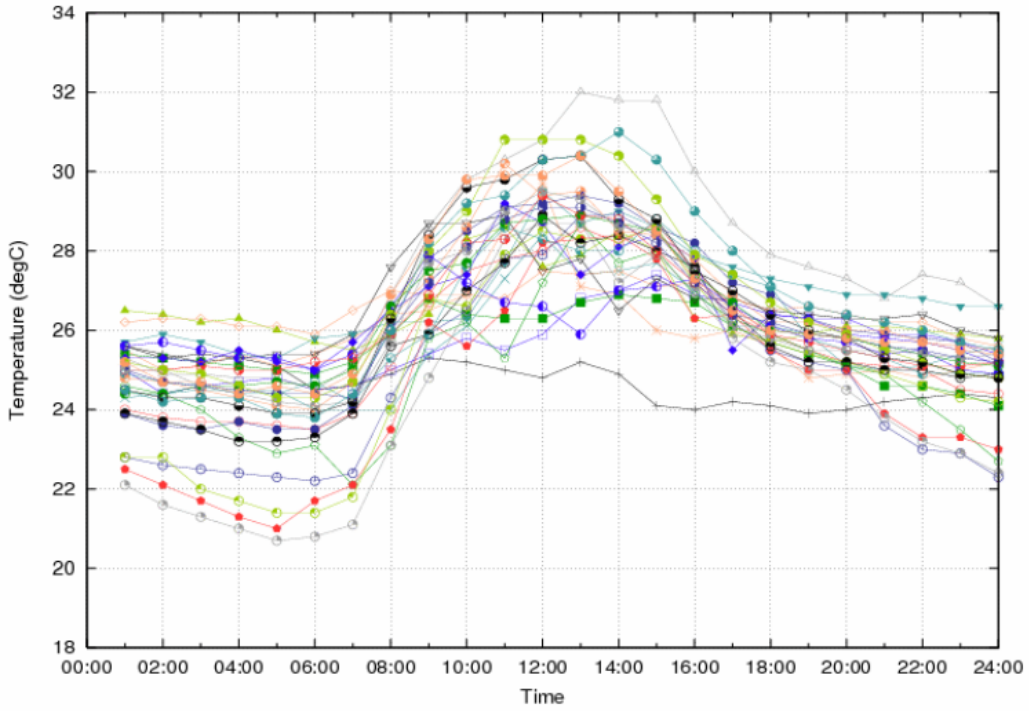

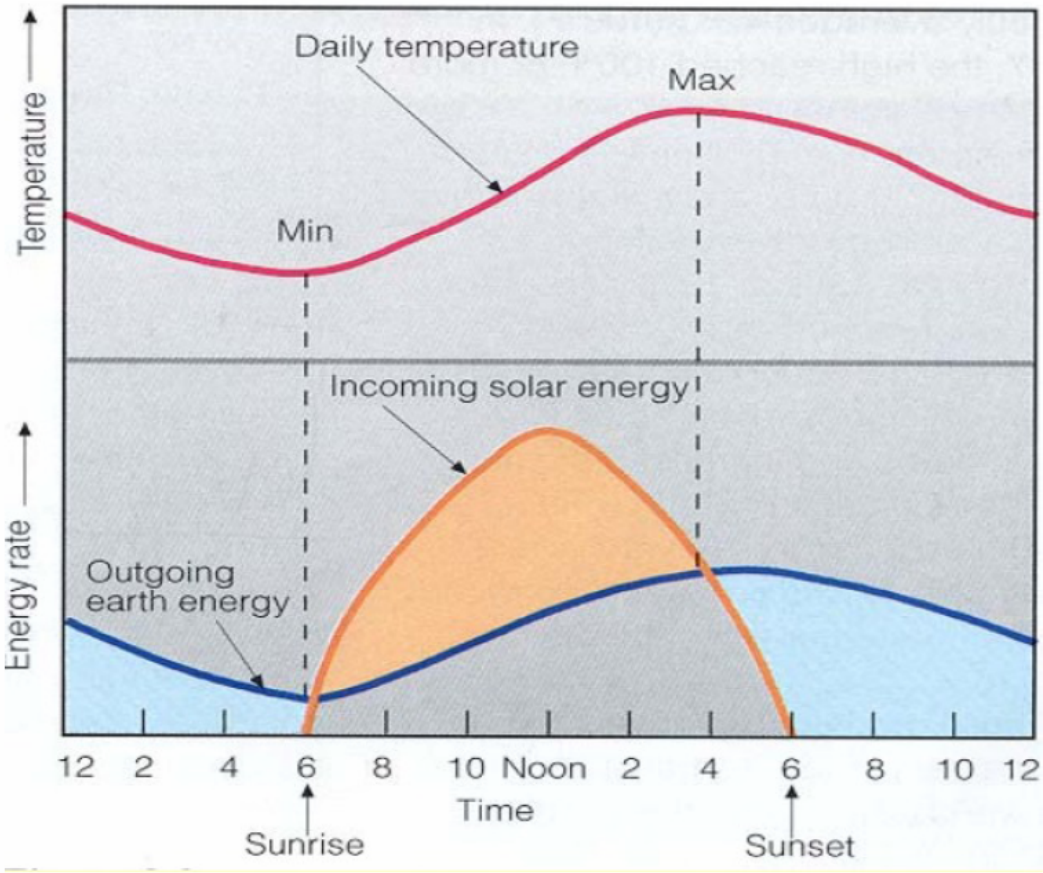

而在阿里山上的氣溫趨勢，推測可能是接近中午通常會有雲升起，減低了太陽幅射的能量，而且地表附近沒有太多人爲的建築物吸收太陽輻射，延遲輻射所產生的升溫效應，所以最高溫會出現在午前一小時左右。不過這也是初步推測，實際情況可能仍待進一步研究。

日月潭跟平地差不多趨勢(Altitude: 1017.5m)：

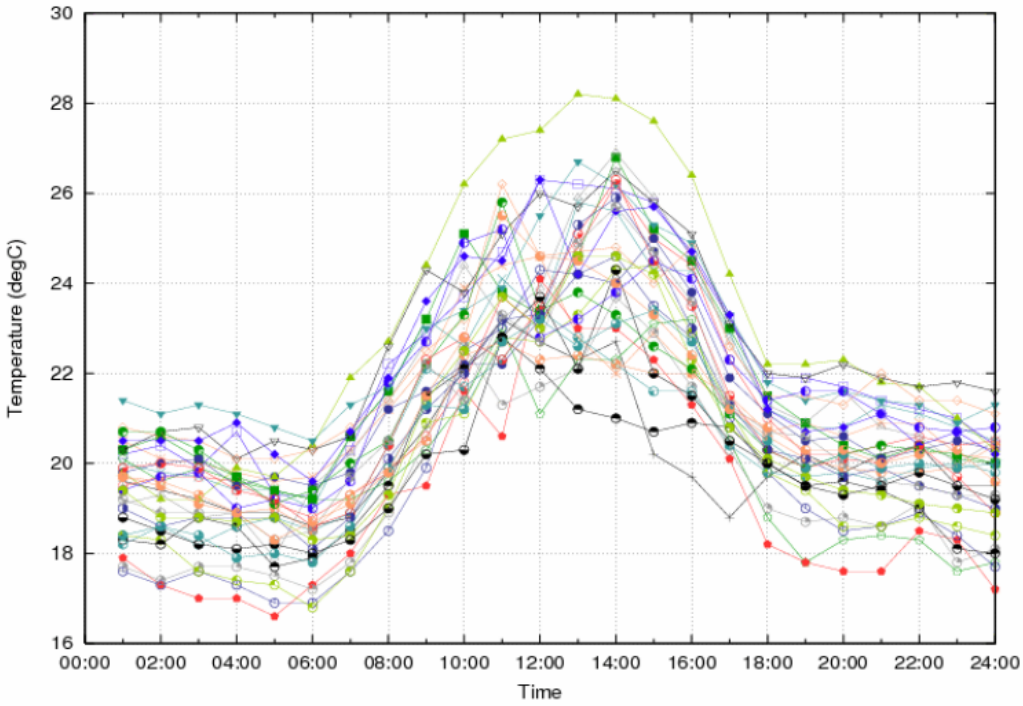

四、風的資料：

2003-2005 年 Campbell 氣象站統計的風速資料如下。由於颱風對於瞬間最大風速及平均最大風速都會有顯著的影響，所以我們把有發布颱風警報的時間及其前後一天的資料去除，可以看出風速的大約趨勢。另外由於測站距地面僅約兩公尺，未達建議測站高度（距地約 10-20 公尺），所以容易受地形及地物之影響，造成測量出的風速值偏低，所以風速資料僅爲參考用。

下圖爲 Campbell 氣象站手冊所提供的安裝參考建議，建議距離週圍地物至少約十倍地物高度的距離，不過鹿林前山腹地有限，所以未能達到其要求。

Wind Speed and Direction

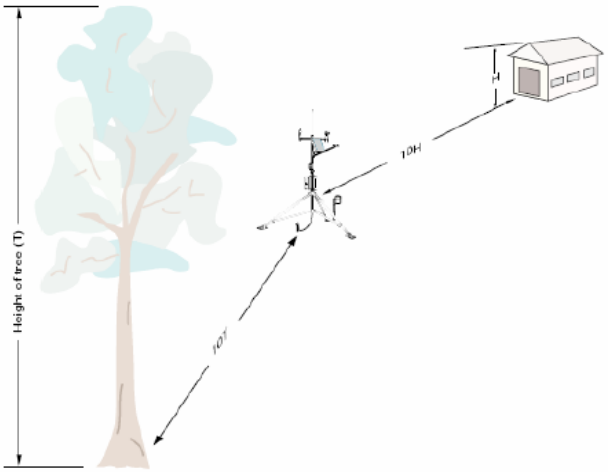

Wind sensors should be located over open level terrain. The EPA recommends the wind sensor be a distance of at least ten times the height of nearby buildings, trees, or other obstructions.

- 2003 年風速資料（橘色部分爲颱風）：

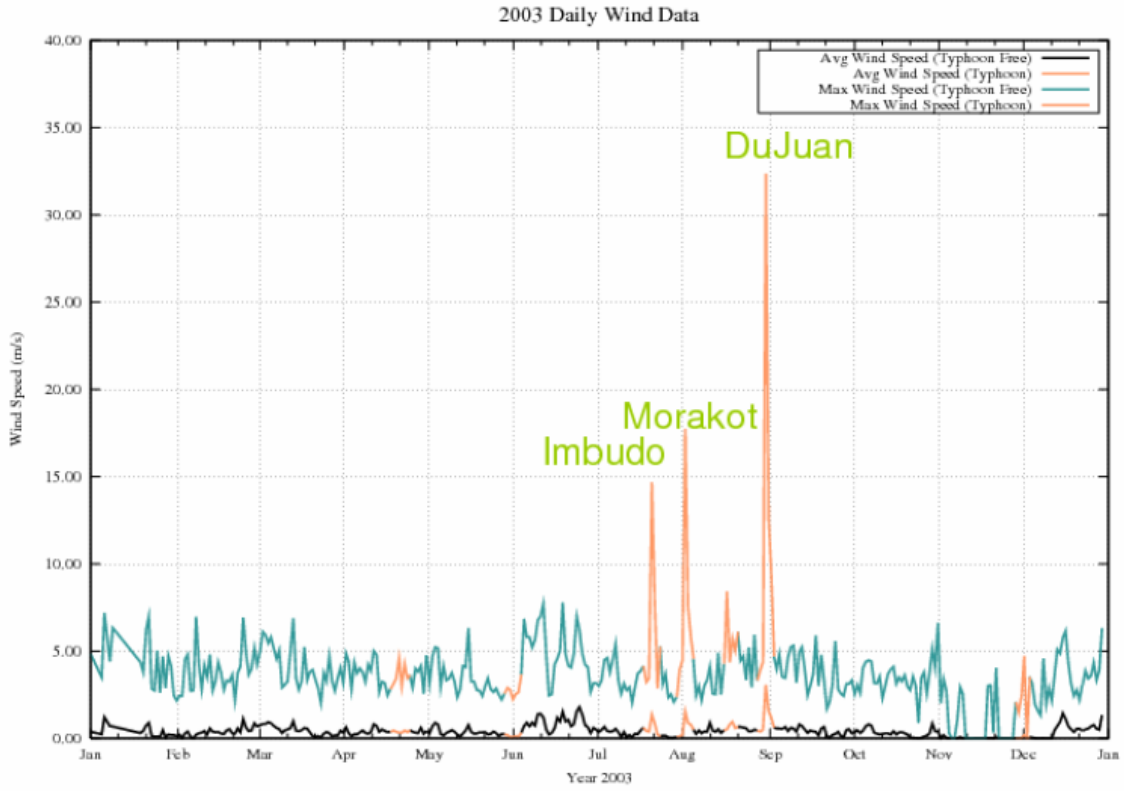

- 2004 年風速資料（橘色部分爲颱風）：

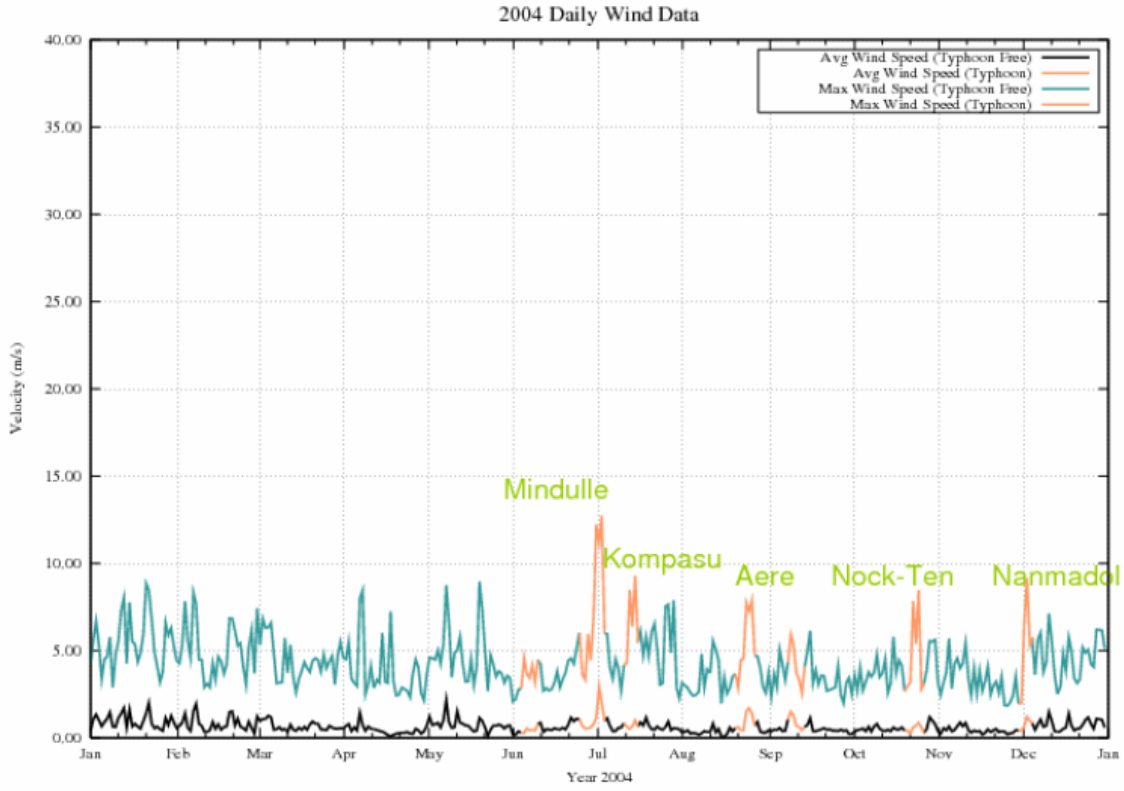

- 2005 年風速資料（橘色部分爲颱風）：

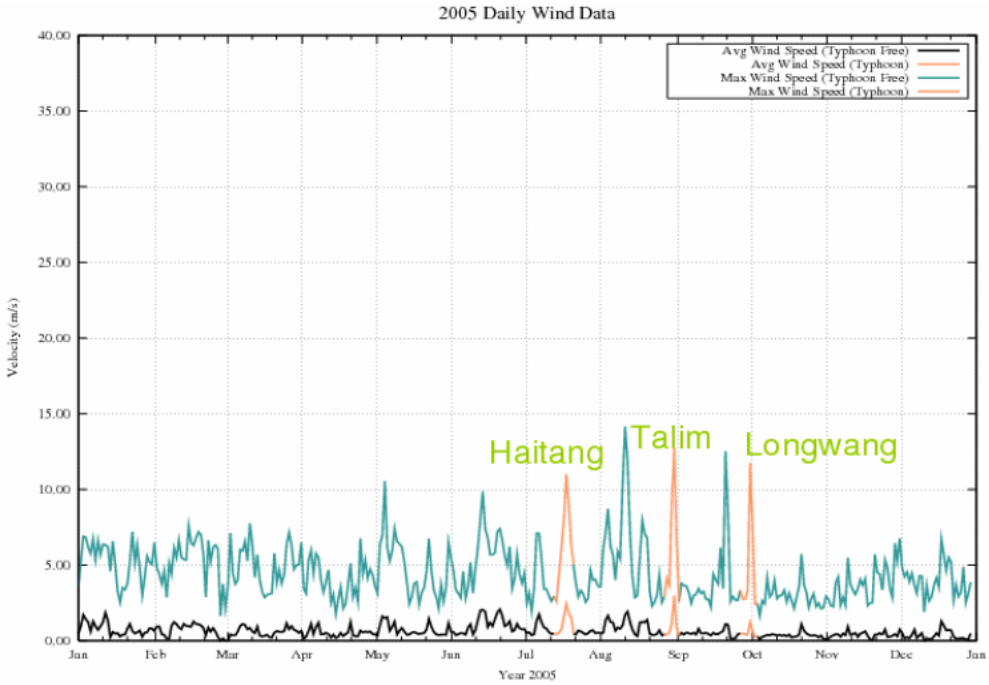

2003-2005 年開始有風速的記錄以來，2003 年杜鵑颱風帶來最大風速的記錄，而玉山氣象站 1947 年以來的最大風速（51.1m/s）也是在那時創下的。

- 每月風速的 Variance 比較：
  取出上述去掉有颱風警報發布時間的資料，我們逐年看每個月風速的 Variance。可以發現：一般而言， 5 到 8 月的風速變化較大，可能是由於此時的風面、低壓系統對於台灣影響較大的原因。而除了夏季之外，冬季的 12 到 2 月的 Variance 也稍大一些，這可能是由於東北季風（在高山處爲西南風，容後說明）在這個季節的變化對平均風速造成的影響。所以看起來風速較穩定的月份是 9 到 11 月份，觀測條件或許較佳。（圖經過 smooth 化）

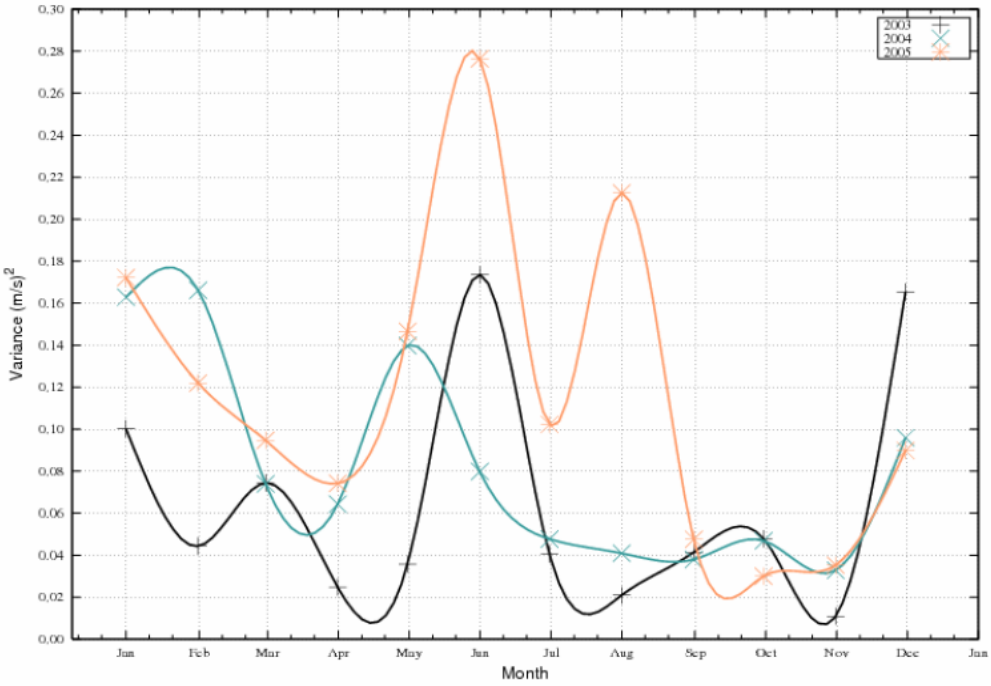

- 每月風向比較：

從圖中可看到，可能是由於地形的關係，或是測站位置不適當（造成某些方向的地形風），所以除了夏天的月份（八、九、十月）之外，其他月份以西南風爲主。

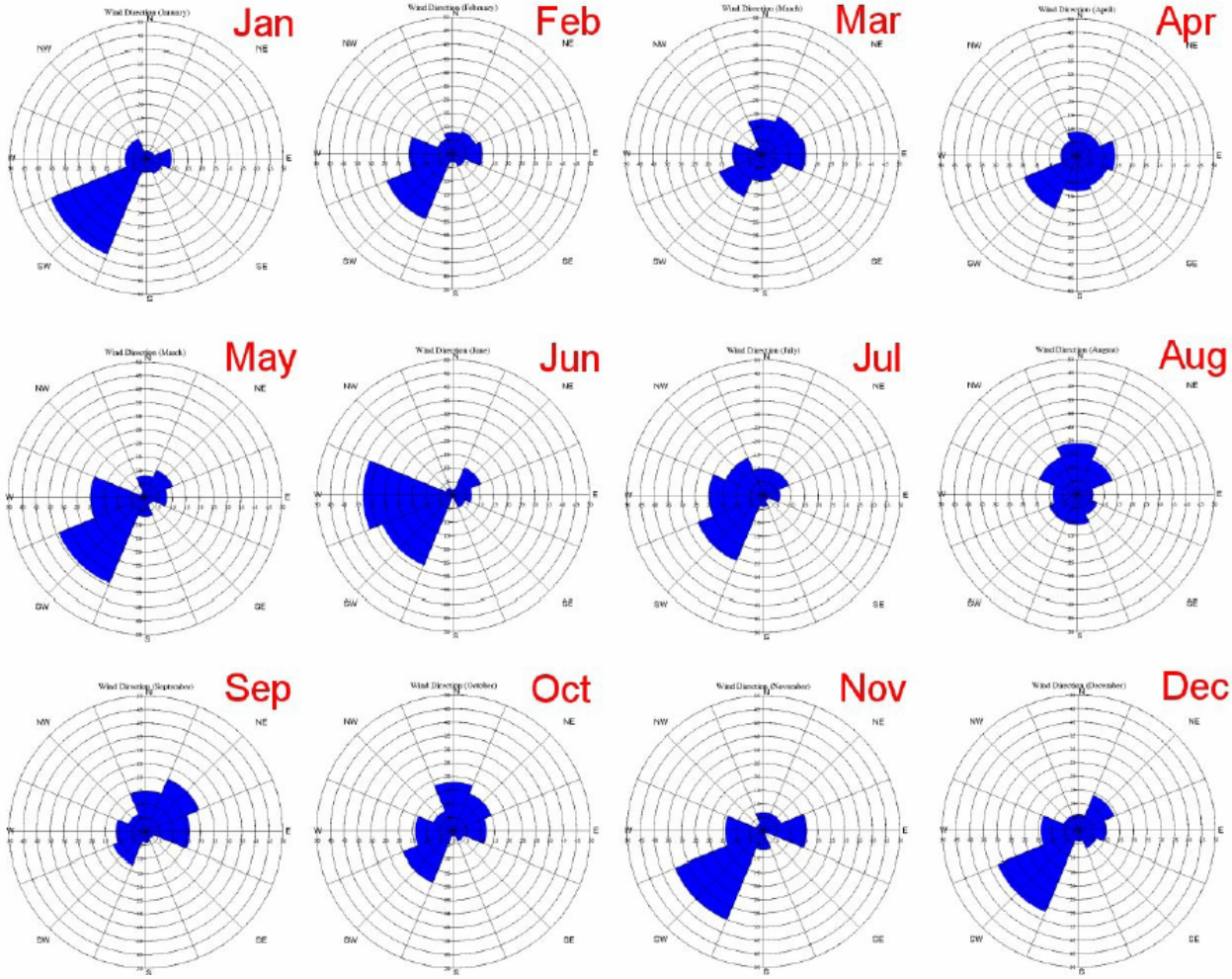

➢ 全年風向趨勢：

將全年的風向作一個統計，可以發現全年的風向以西南風最多（27.79 %）。可能是因爲地形及測站位置的關係。鹿林前山東邊有玉山山脈的屏障，而西邊相對而言是比較空曠的方向。另外，由於台灣冬季三千公尺以上的高山風向均偏西南，而且東北季風通常高度都在兩公里以下，且被東邊的玉山山脈所阻隔。所以天文台全年的東北風風向反而不明顯，反而以西南風居多。不過此現象的成因，仍待進一步的驗證。

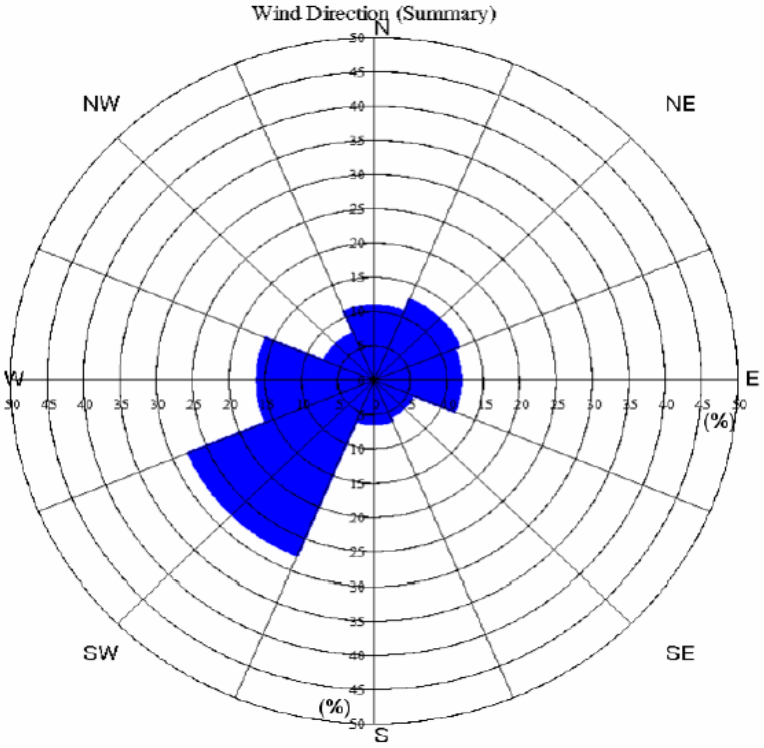

五、濕度分析：

從 2005d66 （7th/March）起，Campbell 氣象站加裝了 humidity sensor，提供了溼度方面的資料。記錄的頻率與其他氣象資訊相同。然而由於溼度計未經絕對值校正，所以最高相對溼度未能達到 100%，所以其值僅供相對參考。（註：一般的溼度計其誤差約在 ±2%~5% 之間）

- 2005 年每天平均的溼度記錄值如下（誤差以 5% 計）：

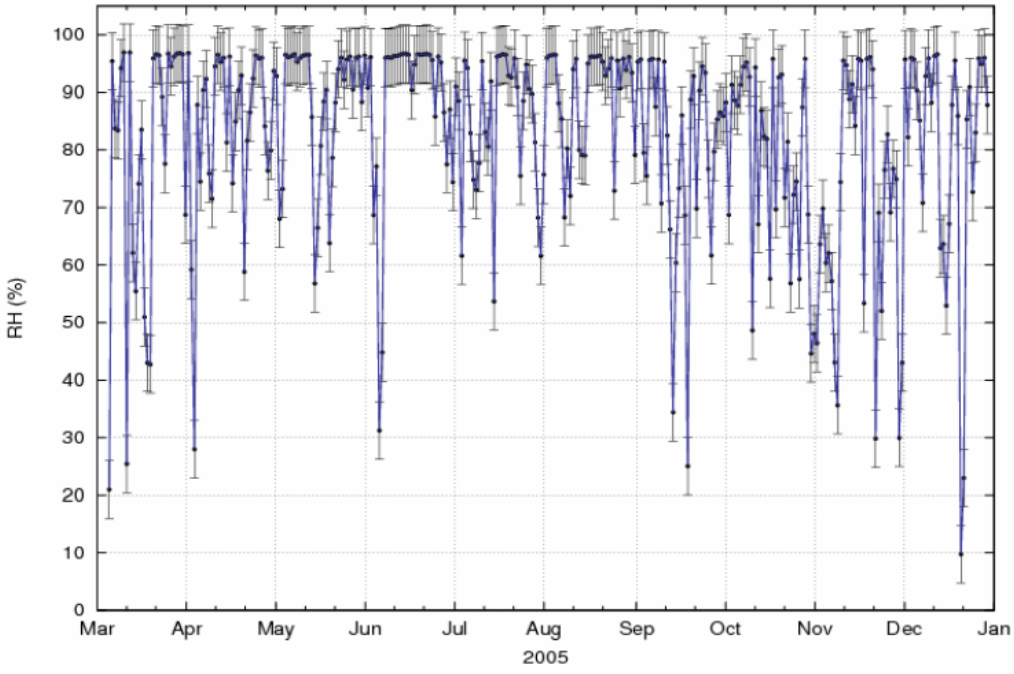

六、降雨資料：

- 每年降雨資料（含颱風）：

我們可以發現最高的降雨都與颱風的來臨有密切的關係，所以颱風對於山上的雨量的

貢獻還是有決定性的影響。

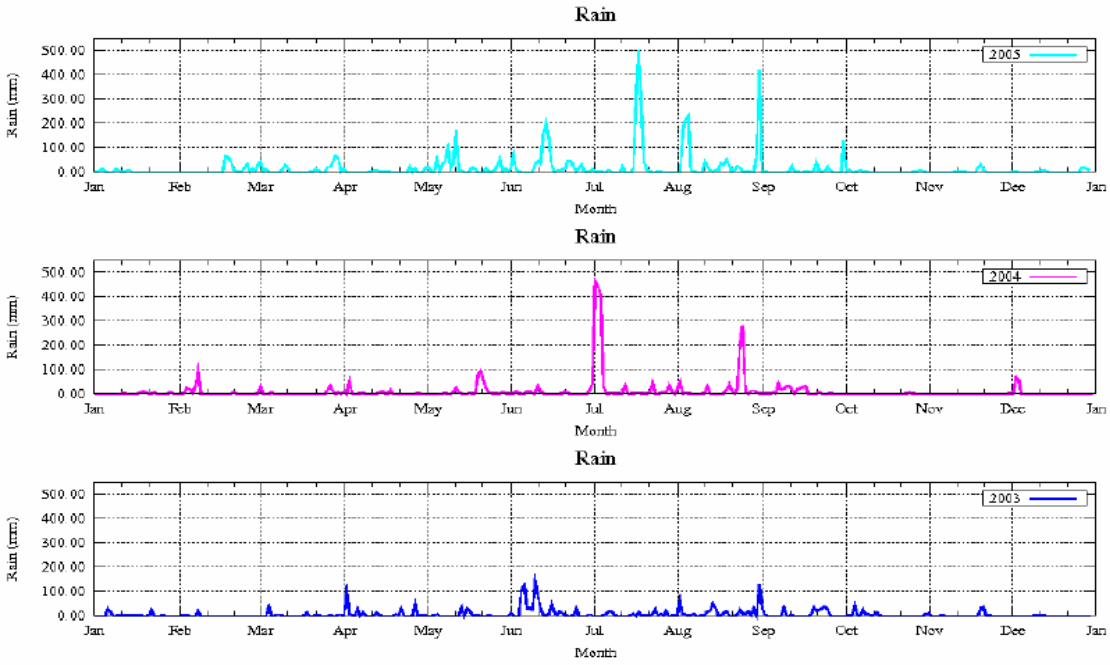

- 每月平均降雨資料（逐年比對）：
  算出每天之平均雨量之後，以每月三十天來計算平均月雨量。
  - 平均七月份降雨最高（401.71 mm）
  - 平均一月份降雨最少（99.95 mm）

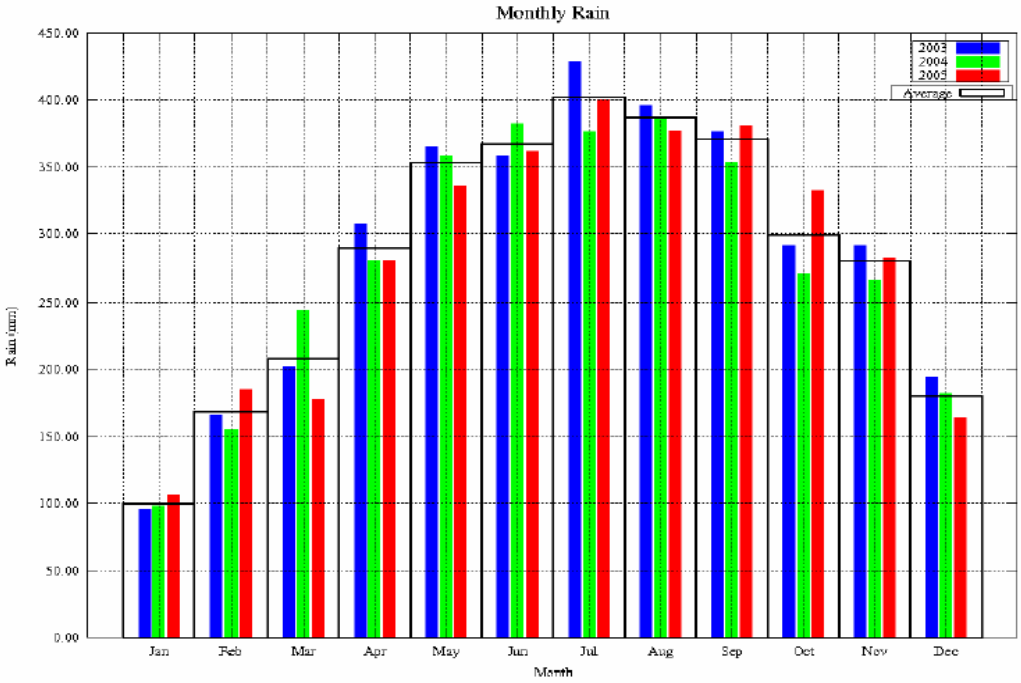

七、近三年颱風資訊：

由於颱風對於降雨及風速有決定性的影響，且颱風來襲時不僅不能進行觀測，天文台亦須作好防颱措施，以避免不必要的儀器、人員損失。以下是 2003-2005 年颱風中心經過

特定範圍的颱風路徑及列表。

- 選取範圍：颱風中心經過（119~123 degE, 21~26 degN）

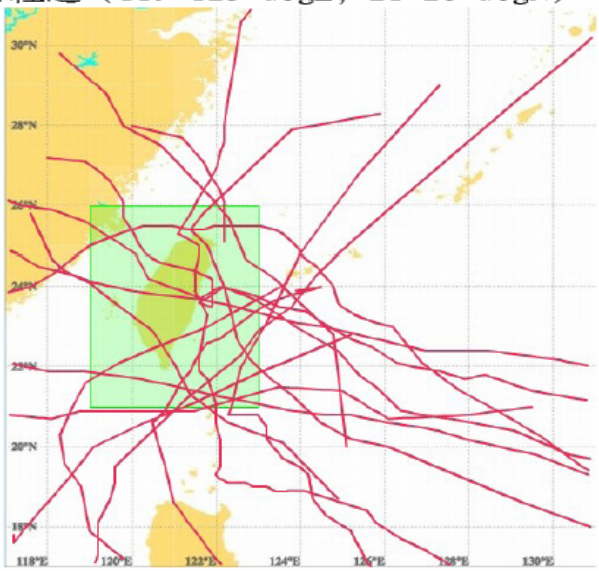

編號	*中文名稱*	*英文名稱*	*警報期間*	*強度*
200302	柯吉拉	KUJIRA	04/21～04/24	中度
200305	南卡	NANGKA	06/01～06/03	輕度
200307	尹布都	IMBUDO	07/21～07/23	中度
200309	莫拉克	MORAKOT	08/02～08/04	輕度
200311	梵高	VAMCO	08/19～08/20	輕度
200313	杜鵑	DUJUAN	08/31～09/02	中度
200319	米勒	MELOR	11/02～11/03	輕度
200404	康森	CONSON	06/07～06/09	中度
200407	敏督利	MINDULLE	06/28～07/03	中度
200409	康柏斯	KOMPASU	07/14～07/15	輕度
200417	艾利	AERE	08/23～08/26	中度
200420	海馬	HAIMA	09/11～09/13	輕度
200424	納坦	NOCK-TEN	10/23～10/26	中度
200427	南瑪都	NANMADOL	12/03～12/04	中度
200505	海棠	HAITANG	07/16～07/20	強度
200513	泰利	TALIM	08/30～09/01	強度
200519	龍王	LONGWANG	09/30～10/03	強度

參考資料：

- 「國立中央大學天文研究所 鹿林天文台年報 2005 No.3」，國立中央大學天文研究所編，2005
- 「鹿林天文台氣象統計 2003-2005」，林宏欽及林啓生，2006
- 「http://www.cwb.gov.tw/V5/information/knowledge/Data/dict/022.htm」

LOT 鏡面重鍍工作報告

張明新、林宏欽、張永欣

LOT 自安裝啓用已經四年，鏡面反射膜已有退化跡象，因此於 2006A 觀測季結束後，在天氣許可的情況下，隨即於 6/8 拆卸主、次鏡並完成裝箱與打包作業。連同吊運主鏡用的夾具，於 6/16 日順利運送下山，隨即陸運送往中正機場通關後，空運送往日本西村製作所進行重鍍工作。

重鍍作業於七月下旬完成，八月份主次鏡自日本運回，海關提領後直接運至天文台，8/30 進行安裝作業，經調整後隨即投入 2006B 的觀測任務，整個重鍍工作自拆卸至重新安裝完畢，共耗時 90 天，總計鍍鏡費、吊運費、陸空運費及保險等費用，鍍鏡作業總費用約 109 萬。

2006/06/15 主鏡吊運下山作業情況

本次望遠鏡的拆裝工作完全由天文台團隊進行，由於這是工作人員第一次進行拆卸作業，由於圓頂內機具的使用限制、專用載具的欠缺等等，整體而言拆卸過程還算順利，但整個工作流程還有許多可以改進的地方。專用載具的缺乏，使得裝卸主鏡室的過程相當困難，且有損壞固定用的螺牙之虞，這是應首先改進的地方，未來在山上設置獨立的鍍膜設備後，在有較頻繁的拆卸需求時，專用載具非常重要，可以避免造成望遠鏡不必要的損傷。

東廣島天文台的主鏡專用載具

藉由此次機會，工作團隊也前往日本西村公司觀摩該公司的小型鍍鏡設備，並實地參與次鏡的鍍鏡工作，並檢視主鏡的處理結果。


西村公司廠內的小型鍍鏡設備

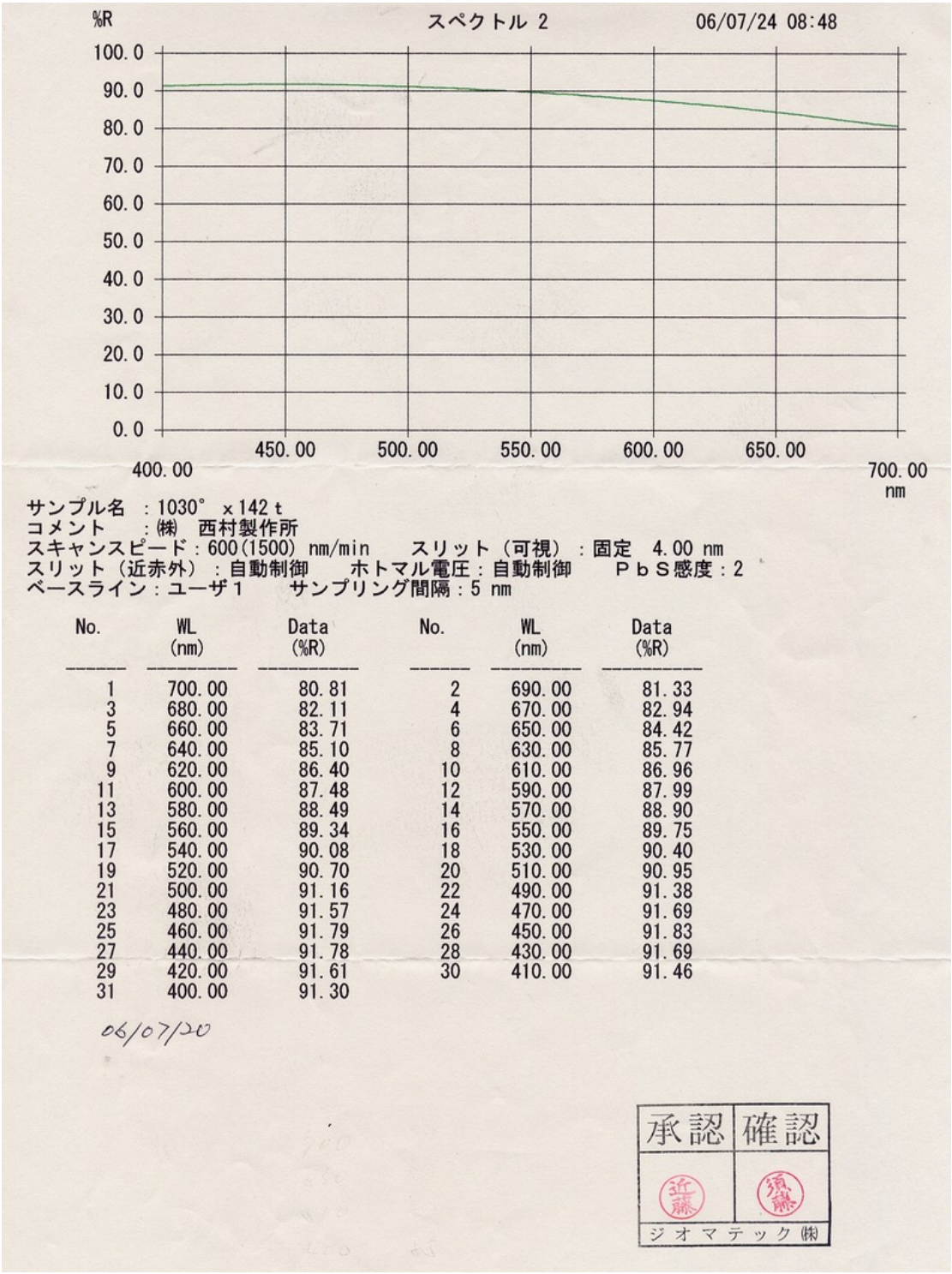

No.	WL (nm)	Data (%R)	No.	WL (nm)	Data (%R)
1	700.00	80.81	2	690.00	81.33
3	680.00	82.11	4	670.00	82.94
5	660.00	83.71	6	650.00	84.42
7	640.00	85.10	8	630.00	85.77
9	620.00	86.40	10	610.00	86.96
11	600.00	87.48	12	590.00	87.99
13	580.00	88.49	14	570.00	88.90
15	560.00	89.34	16	550.00	89.75
17	540.00	90.08	18	530.00	90.40
19	520.00	90.70	20	510.00	90.95
21	500.00	91.16	22	490.00	91.38
23	480.00	91.57	24	470.00	91.69
25	460.00	91.79	26	450.00	91.83
27	440.00	91.78	28	430.00	91.69
29	420.00	91.61	30	410.00	91.46
31	400.00	91.30			

重鍍後主鏡的反射率測量結果圖

另外我們在主鏡卸下之後，趁機測量了一下各個主鏡底支撐的施力狀況，藉此瞭解此設計底支撐運作的原理，並作爲日後調整保養的依據。量測結果如下：

1. LOT 鏡片重量實測爲：253kg
2. 6 組（18 點）底支撐施力總重約爲：216kg (平均 36kg/組，12Kg/點)。
3. 光軸調整位置（3 點）總受力約爲：36kg(平均 12Kg/點)。

LOT 主鏡出廠時原本就有一些缺陷，在中央孔附近有一個缺陷（碎片缺陷），通過副鏡的遮攔，它不在光路中。

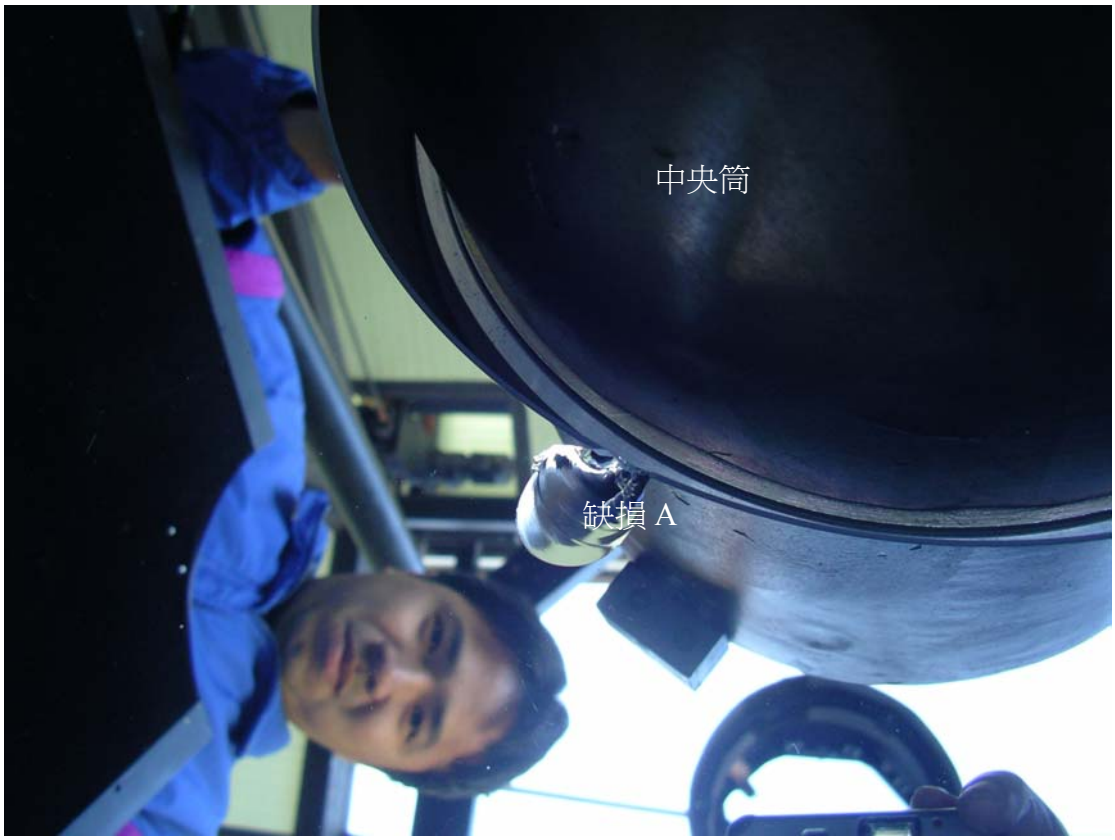

在鏡上也有一些小的缺陷，總面積小於1.5cm^2(估計爲開口氣泡或結石)。

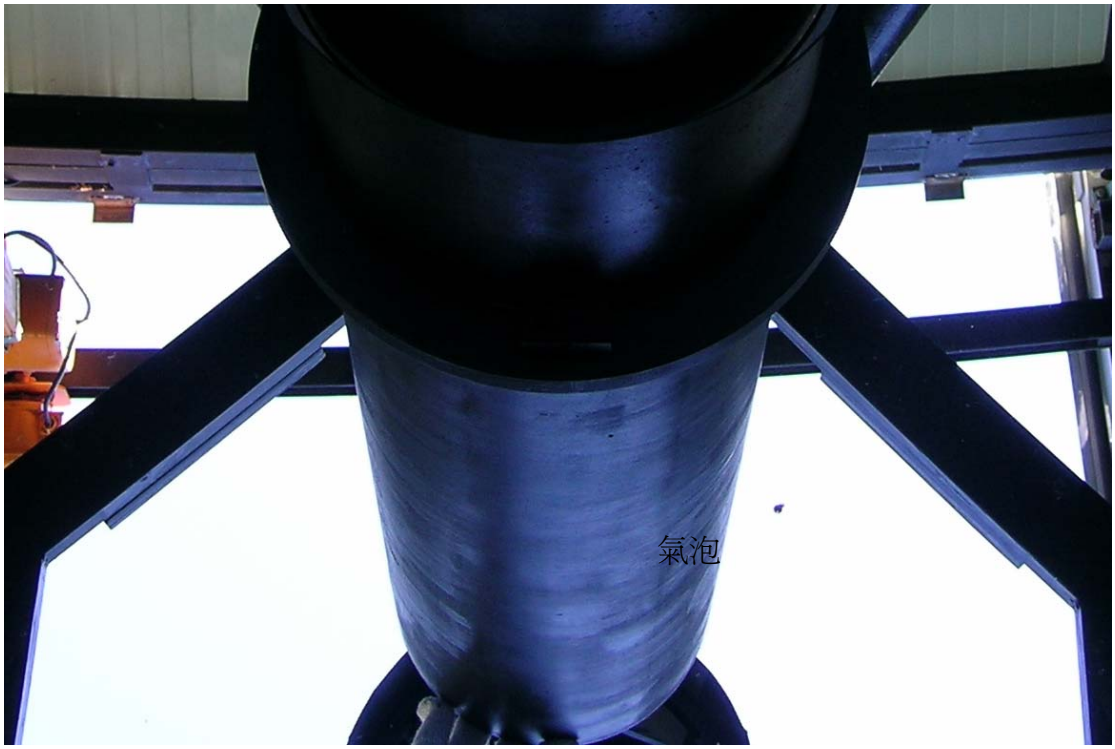

在日本鍍鏡工廠重鍍過程中，疑似使用夾具不當，導致 LOT 主鏡面有 2 個比姆指指甲略大的缺損，位置恰成 90 度角。估計破損區域只會造成極小的減光(<0.02%)，對影像品質幾乎沒有影響。未來可將主鏡旋轉一小角度將缺損區域藏到主鏡倒扣下方。

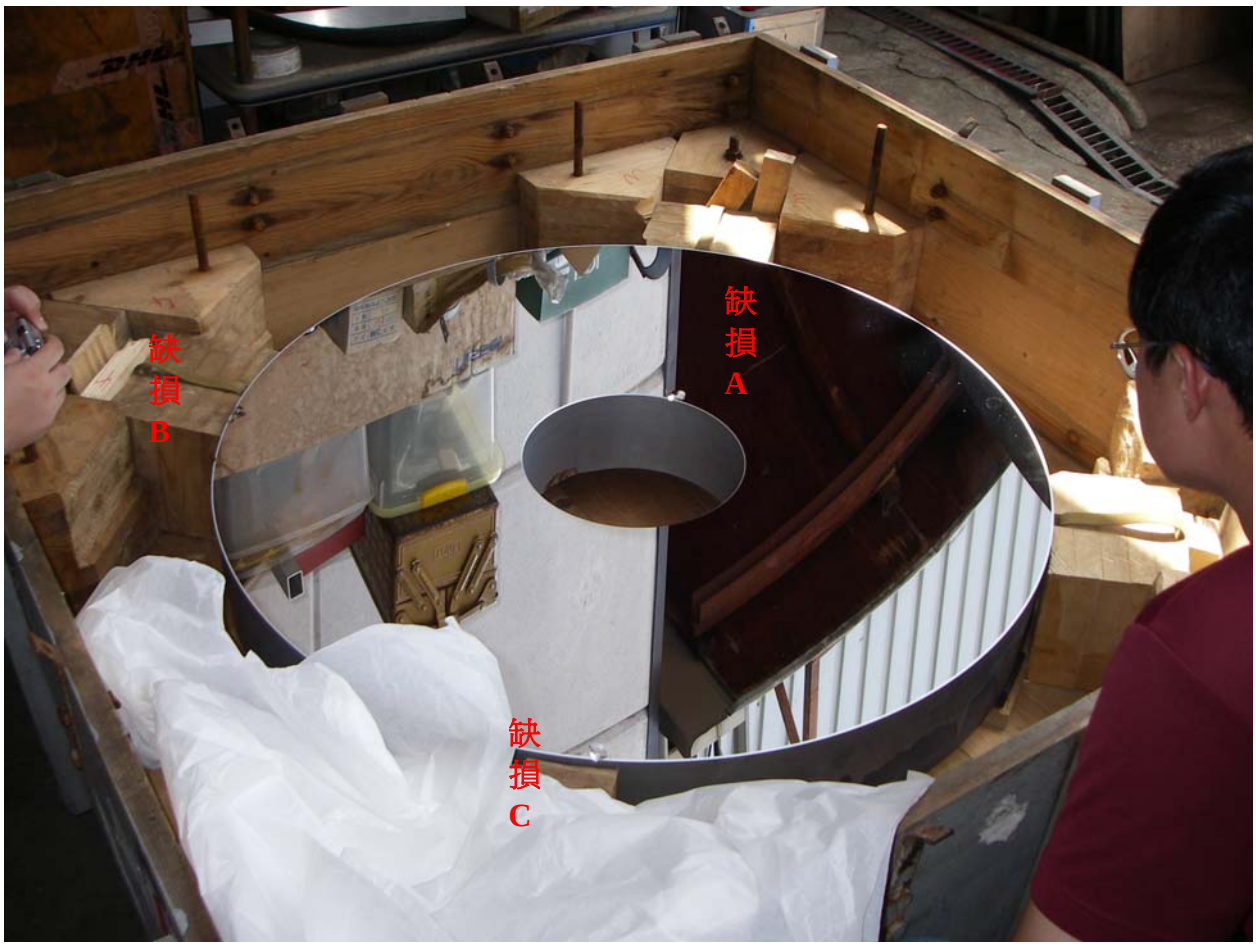

重鍍後開箱檢驗時，發現新的缺損 B、C（上圖），安裝完後在主鏡上之缺陷相對位置如下，（氣泡缺陷位置剛好被中央筒擋住）

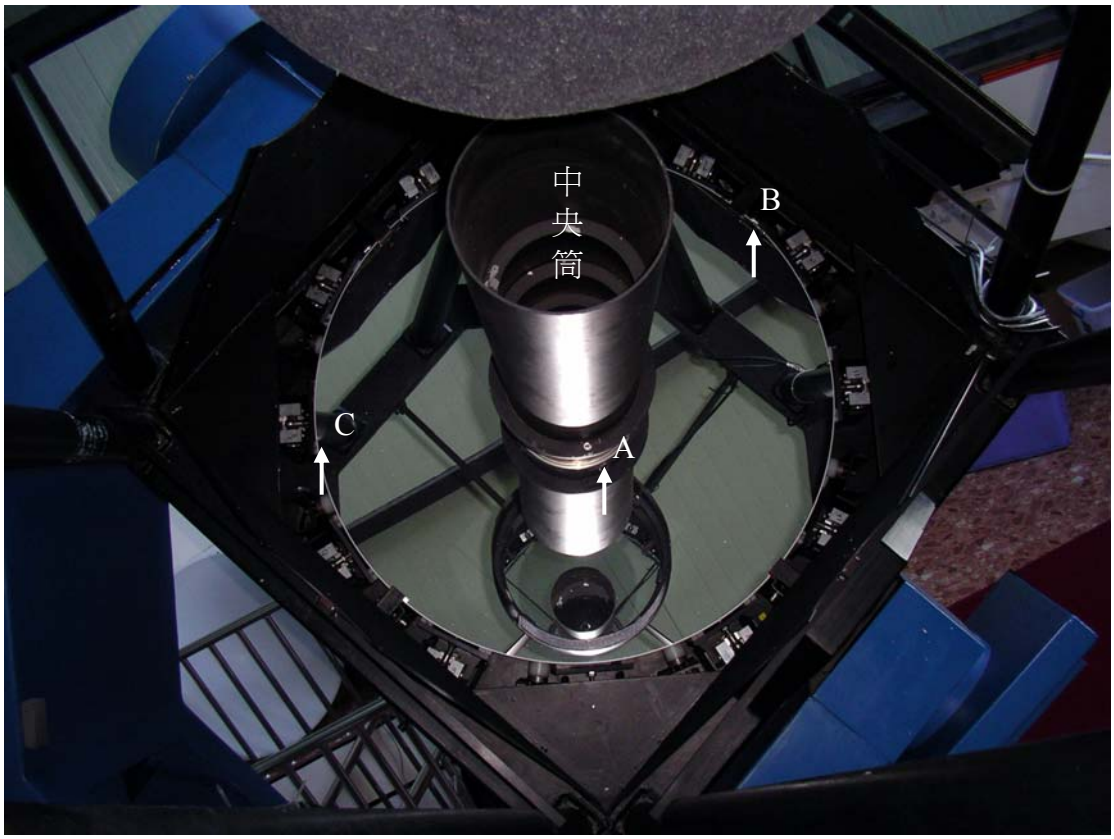

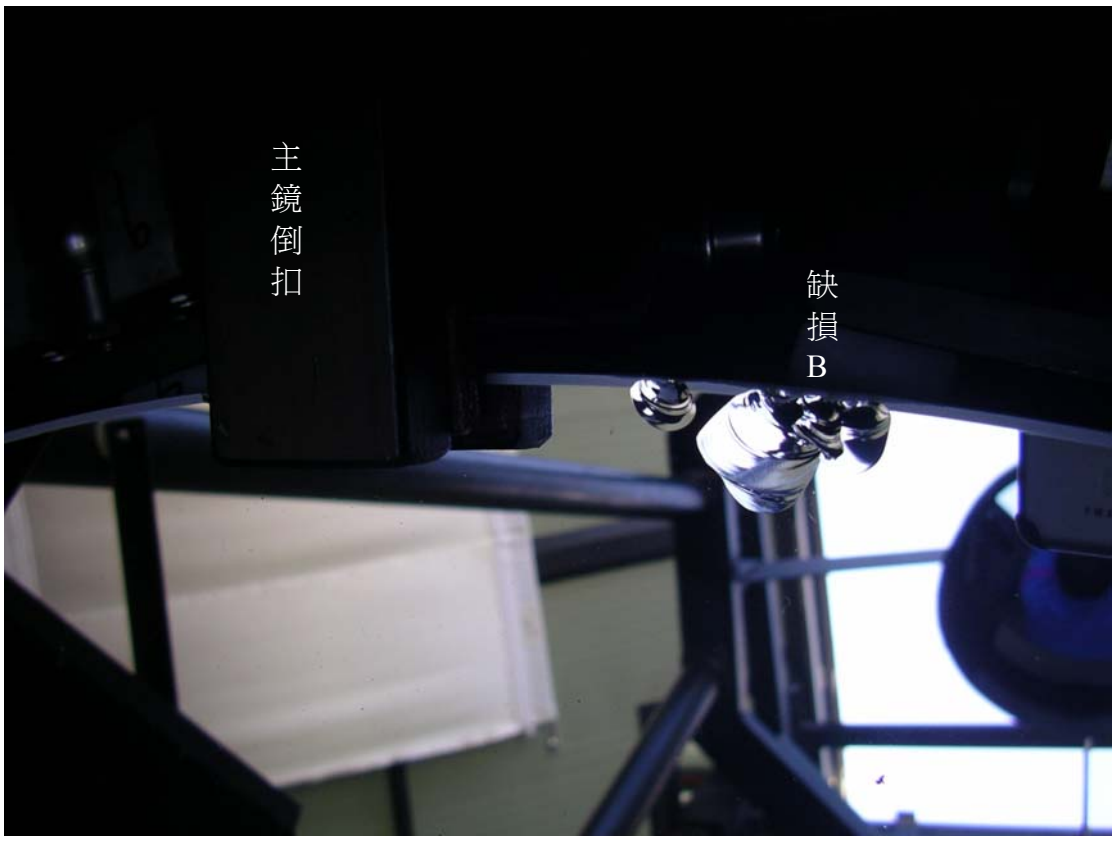

缺損 B 放大圖

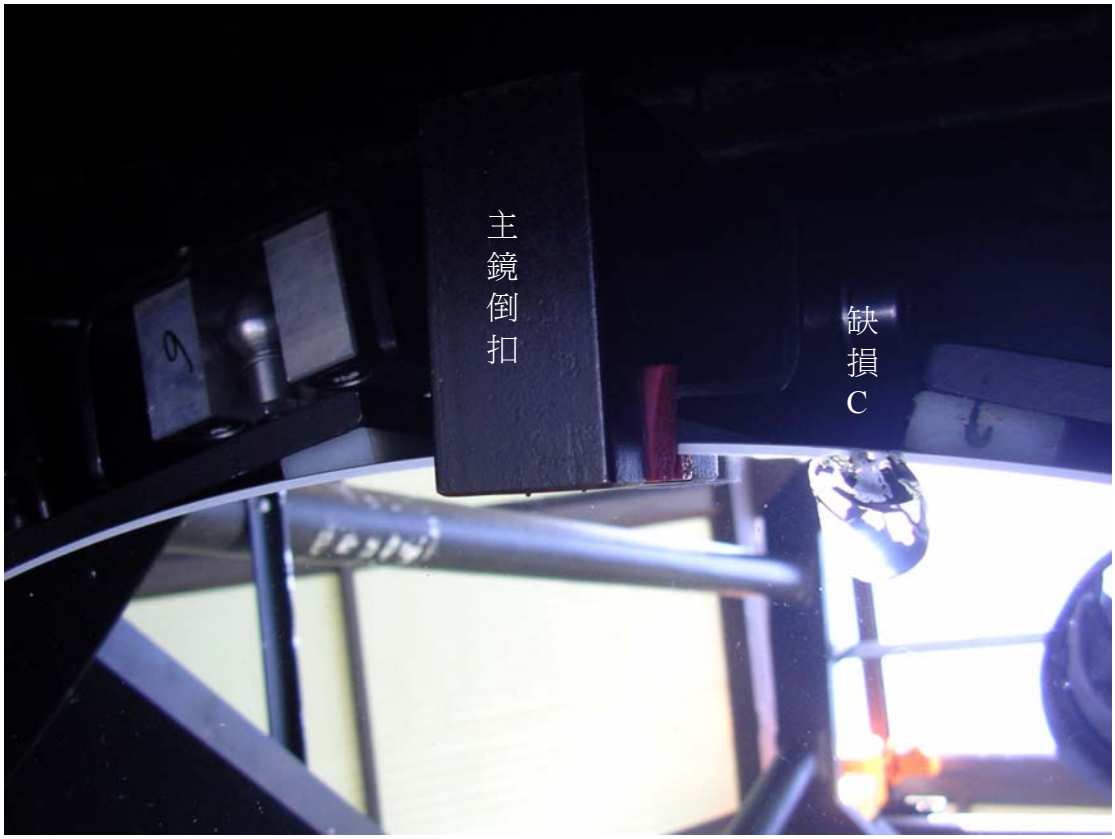

缺損 C 放大圖

鹿林山天文台周遭地震統計分析

楊庭彰

2007/01/03

一、前言（台灣地質簡介）：

台灣是地震發生較頻繁的地區，所有的建築在建造時一定要考量到地震發生的因素，以免造成生命財產的重大損失。

台灣是歐亞大陸板塊及菲律賓板塊的交界地帶，在板塊的交界處由於隱沒帶的地質作用，造成地質壓應力持續累積，累積到地殼發生剛性變形或是錯動時，就會有規模大小不同的地震產生。圖中爲板塊、地震及台灣的關係（箭頭尖端爲上磐）。

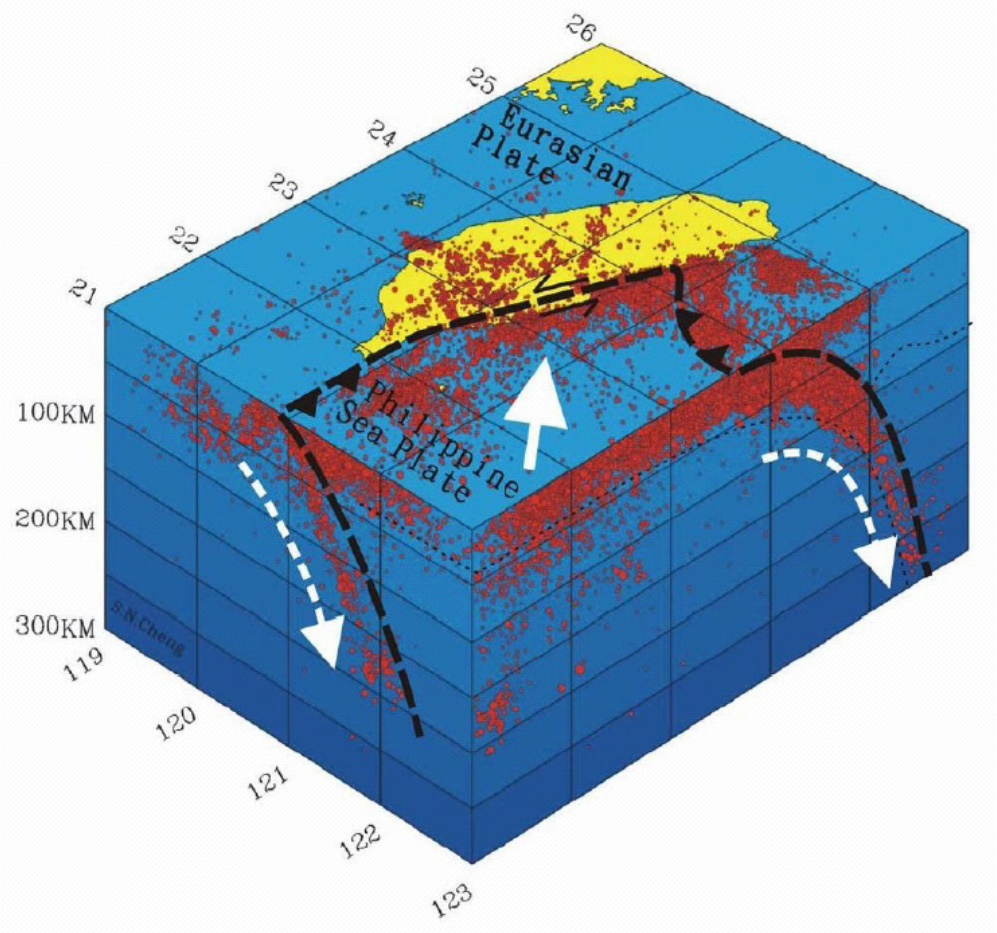

圖 1: 台灣地震發生的位置分佈圖（「地震觀測與災害」上課內容，林正洪）。

由圖可見，宜蘭外海及東部沿海一帶爲主要發生地震的區域，此處爲板塊交界前緣。而台灣西部麓山帶一帶也有一系列的逆衝斷層，斷層之間的岩層錯動也是造成地震的主要成因之一，如 1999 年在集集發生驚天動地的 921 集集大地震，就是車籠埔斷層錯動所造成的災害（如圖二）。

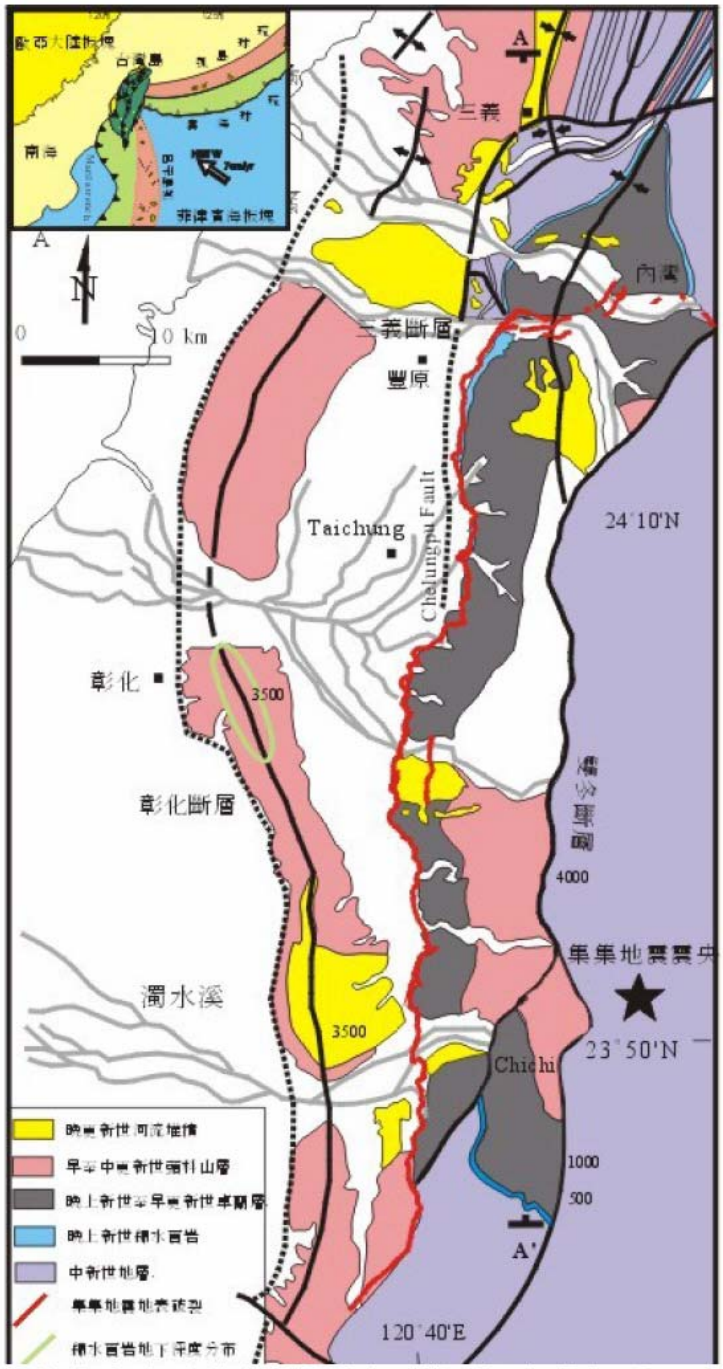

圖 2: 集集大地震所造成的地表破裂（紅色線）（From: 活動斷層調查報告——車籠埔斷層調查，李元希、盧詩丁、石同生、林偉雄、林燕慧、劉彥求、黃存慧）

二、資料來源：

這次分析的資料來源爲*國立中央大學應用地質研究所工程地質與新科技研究室*下的一個*「台灣地震資料查詢」*的網頁[1]，還有中央氣象局的 RTD 速報系統網頁[2]。其主要資料均爲中央氣象局所提供。其網頁介面提供了一個便於我們查詢的管道，記錄的資料主要爲從 1900 到 1995 年這段時間內的測量資料。我們可以選取適當的震央發生區域

1 該網址在：http://gis.geo.ncu.edu.tw/gis/eq/，爲中央大學應用地質研究所工程地質與新科技研究室下的一個網頁。

2 該網址在：http://scman.cwb.gov.tw/rtd/index.htm，爲中央氣象局所維護。

而獲得適當的資料。從這些資料中，我們就可以看出在鹿林天文台附近近百年來大致上的地震趨勢。

從網頁資料統計中，我們取出規模 4-8 級的地震畫出逐年次數分佈圖，如下：

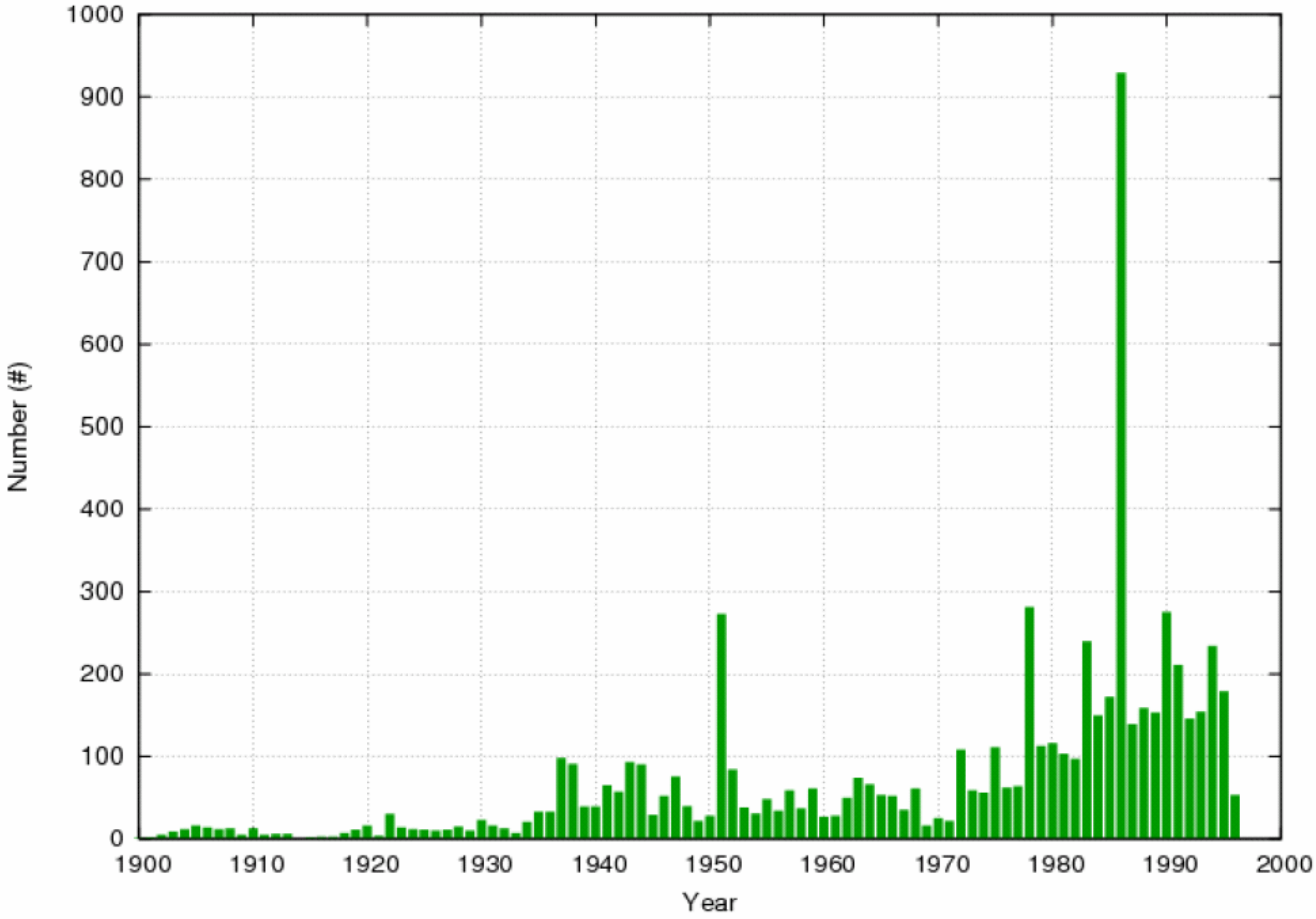

圖 3: 1900 至 1996 年 4-8 級地震分佈圖

如圖所示，資料量逐年增加，可能是因爲儀器、測量技術及記錄有大的突破及改善所致。不過從地震的次數分佈其實無法顯示地震所釋放的能量，而且在大地震之前或後通常均會伴隨著比較多的前震 (foreshock) 及餘震 (aftershock)。所以地震次數的分佈只能常作一個參考。

台灣地區的地震主要是由於板塊之間的擠壓造成的，而每年板塊的相對移動速率的變化量不會相差很多，所以可視爲是接近定值。而板塊的相對位移就造成能量的累積，能量的累積如果每年是差不多的，當一次大地震來的時候就會把能量大量釋放，而其後續許多的餘震其能量釋放亦相當可觀。所以當大地震後的幾年內，可能地震量也較少，而且規模也較小。直到下一次的地震發生。

從單一年的地震資料（如 1986 年的地震資料），我們可以看出，在大地震之前及之後，有較明顯的前震及餘震產生。所以當明顯的前震現象產生時，我們就要注意是否爲大地震發生的前兆，採取必要的預防措施。不過，總體而言，地震的預防是很困難而籠統的。

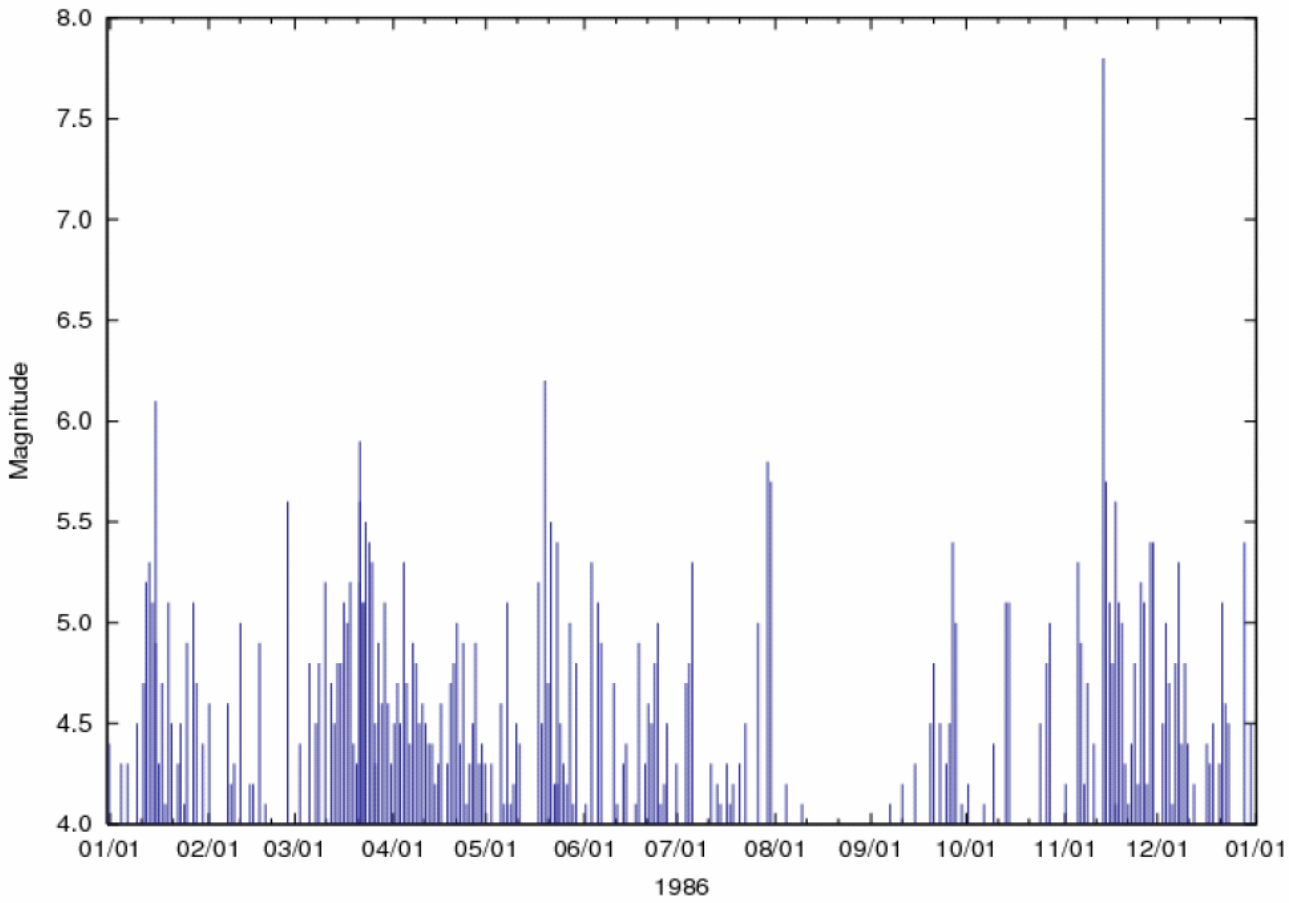

圖 4: 1986 年 4 級以上地震發生的時間及規模

以上的地震資料選取區域涵蓋了台灣附近的區域，如下：
Latitude: 21-26 °N
Longitude: 119-123 °E

如下圖所示：

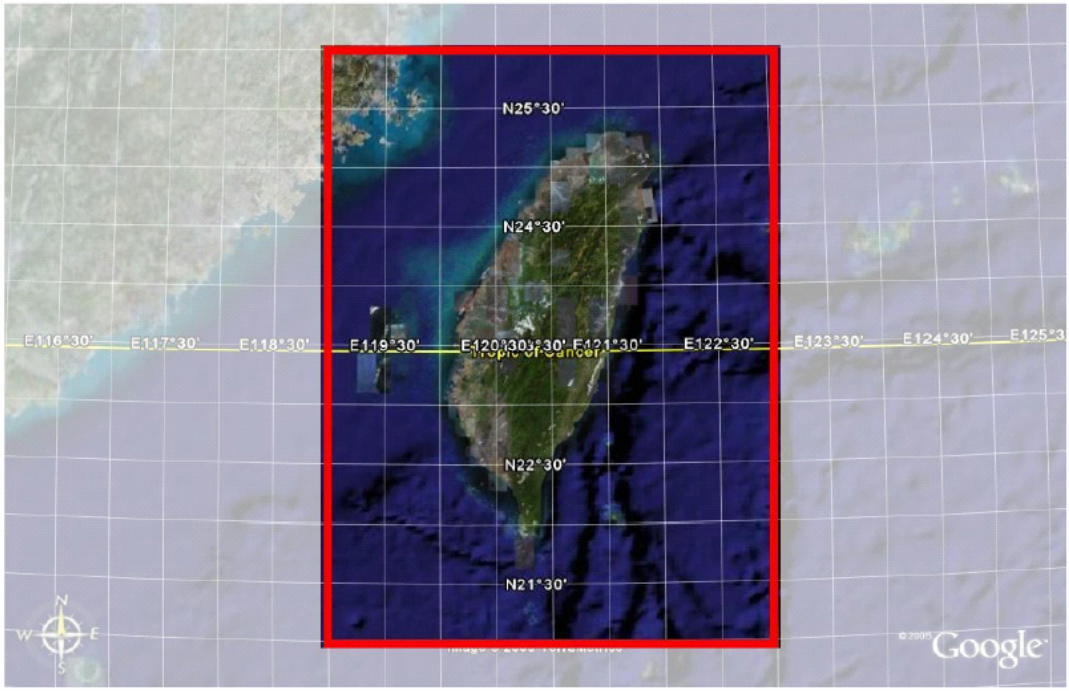

圖 5: 地震事件選取範圍（全台灣）

較局部的資料將在後文提及。

三、地震次數統計：

首先我們先來看看地震在台灣各地的分佈情形。從「*台灣地震資料查詢*」的網頁中，我們可以得到從 1900 到 1995 年各地地震發生次數的分佈圖。我們取規模爲 4-8 級的地震作統計，結果地震分佈的次數如下：

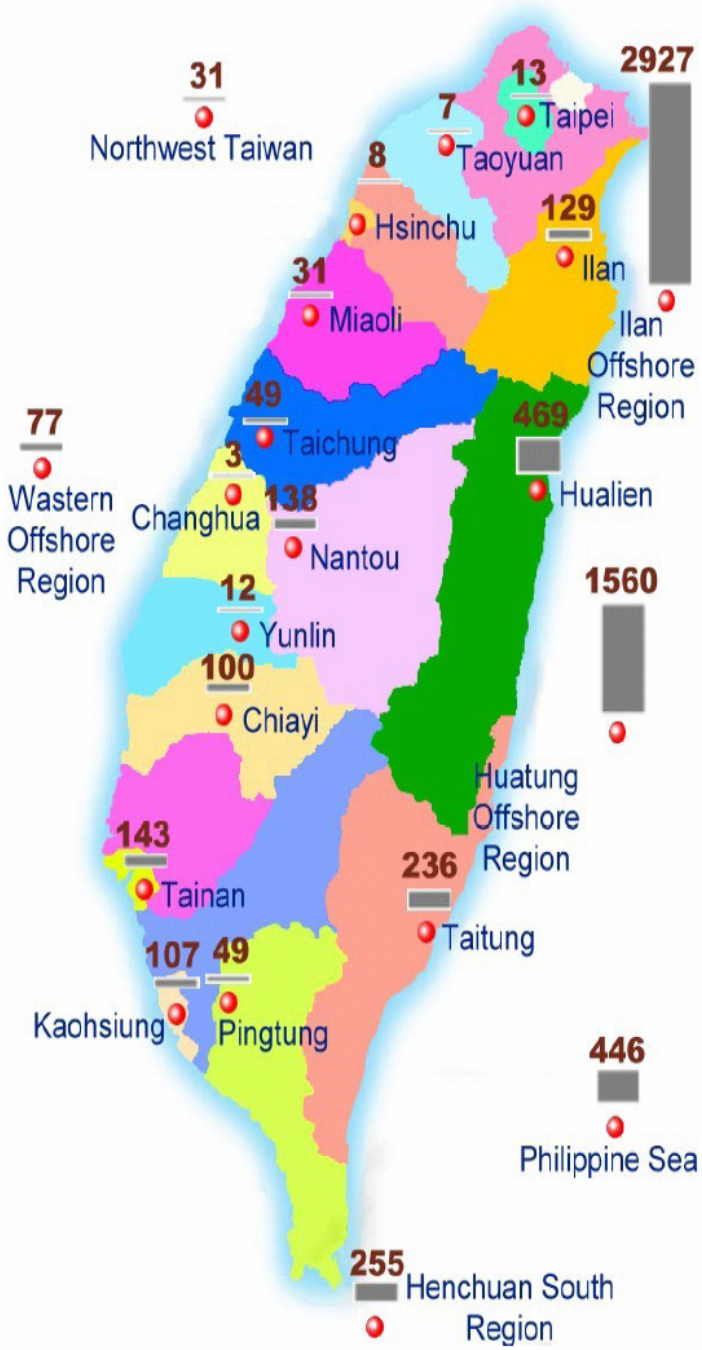

圖 6: 1900 至 1996 年各地地震次數分佈統計

從圖中我們可以發現宜蘭及花東外海爲地震發生最頻繁的地區，結果是很合理的。因爲當地剛好是菲律賓海板塊及太平洋板塊交界處，地震活動當然頻繁。而在台灣西部

也有一些地震，主要是由於一系列逆衝斷層的活動所導致。而鹿林天文台就位於台灣西部麓山帶附近，所以一般而言，對於相同規規模的地震而言，在台灣西部發生的地震對鹿林天文台影響會比較大一些，因爲距離較近之故。

四、地震規模統計：

由氣象局的 The Taiwan Rapid Earthquake Information Release System (RTD) 網站資料我們可以得到各年不同規模地震的次數分佈圖，如下：

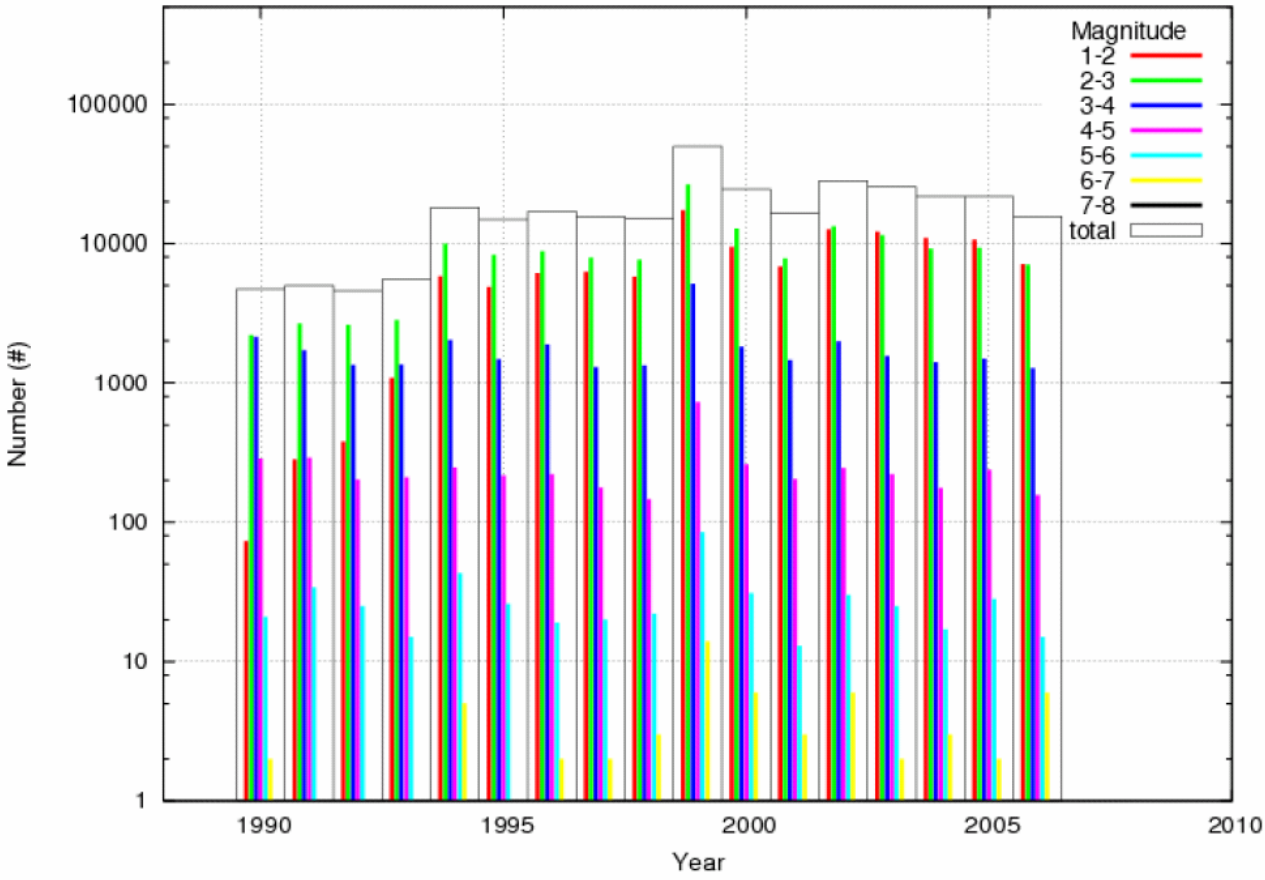

圖 7: 1990 年至 2006 年地震規模與次數統計

由圖中可發現除了 1-2 級地震的次數分布之外，其餘地震的次數分布隨著規模的增加而約略呈現指數遞減 (power law decay) 的情形。規模較大的地震會釋放較多的能量，所以平均再發的時間會較長。而小規模的地震就常常發生，平均每天有數次的小地震發生。而 1-2 級地震次數不如預期的多，這可能是由於測站記錄的問題，或是儀器記錄的限制所導致。

五、局部分析：

由於地震對一個地點所造成的危害與兩大要素：震央距及規模有關。所以爲了評估鹿林天文台所可能造成的地震損害，我們選取以鹿林天文台周圍五十公里爲半徑的圓，我們定義爲 Hazard Zone，即爲地震發生時的高危險區。當大規模地震發生在這個區域時，對於天文台的威脅性要較其他地區高出許多。如下圖所示：

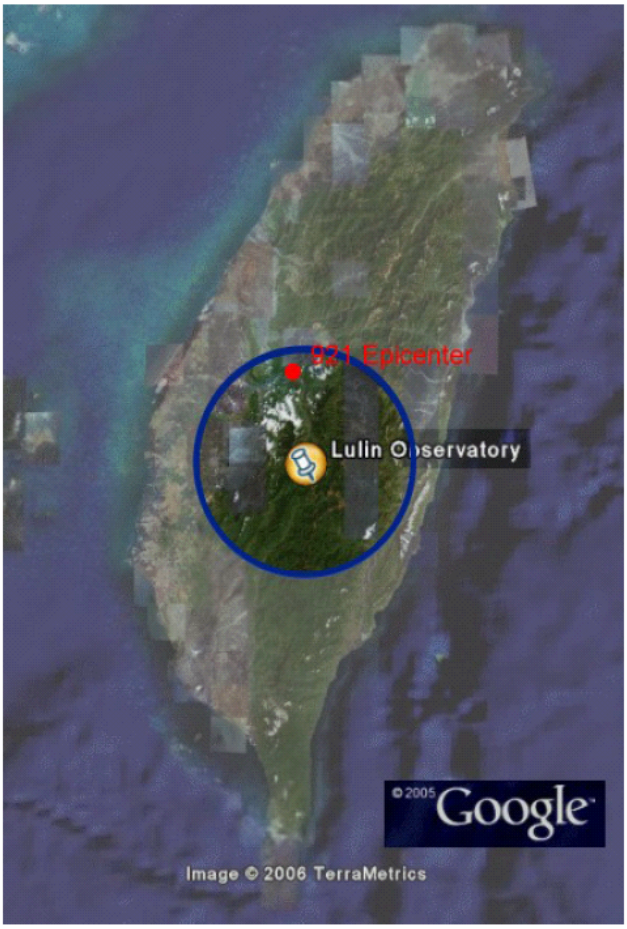

圖 8: 我們自行定義的 Harzard Zone 範圍

從 1900 到 1996 共有 6781 個芮式規模 (Richter Scale) 大於 4 的地震記錄，而在落在此選取區域中的事件有 399 個，佔所有發生地震約 5.9 %。其中不同規模的次數分佈如下表：

Richter Scale (M_R)	***Number***
4-5	334
5-6	57
6-7	5
7-8	3

深度分佈如下表：

Depth (km)	***Number***
0-10	278
10-20	78
20-30	33
30-40	10

一般而言，淺層地震的規模通常會比較小，而發生頻率會較頻繁，每次發生時所釋放的能量較小。而深層地震則相反，發生的頻率要低，不過發生時對於天文台造成的威脅就不容小覷。

六、PGA 超越機率圖：

在「*台灣地震資料查詢*」網頁中，提供了一個「場址 PGA 年超越機率」的試算連結。PGA 是 Peak Ground Accretion（最大地表加速度）的縮寫。網頁內容是使用蔡主權等人在 1987 年所提出的文章中的模型來作爲計算標準。該連結提供了四種模型的計算，我們可以藉由其計算的結果來評估天文台在地震發生時的最大地表加速度的理論發生機率。

我們取鹿林天文台的座標爲中心，向外積分半徑爲 100 km，所得到的結果如下圖所示：

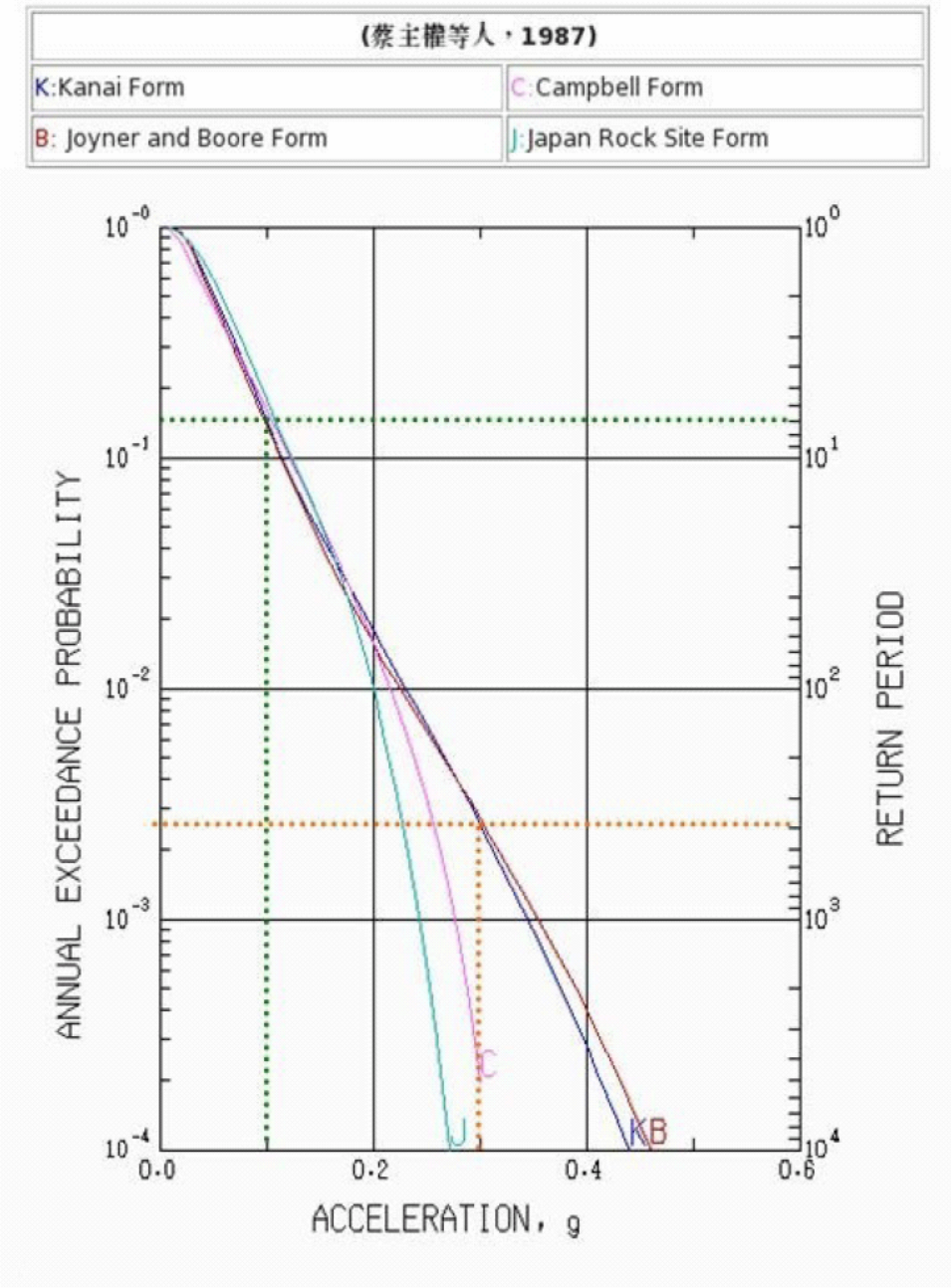

圖 9: 鹿林天文台 PGA 超越機率圖（From: http://gis.geo.ncu.edu.tw/gis/eq/eq_PGA.htm）

我們如果考慮到較極端的 B 模型，也就是 Joyner and Boore Form 的話，如果要發生 0.3 g 的最大地表加速度，則鹿林天文台平均發生的周期約爲 500 年。如果是 0.1 g 的

話，則發生的平均周期約爲 7 年。不過此結果亦爲參考用，我們只能算出一個平均發生的頻率（周期），而不能真正地預測地震何時會發生。

七、災害及預防：

至今還沒有真正能對地震作預測 (forecast) 的方法，而且對於地震發生的機制還沒有徹底的了解。不過有一些嘗試性的預測方法，如測地下水位法、地磁及地電法、活斷層及褶曲等等，都是地質學家正在積極研究的方法。不過目前最佳的因應之道還是作好在建築建造時的防震設計，及相關人員在災難發生時的臨時應變訓練及後續損害控制，這才是減少儀器損壞及生命財產損失之道。

八、結語：

這篇文章因爲受限於技術及知識的侷限，所以只能當作參考用。如果真的要對建築本體的強度作評估，建議還是請專業的工程顧問公司來作評估較爲妥適。也較能符合工程施工的需求。

參考資料：

- 「地震觀測與災害」上課內容，林正洪。(http://www.earth.sinica.edu.tw/~lin/contents.htm)。
- 活動斷層調查報告——車籠埔斷層調查，李元希、盧詩丁、石同生、林偉雄、林燕慧、劉彥求、黃存慧。
- Tsai, C. C., C. H. Loh and Y. T. Yeh (1987). Analysis of earthquake risk in Taiwan based on seismotectonic zones, Memoir of the Geological Society of China, 9, 413-446.
- 中央氣象局地震百問 (http://scman.cwb.gov.tw/eqv5/eq100/eq100.htm)。

2006/01~2007/02 LOT 執行計畫列表

IANCU/LOT Observing Time 2006A (January/2006 – May/2006)

No.	Project	PI
1	A multi-wavelength study of the merger candidate-ACO S0721	何佩勵
2	Monitored the unusual comet 73P/Schwassmann-Wachmann 3-C	林忠義
3	Supernovae Search and Follow-up Observation	陳英同
4	Photometric Observation of Asteroids with Comet-Like Orbit	木下大輔
5	A test of star formation theories in galaxies from near-infrared and Hα imaging	夏志浩
6	Target of Opportunity of GRBs and XRFs follow-up observation	黃麗錦
7	A Deep Search for Transiting Exoplanets and Variable Stars in NGC 2099(M 37)	胡瑞華
8	Photometry on Variable Candidates from the Pisgah Survey	陳岸立
9	UBV photometry on galactic open clusters with poor age and distance determination: Formation and evolution of high galactic latitude open clusters	陳錦威
10	The photometric study of the candidate of binaries in Bipolar planetary nebulae- M4-18 and NGC 3242	夏志浩
11	Ground based observation of asteroid sample return mission target	Masanao Abe
12	Time-resolved photometry for superhumpers	陳炳志
13	天文觀測 II 戶外教學	周翊
14	NTU Center for Information and Electronics Technologies Advanced Communication Systems and Technologies Laboratory	吳靜雄
15	Precession of Splitted Cometary Nucleus---Proving Internal Structure of the Comet 73P/Schwassmann	木下大輔
16	Galactic structure from apparent luminosity function	高仲明
17	The Photometry of selected eight open clusters with log(age)=8-9, NGC 1528 and NGC 1708	傅學海
18	Image reconstruction of double Stars and central part of M42 by speckle masking method	傅學海
19	Wholr-Earth Telescope Determination of Whita Dwarf Convertive Parameters	陳文屏
20	The Hα Survey of bright galaxies in galactic cluster Abell 1213	黃崇源
21	Identification of the Optical Counterparts of high-mass X-ray binaries	黃崇源

IANCU/LOT Observing Time 2006B (September/2006– February/2007)

No.	Project	PI
1	Shake-Down Observations and Calibration of the New Spectrograph	Wen-Ping Chen
2	A Deep Search for Transiting Exoplanets and Variable Stars in NGC 7245	胡瑞華
3	The UBVRI Photometry of Open Clusters with age ≧ 100M yrs	Hsieh-Hai Fu
4	Webcam CCD Speckle Observations of Binary Stars	Hsieh-Hai Fu
5	Photometric Observations of Asteroids with Comet-Like Orbit	Kinoshita Daisuke
6	Low Resolution Spectroscopy of (3200) Phaethon during Commissioning Phase of Lulin Compact Spectrograph	Kinoshita Daisuke
7	Supernova follow-up Observations	陳婷琬
8	Supernovae Search	Ying-Tung Chen
9	Target of Opportunity of GRBs follow-up observation	Wing-Huen IP
10	Photometry Observation of 73P/SW-C & -B and Halley-like Comet	Lin, Zhong yi

	177P/Barnard 2	
11	Photometry and Dynamics Characteristics of Selected Open Clusters	吳志剛
12	觀測天文學實習	黃崇源
13	NTU Center for Information and Electronics Technologies Advanced Communication Systems and Technologies Laboratory	吳靜雄
14	Ground based observation of asteroid sample return mission target	Masanao Abe
15	The Photometric study of the Candidates of Binaries in the Nuclei of Bipolar planetary nebulae Ⅰ – M 4-18	夏志浩
16	Calibration Program of Lulin Compact Spectrograph (LCS) Ⅰ: A basic test and observational parameters for the instrument of LCS	夏志浩
17	Triggered Star Formation at High Galactic Latitude	李昫岱
18	A study of rotational variability in 2003 UB313 and other large Trans-Neptunian Objects	Wing-Huen IP
19	Identify of the high-mass x-ray binary	黃國斌
20	A Test of Star Formation Theories	陳以忱
21	巡星觀測網的可行性研究 The Feasibility Study of a Transit Survey Network	江瑛貴

2006 駐站人員年度工作報告

(I) 駐站觀測助理 林啓生

一、LOT 部分

1. 協助申請使用 LOT 的研究人員觀測，比較特別是 5 月份前後的 73P 彗星觀測
2. 協助 2006 年 6 月拆卸 LOT 鏡片，2006 年 8 月安裝及調整 LOT 鏡片
3. LOT 及圓頂故障的排除
4. 協助外國研究者使用 LOT 從事觀測工作

二、SLT 部分

1. 成爲 LUSS 一員，使用 SLT 拍攝特定天區，搜索新的小行星，成果豐富
2. 使用 SLT 協助麗山高中陳漢洲同學拍攝特定的太陽系外恆星所屬行星凌日過程
3. 協助 SLT-RC16 故障的排除，更換配件及圓頂故障的排除
4. 協助研究人員使用 SLT 觀測特定星體，如 GRB、NEO、小行星和彗星等等

三、LELIS 部份

1. 協助 LELIS 助理有關 LELIS 臨時交辦的事情，如圓頂故障排除，望遠鏡故障的排除，電腦的重新開機等

四、TAOS 部份

1. 協助 TAOS 人員有關 TAOS 臨時交辦的事情 ， 如量測望遠鏡上某個硬件的大小，電腦的重新開機等

五、一般行政部份

1. 協助公共電視台的攝影製作小組拍攝專輯影片
2. 爲多個大學天文社及救國團辦理的活動及新加坡的中學講解參觀鹿林天文台
3. 協助整理鹿林天文台的環境衛生工作
4. 燒錄 LOT 及 SLT 的備份觀測資料
5. 幫忙接送研究觀測人員往返本天文台
6. 接待各級長官參觀導引本天文台

(II) 駐站人員 石俊雄

1. 天文台內務清潔及環境整理.
   值班期間負責天文台裡外之清潔工作打掃拖地，吊運垃圾.換洗床被單套，登山步道清潔及天文台周圍雜草修剪，並且例行做天文台機械之維修，以確保機械正常運作。
2. 炊煮
   負責觀測人員糧食，每周至少一次下山購買食物及日用品，補給觀測人員，讓其能專心研究觀測。
3. 協助觀測.
   協助 TAOS 人員作遠距離觀測，並做簡易之維護，支援天文營山上教學，負責接待來賓，並隨時聽指示支援觀測人員。
4. 監督工程.
   監督天文台正在運作之工程，並給予適當之支援。
5. 防颱工作
   台灣每年夏季初到秋季都有颱風威脅，天文台位於鹿林前山頂，颱風威脅更甚，因此防颱工作.更爲重要，除了一般所要注意的防颱工作，更要在每一個能固定的地方確實做到，

一點都不能疏忽，並且幫望遠鏡穿衣服，以防淋雨。

6. 參加校運

每年一度回校支援理學院參加學校運動會理學院爭取榮譽。

(III) 駐站人員 汪榮進

1. 例行工作，將學校研究人員或客人，由阿里山、石桌、嘉義市接駁上山。
2. 固定每週二下山補給日常生活用品。
3. 每個禮拜交接時檢查大水塔的儲水量，測水龍頭水質讀數，逆滲透水質讀數檢查天文台水塔有無漏水現象。
4. 雨季時因雜草生長速度較快，每一個半月修剪一次，冬天因爲結霜的緣故雜草會枯萎。
5. 颱風季節如有災害發生，視災害的嚴重性，災害較嚴重者回報學校，較輕微者自行處理。
6. 每日例行工作內務整理，室內清潔，中餐及晚餐的準備，人員下山後清洗床被單套。
7. TAOS 協助觀測，作一些簡單的維修及故障排除，回報當下的天氣概況。
8. 冬天時期山上容易結冰造成水管破裂或加壓馬達爆裂，利用融冰時從山下打水上山，如沒再打水上山，需在 10 點以前關閉馬達，枯水期必要時會請一個助理下山載水上山。
9. 6 月份將望遠鏡鏡片裝箱送日本鍍鏡，8 月份送回鹿林天文台重新組裝，也已正常運作。
10. 6 月份至 9 月 21 日，我在嘉義縣的新港鄉參加配電線路訓練，因此無法上山值班，由石俊雄、杜進全、石浩偉協助代班，非常感謝他們，也感謝學校給我這個難得的機會學習更多的知識，在未來也請學校給其他想要學習的人機會。
11. 今年 12 月的 26 日一場地震，天文台安然無恙。
12. 消防安全檢查以及汰舊換新。
13. 協助孫老師網路數位化天文觀測戶外教學。
14. 協助公共電視採訪。

(IV) 駐站人員 杜進全

1. 從鹿林山莊步道到天文台兩邊草都已砍好，植草磚水溝也已清理處理好。
2. 天文台上面有種植綠化，成效目前仍不是很明顯，但可以期待。
3. 每禮拜採買，雨季及有颱風疑慮時天，會採買約半個月份的糧食備用。
4. 住的方面，冬天缺水比較麻煩，床單需一段時間才會拿下山送洗。
5. 人員接駁運作正常。
6. 天文台夏天容易有斷電現象、冬天則容易斷水，需特別注意。

(V) 駐站人員 石皓偉

1. 上山人員常購買零嘴抵住宿費用，住宿收入與食物支出時常不平衡。
2. 食物庫存的量與質有慢慢的改善。
3. 駐站人員目前都有受烹飪訓練課程，石俊雄已通過考試，其他人正加緊練習準備當中。
4. 上山人員儘量於前一星期申請，人數可以控制的話，補給及車輛的花費就會少一點，可減少不必要的開銷。

附錄

NCU/LULIN LOT/1m OBSERVING PROPOSAL

Semester: 2007B

※ Observing time is allocated on a 6-month basis, March-August (A), and September-February (B).

※ The proposal, either in Chinese or English, should be sent to the Time Allocation Committee, preferably via email at tac_lulin@astro.ncu.edu.tw, or via post to Graduate Institute of Astronomy, National Central University, 300 Jungda Road, Chung-Li 32054 Taiwan. Inquiries regarding observing requests or instrumentation can be directed to the same email contact.

※ If time is granted, please fill out the Lulin Lodging Request Form before the observing run (http://www.lulin.ncu.edu.tw/TAC/LulinApplication.htm).

※ At times a time-honored event may require interruption of an ongoing project. The observer will be notified, and consulted for service observations if a mutual agreement can be reached.

---

1. Title of the Proposed Observing Program

---

2. Abstract (limited to 200 words)

---

3. Category

☐Solar System ☐Exoplanets ☐Stars Star Formation ☐Compact Objects
☐Interstellar Medium ☐Nearby Galaxies ☐AGN ☐Cosmology
☐Cluster of Galaxies ☐Gravitational Lenses ☐Large Scale Structure ☐Distant Galaxies
☐Others

---

4. Principal Investigator

Name:
Institute:
Address:
E-mail:
Phone/Fax:

---

5. Co-Investigators

Name / Institute	Name / Institute	Name / Institute

---

6. Link to Thesis Work

☐This observing program is linked to a PhD thesis
☐This observing program is linked to a master thesis

Name of the student(s):

---

7. Time Request

Instrument (LCI/LCS)	Number of Nights	Moon Phase (D/G/B)	Preferred Date	Acceptable Date	Remarks (Hi or Lo-Res for LCS)

Total requested number of nights:
Minimum acceptable number of nights:

---

8. Scheduling Constraints

---

9. Instrument Requirements

---

10. Observing Experiences

---

11. Backup Program in Poor Weather Conditions

---

12. Publications related to LOT usage

---

13. Status of Previous Observations if LOT observing time has been allocated to P.I. before

---

14. Target List

Object	RA (2000.0)	Dec (2000.0)	Magnitude	Angular Size	Exposure	Remarks

15. Scientific and Technical Justifications (limited to two additional A4 pages, including figures)

This page is intentionally left blank.

相關報導

兩岸合作　發現 5 顆新小行星

原文轉載自【2006-03-27/蘋果日報/A11】

台灣天文學界又有重大發現！中央大學天文所位於南投的鹿林山天文台今年三月五日起，與大陸天文觀測家葉泉志合作進行搜索小行星的「巡天計劃」，至今共發現五顆新小行星，這次發現是繼二００二年的「鹿林一號」、二００五年的「NCU90」後，台灣第三次發現新小行星，未來經過國際小行星中心測定運行軌道參數後，發現者可取得該小行星永久命名權。

鹿林山天文台長林宏欽指出，「巡天計劃 」是由葉泉志策劃，再由天文台工作人員林啓生、楊庭彰以口徑四十公分的望遠鏡進行拍攝，三月五日起，兩天內就在室女座發現一顆直徑約兩公里、向西北方向移動的亮度十九等（亮度愈大表示星體愈暗，太陽亮度爲負二十六等）目標，位於在火星及木星間的小行星帶，經核對確定是顆新目標，暫定編號爲「2006 EM67」。

有助了解太陽系發展

林宏欽表示，在發現第一顆小行星後，緊接林啓生、楊庭彰又陸續在三月九、十、十九日三天發現四顆小行星，不到一個月內就發現五顆小行星，成果非常難得。台北市立天文館館長邱國光也說，要精確發現體積、亮度較小的小行星相當不容易。

中央大學天文所副教授孫維新表示，一般相信，小行星是太陽系產生過程中的遺跡，有助了解太陽系早期發展的過程，並可提早發現「近地小行星」的軌道，預防地球可能遭撞擊的災難。

【張勵德／台北報導】

玉山設亞洲首座空氣測站

原文轉載自【2006-04-09/蘋果日報/A13 版】

玉山國家公園中的鹿林山將出現亞洲首座設備最新的空氣品質背景測站，4 月 13 日起正式運轉；目前已裝設完成價值 2000 多萬元的極精密微量氣體、汞以及微粒監測等儀器，未來將與國際監測資訊即時接軌，並補強全球空氣品質監測站的空缺，提供中國大陸、東南亞污染物長程輸送對台灣及國際之影響數據。

受美國環署青睞

環保署指出，台灣位處東亞大氣污染物及南亞生質燃燒傳送的下風處，位居樞紐，其中又以海拔 2862 公尺高的鹿林山地理觀測位置最佳，當地因高度夠，不受局部區域空氣污染物干擾，可據以量化境外空氣污染物的影響程度，更可作爲上游中南半島、中國南方、西太平洋夏威夷等地區一線的大氣污染監測中繼站，因此得到美國環保署、太空總署、海洋大氣總署等單位青睞。

兩年來透過台美環保技術合作，完成技術移轉，並將正式啓用，未來將添購二氧化碳分析儀，以了解地球暖化現象。

空氣品質背景測站資訊

◎運轉啓用日期：今年 4 月 13 日

◎地點：玉山國家公園（嘉義、南投交界的鹿林山，海拔 2862 公尺）

◎設備：一氧化碳分析儀、大氣汞分析儀、光學輻射儀、酸雨採樣器、能見度儀、自動

氣象觀測系統

◎功能：掌握大陸及東南亞污染物長程輸送，爲亞洲地區設備最先進空氣品質背景測站

◎造價：新台幣 2000 多萬元

資料來源：環保署、中央大學大氣物理所教授林能暉

【李宗衡／台北報導】

將與國際接軌 提供監測數據 鹿林山空氣測站啓用

原文轉載自【2006-04-14/中國時報/C3 版】

環保署在塔塔加鞍部的鹿林山，設置台灣第一座國際級空氣品質背景測站，十三日開始運轉，未來將提供微量氣體、汞及微粒監測數據，透過資料交換，讓台灣與國際接軌，並促進國內學者與國際進行同步研究。

昨天上午，鹿林山空氣品質背景測站啓用典禮，在海拔 2862 公尺的鹿林山舉行，包括美國環保署、太空總署、海洋大氣總署，及日本、韓國及香港的學者專家，都參與環保史上意義重大的儀式。

環保署副署長林達雄表示，鹿林山背景測站觀測項目，與國際背景測站相同，設置極精密的微量氣體、汞與微粒監測儀器，可以掌握東南亞汙染物在空中長程飄送，對台灣及國際的影響，因此，鹿林站也是亞洲地區極爲重要的背景測站。

由於中國近年來日益工業化，汙染物排放強度也隨著增加，並透過季風跨國傳輸。台灣正處於這些汙染物傳輸路徑上，直接受到影響，因此，對汙染物傳輸現象監測益形重要。背景測站設置目的，是爲了監測大區域空氣品質，必須不受當地汙染影響，因此，環保署依據國際大氣背景站設置條件，選擇在海拔較高的鹿林山設站。

林達雄表示，美國海洋大氣總署在全球卅多個地點，設置背景測站，每周以容器裝氣體，送回美國進行分析，據以掌握大規模環境中，汙染物流動的情況。鹿林山空氣品質背景測站，與國內的中央大學、元智大學合作，進行採樣實驗，與國際進行同步研究；並透過資料交換與學術研究，與國際合作，參與國際環保事務。

【廖志晃／信義報導】

73P 彗星近地球　明起好觀星

原文轉載自【2006-05-10/中國時報/A10 版】

過去二個月快速分裂，加速瀕臨「死亡」的７３Ｐ彗星，已成爲今年全球天文界最熱門的觀測焦點！中央氣象局天文站表示，７３Ｐ彗星明日通過近地點以後，開始進入最佳觀測期，即使是業餘的天文迷，透過雙筒望遠鏡，就有機會看到最大、最明亮的 C 與 B 兩個分裂彗核。

７３Ｐ彗星是在一九三○年五月二日被德國漢堡天文台發現，公轉太陽一周約需五．四年，繞行太陽的橢圓軌道遠日點在木星軌道附近，近日點則是在地球軌道偏內側處。氣象局天文站技士鄭振豐表示，７３Ｐ彗星會引起國際矚目，最主要是因爲它正處於快速分裂的狀況，是全球天文觀測家首次可以在這麼近的距離觀察一顆彗星如何走向「死亡」的過程。

正在位於玉山塔塔加鹿林天文站進行觀測研究的中央大學天文研究所博士生林忠義表示，７３Ｐ是在一九九五年回歸周期通過近日點時，首次被發現分裂成Ａ、Ｂ、Ｃ三個彗核，

到兩千年回歸周期再經過近日點時，A 彗核就消失不見了。天文學界都認爲，經過今年的回歸周期之後，可能連Ｂ、Ｃ彗核都會粉身碎骨，到了下一次回歸周期，就什麼都看不見了。

鄭振豐表示，７３Ｐ彗星在明日通過近地點、到六月初通過近日點是最佳觀測期，尤其是明日到十四日之間，是該彗星最接近地球的時間，可以讓天文迷觀測到最大、最明亮的彗核。但因十二日正好是滿月，如果太亮的話，也會影響觀測品質。

【李宗祐/台北報導】

台灣業餘天文界第一顆 發現超新星 墾丁兩人搶頭香

原文轉載自【2006-07-22/中國時報/A8 版】

「號外！號外！墾丁『星星村天文台』村長蔡元生和台長呂科智發現台灣業餘天文界首顆超新星」（見右圖、蔡元生提供）！國際天文聯合會昨日發布通報，確認蔡、呂在本周二發現的新天體爲超新星，並給予「sn2006ds」編號。

中央大學鹿林天文台台長林宏欽表示，超新星是質量爲太陽的數十倍、甚至是幾百倍的恆星爆炸，所釋放出來的光芒。一個星系（如銀河系）平均一百年會出現一顆超新星，一個人一輩子可能只有一次機會看到超新星。蔡元生和呂科智以業餘觀測家的身分，發現超新星非常不容易。

中央氣象局天文站技士鄭振豐指出，觀測搜尋超新星近幾年來，在美日等國業餘天文界蔚成風潮，台灣則剛在起步中。鄭振豐表示，台灣過去除了中央大學與美國柏克萊大學和中國大陸北京天文台，合作「超新星巡天計畫」，從二００四年起陸續發現十二顆超新星以外，業餘天文界還沒有人發現過超新星，蔡呂兩人首開國內先例。

蔡元生表示，他和呂科智是在十八日（周二）深夜利用四十公分口徑的望遠鏡，瞄準天頂偏南的 PGC70011 星系進行觀測，發現該星系附近好像多出一顆星體。蔡元生指出，剛開始他還有點懷疑，經過重複比對後，他忍不住在心裡呼喊：「這次真的讓我找到了嗎？」馬上在周四早上撰寫觀測報告，連同照片利用電子郵件向國際天文聯合會通報。

昨日上午，國際天文聯合會以電子郵件回覆，並發布正式通報，蔡元生才相信自己真的找到台灣業餘天文界第一顆超新星，讓他十分高興。蔡元生說，自從知道中央大學與美國合作「超新星巡天計畫」以後，他就很想自己做做看，卻一直等到自資籌建的墾丁「星星村天文台」，在去年底完工啓用以後，才開始有計畫的巡天。

蔡元生表示，過去幾個月來，他與呂科智共同鎖定約一千個星系進行觀測，「晚上我先睡覺，由呂科智負責操作望遠鏡拍攝。白天再由我負責比對前晚拍攝的影像。」蔡元生指出，只要是好天氣，他們每天可次觀測拍攝一百五十個左右的星系，有時候甚至可以狂拍四、五百個。「有好幾次曾拍到過超新星，常因爲來不及比對完，人家就先找到了。」蔡元生說，搜尋超新星競爭非常激烈，幾乎全世界都有人找看，晚幾分鐘，就會被別人捷足先登。

【李宗祐／台北報導】

中央大學與夏威夷大學洽談合作泛星計畫

原文轉載自 【2006-08-21/中央社】

中央大學副校長葉永烜今天表示，中央大學天文研究所正積極與美國夏威夷大學洽談合作「泛星 Pan-Starrs」計畫，目的是要大量搜尋及發現在太空中運行的小行星或彗星，而資源

的互通有無與合作，預期會使研究更可以預期。

葉永烜並以中央大學在台灣南投鹿林天文台進行的「鹿林巡天計畫」獲得優異觀測績效爲例，即最近獲得國際天文總會小行星中心（IAU：MinorPlanetCenter ）確認觀測發現超過一百零一個小行星等新天體，表示中央大學這項自發性的研究成果，證明中央大學有發現小行星的實力，將爲與美國的合作奠定良好基礎。

中央大學這項自發性的研究成果，在偶然中還獲得中國大陸十七歲的天文愛好者葉泉志從網路上友善參與，協助規劃觀測。中央大學鹿林天文站站長林宏欽說，三月時的高中生葉泉志已研究小行星並搜索多年，從 NEAT、BATC、 DSS 等資料庫已發現多顆小行星，嫻熟小行星的巡天之道。中央大學在向晴天鐘網站（http://www.y234.cn/ ）申請鹿林天文台晴夜率預測時，意外得到葉泉志的友善回應，雙方開始展開合作計畫。林宏欽表示，如今，葉泉志剛考上中山大學大氣科學系，在網路聊天當中，葉泉志也說如果有機會，願意到台灣來看看。

葉永烜表示，這項偶然的兩岸合作研究模式，都是研究人員的主動與興趣促成，從科學研究來說是最好的事情，如果有更好的儀器資源互通有無與研究機會，成就會更可以預期，歐美科技發達很多情形是互相合作的相乘效果，值得大家思考。

【中央社記者翁翠萍台北二十一日電】

兩岸合作　鹿林巡天計畫半年　發現逾 101 顆小行星

原文轉載自 【2006-08-21/中央社】

國立中央大學今年三月以「鹿林巡天計畫（LUSS）」開始有計畫觀測小行星，並獲得中國大陸十七歲的天文愛好者葉泉志從網路上友善參與，協助觀測，短短半年來，經國際天文總會小行星中心確認，已經發現超過一百零一顆小行星，台灣鹿林天文台成爲亞洲發現小行星最活躍的地方。

中央大學天文研究所教授兼副校長葉永烜表示，移動天體當中，有些屬於近地天體（NEOs），其中少數軌道與地球相交，當地球與這些近地天體交會時，對於地球是具有威脅性的。所以，巡天觀測可以讓人們瞭解這些地球附近移動天體的分佈狀況，幫助人類及早因應可能發生的災難。

中央大學天文研究所鹿林天文台設在距離亞洲第一高峰玉山登山口塔塔加附近標高近三千公尺的高山上，目前擁有的天文望遠鏡口徑最大是一公尺，「鹿林巡天計畫（LUSS：LulinSkySurvey）」只使用口徑四十公分的小型望遠鏡進行半自動巡天觀測，每月統計觀測結果，平均每個月發現十五顆到二十顆新天體，對於小型望遠鏡的觀測可說成效卓著。

葉永烜說，到半個月前，經國際天文總會小行星中心（IAU：MinorPlanetCenter）確認，台灣鹿林天文台累計觀測到一百零一顆新天體，其中有三個是七十三片彗星碎片，其餘都是小行星，到現在，應該又再觀測發現到更多小行星了！

台灣的小行星發現也是從中央大學開始，但都是比較偶然的發現，包括二００二年十一月二十五日兩位研究生張智威、陳秋雯使用鹿林一米望遠鏡觀測 4708 號小行星時，意外發現「鹿林一號小行星」（Lulin1），暫定編號爲 2002WT18，成爲台灣發現的第一顆小行星。

二００五年，中央大學天文所博士後研究員木下大輔與博士生黃癸雲在觀測伽瑪射線爆

發源 GRB20050408 餘暉時，意外發現第二顆，爲紀念中央大學創校九十週年，暫名爲「中央大學 90（NCU90）」。

鹿林巡天計畫偶然的兩岸合作模式，係透過大陸葉泉志策劃，選定觀測天區，再由台灣鹿林天文台站長林宏欽、林啓生、楊庭彰等人輪流進行遠端遙控，以半自動化排程方式觀測，半年來逐步改善，觀測及發現效率愈來愈高。

林宏欽說，鹿林巡天計畫與國外其他大型巡天計畫如 LINEAR、NEAT 等相比，只能算是小巫見大巫，重要的是，「在這個世界的舞台上，台灣沒有缺席！」

【中央社記者翁翠萍台北二十一日電】

中央大學：天體中唯有小行星可由發現者命名

原文轉載自 【2006-08-21/中央社】

國立中央大學今天發布設在南投山區鹿林天文台觀測小行星的優異成果，並表示小行星是目前唯一可以由發現者命名並得到世界公認的天體。

中央大學指出，根據天文相關網站 http://www.pep.com.cn/200503/ca637870.htm 資訊，發現者擁有小行星的命名權，命名權在十年內隨時可以行使。但所有小行星的命名，須報經國際小行星中心和小行星命名委員會審議通過後，才公布於世，成爲所發現天體的永久名字，並爲世界各國公認。

發現小行星有標準程序，即觀測到一顆小行星後，不能立刻確定是否爲一顆新發現的小行星，可以自己先給它一個臨時編號，例如中央大學發現的 Lulin1 鹿林一號。當這顆小行星在不同的夜晚被觀測到，並報告國際小行星中心，確認是新發現的小行星之後，即可得到一個國際同一格式的「暫定編號」2002WT18（K02W18T）。

中央大學指出，當一顆小行星至少四次在回歸中心被觀測到，並且精確測定出其運行軌道參數後，它就會得到國際小行星中心給予的永久編號，如台灣發現的「蔡氏小行星」，永久編號爲 2240。

【中央社記者翁翠萍台北二十一日電】

大陸高中生領航　中大發現 115 顆小行星

原文轉載自【2006-08-22/聯合報/A5 版】

電影「世界末日」、「彗星撞地球」中，說的都是地球被小行星或彗星撞出大問題；中央大學和十八歲的中國大陸高中生葉泉志合作，最近半年就發現一百一十五顆從前未知的小行星，對全球都有幫助。

一般認爲，恐龍在六千五百萬年前滅絕，就是因爲一顆直徑約十一公里的小行星，撞到墨西哥猶加敦半島，揚起巨量灰塵遮蔽陽光，綠色植物無法進行光合作用，導致食物鏈被破壞；西元一九０八年，一顆直徑六十公尺的星體，撞到西伯利亞，造成方圓四十公里內的森林全毀，爆炸威力相當於日本廣島原子彈的六百倍，證明地球隨時可能面臨來自外太空的嚴重威脅。

人類一直在尋找小行星，希望減低這種威脅，中大副校長葉永烜表示，中大鹿林山天文台在二００二年和二００五年，先後發現兩顆小行星「鹿林一號」和「中央大學九十」（爲紀

念中大創校九十周年），爲人類盡一份心力。

鹿林山天文台站長林宏欽表示，他們是從網路找到葉泉志的個人網站「晴天鐘」，發現葉泉志收取全世界公開氣象資料庫的資訊，自己寫程式預測夜間天氣，於是請葉泉志幫忙提供台灣地區夜間天氣。

葉泉志當時已根據其他天文台的觀測資料，找到許多小行星，但這樣做的命名權屬於天文台；因此葉泉志提出「鹿林巡天計畫」，由他規畫每晚觀測天空那些區域，中大再用鹿林山天文台的望遠鏡觀測，並將資料傳給他，他再從中分析比對，找出可能的新小行星，然後雙方分享命名權。

林宏欽指出，葉泉志的分析，中大也可以做，但葉的經驗豐富，分析速度快很多，於是雙方從今年三月初開始合作。鹿林山天文台可看見廿星等的小行星（星等愈小愈亮，六等爲肉眼可視極限，北極星約爲二等），大約是數公里大小，從三月到現在，已發現一百一十五顆新小行星，平均每三天就可發現兩顆。

林宏欽說，天文學家認爲有幾十萬顆小行星，位於火星和木星之間的「小行星帶」，其中百分之九十九不會靠近地球，但部分仍可能對人類造成威脅；不過到目前爲此，天文學界還沒有發現可能撞到地球的小行星。

【記者李名揚／台北報導】

國際小行星中心　確認才算數

原文轉載自【2006-08-22/聯合報/A5 版】

全世界有許多天文台在找小行星，若認爲找到現有資料中不存在的星體，把資料送到「國際小行星中心」，確認爲新小行星，發現者就可爲此小行星正式命名，但「發現者」指的是觀測到的天文台，而非分析、比對的人。

一顆新的小行星，至少要在不同的三個夜晚被觀測到，國際小行星中心才能據以計算軌道，且三個夜晚間隔愈久，計算出來的軌道愈精確；從發現者把資料報給國際小行星中心到正式命名，最快要一年，若這顆小行星不易觀測，可能得等上好幾年。

【記者李名揚】

兩岸合作巡天　半年發現 101 小行星

原文轉載自　【2006-08-22/中國時報/A8 版】

台灣科學界也有「一〇一」個傲視全球的新發現！中央大學天文所鹿林天文台與大陸十七歲青年學生葉泉志合作「鹿林巡天計畫」（ＬＵＳＳ），半年內發現一〇一顆小行星，全部經過國際天文總會小行星中心確認。

中大副校長、國際知名天文學者葉永烜指出，我國每個月平均發現十五顆小行星，在全球名列前茅。特別的是，其他國家都是用一米到二米口徑望遠鏡搜尋小行星，我國則用四十公分的小型望遠鏡觀測，可說是國際間最小的「巡天」望遠鏡。

盼找出恐威脅地球行星

葉永烜表示，鹿林巡天計畫由大陸高中生葉泉志策畫，選定觀測天區，鹿林天文台長林宏欽和觀測員林啓生、楊庭彰等輪流以遠端遙控操作玉山塔塔加的望遠鏡，觀測搜尋小行星。

今年三月至今，陸續發現超過一百顆新天體，其中一〇一顆由國際天文總會小行星中心確認爲新小行星。

林宏欽表示，葉泉志只是高中生，卻已研究搜索小行星多年，與台灣合作前，陸續透過美國航空暨太空總署「近地小行星追蹤計畫」（ＮＥＡＴ）等影像資料庫發現多顆小行星，可精準計算小行星可能出現天區。中大今年初向他的天文網站「晴天鐘」（www.y234.cn）申請鹿林天文台晴夜率預測時，開始和葉泉志合作。

葉永烜指出，目前發現的一〇一顆小行星，經初步計算約有一、兩顆的運行軌道會與地球軌道交會，可能與地球碰撞，該校已將相關資訊通報國際天文總會小行星中心。

葉永烜強調，「巡天計畫」主要目的是找出所有可能進入地球軌道與地球碰撞的小行星，我國也組成跨校研究團隊，與美國夏威夷大學合作「泛星 Pan-Starrs」計畫，希望今年底起五到十年內，找出所有可能威脅地球安全的小行星或彗星。

【李宗祐/台北報導】

幕後功臣葉泉志　17 歲天文異人

原文轉載自　【2006-08-22/中國時報/A8 版】

中央大學的玉山塔塔加鹿林天文台半年不到發現一〇一顆小行星，觀測團隊夙夜匪懈的努力，功不可沒，但就讀大陸廣州第七中學的天才高中生葉泉志精心規畫觀測天區，是促成兩岸成就的最大幕後功臣。中大副校長葉永烜說：「這個小孩是個不可思議的異人！」

鹿林天文台台長林宏欽表示，大陸「晴天鐘」網站提供各地未來四十八小時天文觀測晴夜率預測，供天文愛好者研擬觀測計畫參考。今年初，我方以電子郵件向該網站申請協助提供鹿林天文站晴夜率預測。

「晴天鐘」網站站主葉泉志回信答應幫忙，並利用「近地小行星追蹤計畫」（ＮＥＡＴ）資料，對中大之前發現的鹿林一號小行星進行定軌觀測，讓鹿林兩顆一直未獲編號的小行星（Lulin2、Lulin）得到國際天文總會小行星中心認證編號。

當時葉泉志也希望用鹿林天文台四十公分口徑望遠鏡搜尋小行星。葉泉志和台灣合作前，已利用ＮＥＡＴ影像資料庫發現多顆小行星，但都是分析其他研究機構拍攝的影像所得，不是自行觀測，因此無法取得小行星命名權。而以往鹿林發現的小行星並未系統性觀測，都是觀測過程意外發現，也未進行後續觀測，因此多年來發現的小行星一直未永久命名。

林宏欽指出，葉泉志的提議促成雙方合作搜尋小行星。三月五日起，中大研究生利用四十公分望遠鏡搜索小行星和彗星，葉泉志負責資料處理及分析，希望系統性觀測及持續追蹤，發現並取得小行星永久命名權。

沒想到，三天後，台灣觀測團隊就在室女座發現一顆向西北方向移動的新小行星，接著又在觀測 2006EE 近地小行星影像時，發現另外三個新小行星。就這樣，海峽兩岸第一顆非專業小行星出爐了，並在半年內快速增加到一〇一顆，成爲兩岸天文觀測合作的最佳典範。葉泉志也終於如願以償，達到自己命名小行星的願望。

【李宗祐/台北報導】

兩岸合作　發現 115 顆小行星

原文轉載自【2006-08-22/蘋果日報/A10 版】

中央大學天文所鹿林天文台和大陸年僅十七歲的天文愛好者葉泉志，合作執行鹿林巡天計畫（Lulin Sky Survey，簡稱 LUSS）後，半年發現一百一十五顆小行星。

對人類意義重大

中央大學副校長、天文所教授葉永烜昨表示，該校二００二年發現第一顆小行星，今年又發現一百一十五顆，經國際天文總會小行星中心（IAU：Minor Planet Center）確認，成亞洲發現小行星最活躍處。

葉永烜說，觀測小行星對人類意義重大，因小行星軌道太接近地球，可能會碰撞地球，六千五百萬年前一顆小行星軌道和地球相交擦撞造成恐龍滅絕；目前新發現小行星，軌道都不太接近地球，不致有相交擦撞危險。他強調，該校觀測團隊無意間在網路上發現葉泉志架設的「晴天鐘」天文網站，提供軌道計算與比對資料，促成雙方合作。

【楊桂華／台北報導】

９／３太空船撞月球　天文迷等著看

原文轉載自【2006-08-25/中國時報/A8 版】

歐洲太空總署(ＥＳＡ)首艘探月太空船「史邁特一號」(SMART-1)歷經近三年太空飛行和觀測任務後，預定九月三日撞擊月球表面，結束探月任務。為協助ＥＳＡ解開月球起源之謎，國家太空中心昨日號召國內天文迷，同步觀測記錄月球表面被擊前後的變化。

國家太空中心主任吳作樂指出，史邁特一號九月三日在第 2890 軌道撞擊月時間為台灣下午一時四十一分，因白天無法進行觀測，但科學界預測，太空船撞擊月球產生的灰塵很可能延遲十幾個小時後才出現，剛好是台灣的午夜，應可看到碰撞後的煙塵。

吳作樂表示，撞擊時間也可能延後到第 2891 軌道，時間是台灣九月三日傍晚六時四十六分，天色尚未全暗，仍有機會看到史邁特一號撞擊月球全部過程及煙塵。國家太空中心將彙整台灣地區天文迷觀測資料，傳送ＥＳＡ研究參考。

國家太空中心也與中央大學天文研究所教授孫維新表示，中大動員鹿林天文台和墾丁天文台加入觀測，業餘天文迷若有廿四公分以上口徑的望遠鏡，也可加入觀測。

【李宗祐/台北報導】

歐洲太空船 3 日撞月　中央大學天文台助觀測

原文轉載自【2006-09-01/中央社】

歐洲太空總署（ESA ）SMART-1 太空船預定三日撞擊月球表面，希望全球專業及業餘天文台協助做地面光學觀測，以獲得撞擊前後的光學影像，提供做為月表科學研究。台灣中央大學的鹿林天文台、墾丁天文台將使用專業天文望遠鏡在當天進行月面觀測，為全球科學研究合作貢獻一分力量。

SMART-1（SmallMissionsforAdvanced ResearchinTechnology）太空船是歐洲太空總署第一艘探月太空船，二００三年九月二十七日格林威治時間二十三時十四分（相當台北時間二十八日七時十四分）由亞利安五型火箭承載，從法屬圭亞那 Kourou 基地發射升空。四十二分鐘後，成功進入地球同步軌道。三百六十七公斤的 SMART-1 太空船隨後展開漫長的月球探測

之旅，歐洲也成爲繼蘇聯、美國與日本之後，第四個發射月球探測太空船的成員。

中央大學表示，雖然人類已於二十世紀六０年代登陸月球，但對月球的瞭解仍有限，尤其是月球起源與「地—月關係」等，探測月表有沒有含水的目標已由另一艘探月太空船於一九九九年撞擊月表時觀察沒有發現，這次撞月任務以研究月表土壤的地質構造與組成爲主。

歐洲太空總署一九九四年制訂月球探測計畫，主要目標除了科學研究，還希望開發月球資源。SMART-1 配備了紅外與 X-射線儀器，以繪製詳細的月球礦物分佈與元素含量圖，並可精確繪製月球三維地圖，詳細研究月球地形、表層土壤構造、岩層化學成分，及地表下的水冰等，這些資訊不僅可提供科學家對於類地行星與月球起源的線索，也可做爲未來開發月球資源時的參考。

SMART-1 發射升空後，不使用傳統火箭，而使用離子引擎逐步推進到月球軌道上，這種新技術是電離八十二公斤氙氣，讓電離後產生的離子以一萬六千公里時速噴出，提供約 70mN（千分之七十牛頓）的向前推力，雖然力量很小，但可持續甚久，甚至可達一年。專家認爲離子引擎是未來太空飛行的主要發展方向，其效率爲傳統化學火箭的十倍以上，不僅可使太空船重量減輕，也降低發射成本。如果這次任務成功，二０一三年的水星探測太空船也將採用同樣設計的引擎。

SMART-1 主要任務在做離子引擎技術測試，對月面的科學觀測及研究僅爲輔助性任務，但技術測試及觀測任務告一段落時，歐洲太空總署決定充分發揮 SMART-1 的剩餘價值，使用太空船撞擊月球表面，以研究月表的地質構造及組成。

撞擊是否產生可觀視覺效果，科學家不表樂觀，因爲 SMART-1 將以掠射（Grazing）方式擦撞月表，撞擊月表速度每秒二公里，即時速七千二百公里，速度不快，因此撞擊產生的光學特徵可能不明顯，估計大約爲視星等十六等亮度，即使能觀測到撞擊那一剎那亮度最強時，也需用較大型望遠鏡才可能偵測到明顯的光學變化。

若當天台灣入夜時撞擊已經結束，則因撞擊點爲月球暗面，估計不會有明顯光學特徵產生，而需等幾天後，撞擊點重新被太陽照射時，可拍攝撞擊點作爲比較。

SMART-1 預定撞擊月面的軌道是第二八九０號軌道，其次的可能性是提前到第二八八九號軌道，第三種可能性是延後到二八九一號軌道發生撞擊。前兩個可能性撞擊時間是在台灣的白天，台灣無法觀測，第三種撞擊時間爲台灣時間傍晚六時許，台灣地區勉強可以觀測。因此台灣這次不會扮演關鍵的地面支援角色，但中央大學師生仍會在鹿林天文台及墾丁天文台進行觀測。

【中央社記者翁翠萍台北一日電】

太空船撞月球 明天上演

原文轉載自【2006-09-02/聯合晚報/6 版】

歐洲航太總署（ESA）的 SMART-1 太空船，明天將撞擊月球表面，探測月球土壤成分。中央大學的鹿林天文台及墾丁天文台也參與這項全球科研合作協助觀測，台北市立天文台表示，撞擊所揚起的塵土被陽光照射下，用雙筒望遠鏡就可以觀察到。

SMART-1 預定於台北時間明天 (3 日)下午 1 時 41 分，撞擊位在月球南半球的卓越湖，明天是農曆 11 日的「凸月」，撞擊點位於接近月球日夜分界線的暗面。

台北市立天文館表示，雖然太空船僅以每秒 2 公里的速度撞擊，但撞擊所揚起的塵土被陽光照射下，透過業餘觀測用望遠鏡便可觀察到。如果預定撞擊的時間延後到台北時間 3 日傍晚 6 時 46 分，台灣上空已可見月球，可進行短曝光觀測，此時月亮在東南方仰角約 30～40 度的位置上。

中央大學天文所副教授孫維新，是台灣地區同步觀測行動的召集人，明天傍晚將和天文同好在墾丁天文台參與觀測。他表示，撞擊時間如果發生在台北時間的下午，雖無法觀測撞擊當時的景象，但仍可藉由撞擊前後的影像，比對物質噴出、沈澱的狀況。

孫維新指出，367 公斤重的 SMART-1 太空船是歐洲太空總署首艘探月太空船，配備了紅外線與 X-射線儀器，以繪製詳細的月球礦物分布與元素含量圖，並可精確繪製月球三維地圖，詳細研究月球地形、表層土壤構造、岩層化學成分，及地表下的水冰等。這些資訊不僅可提供科學家對於類地行星與月球起源的線索，也可做爲未來開發月球資源時的參考。

這次讓太空船撞擊月球表面，更要藉由揚起的灰塵，研究月表土壤的元素。但撞擊當時是否會產生可觀的視覺效果，科學家並不表樂觀，孫維新解釋說，因爲 SMART-1 太空船是以掠射（Grazing）的方式擦撞月球表面，撞擊月球表面的速度約爲每秒鐘 2 公里，也就是時速 7200 公里，這樣的太空速度並不快，因此撞擊所能產生的光學特徵，約爲星等 16 等的亮度，撞擊那一剎那，需要使用較大型的望遠鏡才可能偵測到明顯的光學變化。

SMART-1 預定撞擊月面的軌道是第 2890 號軌道，次一級的可能性是提前到第 2889 號軌道，第三種可能性是延後到 2891 號軌道發生撞擊。前兩個軌道撞擊時間是在台灣的白天，台灣皆無法觀測，只有 2891 號軌道的撞擊時間爲台灣傍晚 6 時許，台灣地區勉強可以觀測。

【記者王彩鸝/台北報導】